Understanding tyrosine kinase domain plasticity through identification of protein residues involved in the control of the conformational transition

Boubeva, Ralitza

UNIVERSITÉ DE GENÈVE
Section des sciences pharmaceutiques
Laboratoire de biochimie pharmaceutique

FACULTÉ DES SCIENCES
Professeur Leonardo Scapozza

Understanding tyrosine kinase domain plasticity through identification of protein residues involved in the control of the conformational transition

THÈSE

présentée à la Faculté des sciences de l'Université de Genève
pour obtenir le grade de Docteur ès sciences, mention sciences pharmaceutiques

par

Ralitza Boubeva
de
Sofia (Bulgarie)

Thèse N°:4300

Genève
Atelier de reproduction Repromail
2011

Contents

Abbreviations 6

Summary 9

Résumé 14

CHAPTER 1 20

1. From structure to function: A historical view 21

2. Protein dynamics: from hypothesis to structural evidences. 23

3. Protein dynamics: the time-scale issue 28

3.1. Experimental methods for studying "slow" protein dynamics 30

3.2. Computational methods for studying protein dynamics 31

3.3. Experimental methods for studying "fast" protein dynamics 32

4. Protein tyrosine kinases 34

4.1. Protein structure and dynamics of the tyrosine kinases 38

4.2. Discovery, physiological role and oncogenicity of c-Src 45

4.3. Structure and plasticity of c-Src 49

5. Aim and workflow of the thesis 53

CHAPTER 2 54

1. Abstract 55

2. Introduction 56

3. Materials and Methods 60

3.1. Protein Expression 60

3.2. Protein Purification 60

3.2.1. c-Src KD purification for activity, inhibition assays and for crystallization 60

3.2.2. c-Src KD purification for ITC studies 61

3.2.3. c-Src KD purification for CD studies 62

3.3. Protein quantification 63

3.4. In vitro protein activity assay 64

3.4.1. UV-based tyrosine kinase assay 64

3.4.2. Autophosphorylation reaction monitored by Western Blotting 66

3.5. CD spectra 67

3.6. Thermal denaturation 67

4. Results and discussion 69

4.1. c-Src KD purification for kinase assay and crystallyzation 69

4.2. c-Src KD purification for ITC studies 76

4.3. c-Src KD purification for CD 81

5. Conclusion 88

CHAPTER 3 *.....90*

1. Abstract 91

2. Introduction 92

3. Materials and methods 102

3.1 Rational design of c-Src kinase domain site point mutants 102

3.2 Site-directed mutagenesis 105

4. Results and discussion 107

5. Conclusion 112

CHAPTER 4 *.....113*

1. Abstract 114

2. Introduction 115

3. Materials and Methods 123

3.1 In vitro tyrosine kinase activity assays 123

3.1.1 UV-based tyrosine kinase assay 123

3.1.2 Autophosphorylation reaction by Western Blotting 125

3.2 In vitro c-Src inhibition assays 127

3.2.1 UV-based c-Src inhibition assay 127

3.2.2 Inhibition of autophosphorylation monitored by Western Blot 128

3.2.3 Inhibitory constant (Ki) determination 129

3.3 Circular Dichroism (CD) 130

3.3.1 CD spectra of c-Src WT and mutants 130

3.3.2 Thermal denaturation of uncomplexed c-Src WT and mutants 130

3.3.3 Thermal stability of c-Src WT and c-Src L317I in presence of imatinib 131

3.4 Crystallization 131

3.4.1 c-Src L317I – apo 131

3.4.2 c-Src L317I –co-crystals 132

3.4.3 Data collection, structure solution and refinement 132

3.5 Isothermal Titration Calorimetry (ITC) 134

4. Results and discussion 135

4.1 Autophosphorylation 135

4.2 ATP and substrate kinetics of c-Src WT and c-Src L317I 138

4.3 Dasatinib and pyrazolopyrimidine compound 5 sensitivity of c-Src KD 145

4.4 Using CD to elucidate the influence of L317I on the stability of c-Src KD 148

4.5 Crystal structures of c-Src L317I 155

4.6 Crystal structure of c-Src L317I apo form 156

4.7 Crystal structure of c-Src L317I- imatinib 159

4.8 Crystal structure of c-Src L317I-dasatinib 161

4.9 Crystal structure of c-Src L317I-pyrazolopyrimidine compound 5 164

4.10 Imatinib binding to c-Src L317I: a calorimetric study 168

4.11 H1-H2 naturally occurring mutations in c-Src? 170

5. Conclusion 173

CHAPTER 5 ..... *175*

1. Abstract *176*

2. Introduction *177*

3. Materials and Methods *181*

3.1. Protein expression and purification *181*

3.2. ADP-inhibition assay *182*

3.3. Kinetic analysis *183*

4. Results and discussion *184*

5. Conclusion *188*

CHAPTER 6 ..... *190*

Final conclusions and outlook *191*

Bibliography *197*

Appendix A *212*

Acknowledgements *213*

Abbreviations

ABL	Abelson tyrosine kinase
ACK	Activated CDC42 kinase
ADP	Adenosine diphosphate
ATP	Adenosine triphosphate
AXL	Tyrosine protein kinase receptor UFO
Blk	B lymphocyte kinase
BSA	Bovine serum albumin
CCK	Cholecystokinine
CD	Circular dichroism
CDK	Cyclin-dependent kinase
CRP	Catabolite gene activator
CSK	C-terminal Src kinase
CV	Column volume
DDR	Epithelial discoidin domain-containing receptor
DMSO	Dimethyl Sulfoxide
DNA	Deoxyribonucleic acid
dNTP	Deoxynucleotide triphosphate
DTT	Dithiothreitol
ECM	Extracellular matrix
EDTA	Ethylene diamine tetra acetic acid
EGFR	Epidermal growth factor receptor
ELS	*Escherichia Coli* chaperone system (GroEL, GroES)
EPHR	Ephrin receptor
FAK	Focal adhesion kinase
FES	Proto-oncogene tyrosine kinase Fes
FGFR	Fibroblast Growth factor receptor
Fgr	Gardner-Rasheed feline sarcoma viral (v-fgr) oncogene homolog
FIRST	Floppy inclusion and rigid structure topography

FRK	FYN-related kinase
FRODA	Framework rigidity optimized dynamic algorithm
Fyn	Proto-oncogene tyrosine-protein kinase Fyn
GST	Glutathione s transferase
GTP	Guanosine triphosphate
Hck	Hematopoietic cell kinase
HGFR	Hepatocyte growth factor receptor
Hsp	Heat shock protein
IDR	Intrinsically disordered region
IKK	IκB-related kinases
IMAC	Immobilized metal chelating chromatography
IPTG	Isopropyl β-D-1-thiogalactopyranoside
IR	Insulin receptor
ITC	Isothermal titration calorimetry
JAK	Janus kinase
JM	Juxtamembrane domain
KD	Kinase domain
KJE	*Escherichia Coli* chaperone system (DnaK, DnaJ, GrpE)
LB	Luria-Bertani medium
Lck	Lymphocyte cell-specific protein tyrosine-kinase
LDH	Lactate dehydrogenase
LMR	Lemur tyrosine kinase
LTK	Leukocyte tyrosines kinase receptor
Lyn	Tyrosine-protein kinase Lyn
MD	Molecular dynamics
MES	2-(*N*-morpholino)ethanesulfonic acid
MMP	Matrix metalloproteinase
MUSK	Muscle, skeletal receptor tyrosine protein kinase
MWCO	Molecular weight cut-off
NGFR	Neutrophic tyrosine kinase receptor
nRTK	Non-receptor tyrosine kinase
PAGE	Polyacrylamide gel electrophoresis

PDB	Protein Data Bank
PDGRF	Platelet derived growth factor receptor
PK	Pyruvate kinase
PKA	Protein kinase A
PTK	Protein tyrosine kinase
RET	Rearranged during transfection kinase
RMSD	Root mean square deviation
RNA	Ribonucleic acid
ROR	Receptor related transmembrane tyrosine protein kinase
ROS	Proto-oncogene tyrosine kinase Ros
RSV	Rous sarcoma virus
RTK	Receptor tyrosine kinase
RYK	Tyrosine protein kinase Ryk
SDS	Sodium dodecyl sulfate
SH1	Src-homology domain 1
SH2	Src-homology domain 2
SH3	Src-homology domain 3
SH4	Src-homology domain 4
SlyD	Sensitivity to lysis protein D
SRC	Proto-oncogene tyrosine-protein Kinase Src
STAT	Signal transducer and activator of transcription
SYK	Spleen tyrosine kinase
TB	Terrific broth
TCEP	Tris (2-carboxyethyl) phosphine
TEC	Tyrosine protein kinase Tec
TIE	Tyrosine protein kinase receptor Tie
Vav	Proto-oncogene vav
VEGFR	Vascular endothelial growth factor receptor
WT	Wild type
Yes	Proto-oncogene tyrosine-protein kinase Yes
YopH	Tyrosine-protein phosphatase yopH

Summary of the thesis

The publication of the first structures of proteins at atomic resolution fifty years ago represented a major breakthrough to our present understanding of protein structure and function. Additional studies demonstrated that proteins assume a constant fluctuation of a large number of different conformations and thus brought to the idea that dynamical effects play a major role in protein activity. In fact, intrinsic dynamic properties of proteins have been shown to act as switches and transducers in response to incoming signals and thereby are essential elements for signal transmission in cellular signalling networks.

In this context, with approximately 518 kinases encoded in the human genome, virtually every signal transduction process is wired through the phosphotransfer cascade operated by protein kinases. Protein tyrosine kinases take part in the control of cell growth, metabolism and apoptosis by using a highly conserved catalytic domain to transfer the γ-phosphate of adenosine triphosphate (ATP) onto the hydroxyl group of a substrate tyrosine residue. Any abnormal tyrosine kinase activity can deregulate cell homeostasis and cell-to-cell signalling, which may ultimately lead to cancer and diverse inflammatory diseases.

In medicinal chemistry, the conformational plasticity in protein function and interactions represents a challenge but also an opportunity for the discovery and for the selection of new chemical scaffolds interacting with the target protein.

Our actual knowledge on the tyrosine kinase conformational landscape is based on crystal structures depicting tyrosine kinase domain structures in closed, intermediate and open conformations, according to the position of

several structural determinants described in details in the first chapter of this work.

The aim of this thesis consisted in the identification of key amino acid residues governing the transition from active to inactive protein kinase domain conformation to better understand the molecular basis of the conformational plasticity of tyrosine kinases. We used c-Src tyrosine kinase domain as a case study because of the wealth of structural information on this protein.

To define the residues involved in the regulation of c-Src kinase domain plasticity, we have leaned upon a recent comparative structural study on tyrosine kinase domains. The latter study depicted a pool of 14 residues forming a hydrophobic interface in between the bi-lobed structure of the InsR kinase domain that appeared to be important for the protein conformation and motion. Thus, we first carried out a structural alignment against the kinase domain of InsR and defined the corresponding residues in the kinase domain of c-Src.

To verify experimentally whether the identified residues were indeed controlling the kinase domain plasticity, we have mutated them to the corresponding ones found in tyrosine kinases (c-Abl, c-Kit, Syk) that are inhibited in a nanomolar range by the DFG-Asp out conformation specific inhibitor, *i.e* imatinib. The wild type kinase domain of c-Src is only inhibited by imatinib at high concentration (IC_{50}=220µM). This is due to the thermodynamic penalty conformation of the DFG-motif (*i.e* DFG in an "out" conformation), a key conformational determinant within the kinase domain. Therefore, by mutating one or several residues from the hydrophobic interface of c-Src to the corresponding ones of c-Abl, c-Kit and/or Syk we constructed 8 c-Src kinase domain mutants (as detailed in Chapter 3) with the aim at answering to the following questions: Do residues from the hydrophobic interface in c-Src influence the

conformational prevalence of c-Src? If yes, how do they do it? Is it by stabilizing a DFG-favourable conformation for imatinib binding or by influencing dynamically the transition from DFG-out to DFG-in conformation?

We expressed all c-Src kinase domain mutants together with the wild type c-Src kinase domain and purified them in milligram amounts according to two main types of biophysical and biochemical protein characterization assays necessary to reply to the addressed issues. In Chapter 2 we report the protocols for c-Src purification tailor-made for each type of protein characterization assay, namely for kinase assay and crystallization, for isothermal titration calorimetry (ITC) studies as well as for circular dichroism (CD) studies.

The first category of assays investigated the influence of the mutated residues on the dynamics of the DFG-flip and was conducted in presence of elements essential for c-Src catalysis, notably Mg^{2+}, peptide substrate and ATP. The second category of assays was meant to follow the role of the mutations on the conformational prevalence of the c-Src kinase domain. The latter were referred to as "static" assays and were conducted without Mg^{2+}, and ATP. Results from protein characterization assays are detailed in Chapter 4.

Kinetics and circular dichroism data showed that all c-Src mutants were active and properly folded, with a decreased thermodynamic stability of c-Src kinase domains carrying mutations of hydrophobic residues from the N-lobe of the kinase domain.

Data from UV-coupled imatinib inhibition assay demonstrated that all c-Src mutants were more sensitive to imatinib inhibition than the wild type kinase domain when their unphosphorylated form was pre-incubated with the inhibitor before addition of Mg^{2+}, and ATP. c-Src variants carrying mutations of hydrophobic residues from the N-lobe of the kinase domain, showed higher sensitivity to the inhibition than c-Src variants carrying mutations of hydrophobic residues from the C-lobe of the kinase domain. Among them c-Src L317I exhibited an inhibition by imatinib in the nanomolar range (IC_{50}=4nM) which was comparable to the one of c-Abl (IC_{50}=25-200nM) in both the UV-coupled inhibition assay as well as in an orthogonal autophosphorylation inhibition assay. Thus we could show that the identified residues from the hydrophobic interface in c-Src appear to have a net impact on the conformation of the kinase in particular at the level of the DFG-motif.

c-Src L317I revealed also a higher sensitivity to the inhibition with pyrazolopyrimidine 5 compound. Since the pyrazolopyrimidine 5 compound has been reported as an inhibitor that binds to the DFG-out conformation without thermodynamic penalty, we could presume that L317I mutation influences the plasticity of the kinase domain of c-Src not only at the level of the DFG-motif but also, to a lesser extent, of the A-loop, influencing the whole rotation of the N-and C-terminal domains.

The c-Src L317I in complex with imatinib showed that the mutation did not influence the binding mode of the inhibitor and the expected DFG-out conformation of the protein. Surprisingly, the crystal structure of c-Src L317I-apo revealed a new DFG motif conformation although still adopting the “in” conformation.

Performed in parallel, ITC measurements for imatinib binding to L317I and WT c-Src kinase domains depicted as well a discrepancy in comparison

with inhibition data; K_D values for the mutant and the wild type protein were similar and both in the µM range (7.2µM and 7.4µM, respectively).

Thus, the crystal structure of c-Src L317I apo-form and thermodynamic characterization of imatinib binding to the mutant suggested that an Ile at position 317 in c-Src does not act on the conformational prevalence of the kinase domain but at the level of the DFG dynamical transition from an "out" to an "in" position.

To assess experimentally this hypothesis and whether the DFG-flip takes place within the catalytic cycle of c-Src tyrosine kinase in order to release ADP, we have adapted a kinase radiometric inhibition assay in which ADP was used as inhibitor against c-Src WT and c-Src L317I kinase domains. The apparent ADP dissociation constant for c-Src L317I (K_i =1.0µM) was found to be 1 log higher than for c-Src WT (K_i =0.1µM), indicating that ADP binds less tightly to c-Src L317I than to c-Src WT. This implies that the formed product ADP was released faster by the mutated kinase domain and could suggest that the faster release of ADP by the mutated kinase was due to the higher rate of the DFG-flip in c-Src L317I. K_i values were also in agreement with kinetic data which showed that the mutant had higher K_{cat} than WT c-Src. Thus, the reduced sensitivity to ADP inhibition in c-Src L317I supported experimentally the assumption that the flip of the DFG motif is the most probable molecular mechanism for the release of ADP at the end of the kinase catalytic cycle.

In conclusion, we could identify key residues in c-Src which dictate the conformational plasticity of the kinase domain mainly by influencing the rate of the DFG-flip. Furthermore, we could demonstrate that the flip of the DFG-motif is the most probable molecular mechanism for the release of ADP at the end of the kinase catalytic cycle and that both DFG-in and DFG-out conformations are present within the catalytic cycle of c-Src.

Résumé de la thèse

La publication des premières structures cristallographiques de protéines à résolution atomique il y a 50 ans fut un progrès qui a contribué considérablement à nos actuelles connaissances sur la structure et la fonction des protéines. Des études subséquentes ont démontré que les protéines sont en perpétuelle fluctuation entre plusieurs conformations différentes et que les effets dynamiques que subit la structure protéinique (*i.e* sa plasticité), jouent un rôle déterminant pour son activité. D'ailleurs, les propriétés dynamiques des protéines ont été démontrées être essentielles pour la transmission de signaux au niveau de la communication intra- et extracellulaire.

En sachant que plus que 518 protéines kinases sont codées par le génome humain, on pourrait prétendre que presque chaque signal cellulaire est transmis via la cascade de phosphorylation opérée par cette famille de protéines. La sous-famille de protéine tyrosine kinases est en effet impliquée dans le contrôle du métabolisme, de la croissance cellulaire et du processus d'apoptose au travers son action catalytique qui consiste à transférer le γ-phosphate de l'adénosine triphosphate (ATP) sur le groupe hydroxyle de la chaine latérale d'une tyrosine, contenue dans le substrat de l'enzyme. Toute activité kinasique anormale peut donc déréguler la transmission et l'homeostase cellulaire et constituer l'origine de processus cancéreux et inflammatoires.

En chimie pharmaceutique, l'étude de la plasticité conformationnelle des protéines présente un défi, mais également une opportunité pour la découverte et la sélection des effecteurs potentiels de protéines cibles.

Nos actuelles connaissances sur l'éventail de conformations que les tyrosine kinases peuvent occuper reposent sur un large nombre de structures cristallines démontrant les kinases dans leur forme ouverte, fermée ou intermédiaire en fonction de la position de plusieurs déterminants structurels, décrits en détail dans le premier chapitre de ce travail.

Afin de mieux comprendre le mécanisme qui contrôle la plasticité kinasique au niveau moléculaire, le but de cette thèse consistait à identifier les acides aminés qui gouvernent la transition du site catalytique d'une tyrosine kinase de sa conformation active à sa conformation inactive et *vice-versa*.

Nous avons utilisé le domaine catalytique recombinant de la tyrosine kinase c-Src comme étude de cas, car de nombreuses informations structurelles étaient déjà disponibles sur cette tyrosine kinase.

Notre approche pour définir les résidus impliqués dans la régulation de la plasticité de c-Src a été établie sur la base d'une récente étude structurelle qui a comparé *in silico* les structures connues de différents domaines kinasiques. Cette étude a montré la présence d'un groupe de 14 résidus dans la structure du récepteur de l'insuline (InsR), essentiel pour la plasticité des kinases. Ce groupe d'acides aminés est majoritairement constitué de résidus hydrophobiques formant par conséquent une interface hydrophobique entre le N-lobe et le C-lobe des domaines catalytiques des tyrosine kinases.

Ainsi, avons-nous conduit un alignement structurel contre la structure tertiaire du récepteur de l'insuline pour définir les résidus correspondants dans c-Src.

Afin de valider expérimentalement que les 14 résidus identifiés dans la structure de c-Src contrôlent effectivement la plasticité du domaine kinasique, nous les avons mutés pour transformer c-Src en un des domaines kinasiques de c-Abl, c-Kit, Syk ou PDGFR. Ces derniers sont inhibées par des concentrations nanomolaires d'un inhibiteur specifique pour la forme DFG-Asp-out, *i.e* imatinib. Ceci, en sachant que le domaine kinasique de c-Src n'est par inhibé par imatinib avec une affinité d'intérêt clinique (CI_{50}=220μM). La raison structurelle pour l'inhibition difficile de c-Src par imatinib est due à la conformation du motif DFG dans c-Src. Cette triade de résidus, qui est un des déterminants conformationnels des tyrosine kinases, est en position thermodynamiquement défavorable pour la pénétration de l'inhibiteur au site de liaison d'ATP dans c-Src.

C'est pourquoi, en mutant un ou plusieurs résidus de l'interface hydrophobique de c-Src en correspondants en c-Src, c-Kit, Syk ou PDGFR, on a produit huit mutants de c-Src dans le but de répondre aux questions suivantes : Est-ce que les résidus qui ont été mutés dans c-Src influencent la conformation thermodynamique du motif DFG dans c-Src et si c'est le cas, de quelle manière? Est-ce que c'est en stabilisant la position du DFG dans la conformation favorable à la liaison d'imatinib ou bien, en facilitant la vitesse de transition de la conformation défavorable à la conformation favorable?

On a commencé par exprimer et par purifier le domaine kinasique de c-Src non muté (WT) ainsi que celui de tous les mutants dans leur forme non-phosphorylée selon des protocoles (cf. Chapitre 2) en fonction de deux types d'expériences biophysiques et biochimiques qui étaient nécéssaires pour répondre aux questions adressées plus haut.

La première catégorie d'expériences a été conçue pour vérifier si les résidus qui ont été mutés dans c-Src influencent la conformation thermodynamique du motif DFG en facilitant sa transition conformationnelle. Pour cela cette catégorie d'expériences a été réalisée en la présence de facteurs essentiels pour l'activité catalytique de la protéine, notamment Mg^{2+}, substrat peptidique et ATP. La deuxième classe d'expériences visait à vérifier si les résidus qui ont été mutés dans c-Src stabilisant la position du DFG dans la conformation favorable à la liaison d'imatinib. Ce type d'expériences a été effectué sans Mg^{2+} et ATP. Les résultats ont été détaillés dans Chapitre 4.

L'analyse cinétique et par dichroïsme circulaire a montré tous les domaines kinasiques exprimés et purifiés pour cette étude étaient actifs et correctement repliés en leur structure tertiaire.

La stabilité thermodynamique des domaines kinasiques de c-Src qui contenaient de mutations au niveau du N-terminal lobe était réduite par rapport au *wild type* et les autres mutants.

Les résultats du test d'inhibition ont montré que tous les mutants de c-Src générés dans cette étude étaient plus sensibles à l'inhibition par imatinib que le domaine kinasique de c-Src WT quand leur forme nonphosphorylée a été pré-incubée avec l'inhibiteur avant l'addition de Mg^{2+} et ATP. D'ailleurs, les domaines kinasiques de c-Src qui contenaient des mutations au niveau du N-lobe étaient inhibés par imatinib plus facilement que celles qui contenaient des mutations au niveau du C-lobe. Parmi eux, c-Src L317I a produit l'effet majeur avec une inhibition au niveau du nanomolaire (CI_{50}=4nM), comparable à celle de c-Abl (CI_{50}=25-200nM). L'inhibition de c-Src L317I dans la basse zone du nanomolaire a été également confirmée par l'essai orthogonal où l'inhibition d'autophosphorylation de la kinase par imatinib a été suivie par Western Blot.

Grace aux tests d'inhibition on a pu confirmer que les résidus qui ont été mutés dans le domaine kinasique de c-Src influencent la thermodynamique de la conformation du motif DFG dans c-Src.

c-Src L317I a été également plus fortement inhibé par le composé pyrazolopyrimidine 5 que c-Src WT. Ce dernier inhibiteur lie c-Src WT dans la basse zone du nanomolaire et sans la barrière thermodynamique que constitue la conformation du motif DFG. C'est pourquoi on a pu présumer que la mutation L317I influence la conformation thermodynamique de c-Src pas uniquement au niveau de la triade DFG, mais également, dans une moindre mesure, au niveau de la loop d'activation tout en influant sur la plasticité du domaine kinasique entier.

La structure crystalline du complexe formé par c-Src L317I et imatinib a démontré que la mutation n'influençait ni la disposition de l'inhibiteur ni l'adoption de la conformation DFG-out de la part de la protéine.

C'est la structure apo- de c-Src L317I qui a révélé une nouvelle conformation de la triade DFG, tout en affichant le motif dans sa position « in ».

Conduites en parallèle, les expériences par ITC ont été en désaccord avec les résulats de tests d'inhibition on c-Src L317I mais en accord avec la structure c-Src L317I-apo. En effet, les valeurs des constantes de dissociation (K_D) qui traduisent l'affinité du ligand pour la protéine étaient comparables pour c-Src WT et c-Src L317I et dans la zone du micromolaire (7.4µM et 7.2µM, respectivement).

Or, la structure crystalline de c-Src L317I-apo et la caractérisation thermodynamique de l'affinité de c-Src L317I pour imatinib par ITC, nous ont conduit vers l'hypothèse que la mutation L317I dans Src ne stabilise

pas la position du DFG dans la conformation favorable à la liaison d'imatinib mais facilite la dynamique de sa transition conformationnelle.

Afin de vérifier cette dernière hypothèse expérimentalement, on s'est basée sur des études suggérant que la rotation du motif DFG est importante pour libérer un des produits de la réaction du phosphotransfer, à savoir l'adénosine diphosphate (ADP).

Pour cela, on a établi et conduit un essai radiométrique d'inhibition où ADP a été utilisé en tant qu'inhibiteur de c-Src L317I et de c-Src WT, respectivement. Les résultats de cette expérience ont montré que la constante de dissociation apparente pour c-Src L317I était significativement plus élevée (K_i =1.0μM) que celle pour la protéine non mutée (K_i =0.1μM) indiquant que ADP se lie moins fort à c-Src L317 qu'au c-Src WT. Ces données étaient en accord avec les résultats de l'étude cinétique où le mutant a montré une K_{cat} plus élévée que c-Src WT et impliquent qu'ADP est relâché plus rapidement par le mutant dû à l'augmentation de vitesse de rotation du motif DFG. Ainsi, la sensibilité réduite à l'inhibition par ADP chez c-Src L317I représente-elle un soutien expérimental à l'hypothèse que la rotation du motif DFG est le mécanisme moléculaire qui expulse la molécule d'ADP à la fin du cycle catalytique de la kinase.

En conclusion, on a pu identifier des résidus importants pour la régulation de la plasticité au sein du domaine kinasique de c-Src. On a également démontré expérimentalement que cette régulation est effectuée principalement au niveau de la rotation du motif DFG. Sur cette base, on suggère que ce mécanisme est fort probablement la façon de libération de la molécule d'ADP à la fin du phosphotransfer et que les conformations « in » et « out» du motif DFG sont présentes lors du cycle catalytique de c-Src.

CHAPTER 1

Introduction

1. From structure to function: A historical view

> *Le nom protéine que je vous propose pour l'oxyde organique de la fibrine et de l'albumine, je voulais le dériver de πρωτειος, parce qu'il paraît être la substance primitive ou principale de la nutrition animale.*
>
> Letter from J. Berzelius to G. Mulder, 10 July, 1838

That is how the "protein" history officially started even though substances we now call proteins grabbed the interest of early-day chemists years ago because of their close association with life processes. The French chemist Antoine Fourcroy recognized the three distinct varieties of protein from animal sources in 1789, albumin, fibrin and gelatine. They were often collectively called "albumins" in recognition of the prototype derived from egg white ("Eiweisskörper", german). Later on, when the distinction between elements and compounds was sorted out, Jacob Berzelius and Gerrit Mulder described the common elemental composition of proteins based on the presence of C, H, O, N, and S.

By 1900, the notion that proteins are build up from amino acids was accepted as the discovery in protein progressed; Leucine was described first in 1819 and Threonine was the last one found in 1936. Important findings which contributed to this theory were the announcement of the nature of the peptide bond at the same meeting on the same day in 1902 by Franz Hofmeister (in the morning) and by Emil Fischer (in the afternoon) and leading to the announcement of the first protein amino acid sequence (i.e. bovine insulin) in 1949 by Fred Sanger.

The contribution of Emil Fischer to protein science is all the more significant as he was the first to propose a model for enzyme activity [1]. This model, resulting from the work of Fisher on the enzymatic degradation of glycosides, is mostly known as "lock-and-key" principle (Figure 1.1). As figuratively suggested, it implies the structural selectivity of a protein for its substrate. Remarkably, the "lock-and-key" theory was published decades before any protein three-dimensional structural data was available and before accepting the idea that enzymes were proteins.

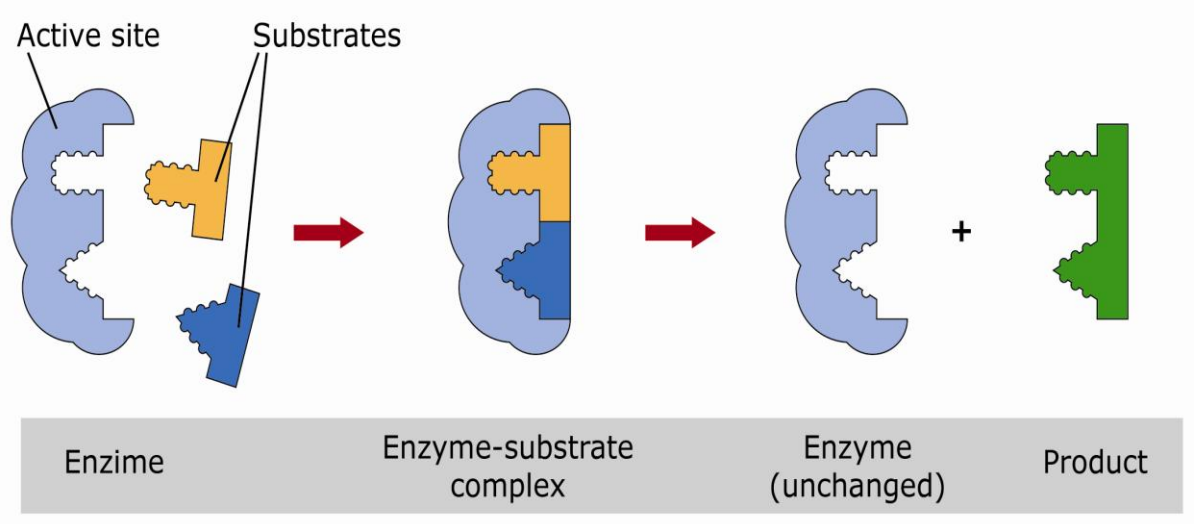

Figure 1.1: The "lock and key" model for enzyme activity. In the lock and key mechanism the substrates (in yellow and in dark blue) have a complementary fit to the enzyme's active site. Modified from [2].

For almost five decades, the three-dimensional (3D) structures of proteins were studied indirectly. Details of a mechanism and its relationship to structure could only be inferred from the properties of the protein [3]. The crystallization of jack bean urease [4] and bovine pepsin [5] clearly classified enzymes as proteins. Later on, Max Perutz and John Kendrew reported the first structures of human enzymes, haemoglobin [6] and myoglobin [7]. The latter findings provided a structural explanation of the "lock-and-key" model of enzyme catalysis and fixed the representation of enzymes as rigid 3D entities for the next decades.

2. Protein dynamics: from hypothesis to structural evidences.

Interest in enzyme structure and function continued their expansion and several mathematical models were established to describe enzyme activity and inhibition.

In the early 1960s, it was one of these models, namely the non competitive enzyme inhibition, which set Daniel Koshland thinking that Fischer's "lock-and-key" principle needed modification.

Non-competitive inhibition was explained as the inhibitor blocking the enzyme action without affecting the binding of the substrate. No lock and key concept was available to explain such a result, bringing Koshland to suggest a new theory for enzyme action.

The "induced fit" theory was proposed in the following terms "a) the precise orientation of catalytic groups is required for enzyme action, b) the substrate causes an appreciable change in the three dimensional relationship of the amino acids at the active site, and c) the changes in the protein structure caused by the substrate will bring the catalytic groups into the proper alignment, whereas a nonsubstrate will not"[8]. In other words, the "induced fit" theory of Daniel Koshland pointed for the first time the flexibility of enzymes as an essential point of enzyme activity and established a link between protein three-dimensional structure and function (Figure 1.2).

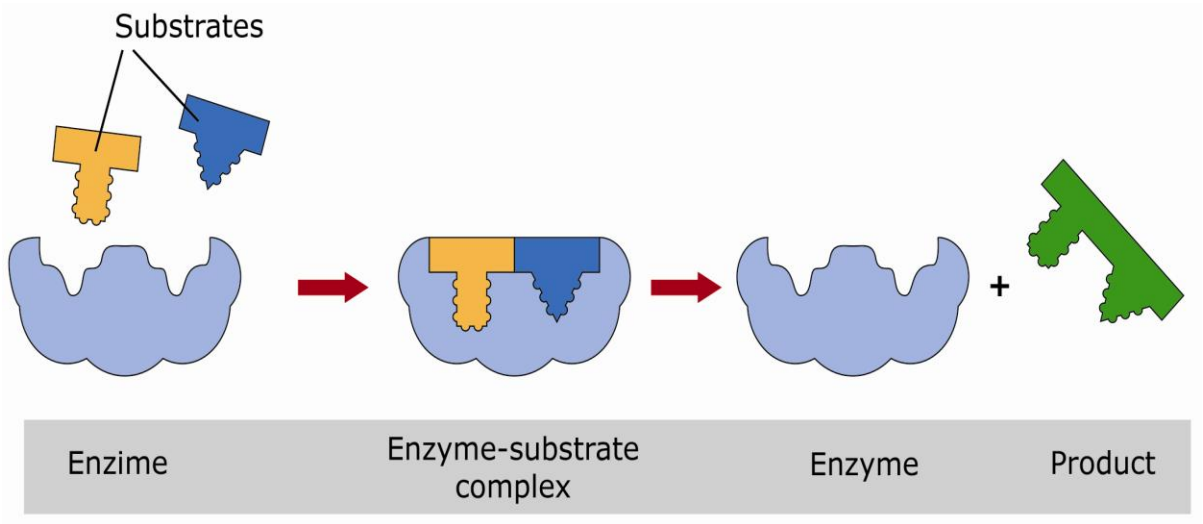

Figure 1.2: The "induced fit" mode for enzyme activity. Binding of the first substrate (yellow) induces a physical conformational change in the protein that facilitates binding of the second substrate (dark blue), with a far lower energy than otherwise required. When catalysis is complete, the product is released, and the enzyme returns to its uninduced state. The induced fit model has been compared to a hand-in-glove model, wherein it may be difficult to insert the first finger into the proper place, but once done, the other fingers go in easily because the glove is yet properly aligned. Modified from [2].

The experimental evidence for enzyme dynamics was provided by Steitz et al. a decade later with the crystal structures of carboxypeptidase [9] and hexokinase [10]. Steitz showed that the engulfing of the substrate glucose by hexokinase occurred precisely as the induced fit predicted, thus giving visual proof that ligand-induced conformational changes were real and significant. The vision on proteins as flexible macromolecules was founded. Further crystallographic studies confirmed the existence of different protein conformations in the presence but also in the absence of substrate [11]. Based on the observed ligand-induced conformational changes, Gerstein et al. [11] divided protein motions in "hinge domain" and "shear" motions.

Additional studies demonstrated that proteins assume a constant fluctuation of a large number of different conformations [12-16] and that protein motions are intimately linked to the nature of the environment (protein slaving) [17]. Hence, in a modern vision proteins are seen as soft materials that sample a large number of conformations around the average structure as a result of thermal energy. The organisation of their conformational space can be described by a multidimensional energy landscape that defines the relative probabilities of the conformational states (thermodynamics) and the energy barriers between them (kinetics) [12, 18-22].

All these findings brought to the idea that dynamical effects play a major role in enzyme catalysis [23-27]. Although this idea has been challenged several times [28-30], it continues to attract considerable attention since it relates the catalytic power of enzymes to their flexibility [18, 31-37].

A substantial amount of research has been performed to describe the forms and timescales of the internal motions in enzymes related to their catalytic function [37]. It has become clear that the motions required vary according to the step of the functional process. External, whole molecule diffusive Brownian dynamics determines the initial enzyme-substrate encounter [38]. In some cases conformational flexibility is required for substrate access [39, 40] and/or product release [41]. For the steps in between, a distinction should be drawn between reaction dynamics along the reaction coordinate and other fluctuations required for progress along the reaction coordinate to be made. Dissociating the functionally important motions from the thermal noise is still an important challenge in enzymology since the amplitude of the conformational changes that accompanies enzyme activity is variable among different proteins (hydrolases vs. GTPases and kinases). To avoid semantic confusion about the term protein dynamics, we adopt here the definition of Henzler-Wildman & Kern [18] who describe it as "any time-dependant change in atomic coordinates".

Recently, the role of protein dynamics has been also recognised in even larger scale processes. Intrinsic dynamic properties of proteins have been shown to act as switches and transducers in response to incoming signals and thereby as essential elements for signal transmission in cellular signalling networks [42] (Figure 1.3).

Protein dynamism could be also viewed as a foundation stone of protein evolvability [43]. In this "avant-garde view" protein dynamics can be considered as facilitating the divergence of new functions within existing folds and as a source of entirely new folds. Thus, giving future research directions in the area of understanding protein dynamism.

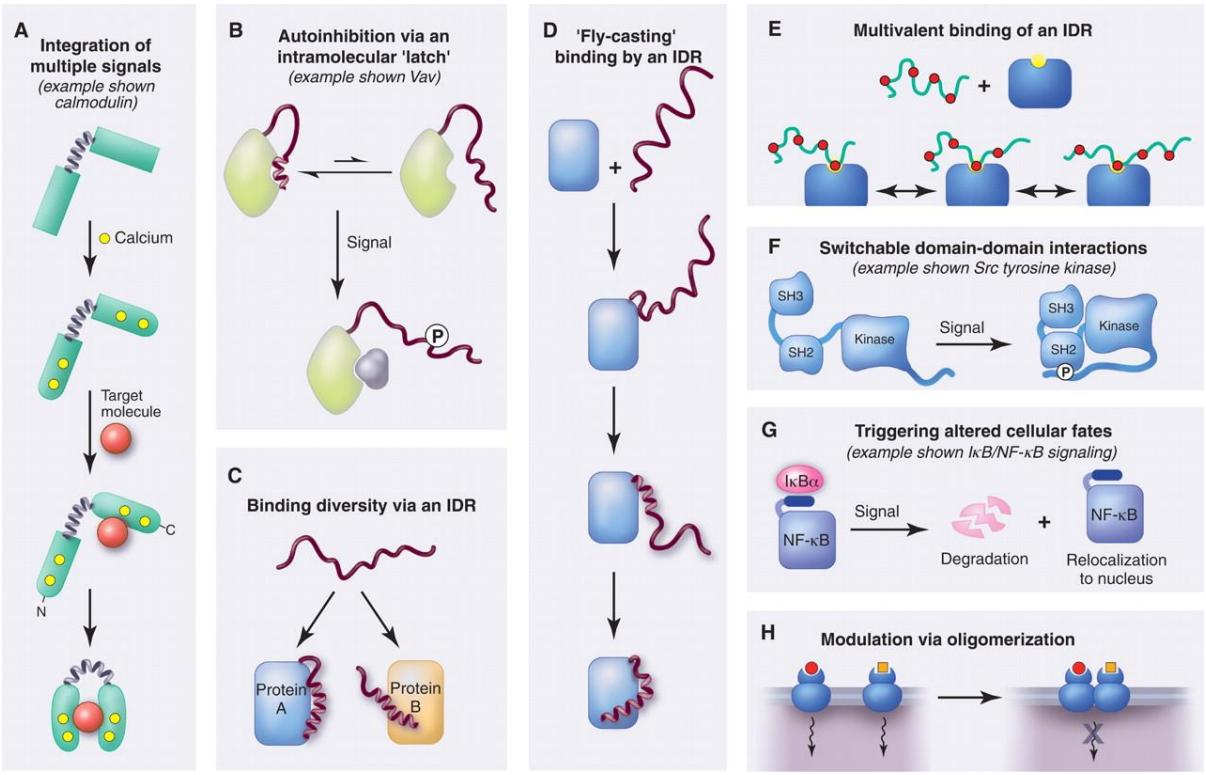

Figure 1.3: Dynamic properties in signaling. A: Multiple signals can create a response. In the case of calmodulin, first calcium (yellow circles) is sensed, which favours binding to myosin light chain kinase (red circle), leading to enhanced likehood of binding to a second binding site [44]. **B:** Intramolecular autoinhibition can occlude a downstream target interaction site. Opening of the autoinhibitory domain (in Vav) can be favoured by an upstream signal such as phosphorylation [45]. **C:** An intrinsically disordered region (IDR) can confer binding diversity on a signalling protein, enabling two targets to be recognized [46]. **D:** IDRs also enable a stepwise association with a target [47]. **E:** Multivalent binding can be mediated by an IDR that harbours several potential binding sites (small red circles) that each transiently occupy a single site on the target [48]. **F:** Dynamic domain-domain rearrangements can be triggered by signals such as phosphorylation [49]. **G:** Disruption of complexes can reveal signals for relocalization in the cell and degradation [50]. **H:** Receptor complexes enable higher-order modulation of responses to two different signalling ligands (red circle and yellow square) [51]. Modified from [42].

3. Protein dynamics: the time-scale issue

As previously described, the three dimensional crystal structures evidence the dynamical nature of proteins as well as the amplitude of their motions. Nevertheless, to fully describe a protein in action, two additional components are still needed: the directionality of the motion, and the timescale of the dynamic process.

A major obstacle is that it is not possible to watch experimentally individual atoms moving within a protein. Instead, multiple biophysical and biochemical methods are needed to quantify the properties from which the dynamics can be inferred.

Protein motions can be divided into "slow" and "fast" timescale fluctuations (Figure 1.4) that need a different combination of experimental and *in silico* techniques for their characterization. We present here the major experimental and computational methods according to the timescale of the dynamical process.

Dynamics on a "slow" scale define fluctuations between kinetically distinct states (tier-0) that are separated by energy barriers of several kT (the product of the Bolzmann constant and the absolute temperature), corresponding to timescales of microseconds to milliseconds [52]. These fluctuations consist of large-amplitude domain motions. Proteins are not static between tier-0 states, but fluctuate among closely related structures on longer timescales. Dynamics involving transitions between tier-0 states include enzyme catalysis [53], signal transduction [54] and protein-protein interactions [55]. Fast timescale dynamics (tier-1 and tier-2) define fluctuations within the frame of a given tier-0 conformation. These are local, picosecond (side-chain rotations) to nanosecond fluctuations (loop motions) implicated in the entropy of the system [18].

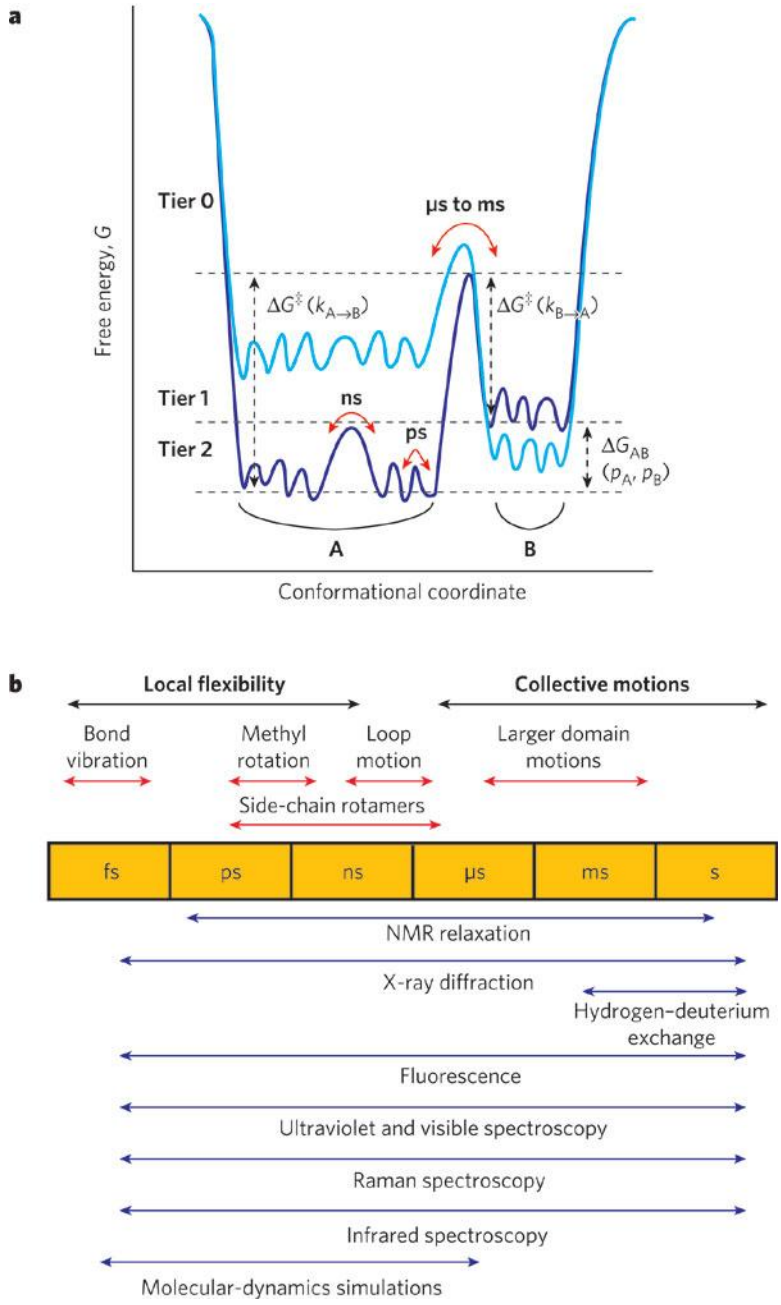

Figure 1.4: Amplitude and timescale of protein motions. A. Hierarchy of protein dynamics and the energy barriers. Each tier is classified following Frauenfelder et al. [12]. A state is defined as the minimum in the energy surface, whereas a transition state is the maximum between the wells. The population of the tier-0 states A and B ($p_{A,}$ p_B) are defined as Boltzmann distributions based on their difference in free energy (ΔG_{AB}). Lower tiers describe faster fluctuations between closely related states within each tier-0 state. Ligand binding, protein mutation and changes in external conditions shift the equilibrium among the states. **B.** Timescale of dynamic processes in proteins and the experimental methods that can detect fluctuations on each timescale. Modified from [55, 56].

3.1. Experimental methods for studying "slow" protein dynamics

Nuclear magnetic resonance (NMR) spectroscopy, cryo-electron microscopy and small angle X-ray scattering provide near-atomic to atomic resolution snapshots of tier-0 conformations [55]. However, these methods cannot measure the timescales between different tier-0 states. Actually both structures and kinetics can be determined simultaneously by using Laue X-ray diffraction [57]. Alternatively, hydrogen-deuterium exchange coupled to either mass spectrometry or NMR spectroscopy provides means to detect global or local motions on a millisecond timescale [58, 59].

NMR methods present several advantages. They provide atomic resolution and timescales of conformational transitions for high molecular weight systems [60, 61]. Dynamic information is extracted from relaxation of nuclei following an excitation, using a variety of experiments to span dynamics on timescales from picoseconds to seconds and to assess several types of nuclei (^{1}H, ^{2}H, ^{13}C and ^{15}N) [62-64]. In contrast to most other spectroscopic techniques, enzyme dynamics during catalysis can be followed in solution[56].

Classical biophysical methods such as fluorescence [65], circular dichroism [66], UV/visible absorbance, infrared spectroscopy [67], Raman spectroscopy [68] and electron paramagnetic resonance [69] represent a source of complementary kinetic information to the above stated higher-resolution techniques. These lower-resolution methods access a large range of timescales (Figure 1.4) with high precision, while providing information for one or a few sites or an average over the entire system [18].

3.2. Computational methods for studying protein dynamics

Computation can complement the experimental methods to fully describe protein dynamics: the precise position of each atom at any instant in time for a protein molecule can be followed. At least one known high-resolution structure is the ideal starting point. Moreover, molecular dynamics simulations can answer why things move, as the underlying forces and corresponding energies are included in the simulation [18]. Nevertheless, a critical look at the energies is needed because the description of the protein-solvent system during simulations is still not optimal [70].

There are stochastic approaches, like Montecarlo, and deterministic ones, such as molecular dynamics (MD) simulation. In general, the protein is described by atomic coordinates and charges, then several cycles of computation are run and the obtained trajectory represents possible states of the evolution of the system [71].

In opposition to fast protein motions in the picosecond-to-nanosecond timescale that can be routinely studied by MD simulations, the microsecond-to-millisecond timescales are currently out of reach for conventional molecular dynamics simulations eventhough some recent publications describe microsecond simulations on small proteins [72, 73].

To overcome this restriction a large variety of approaches have been developed, including normal mode analysis [74], Gaussian network models, floppy inclusion and rigid structure topography (FIRST) [75], framework rigidity optimized dynamic algorithm (FRODA) [76] and Gō models [77]. Alternatively, dynamics simulations are accelerated by external force to access this timescale (targeted, steered and accelerated MD simulations [70, 78]), or prior knowledge about features of the reaction coordinate (umbrella sampling [79]) or the transition end points (transition path sampling [80]) is necessary[18].

3.3. Experimental methods for studying "fast" protein dynamics

The polypeptide backbones and side chains of proteins are constantly moving due to thermal motions and kinetic energy of the atoms. Classical X-ray protein crystal structures can provide information about the fluctuations of atoms (tier-1 and tier-2) around their average positions (tier-0) via the mean square atomic displacement, better known as the atomic temperature factor or the B-factor [15, 81]. It should be noted that B-factors cannot be interpreted as reflecting exclusively the dynamic disorder of atomic fluctuations. They measure the static disorder resulting form structural disparities in different unit cells as well.

Recent advances in Laue X-ray technology have allowed measuring of the purely dynamic component within the limit that structural changes are small enough to be tolerated within the crystal lattice [82]. This was shown to be the case in myoglobin where pico-to-nanosecond side-chain motions in the active site are synchronized with the carbon monoxide migration within the protein [83].

Fast protein dynamics can be characterized in terms of amplitude and timescale of bond fluctuations when using NMR relaxation methods [18, 62]. Picosecond-to-nanosecond NMR spectroscopy has been used widely for quantifying the entropic contribution of proteins to macromolecular binding [84, 85].

Relaxation methods are typically conducted with NMR active bond such as the ^{1}H-^{15}N pair [63, 86]. In addition, many experiments that provide complementary information to the ^{15}N studies have been developed, such as methods that measure the correlated motions of successive residues in proteins [87, 88] or the dynamics of the backbone carbonyl Cα bonds [89].

Side chain motions in proteins are also amenable to study with the use of spin relaxation techniques [90]. In particular the use of deuterium nucleus as a probe of side chain methyl group dynamics has seen substantial advances in recent years [62].

In addition to the atomic-resolution methods, most of the low-resolution methods such as fluorescence, ultraviolet, visible, infrared and Raman spectroscopy can also be used for defining dynamics down to the picosecond timescale (Figure 1.4). Another three low-resolution techniques find an application in this field, namely neutron scattering [91], femptosecond spectroscopy [92] and four dimensional ultrafast electron diffraction, crystallography and microscopy [93].

In presence of such a vast toolset for exploring protein dynamics, an optimal description of the process requires connection between different timescales and amplitudes of motions. Since the ultimate goal is to understand how proteins function in real time, several of the above mentioned methods should be combined [18]. In our work we will also present the importance of choosing the right combination of experimental techniques for exploring different protein motions as well as the importance of providing the appropriate protein preparation for each of the chosen methods (cf. Chapters 2 & 3).

4. Protein tyrosine kinases

Protein tyrosine kinases (PTKs) are critical components of the cellular signalling pathways [94]. They are involved in diverse biological processes, such as control of cell growth, metabolism and apoptosis [95, 96].

PTKs catalyze protein or peptide phosphorylation by using a highly conserved catalytic domain to transfer the γ-phosphate of adenosine triphosphate (ATP) onto the hydroxyl group of a substrate tyrosine residue (Figure 1.5) [97].

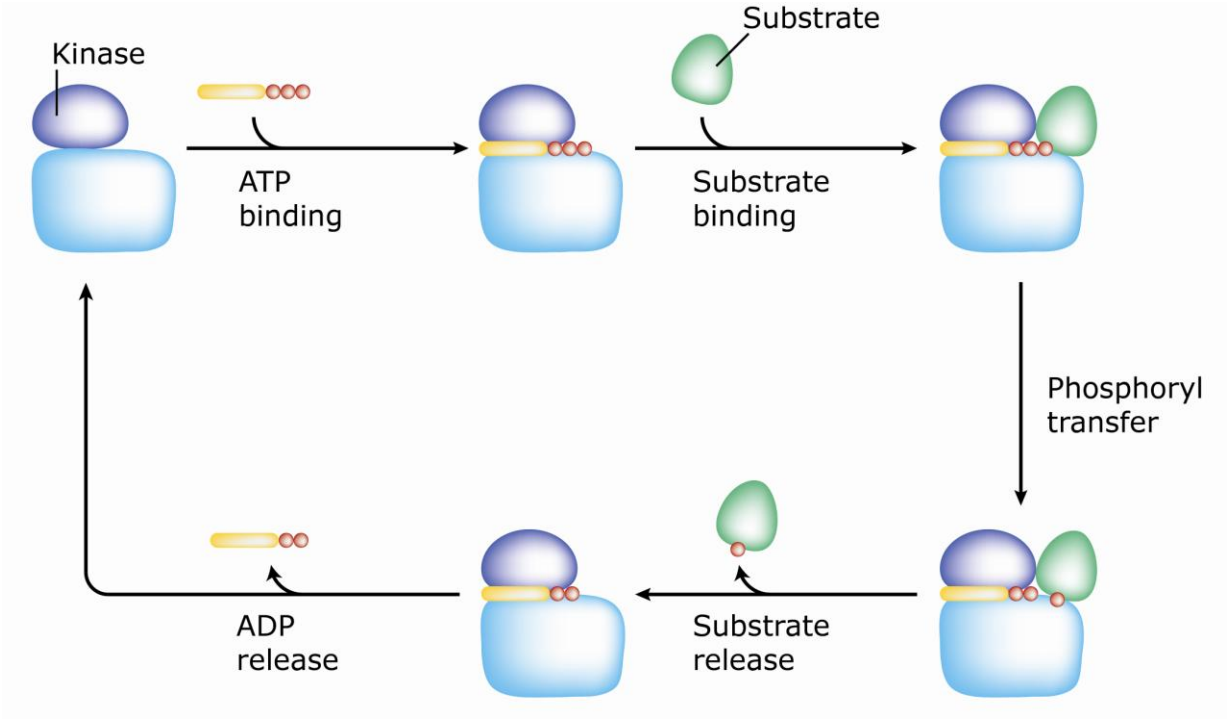

Figure 1.5: The basic cycle for substrate phosphorylation by a kinase. Starting top left, ATP binds to the active site of the kinase. This is followed by binding of the substrate to the active site. Once bound, the γ-phosphate of ATP (red) is transferred to a Tyrosine residue of the substrate. After phosphorylation, the substrate is released from the kinase. The last step shown is the release of ADP from the active site. The order of the steps differs for different kinases. Taken from [98].

Kinase activity may be modulated by phosphatases, upstream kinases, cofactors and ligands and by interactions with other activating or regulatory proteins [99, 100]. Perturbation of PTK signaling by mutations and other genetic alterations may result in deregulated kinase activity and lead most prominently to malignant transformation or diabetes and inflammatory diseases [101]. Therefore, their activity is strictly regulated.

There are 518 kinase sequences encoded in the human genome (1.7%), of which 430 are considered catalytically active [95, 102]. According to the sequence similarity, the largest subgroup of the human protein kinases, among the eight PK groups, is the tyrosine kinase family with 93 members [103]. This family can be divided into receptor tyrosine kinases (RTKs) and non-receptor tyrosine kinases (nRTKs). The receptor and non-receptor tyrosine kinases are further classified into 20 and 10 families, respectively (Table 1.1).

RTKs are transmembrane proteins which are structurally divided in three domains: a ligand-binding extracellular domain, a transmembrane helix domain and a cytoplasmic domain that possess the tyrosine kinase catalytic activity [94].

nRTKs are cytoplasmic or nucleic proteins that respond to extracellular stimuli via regulatory domains. Some of them can bind to cell membranes via an N-terminal lipid. In general they contain a tyrosine kinase catalytic domain (SH1) and different domain modules also known as regulatory domains. The regulatory domains in nRTKs are: the Src homology 2 (SH2), Src homology 3 (SH3), the Actin-binding, the DNA-binding, the Focal adhesion-binding, the Integrin-binding, the Pleckstrin homology (PH) and the Btk domains. Different combination and distribution of such protein portions diversify the topology of the elements of the enzyme family and contribute to specific protein regulation, localization and substrate specificity [94, 104].

Table 1.1: Publically available data for PTKs

Family	Subfamily	Protein	Entry code
RTK	**PDGFR**	PDGFRα: Platelet derived growth factor receptor α	P16234
		PDGFRβ: Platelet derived growth factor receptor β	P09619
		Cdf1r: Colony-stimulation factor-1 receptor	P07333
		Kit: Stem-cell factor receptor	P10721
		Flt3: Fms-like kinase receptor	P36888
	EGFR	EGFR1: Epidermal growth factor receptor 1	P00533
		ERBB2: Epidermal growth factor receptor 2	P04626
		ERBB3: Epidermal growth factor receptor 3	P21860
		ERBB4: Epidermal growth factor receptor 4	Q15303
	IR	INSR: Insulin receptor	P06213
		IGF1R: Insulin-like growth factor receptor	P08069
		INSRR: Insulin receptor-related protein	P14616
	VEGFR	Vegfr1: Vascular endothelial growth factor receptor 1	P17948
		Vegfr2: Vascular endothelial growth factor receptor 2	P35968
		Vegfr3: Vascular endothelial growth factor receptor 3	P35916
	FGFR	Fgfr1: Fibroblast growth factor receptor 1	P11362
		Fgfr2: Fibroblast growth factor receptor 2	P21802
		Fgfr3: Fibroblast growth factor receptor 3	P22607
	EPHR	EphrA1: Ephrin receptors A1	P21709
		EphrA2: Ephrin receptors A2	P29317
		EphrA3: Ephrin receptors A3	P29320
		EphrA4: Ephrin receptors A4	P54764
		EphrA5: Ephrin receptors A5	P54756
		EphrA6: Ephrin receptors A6	Q15375
		EphrA7: Ephrin receptors A7	P29322
		EphrA8: Ephrin receptors A8	Q5JZY3
		EphrB1: Ephrin receptors B1	P54762
		EphrB2: Ephrin receptors B2	P29323
		EphrB3: Ephrin receptors B3	P54753
		EphrB4: Ephrin receptors B4	P54760
		EphrB5: Ephrin receptors B5	O15197
	CCK	Ptk7: Tyrosine protein kinase-like 7 Cck4	Q13308
	NGFR	Nrtk1: Neutrophic tyrosine kinase receptor type 1	P04629
		Nrtk2: Neutrophic tyrosine kinase receptor type 2	Q16620
		Nrtk3: Neutrophic tyrosine kinase receptor type 3	Q16288
	HGFR	Met: Hepatocyte growth factor receptor	P08581
		Ron: Macrophage-stimulating protein receptor	Q04912
	AXL	Ufo: Tyrosine protein kinase receptor UFO	P30530
		Merk: Proto-oncogene tyrosine protein-kinase MER	Q12866
		Tyro3: Tyrosine protein kinase receptor Tyro3	Q06418
	TIE	Tie: Tyrosine protein kinase receptor Tie-1	P35590
		Tie2: Tunica interna endothelial cell kinase Tek	Q02763
	RYK	Ryk: Tyrosine protein kinase Ryk	P34925
	DDR	Ddr1: Epithelial discoidin domain-containing receptor 1	Q08345
		Ddr2: Epithelial discoidin domain-containing receptor 2	Q16832
	RET	Proto oncogene tyrosine protein kinase receptor RET	P07949

	ROS	Ros: Proto oncogene tyrosine protein kinase ROS	P08922
	LTK	Ltk: Leukocyte tyrosine kinase receptor	P29376
		Alk: Anaplastic lymphoma kinase	Q9UM73
	ROR	Ror1: Tyrosine protein kinase transmembrane receptor ROR1	Q01973
		Ror2: Tyrosine protein kinase transmembrane receptor ROR2	Q01974
	MUSK	Musk: Muscle, skeletal receptor tyrosine protein kinase	O15146
	LMR	LMTK1: Lemur tyrosine kinase 1	Q6ZMQ8
		LMTK2: Lemur tyrosine kinase 2	Q81WU2
		LMTK3: Lemur tyrosine kinase 3	Q96Q04
	SuRTK106	STYK1: Tyrosine protein kinase STYK1	Q6J9G0
nRTK	**SYK**	Ksyk: tyrosine protein kinase Syk	P43405
		Zap70: zeta-associated protein kinase	P43403
	FRK	Frk: FYN-related kinase	P42685
		Ptk6: Breast tumor kinase	Q13882
		Srms: Tyrosine protein kinase Srms	Q9H3Y6
	FES	Fes: Proto oncogene tyrosine protein kinase Fes/Fps	P07332
		Fer; Proto oncogene tyrosine protein kinase FER	P16591
	FAK	Fak1: Focal adhesion kinase 1	Q05397
		Fak2: Focal adhesion kinase 2	Q14289
	CSK	Csk: C-terminal Src kinase	P41240
		Matk: Megacaryocyte-associate tyrosine protein kinase	P42679
	ACK	Ack: Activated CDC42 kinase 1	Q07912
		Tnk1: Non-receptor tyrosine protein kinase TNK1	Q13470
	JAK	Jak1: Janus kinase 1	P23458
		Jak2: Janus kinase 2	O60674
		Jak3: Janus kinase 3	P52333
		Tyk2: Non-receptor tyrosine protein kinase TYK2	P29597
	TEC	Tec: Tyrosine protein kinase Tec	P42680
		Bmx: Bone marrow tyrosine kinase gene in chromosome X protein	P51813
		Btk: Briton tyrosine kinase	Q06187
		Itk: Tyrosine protein kinase ITK/TSK	Q08881
		Txk: Tyrosine protein kinase TXK	P42681
	ABL	Abl1: Abelson murine leukemia viral oncogene homolog 1	P00519
		Abl2: Abelson murine leukemia viral oncogene homolog 2	P42684
	SRC	Src: Proto oncogene tyrosine protein kinase Src	P00523
		Lck: Lymphocyte cell specific protein tyrosine kinase	P06239
		Fgr: Proto oncogene tyrosine protein kinase FGR	P09769
		Fyn: Proto oncogene tyrosine protein kinase Fyn	P06241
		Yes1: Proto oncogene tyrosine protein kinase Yes	P07947
		Blk: B lymphocyte kinase	P51451
		Hcks: Hempoietic cell kinase	P08631
		Lyn: Tyrosine protein kinase Lyn	P07948

4.1. Protein structure and dynamics of the tyrosine kinases

In 1991 the first three dimensional atomic disposition of the catalytic core of a protein kinase in apo-form and in complex with substrate was acquired by solving the X-ray structure of c-AMP-dependent tyrosine kinase [105, 106]. To date, the ptotein tyrosine kinase family has the best structural coverage in the kinome with 35 out of 93 members having structures in the public domain and many more with clinical relevance being known within pharmaceutical industry [107].

At the level of the catalytic domain the conservation of the folding and the secondary structures among tyrosine kinases are bigger compared to the primary structure (in some cases below 20% identity). Common to all tyrosine kinase domains is a two-subdomain architecture consisting in an N-terminal lobe, with five-antiparallel-stranded β-sheets and a prominent α-helix (α-C helix) and a C-terminal lobe, with mainly α-helixes. ATP binds in the cleft between the two lobes (hinge region) and the part of the substrate with the tyrosine residue interacts with amino acids in the C-terminal lobe (Figure 1.6).

It is likely that the sequence variability among kinases, achieved throughout their evolution [108], characterizes versatile protein substrate specificities and mechanisms for control in order to differentiate the same enzymatic mechanism for a wide range of physiological roles [71]. On the other hand, the similarity of tertiary structures results from the constraints of the special arrangement of residues important for catalysis, so that the structural elements that are including such residues tend to have the same relative orientation (Figure 1.6) [100].

These elements include the activation loop (A-loop). The conformational transition of the A-loop goes from a close conformation to an open conformation with a spatial flip over a distance of about 10Å. When the loop is closed it is directed to the ATP-binding site. Thus, it blocks the binding of cofactor and substrate by imitating the substrate. In the open conformation the A-loop folds on the side of the C-lobe to make the reaction center accessible to the reagents and to form a platform for the positioning of the kinase substrate.

In most tyrosine kinases, the phosphorylation of a tyrosine in the A-loop stabilizes the open conformation through electrostatic interactions between the phosphate and basic residues of the A-loop and from the catalytic loop [109]. Nevertheless, several structures of phosphorylated kinases show some disorder in this region, indicating that the binding of the substrate might be still necessary to fully stabilize the open conformation of the loop [100]. In addition to the highly conserved site used to stabilize the open conformation, some kinases have secondary phosphorylation sites in the A-loop, each with different roles. For instance, the insulin like growth factor receptor has three tyrosines, which are phosphorylated sequentially leading to progressive increase of protein activity and downstream signaling [110, 111]. Similarly EGFR1 kinase is phosphorylated sequentially on five tyrosine residues from the A-loop [112]. In some tyrosine kinases, the A-loop can adopt an open conformation without the electrostatic stabilization of a phosphate [113, 114]. In the case of Csk it is the positioning of the regulatory SH2 and SH3 domains, which orients the αC helix in a way that the latter stabilizes the open conformation of the A-loop [100, 114].

Another structural element which undergoes an important flip during tyrosine kinase dynamics is the highly conserved amino acid triad (Asp-Phe-Gly) at the N-terminal of the A-loop. This so called DFG motif contains an Asp residue coordinating a magnesium ion which positions the phosphates of ATP for phosphotransfer, and a Phe which is responsible for the positioning of the α-C helix and the A-loop during phosphotransfer and ADP release. The DFG motif can thus interfere with binding of ATP depending on the adopted conformation:

- Asp-out: the aspartate points out of the reaction center while the Phe is in hydrophobic contact with residues at the ATP binding site.

- Asp-in: the aspartate points in the reaction center to coordinate the magnesium ion.

Finally, a third important element of the A-loop is the C-terminal part of the loop, which consists of the P+1 loop with conserved PxxW sequence and helix αEF, both important for substrate recognition [109].

The α-C helix is also a substructure, which demonstrates significant motions during protein tyrosine kinase dynamics. It moves in order to bring its conserved glutamate to the right distance for a salt bridge with the conserved N-terminal Lys from strand β3. This salt bridge positions the side chain of the lysine in order to coordinate the α- and β-phosphates of the ATP molecule. The conformational variation of this structural element is defined by two extreme positions, the “swung-in”, when the Glu is in the right position for catalysis and the “swung-out” reached with combination of movements around its main axis, out of the reaction center [115].

The extended conformation of the P-loop (strand β1 and strand β2) also has a role in coordinating the phosphates of ATP. The strand β6 forms part of the catalytic loop which contains an Asp that orients the tyrosine hydroxyl group of the substrate and thus facilitates the nucleophilic attack of the ATP γ-phosphate by removing the hydrogen atom of the tyrosine [116]. The catalytic loop is the only structural element that does not differ between the active and inactive states.

Apart of the three main structural elements (A-loop, α-C helix and P-loop), another critical element of kinase flexibility is the relative positioning of the N- and C-lobes of the kinase [117].

The motion of the two lobes has been described as twisting and bending. The rotation of the lobes with respect to each other is thought to be normal and is a requirement for catalytic activity [118]. Restriction of this motion for example by the binding of regulatory domains in c-Src or HcK inactivates the latter kinases [119, 120] and mutations in the linker between the regulatory domains which restore the flexibility of the lobes produce a more readily activated kinase [100, 121].

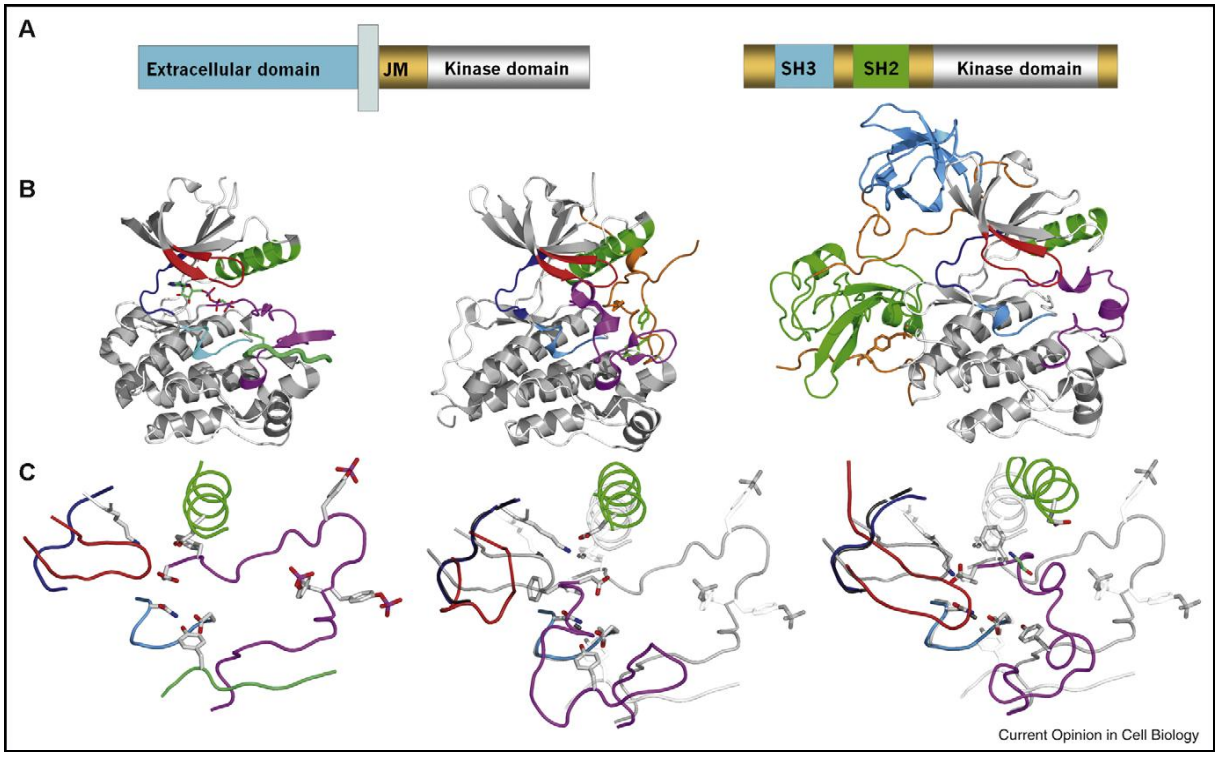

Figure 1.6: Different conformational states in kinase domains. A. Typical domain structures of a RTK (left) and NRTK (right). **B.** Structural elements mentioned in the text: C-helix-green, P-loop-red, Hinge-blue, Catalytic loop- cyan, A-loop-magenta, substrate peptide-light green. On the left, structure of IGF1R kinase in an active conformation (PDB ID: 1K3A). In the middle, structure of c-Kit in an inactive conformation (PDB ID: 1M7N). The A-loop, including the DFG-motif are in inactive conformations. On the right, Structure of c-Src in an assembled inactive state with the SH3 (cyan) and SH2 (green) domains present (PDB ID: 2SRC). Here, the A-loop and the αC-helix adopt inactive conformations. **C.** Details of the structural elements that move away from the active conformation to the inactive one such as the DFG-out conformation (Abl, PDB ID: 1IEP) or the c-Src inactive (c-Src, PDB ID: 2SRC). The grey "shadows" show the initial position of the structural elements in the active conformation. Modified from [107].

The opening angle of the cleft between the two lobes can also indicate the conformational state of a kinase (Figure 1.7). Open kinase structures show similar opening angles resulting from the accommodation of common substrate (ATP) and cofactor (Mg^{2+}). Closed kinase structures, however, reveal a large range of interlobe angles, from relatively closed compared to the open conformation, to much more open conformations. Opening angles often reveal the mode of interaction between the kinase domain and the regulatory kinase domains.

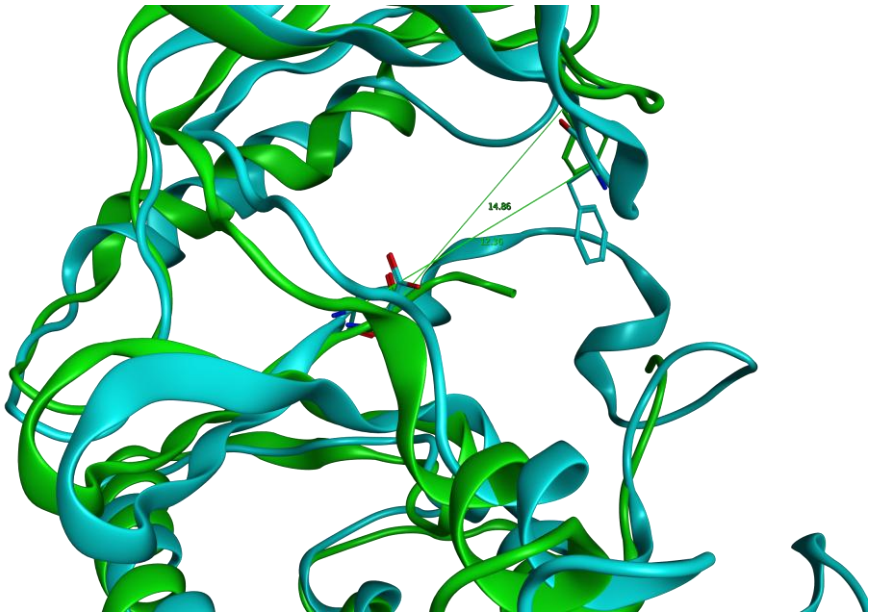

Figure 1.7: Opening angle within the hinge region between the closed c-Src kinase domain (PDB ID: 2OIQ) and the opened c-Src kinase domain (PDB ID: 1Y57). The ribbon structure of the c-Src in closed conformation is color-coded in aqua and the ribbon structure of the opened c-Src is depicted in green.The opening angle is depicted between residues Phe278 from the P-loop and the Asp404 from the DFG-motif, both shown in sticks.

The structural role of the SH2 and SH3 kinase regulatory domains has been described as an inducible snap-lock mechanism, where flexible linkers rigidify when they bind their partners [100, 121, 122]. In Hck and in c-Src, the C-terminal phosphotyrosine behaves as a latch and the SH2-SH3 domains behave as a lock.

Any disruption of the assembled inactive state leads to an increase of the kinase domain flexibility and facilitates the phosphorylation of the A-loop tyrosine. When the kinase is active, the SH2 and SH3 domains are accessible for protein-protein interactions and downstream signalling [123]. There are also cases, in which only the SH2 [124] or only the SH3 [123] domains are sterically free for downstream signalling interactions, thus probably determining the signalling network [100].

In the case of c-Abl and Csk, the latch is not a C-terminal phosphotyrosine. In c-Abl it is a C-terminal myristoyl-binding site [125]. Binding of myristoyl ester in the C-lobe pocket stabilizes a conformation which allows the SH2 domain to make a contact with the C-terminal lobe of the kinase. In Csk, the SH3-linker-SH2-linker region seems to stabilize the active conformation of the α-C helix and thus the A-loop [100, 126].

Another region involved in kinase dynamics and regulation is the juxtamembrane region (JM) in the case of most RTKs. For example, the structure of the Flt3 kinase shows that the N-terminal part of the JM region blocks and stabilizes the closed conformation of the kinase by packing against the α-C helix, P-loop and the A-loop [100].

Finally, exploring the structures and dynamics of isolated domains or entire proteins is still far from giving an understanding on how they interact with other domains or with other proteins due to the transient nature of the protein-protein interactions [127]. Nevertheless, the impressive amount of structural information on tyrosine kinase regulation and catalysis collected over the past 30 years has been successfully used to help drug discovery [107], which counts to date over ten clinically approved protein kinase targeted inhibitors [128].

4.2. Discovery, physiological role and oncogenicity of c-Src

In 1911, Peyton Rous discovered a new virus as the cause for the avian cancer called sarcoma [129]. This virus, called Rous sarcoma virus (RSV) in honour to its discoverer, was the first oncovirus to be described. The RSV is a member of the *Retroviridae* family and has a genome composed by a single strand RNA that codifies for four genes. In 1970, the gene responsible for the transforming properties of RSV was found. It was called *v-src* (or viral *src*) [130-132] and was the first of numerous viral oncogenes to be described [133]. *v-src* was subsequently shown to encode a tyrosine-specific protein kinase [134-136]. In 1976, Bishop and Varmus reported that a homologous gene to *v-src* was present in the genomic DNA of chicken cells and this cellular precursor or proto-oncogene was called *c-src* (or cellular *src*). A cellular *src* gene was also found in human cells as the precursor of the human c-Src protein [136]. The discovery of a cellular counterpart of a viral oncogene was an important step in oncology since it led to the idea that certain cellular genes might be at the origin of human cancers [133].

In healthy individuals, c-Src is expressed primarily in cells of hematopoietic origin; however, it displays a much more ubiquitous pattern of expression, with particularly high levels in platelets, neurons, and some epithelial tissues. It is an enzyme that interacts with numerous substrates involved in the regulation of cellular proliferation, adhesion, invasion and motility.

Two principle subcellular structures regulate adhesion, invasion and motility: focal adhesions and adherens junctions, both of which are regulated by c-Src (Figure 1.8) [137, 138].

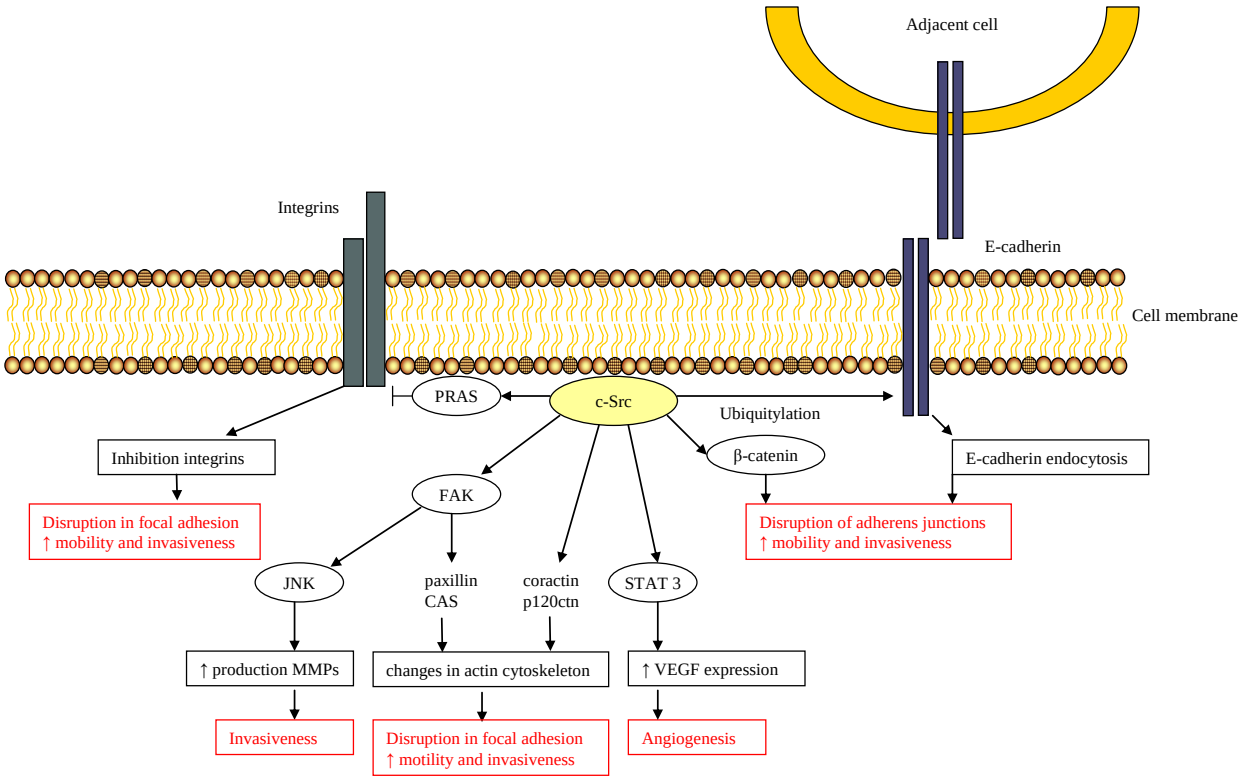

Figure 1.8: Effects of c-Src on tumour-cell behaviour. c-Src promotes the loss of cell-to-cell adhesion by stimulating the ubiquitylation of E-cadherin and its endocytosis. Turnover of focal adhesions is also required for motility and invasiveness and c-Src promotes this in various ways. Several of these mechanisms are mediated by the binding and activation of FAK, which phosphorylates substrates such as paxillin and CAS to bring about changes in the cytoskeleton that lead to focal adhesion disruption. c-Src also leads to changes in the expression on several genes that contribute to tumour progression. Activation of FAK leads to increased expression of the matrix metalloproteinases MMP2 and MMP9 which degrade the ECM components and favour invasion and metastasis. STAT3 activation by c-Src leads to increased expression of the VEGF promoting malignant angiogenesis. Modified from [139].

Focal adhesions are dynamic supramolecular structures composed of over 50 different proteins that assemble to allow cells to adhere to the extracellular matrix (ECM) and disperse to promote cells to move along or away of the ECM [139, 140]. The expression of c-Src leads to disruption of the focal adhesions and cell suspension. c-Src promotes also the loss of cell-to-cell adhesion by disrupting the adherens junctions. Adherens junctions are protein complexes composed of cadherins and catenins that occur at junctions in epithelial tissues. c-Src activation affects both protein families that build up the adherens junctions. It stimulates the E-cadherin inhibition through ubiquitylation and phosphorylates β-cathenin which precludes its binding to E-cadherin [141].

Since both, focal adhesion and adherens junctions are hindered by c-Src phosphorylation, c-Src-transfected fibroblasts and cancer cells show higher levels of motility [139].

The role of c-Src in cellular invasion is mediated through the effect of c-Src on E-cadherin levels. Actually E-cadherin is considered as an invasion suppressor [142].

An additional fundamental step in tumour development is the formation and growth of new arterial blood vessels. c-Src is involved in angiogenesis through phosphorylation of STAT3 (signal transducer and activator of transcription) which increases the expression of the vascular endothelial growth factor VEGF and thus the angiogenesis [143].

Consequently, c-Src is involved in many human tumour type including pancreatic cancer, breast cancer, lung cancer, prostate cancer and most frequently, in colon cancer [144].

The c-src gene is rarely mutated in human cancers, except for some types of colon cancers [145] and the leading mechanisms for c-Src transforming activity are assigned to c-Src overexpression and overactivation [139]. In vivo studies show that in general c-Src has little or no transforming activity in normal cells compared to v-Src. The low transforming activity of c-Src is mainly due to two regulatory elements. The first one is the intramolecular control of c-Src activity by the negative-regulatory Tyr527 (Figure 1.9). The second element of negative regulation is the phosphorylation of the Tyr527 by the C-terminal Src kinase (Csk).

Therefore a recent study explains the low c-Src transforming activity with the presence of intracellular Csk, which down-regulates cSrc oncogenicity. Oneyama et al. report the importance of the cellular c-Src: Csk ratio for the potential of the c-Src transforming activity and assume that it is rather the destruction of the c-Src/Csk balance which is responsible for cell transformation [146].

Nevertheless, c-Src remains a pivotal component of multiple signalling networks that regulate critical cell functions and remains a central therapeutic target for various types of cancer.

4.3. Structure and plasticity of c-Src

c-Src is the most studied member of the nRTK subfamily. The structure of c-Src protein is composed of seven parts: 1) a short membrane anchor or SH4 domain, 2) a unique domain, 3) a SH3 domain, 4) a SH2 domain, 5) a SH2-SH3 linker, 6) a catalytic domain (SH1) and a 7) C-terminal negative regulatory domain (Figure 1.9).

The SH4 domain contains a myristoylation sequence important for inner cell membrane localization. Nonmyristoylated c-Src molecules do not bind to cell membranes. In addition to myristoylation signals, the c-Src SH4 domain contains basic amino acid residues which are substrates for posttranslational palmitylation. Only myristoylated molecules are palmitoylated and consequently this process probably occurs on the membrane. Palmitylation is a reversible process. Thus depalmitylation and repalmitylation may be a mechanism for changing c-Src localization in the cell in response to corresponding stimulation [147].

The unique domain in c-Src is suggested to be responsible for protein-protein interactions [148].

The SH3 domain in c-Src is necessary for interactions with protein substrates and intramolecular bindings controlling catalytic activity and protein localization in the cell. It has a globular structure one side of which is hydrophobic and contains a cluster of acidic residues. The latter part of the SH3 domain binds to proline-rich residues of Src substrates and is important for protein-protein interactions [149].

The SH2 motif is a second globular structure which was identified to bind phosphorylated tyrosine sites [133] and a tyrosine residue (Y_{527}) from the C-terminal negative regulatory domain.

In solution, the two parts of the SH3 and SH2 domains flex freely [150]. But when organized into the assembled state of intact Src, the SH3-SH2 modules have strongly correlated dynamics as demonstrated by Young et al. [121]. They snap together and rigidify the bilobed kinase domain.

The SH1 domain or kinase domain is responsible for the tyrosine kinase activity and plays a crucial role in substrate specificity.

The C-terminal negative regulatory domain harbours Y_{527}, which can interact with the SH2 domain when phosphorylated by the C-terminal Src kinase (Csk) [151].

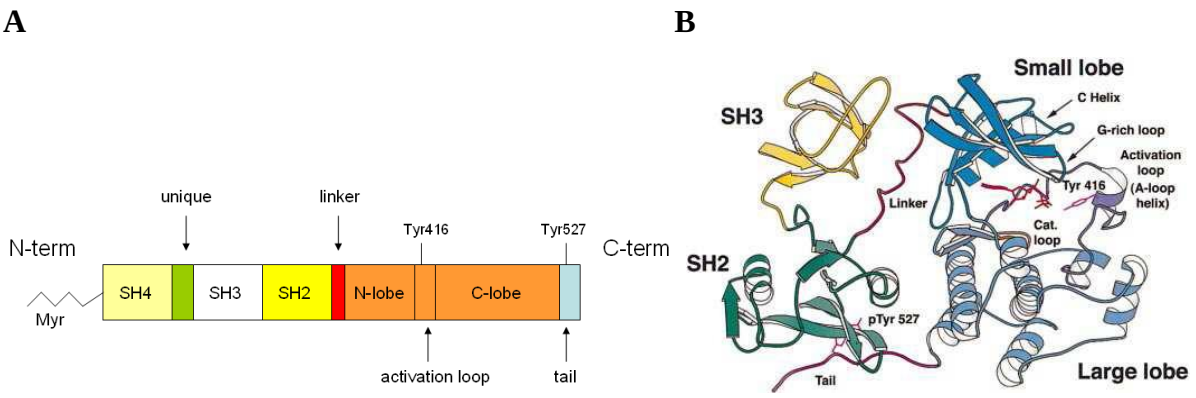

Figure 1.9: c-Src structure. A. The order of the domains in the polypeptide chain of c-Src. **B.** Three dimensional structure of the entire c-Src protein as obtained by Xu et. al [119].

To be catalytically active, c-Src tyrosine kinase undergoes a complex conformational transition which was described by Stephen Harrison as a three step "clamp-latch-switch" process [122] (Figure 1.10).

The "clamp" is the assembly of the SH2 and SH3 domains on the opposite site of the ATP-binding site. The linker connecting SH2 and kinase is the adaptor element that runs through the ligand binding groove of the SH3 domain and interfaces it to the kinase.

The "latch" is the short, Y_{527} containing, C-terminal tail. When the tyrosine is phosphorylated by Csk, it binds the SH2 domain and fastens the clamp in place [119, 122], keeping the kinase domain in a closed conformation.

The assembled state is unlatched by dissociation of the C-terminal tail from the SH2 domain and by dephosphorylation of the exposed $Y_{527.}$ The kinase domain is thus able to open and close (to breath) in order to admit substrates and release the products of the kinase reaction. This "switch" consists in the kinase domain conformational transition between the extreme closed and open conformational states [152, 153].

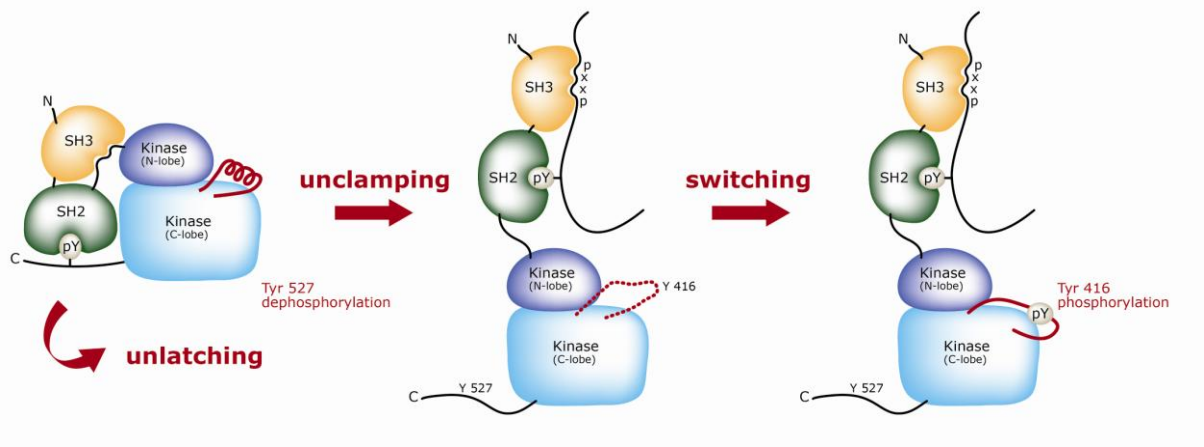

Figure 1.10: Modes of activation for c-Src: unlatching, unclamping and switching. The assembled state is unlatched by dissociation of the C-terminal tail from the SH2 domain and dephosphorylation of the exposed $Tyr_{527.}$ Competing SH2 or SH3 ligands can unclamp the assembled machinery of Src and the kinase domain can then be switched into its active conformation by phosphorylation of a tyrosine in the activation loop (Tyr_{416}). Modified from [122].

Interestingly, when expressed *"in vitro"* without the regulatory modules, the kinase domain of c-Src, like the kinase domains of other tyrosine kinases, could still be trapped in both open and closed conformations, indicating an intrinsic plasticity of the kinase domain.

So far, 36 different c-Src protein kinase structures have been solved providing a general understanding of the reversible switch between distinct states of the kinase. Classified according to the three-dimensional occupation of the structural determinants (DFG, A-loop, Glu310 in the αC-helix) [118], c-Src family are hence available in their active (PDB ID: 3DQW [154]), intermediate (PDB ID: 1QCF [120]) and in inactive state (PDB ID: 1OIQ [155]).

Contributing to the understanding of the dynamical behaviour of c-Src are also numerous computational studies correlating the phosphorylation of Y_{416} to the subsequent movement of the remaining structural elements of the c-Src kinase domain [156-158]. These models involve hydrophobic residues from the N-lobe and the C-lobe that do not form a primary sequence motif or a particular secondary structure but a "spine" of hydrogen bonds that connect and stabilize the primary phosphorylation site and the catalytically important DFG aspartate during kinase activation.

5. Aim and workflow of the thesis

We aimed at the identification of key amino acid residues that are dictating the transition from the active to the inactive protein conformation to better understand the molecular basis of conformational plasticity of tyrosine kinases.

A major challenge of this work was to define whether such crucial residues control protein kinase dynamics by modulating the conformational prevalence of the entire kinase domain or by influencing the dynamics of particular structural elements involved in the conformational transition.

We used c-Src tyrosine kinase domain as a case study because of the wealth of structural and computational information on this protein.

Based on a recent work which depicted a pool of residues between the N-lobe and the C-lobe (H1-H2 interface) important for the InsR tyrosine kinase domain dynamics [71], we first carried out a structural alignment against the InsR and identified the corresponding residues in the kinase domain of c-Src.

Then, we performed site-directed mutagenesis studies to mutate residues from the H1-H2 interface of the c-Src KD as well as residues contiguous to this interface.

To assess the influence of the generated mutations on the conformational plasticity of c-Src KD, we have applied several biochemical (kinetics, inhibition assays) and biophysical methods (protein crystallization, circular dichroism, and isothermal titration calorimetry).

Protocols for protein purification were tailor-made for each experimental approach

CHAPTER 2

c-Src tyrosine kinase domain expression and purification. Three purification methods for three different analytical read-outs.

1. *Abstract*

An important role for structure and dynamics of c-Src tyrosine kinase domain was attributed to a group of amino acids at the H1-H2 interface (cf. Chapter 3).

To investigate on the impact of these residues on c-Src kinase domain conformational dynamics, diverse experimental approaches should be applied. This suggests the use of high amounts of homogenous protein of exceptional stability and purity.

In this chapter we discuss the importance in developing specific protein purification procedures for each experimental pproach. We present three refined c-Src KD purification protocols for enzymatic and crystallization; ITC and CD studies respectively.

2. Introduction

c-Src is the prototype of a nine member family of protein tyrosine kinases (c-Src, Yes, Fyn, Lyn, Lck, Hck, Fgr, Blk, and Yrk) which are tightly associated with cellular membranes but do not span the lipid bilayer [159]. c-Src is virtually found in all higher eukaryotes [160, 161] and is ubiquitously expressed in tissues at different levels[162]. As a cytoplasmic protein, c-Src has a key role in mediating signal transduction via interactions of multiple cell proteins and protein complexes. Thus, c-Src displays a key role in cell adhesion, invasion, proliferation, survival and angiogenesis [139]. Clinical studies have shown that aberrant activation of c-Src is correlated with malignant progression of cancer; high expression levels of c-Src are found in a number of human tumors, including lung, breast, pancreatic, colon and prostate cancers [162-165].

On the basis of these important findings, three small molecule inhibitors (Bosutinib, AZD0530 and Dasatinib) developed against c-Src are currently undergoing early phase clinical testing [166]. Designed as ATP-competitive inhibitors, which is the common substrate of protein kinases (cf. Chapter 1), all these molecules lack of selectivity for c-Src alone [167] and display at least a dual c-Src/c-Abl inhibition profile.

Therefore considerable effort is being invested in understanding the nuanced differences in conformation and dynamics that distinguish one kinase from another [118]. The major part of such studies is performed *in silico* [156-158, 168]. Biochemical, biophysical and structural studies that are needed to complement knowledge on kinase regulation and specificity, are still at a poor state of development for the tyrosine kinases [169]. The lack of biophysical and structural studies on the spatio-temporal changes of tyrosine kinases undergoing the catalytic cycle is mainly due to the need of milligram amounts of conformationally homogenous protein of high stability and purity.

Moreover, recombinant protein preparations should be rationally prepared in respect to the analytical method they will be submitted to, in order to guarantee the correct read-out at the end of the assay.

The chronology of c-Src purification starts 10 years after its discovery in the 1970s. Attempts to purify the entire c-Src kinase from human tissues, and in particular from platelets [170-172], have met with limited success. Post-translational modifications and proteolytic cleavage of the N-terminus during purification has resulted in the isolation of protein of varying size purity and specific activity.

Efforts to overcome this problem have used a number of recombinant expression systems including *Escherichia Coli* [173, 174]. However, most bacterially expressed c-Src aggregates in insoluble protein or remains enclosed into inclusion bodies [175]. Alternative approaches of c-Src production in the bacterium *E. coli* have been described with variable success: to prevent toxicity to host cells, c-Src has been expressed as an inactive protein [176], as a non catalytic fragment in the case of the SH2 domain [177], or as a truncated chimera protein fused to a bacterial protein [178]. The low yields of soluble and active c-Src using bacterial expression made difficult the production of sufficient amounts of protein for biophysical and structural studies. Efforts to solubilize and purify c-Src from precipitates under denaturing conditions and to refold it by dilution yielded active protein that easily aggregated upon concentration [169]. In cases where a GST-tag was used to increase solubility, the heterogeneous autophosphorylation of the kinase arose as another problem [179].

Weijland et al. have described a yeast expression system since c-Src is not down-regulated when expressed in yeast in contrast to expression in bacteria [180]. Production in *Schizosaccharomyces plombe* resulted in extensive phosphorylation of endogenous proteins and the lethal effect could not be counteracted by coexpression of Csk. Toxicity problems in yeast were circumvented by coexpression of an antagonizing protein tyrosine-phosphatase (PEST-PTPase), but due to proteolysis and time requirements, yeast expression is not considered the most convenient procedure in practice [169].

Up to now, the most often used host for expression of recombinant and active c-Src are insect cells (Sf21 or their sub-clone Sf9 from ovarian tissue of *Spodoptera frugiperda*, or Tn5B1-4 cell line originally established from the *Trichoplusia ni* embryonic tissue) [181]. Whereas insect cell culture can provide milligram amounts of protein, this type of expression remains costly and time consuming, with a generation of mutant protein typically in the range of 3-4 weeks.

In 2005 Seeliger et al. reported a c-Src/c-Abl kinase domain expression and purification protocol combining the advantages of a bacterial *E. coli* culture – fast and cheap protein expression; parallel expression of many constructs; possibility of isotope labeling for NMR; no phosphorylation and glycosylation as post-translational modifications – together with a tyrosine-phosphatase (YopH; UniProt KB N°P08538) co-expression [169]. Co-expression with a bacterial phosphatase reduced toxicity and increased drastically soluble protein yields up to ~10mg/Lt of culture, but also resulted in obtaining a conformationally homogenous unphosphorylated protein appropriate for further structural studies.

The latter technique raised notably the amount of c-Src crystallographic studies. 28 crystal structures were reported for YopH coexpressed c-Src KD from 2005 to date (PDB ID: 2HWO, 2HWP,2OIQ, 2QLQ, 2QQ7, 2QI8, 3D7U, 3D7T, 3DQX, 3DQW, 3EN4, 3EN5, 3EN6, 3EN7, 3EL7, 3EL8, 3F6X, 3F3T, 3F3U, 3F3V, 3F3W, 3G6G, 3G6H, 3GEQ, 3G5D, our 3 structures). Purified c-Src following the above described procedure could still not be used with success in some biochemical or biophysical methods as isothermal titration calorimetry (ITC) or circular dichroism (CD), where high amounts of highly homogenous protein should be furnished in addition at specific protein formulation, capable of undergoing the conditions of the particular assay.

Herein we describe c-Src kinase domain bacterial co-expression with YopH phosphatase, coupled to optimized protein purification methods which were tailor-made according to different subsequent read-outs in enzymatic, crystallographic, ITC and CD assays.

3. Materials and Methods

All chemicals were purchased from Applichem, Germany except if otherwise indicated.

3.1. Protein Expression

Co-transformed BL21 (DE3) *E. coli* cells (Merck4Biosciences, Switzerland) were resuspended in 5ml LB medium supplemented with 50ug/ml kanamycin and 50ug/ml streptomycin. The culture was incubated at 37°C, 200rpm till OD_{550}=0.8. Then 1L of selective Terrific Broth (TB) medium (Difco Laboratories, USA) was inoculated with the mini-culture and let at 37°C, 200rpm till OD_{550} reaches 0.8 prior to cooling for 3h at 18°C. Protein expression was induced with 0.2mM Isopropyl β-D-1-thiogalactopyranoside (IPTG) for 16 hours.

Cell cultures were centrifuged at 4°C, 5000rpm for 10min and cell pellets were stored at -20°C.

3.2. Protein Purification

3.2.1. c-Src KD purification for activity, inhibition assays and for crystallization

Cell pellets were resuspended in 30ml buffer A (50mM Tris pH8.0, 500mM NaCl, 5% Glycerol, 25mM imidazole) supplemented with 10mg DNAse (Deoxyribonuclease I from bovine pancreas) and 1mM EDTA. Cells were disrupted by three cycles of homogenisation using a French press. Cell debris and insoluble protein were sedimented by centrifugation at 4°C, 9500rpm for 40min. The filtered supernatant was applied on a 5ml HisTrap HP chelating column (GE Healthcare, UK) equilibrated with buffer A.

The column was washed with 10 column volumes (CV) of buffer A and protein was eluted with a linear gradient 0-100% buffer B (50mM Tris pH8.0, 500mM NaCl, 5% Glycerol, 500mM imidazole) over 30 column volumes at a flow rate of 2 ml/min. Peak fractions containing c-Src KD were pooled and dialysed overnight at 4°C, 50rpm through 6-8 kDa MWCO Spectra/Por® membrane (Spectrum Laboratories) in dialysis buffer (20mM Tris pH 8.0, 100mM NaCl, 5% Glycerol, 1mM DTT).

For crystallization, the N-terminal 6xHisTag was cleaved during dialysis by adding 1000U AcTEV Protease (Invitrogen) to the assembled protein fractions. The dialysed protein was then diluted in 5 volumes of buffer QA (20mM Tris pH 8.0, 5% Glycerol, 1mM DTT), filtered and loaded into a 5ml HiTrap HP column (GE Healthcare, UK) equilibrated with buffer QA.

The column was washed with 10 CV of buffer QA and the protein was eluted with a linear gradient 0-100% buffer QB (20mM Tris pH 8.0, 5% Glycerol, 1mM DTT, 1M NaCl) over 4CV at 2ml/min. The fractions containing c-Src KD were pooled and concentrated to 1ml using the Amicon Ultra 4 falcon tube 10kDa MWCO at 4°C, 3500rpm. The concentrated protein was then filtered and loaded onto a Superdex 75 column equilibrated with buffer S75 (50mM Tris pH8.0, 100mM NaCl, 5% Glycerol, 1mM EDTA). For crystallization buffer S75c was used (21mM Tris pH8.0, 105mM NaCl, 1.05mM DTT). Protein was eluted at 0.5ml/min.

3.2.2. c-Src KD purification for ITC studies

Two main differencies distinguished c-Src KD purification for ITC compared to the purification protocol as described in 3.2.1:

- After Ni affinity purification, fractions containing c-Src KD were directly diluted to 50ml buffer QA to reduce the NaCl content then filtered and loaded on the HiTrap HP column.

- Buffer MES (50 mM MES, 116mM NaCl (ionic strength 154mM), 5% Glycerol, 1 mM EDTA, pH 6.5) was used for gel filtration on the S75 column.

3.2.3. c-Src KD purification for CD studies

Three main differencies distinguished c-Src KD purification for CD compared to the purification protocol as described in 3.2.1:

- The filtrated supernatant from cell lysis was applied on a 5ml Chelating Column (GE Healthcare, UK) charged with CoCl2 (Acros Organics, Belgium) according to the producer's protocol.

- After Co affinity purification, fractions containing c-Src KD were directly diluted to 50ml buffer QA to reduce the NaCl content then filtered and loaded on the HiTrap HP column.

- Buffer CD (20mM Tris pH8.0, 100mM NaCl, 1mM TCEP) was used for gel filtration on the S75 column.

The presence and the purity of recombinant protein were verified after each step of purification on 12% SDS-PAGE and subsequent Coomassie Staining. The absence of protein phosphorylation was confirmed by Western Blot in presence of monoclonal anti-phosphotyrosine antibody clone 4G10® (Millipore) and by ESI-time-of-flight mass spectrometry (TOF MS/MS) on QSTAR XL quadrupole TOF mass spectrometer (AB/MSD Sciex, Canada). For comparison, the expected protein mass for each c-Src mutant was calculated from the amino acid sequences on ProtParam [182].

c-Src proteins at ≥ 95% purity were stored at -80°C.

3.3. Protein quantification

Measurements based on direct protein absorption at 280nm were done using a Cary 50 UV-Vis spectrophotometer (Varian, USA). The concentration of the protein was calculated according to the Lambert-Beer's law. ProtParam software [182] was used to calculate the coefficient of molar extinction of c-Src wild type and mutants. Buffer absorption was subtracted from each value and calculated values were a mean of 3 measurements.

3.4. In vitro protein activity assay

3.4.1. UV-based tyrosine kinase assay

The kinase activity of c-Src was monitored using a continuous spectrophotometric assay [183]. Reactions contained 100mM Tris (pH8.0),1mM DTT, 10mM $MgCl_2$, 275uM ATP, 1mM Phosphoenolpyruvate, 180 uM NADH, 75U/ml pyruvate kinase (PK), 105U/ml lactate dehydrogenase (LDH), 30nM c-Src, 533 uM c-Src peptide substrate (EIYGEFKKK) [184]. Reactions (75µl) were first preincubated for 5min at 30°C and then started through the addition of the peptide substrate. The decrease in absorbance was monitored over 30min at 30°C in a Cary 50 UV-Vis spectrophotometer (Varian, USA) in triplicate for each mutant. For each molecule of NADH used, one molecule of product (ADP and EIY*GEFKKK) is formed. The background protein activity was calculated in a sample without substrate peptide and subtracted from the kinase assays with the substrate peptide.

The specific activity of the recombinant c-Src KD can be calculated as the amount of product (NAD) produced per unit of time per mg of enzyme.

In the UV-based tyrosine kinase assay one molecule of substrate (NADH) used gives one molecule of product (NAD). Therefore the specific activity of c-Src KD can be deduced as the amount of NADH used per unit of time, T (min) and per milligram of enzyme.

$$specific\ activity = \frac{\Delta NADH}{\Delta T * cSrc} \qquad \text{(Equation 1)}$$

The concentration of NADH is given by the Lambert-Beer's law as follows:

$$A = \varepsilon * l * c \qquad \text{(Equation 2)}$$

where c is the concentration of NADH, l is the length of the cuvette (cm) and ε for NADH is $6.22*10^3$ mol^{-1} * l * cm^{-1}. Thus, the normalized specific activity of c-Src is calculated as:

$$\textit{specific activity} = \frac{\Delta A}{\varepsilon * l * \Delta T * cSrc} \quad \{M*min^{-1}*mg^{-1}\} \qquad \text{(Equation 3)}$$

where the variation of the absorbance of NADH over time (ΔA/ΔT) is given by the slope resulting from the activity assay.

3.4.2. Autophosphorylation reaction monitored by Western Blotting

Autophosphorylation of recombinant c-Src WT and mutants were followed by Western Blotting. For this assay 1ug of purified protein was mixed with 5mM $MgCl_2$ and Buffer 75 to a final volume of 20µl. The mix was incubated at 30°C for 5min and the reaction was initiated by adding 200µM ATP. The autophosphorylation was measured at different times of incubation (0sec, 15sec, 1min, 10min and 30min). Reactions were stopped by denaturing the protein with 3xSample Buffer (0.24 M Tris-HCl pH 6.8, 6% SDS, 30% Glycerol, 16% B-mercaptoethanol, and 8.9mM Bromophenol blue).

A negative control was included (no $MgCl_2$, no ATP), as well as a positive phosphorylation control (EGF-Stimulated A431 cell lysate, Millipore, USA). All the samples were boiled for 5min at 95°C and separated on 12% SDS-PAGE. The nitrocellulose membrane and two Watman® papers (with the obtained gel) were equilibrated in water and Transfer buffer (Tris 25 mM pH 8.5, 0.2 M Glycine, 20% Methanol, and 0.05% SDS), respectively, for 30 minutes. The protein transfer was carried out at 19 V, 400 mA, for 1.5 hours, in a Trans-Blot Semi-Dry Transfer Cell (Bio-Rad, UK). Immunodetection was performed on SNAP i.d. Protein Detection System (Millipore, USA) following the standard protocol with the following solutions: 1) Blocking solution (tris buffered saline pH7.6, 0.1% Tween 20, 0.5% non fat dry milk), 2) Washing solution (tris buffered saline pH7.6, 0.1% Tween 20), 3) Primary antibody solution (0.0035mg/ml Monoclonal Anti-Phosphotyrosine-Y_{416} Antibody, clone 4G10 (Millipore, USA) diluted in tris buffered saline pH7.6, 0.1% Tween 20), 4) Secondary antibody solution (0.0015mg/ml Goat Anti-Mouse IgG(H+L)-HRP Conjugate (BioRad, UK).

A FUGI Medical X-Ray film (FUJIFILM Corporation, Tokyo) was used to image the nitrocellulose membrane after 15 seconds of exposure. A picture of each western blot film was taken on Quantity One 4.5.1(Bio-Rad, UK). The densitometric analysis was performed in duplicates using Scion Image (Scion Corporation, USA). Obtained values were corrected for background by subtracting the intensity of the negative control.

3.5. CD spectra

All CD spectra were recorded at 5°C on Jasco model J-815 circular dichroism spectrometer (Tokyo, Japan), equipped with a water cooled Peltier unit in 0.05cm Hellma quartz cuvette model 110-QS (Muellheim, Germany). CD spectra measurements were taken for 10μM protein solutions at a scan rate of 100 nm /min with a data pitch of 0.5nm and a band width of 1nm. Each spectrum represents the average of 2 scans from 800nm to 200nm. Duplicata consisted of a sample from freshly purified protein and from a -80°C overnight frozen sample. Buffer CD (20mM Tris pH 8.0, 100mM NaCl, 1mM TCEP) was used as blank and its spectrum was subtracted from all recorded spectra.

The secondary structure content was estimated by deconvolution procedures using Spectra Manager (Jasco, Tokyo, Japan).

3.6. Thermal denaturation

To define the midpoint of the thermal denaturation curve (T_M) for c-Src WT and mutants, spectra were collected at 220nm within the temperature range of 5°C- 80°C on Jasco model J-815 circular dichroism spectrometer (Tokyo, Japan), equipped with a water cooled Peltier unit in 0.05cm Hellma quartz cuvette model 110-QS (Muellheim, Germany).

For each c-Src mutant and for c-Src WT, CD data were collected from 10uM sample in Buffer CD from both freshly purified protein and from a -80°C overnight frozen sample. The rate of heating was fixed at 1°C /min with data pitch of 1°C and a delay time of 1 sec. T_M calculated with Spectra Manager (Jasco, Tokyo, Japan).

The CD unit used is the mean molar ellipticity per residue (θ) expressed in {deg. cm^2. $dmol^{-1}$. res^{-1}}, where c-Src WT; L317I; L407G; L317_L322I; L317I_L322I; L322I; V377L contained 309 residues and G318, G318_V378L; G318_L323I_V378L contained 310 residues.

4. Results and discussion

4.1. c-Src KD purification for kinase assay and crystallyzation

We took advantage of recent reports where co-expression of a phosphatase with c-Src tyrosine kinase reduces the cellular toxicity that can be associated with milligram amount expression of phosphorylated kinases in bacteria [169, 185]. The YopH phosphatase was obtained from the Kuriyan laboratory, who had demonstrated its use in the production of soluble c-Src [169]. The amino acid sequence of the *yopH* gene product was shown to contain significant homology to the conserved catalytic domains of the eukaryotic protein-tyrosine phosphatase family (PTPas; EC 3.1.3.48) [186]. The recombinant YopH enzyme has absolute specificity for removal of the phosphate from peptides and proteins phosphorylated on a tyrosine residue [187].

Nevertheless, when c-Src KD was expressed and purified in house according to the protocol published by Seeliger et al. [169], the kinase domain remained partially phosphorylated (11% of the total amount of purified protein) (Figure 2.1). Since the initial report indicates the obtention of entirely unphosphorylated kinase domain by the criteria of ESI-TOF mass spectrometry and given the low amount of phosphorylated c-Src, we suggested that autophosphorylation of c-Src is occurring only during the purification procedure. Partial phosphorylation of c-Src takes place when the kinase domain is separated from the phosphatase and because of the imminent presence of variable amounts of residual ATP and divalent cations in buffers along the purification.

To avoid "post-expressional" kinase autophosphorylation we have modified the original purification protocol by adding 1mM 2,2',2'',2'''-(ethane-1,2-diyldinitrilo)tetra acetic acid (EDTA) in buffers for immobilized metal chelating chromatography (IMAC) and gel filtration chromatography. At this concentration, EDTA is used to complex any divalent ion that may catalyze c-Src autophosphorylation without damaging chromatography columns or suppressing kinase activity in subsequent kinase assays. Figure 2.1, below, shows the Western blot of c-Src purified with and without EDTA. In presence of chelating agent during purification, the final protein preparation is not phosphorylated on Y416 or any other tyrosine residue, but shows activity upon addition of 20μM ATP and 5mM Mg^{2+}, suggesting proper folding.

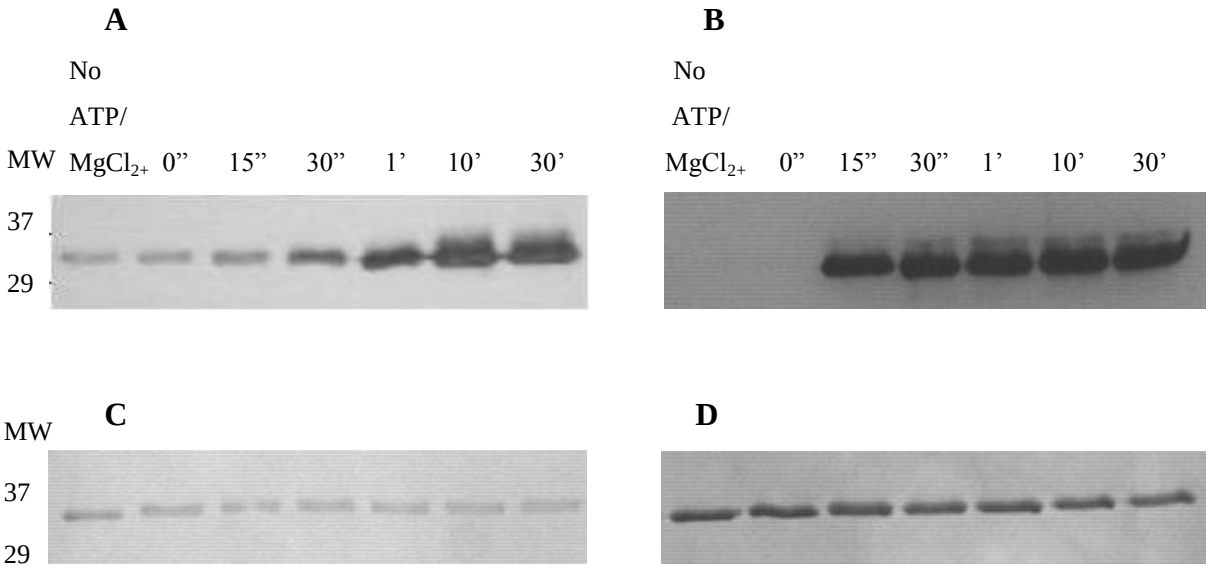

Figure 2.1: Autophosphorylation assay with or without EDTA and ATP probed with anti-phosphotyrosine antibody 4G10® (Millipore, USA). A. Western blot showing the time course autophosphorylation of c-Src WT purified without complexion agent at time 0" and at up to 30' incubation with 20μM ATP and 5mM $MgCl^{2+}$ at 30°C. **B.** Western blot showing the autophosphorylation state of c-Src WT purified with 1mM EDTA at time 0" and at different time point up to 30' incubation with 20μM ATP and 5mM $MgCl^{2+}$ at 30°C. **C.** Loading control for a) by Coomassie staining. **D.** Loading control of b) by Coomassie staining.

In addition to the Western blot analysis, the phosphorylation state of purified c-Src KD in presence of EDTA was assayed by electrospray ionization-time-of-flight mass spectrometry (ESI-TOF MS). The latter analysis confirmed the absence of phosphorylation, indicating that the kinase domain was purified in its inactive conformation (Table 2.1).

Thus the addition of 1mM EDTA to buffers for IMAC and gel filtration chromatography as described in 3.2.1 added robustness to the preparation of homogenous unphosphorylated c-Src. This is of great help for future studies on the conformational transition of the kinase including crystallization.

Modifications to the purification protocol, as described above, did not influence the total protein yield which remained within the range of 5-15 mg/l as previously described [169] and showed similar pattern of purification. A single peak of apparent molecular size of 32.6 kDa eluted from analytical gel filtration, indicating a homogenous preparation of monomeric protein. Protein purity after the last purification step was > 95% by the criteria of SDS-PAGE (Figure 2.2).

Purified c-Src KD stored at 4°C was stable for approximately one week without addition of glycerol, whereas frozen enzyme, with no additional glycerol, could be kept at -80°C for 3 months with no significant loss of activity. Repeated freezing and thawing did not decrease the kinase activity up to three cycles.

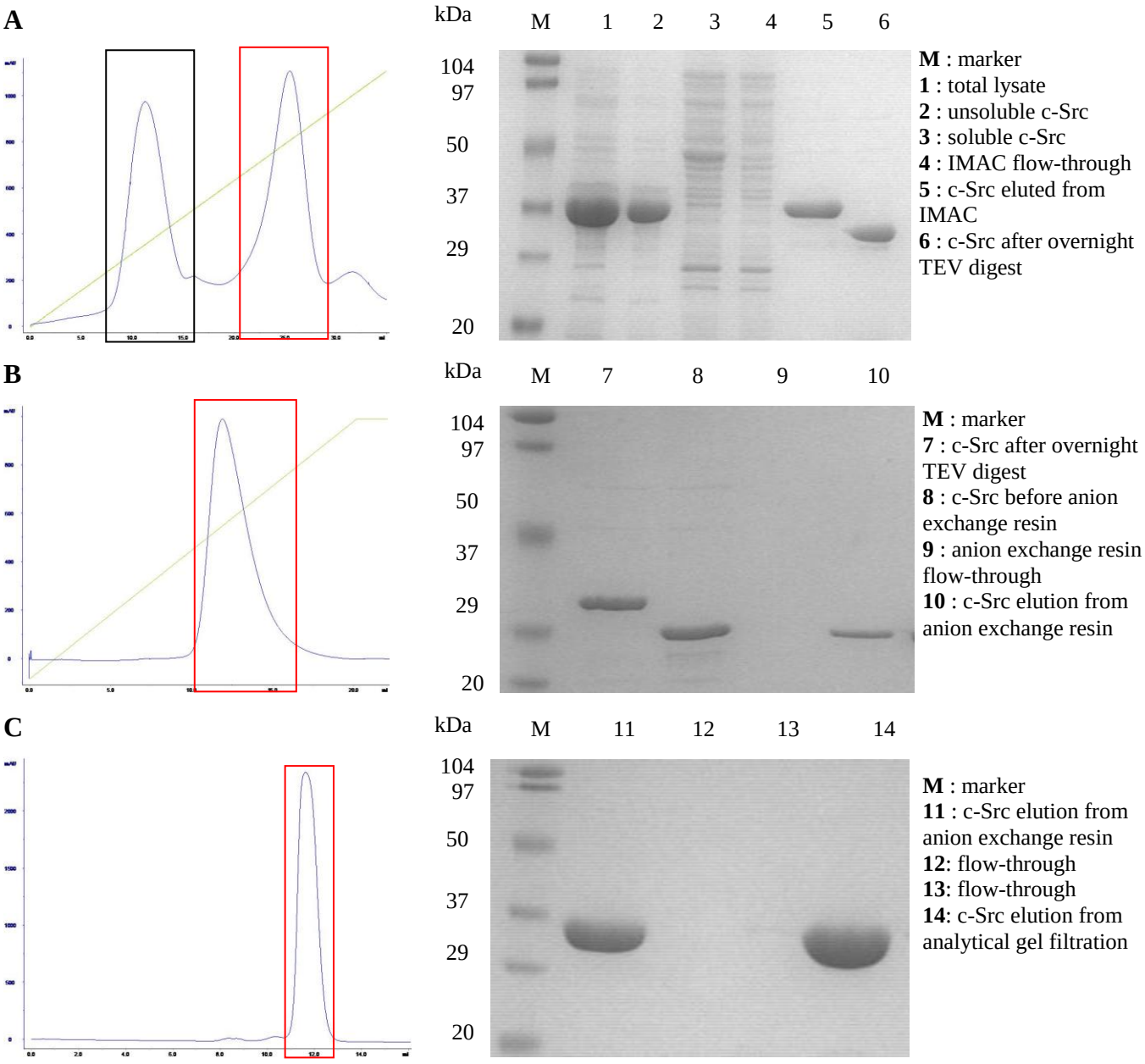

Figure 2.2: Protein purification of c-Src KD in presence of 1mM EDTA. On the left are shown the chromatograms depicting the absorbance (A=280nm) of purified proteins. Fractions highlighted in red boxes corresponded to c-Src KD. Fractions highlighted in black box corresponded to pYopH phosphatase. Green lines show the buffer gradient. On the right are presented 12% SDS-PAGE gels stained with Coomassie Blue after each purification. **A.** Ni-affinity resin; **B.** anion exchange resin; **C.** size exclusion chromatography. Purified c-Src KD appears at 32.6kDa.

Circular dichroism analysis was conducted in order to verify the correct folding of c-Src KD. The analysis revealed a profile compatible with secondary structures that are typical for tyrosine kinase domains [188-191] and for c-Src, in particular [192] (Figure 2.3) indicating a proper folding of the purified Src catalytic domain.

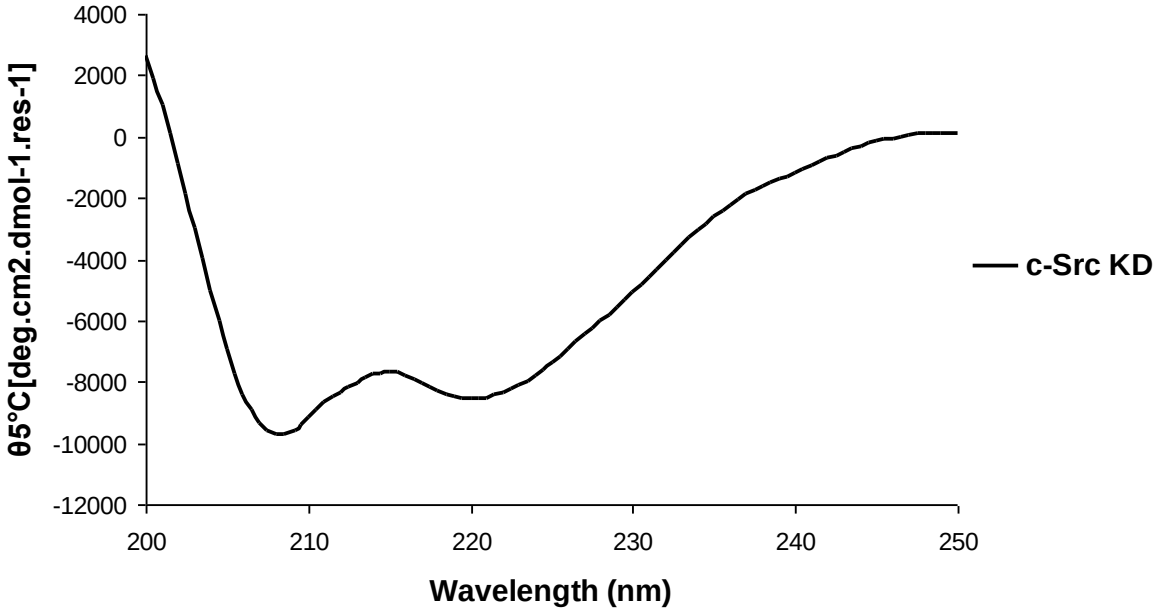

Figure 2.3: CD-spectrum of WT c-Src kinase domain purified in presence of 1mM EDTA. Spectra were recorded as described in Materials and Methods. For each spectrum at least two accumulations were averaged and background corrected.

As the optimized purification protocol generated milligram amount of highly pure, properly folded, unphosphorylated and active c-Src wild type kinase domain, we applied this method for the expression and purification of all previously designed c-Src mutants (cf. Chapter 3).

A summary of the phosphorylation state, specific activity and the recovery of all c-Src kinase domains during purification is reported in Table 2.1.

Table 2.1: Purification of recombinant wild type and mutated c-Src kinase domain.

c-Src KD	Total protein (mg)		Calculated Mass (Da)	Experimental Mass (Da)	Phosphorylation State After Purification *	Specific Activity ** ($M*min^{-1}*mg^{-1}$)
	Lysate	~1000				
WT	Ni affinity	17.1				
	Ion exchange	7.7				
	Gel filtration	6.8	35344.4	35345.20	non- phophosphorylated	0.098±0.005
	Lysate	~1000				
WT (no 6xHis Tag)	Ni affinity	16.5				
	Ion exchange	5.4				
	Gel filtration	4.3	32633.0	32633.5	non- phophosphorylated	0.078±0.011
	Lysate	~1000				
L317I	Ni affinity	14.3				
	Ion exchange	6.2				
	Gel filtration	5.6	35344.4	35347.70	non- phophosphorylated	0.116±0.021
	Lysate	~1000				
G318	Ni affinity	15.2				
	Ion exchange	6.7				
	Gel filtration	5.8	35401.5	35401.57	non- phophosphorylated	0.131±0.01
	Lysate	~1000				
G318_V378L	Ni affinity	14.7				
	Ion exchange	5.9				
	Gel filtration	5.2	35415.5	35415.70	non- phophosphorylated	0.116±0.002
	Lysate	~1000				
L317I_L322I	Ni affinity	16.5				
	Ion exchange	7.4				
	Gel filtration	5.5	35344.4	35344.80	non- phophosphorylated	0.107±0.006
	Lysate	~1000				
L317I_V377L	Ni affinity	15.4				
	Ion exchange	6.1				
	Gel filtration	4.9	35358.4	35358.50	non- phophosphorylated	0.135±0.009
	Lysate	~1000				
L322I	Ni affinity	14.5				
	Ion exchange	7.9				
	Gel filtration	7.1	35344.4	35343.60	non- phophosphorylated	0.183±0.002
	Lysate	~1000				
G318_L323I_V377L	Ni affinity	12.8				
	Ion exchange	4.5				
	Gel filtration	3.2	35415.5	35416.00	non- phophosphorylated	0.138±0.027
	Lysate	~1000				
V377L	Ni affinity	18.3				
	Ion exchange	9.6				
	Gel filtration	7.4	35358.4	35358.70	non- phophosphorylated	0.116±0.007
	Lysate	~1000				
L407G	Ni affinity	16.8				
	Ion exchange	8.7				
	Gel filtration	8.0	35288.3	35289.15	non- phophosphorylated	0.096±0.004

* Assessed by Western Blot and ESI-MS. ** Values represent the average of at least two experiments.

A semi-quantitative analysis of the SDS-PAGE gels after cell lysis showed that the expression procedure generated very high yields (~1000 mg) of total kinase for all expressed c-Src kinase domains. Total amount of protein was similar to recombinant kinases co-expressed in E. coli with other protein phosphatases such as serine/threonine protein phosphatase from the bacteriophage lambda (patent application WO/2004/009831) or with the human PTP1b tyrosine phosphatase [193].

However, more than 90% of all kinase domains were still found in the insoluble fraction (Figure 2.2) even if the expression protocol implements the application of low growth temperature and low amounts of IPTG for induction. Recently several studies have been published on the use of over-expressing folder helpers, so-called molecular chaperones, to prevent kinase aggregation during bacterial recombinant expression. For instance in presence of E.coli chaperones KJE/ELS, homologues of eukaryotic Hsp70/Hsp40, the solubility of Csk, Fyn, Lck and Btk kinases was improved [194-196]. When applied to the c-Src case [197], the use of KJE/ELS chaperones showed two fold increase in solubility, but no change in yields neither in specific activity after IMAC and size-exclusion chromatography. Therefore, no co-expression of bacterial chaperones was implemented in the expression of c-Src kinase domain in this work.

What is significant is that the soluble fraction in all purified kinase variants contained more than 5mg of pure, unphosphorylated, properly folded and active protein that could be readily concentrated (up to 7mg/ml). Thus, tyrosine kinase domains described in Table 2.1 above were successfully used in biochemical and crystallization studies as reported in Chapter 4.

The major aim of this work being the molecular understandings of tyrosine kinase plasticity during the dynamical process of catalysis, kinetic and crystallographic studies of WT c-Src KD versus kinase domains carrying mutations in the H1-H2 interface, were coupled to additional biophysical methods such as ITC and CD. For these studies, tailor-made purification procedures were needed.

4.2. c-Src KD purification for ITC studies

Since the issue of high quantity of pure and active protein was guaranteed by the expression protocol described above, we focused on the development of altered and refined protocol of purification with respect to stability and quality suitable for subsequent microcalorimetric titration of c-Src with imatinib.

As published, the original protocol for calorimetric experiments with c-Src KD was based on a two-day purification procedure containing five main steps, notably Ni-IMAC, overnight dialysis/TEV cleavage of the 6xHis Tag, anion exchange chromatography, analytical gel filtration, P-10 column (GE Healthcare) exchange to ITC buffer conditions [169]. Moreover, the pH for calorimetric titrations with imatinib was fixed at pH 8.0, which is not consistent with the solubility of this kinase inhibitor (pKa = 8).

We have observed that after the two-day purification method for c-Src, the kinase domain precipitates (up to 40%) in the P-10 exchange column. Although appropriate for kinetic measurements (~10min at 30°C) and crystallization (overnight at 14°C), c-Src prepared according to the original procedure was not stable enough for calorimetric experiments where titration is carried out for ~3 hours at 30°C (Figure 2.4, standard protocol, Appendix A).

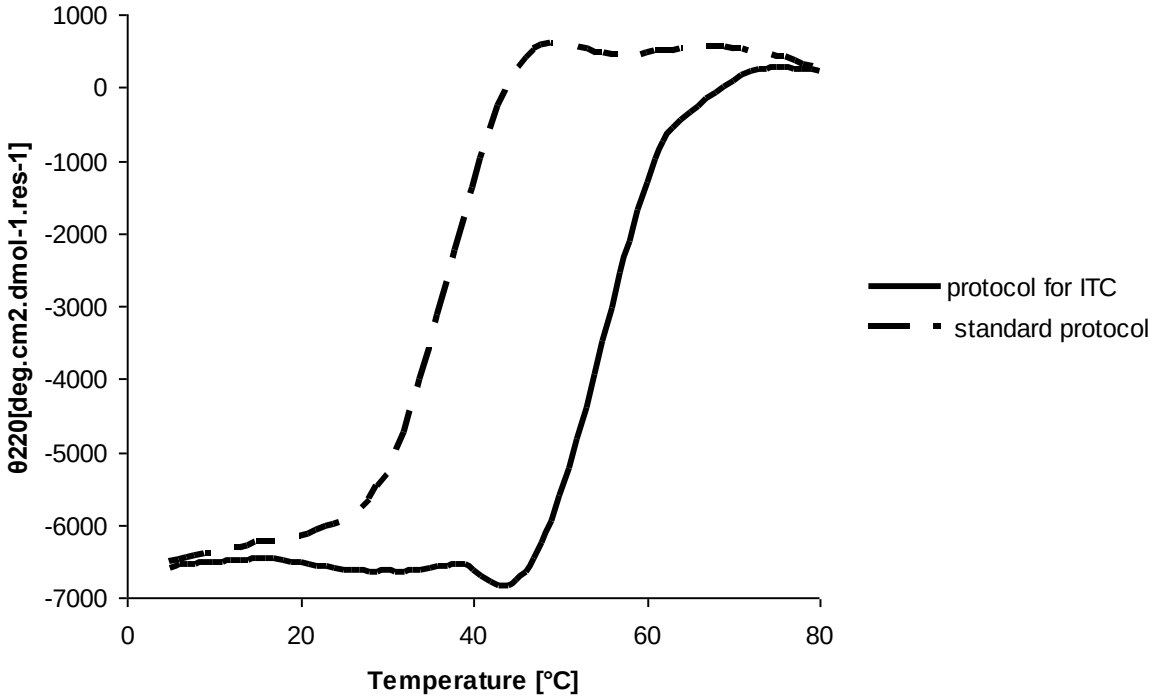

Figure 2.4: Thermal unfolding of uncomplexed c-Src WT KD purified with standard purification protocol over 2 days and of uncomplexed c-Src WT KD purified in one day with optimized protocol for ITC. Unfolding was monitored under the same conditions by CD spectroscopy as described in Materials and methods. Thermal denaturation curves represent the mean of at least 2 measurements and signals are normalized to the buffer. The midpoint of the thermal denaturation curve (T_M) was 37.6 ± 0.1°C for uncomplexed WT c-Src KD purified over 2 days and 53.4±0.1°C for uncomplexed WT c-Src KD purified in one day. T_M values were calculated with Spectra Manager (Jasco, Tokyo, Japan).

To increase protein stability and quality for ITC studies, we have considered three major modifications of c-Src KD purification towards an ITC tailor-made preparation protocol:

- omission of the 6xHis-tag cleavage, since the kinetic properties of the fusion protein are identical to c-Src with cleaved His-tag.
- exchange to the ITC buffer directly on the size exclusion column to avoid protein precipitation on P-10 exchange column.
- pH 6.5 of the ITC buffer to improve imatinib solubility.

The final 3-step purification procedure for ITC yielded higher amount of pure (Figure 2.5) and active (Table 2.2) c-Src kinase domain in one day.

Table 2.2: Purification of recombinant c-Src KD. Comparison between original [169] and optimized purification procedure for ITC.

c-Src KD mutation	Total protein (mg)		Calculated Mass (Da)	Experimental Mass (Da)	Phosphorylation State After Purification *	Specific Activity* ($M*min^{-1}*mg^{-1}$)**
WT	Lysate	~1000				
	Ni affinity	17.1				
	Ion exchange	7.7				
	Gel filtration	6.8	35344.4	35345.2	Non phopsphoraylated	0.078±0.011
WT for ITC	Lysate	~1000				
	Ni affinity	14.9				
	Ion exchange	9.5				
	Gel filtration	7.2	35344.4	35345.2	Non phosphorylated	0.077±0.017

* Assessed by Western Blot and ESI-MS. ** Values are the mean of at least two measurements.

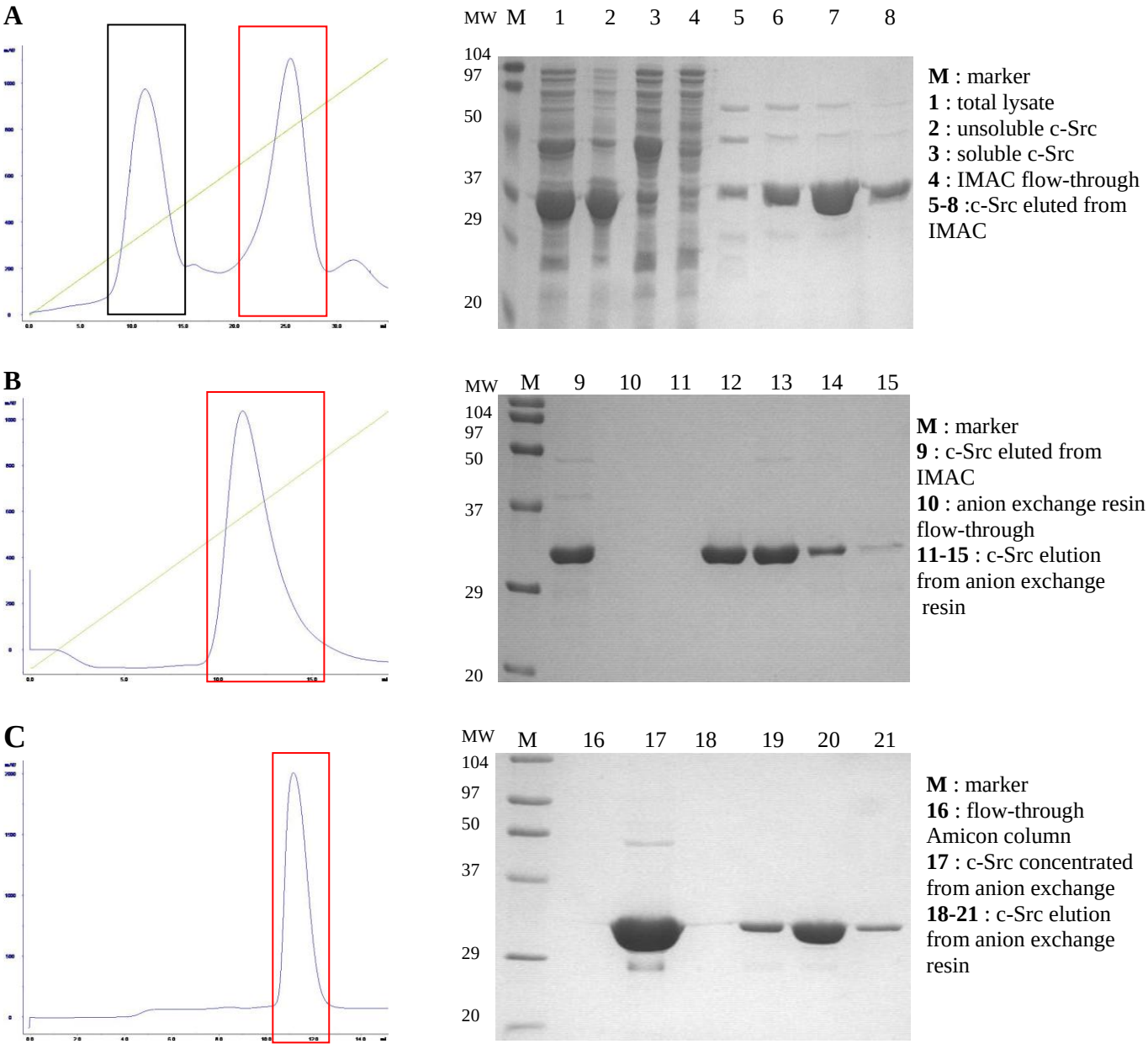

Figure 2.5: Protein purification of c-Src KD for ITC experiments. On the left are shown the chromatograms depicting the absorbance (A=280nm) of purified proteins. Fractions highlighted in red boxes corresponded to c-Src KD. Fractions highlighted in black box corresponded to pYopH phosphatase. Green lines show the buffer gradient. On the right are presented 12% SDS-PAGE gels stained with Coomassie Blue after each purification. **A.** Ni-affinity resin; **B.** anion exchange resin; **C.** size exclusion chromatography. Purified c-Src KD appears at 32.6kDa.

The protein was unphosphorylated and could be autophosphorylated upon incubation with ATP and Mg^{2+} (Figure 2.6).

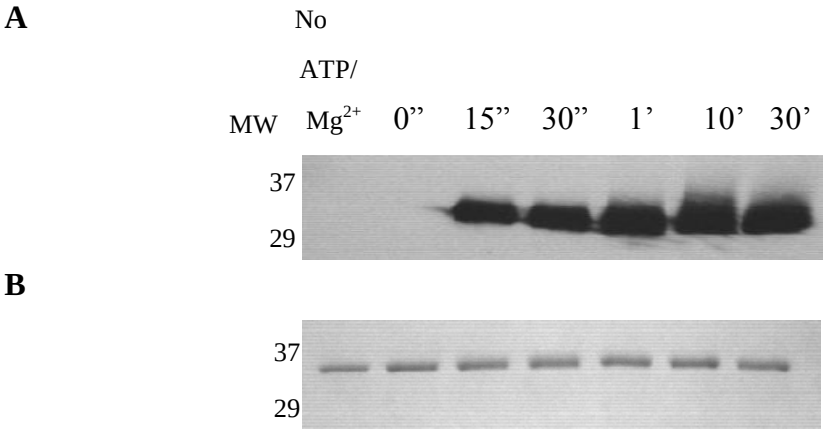

Figure 2.6: Autophosphorylation assay probed with anti-phosphotyrosine antibody 4G10® (Millipore, USA). A. Western blot showing the time course autophosphorylation of c-Src WT purified for ITC at time 0” and at up to 30’ incubation with 20µM ATP and 5mM $MgCl^{2+}$ at 30°C. **B.** Loading control of a) by Coomassie staining**.**

Thermal stability of the protein preparation was significantly increased (T_M=53.4±0.1°C) compared to c-Src purified over two days (T_M=37.6±0.1°C) (Figure 2.4, protocol for ITC) and could reach values that have been measured for the entire c-Src protein and that correspond to the physiological conditions at which chicken c-Src is normally functioning [192].

Improvements at the level of the completeness of c-Src-imatinib binding isotherm and well as on the stoichiometry of the reaction are discussed in Chapter 4, where ITC experiments are presented in detail.

Interestingly c-Src KD from both, standard and ITC purifications was active. Lower thermal stability after a standard purification does not perturb c-Src folding, since such protein purification was used with

success in crystallization (Chapter 4). c-Src KD purified for ITC was not subjected to crystallization within the frames of this work, but differences in the thermal stability of this preparation might be exploited for investigating the influence of protein purification on protein crystallizabilty and conformational prevalence.

4.3. c-Src KD purification for CD

CD studies also required a customization of the purification procedure. Here we have adopted the fast purification protocol as it has been developed for ITC studies since it could generate protein with higher thermal stability. We focused on optimizing two main factors that are important for performing CD studies:

- purity of the sample preparation
- transparency of the buffers.

Protein samples for CD spectroscopy must be highly pure (>95%) by the criteria of high-performance liquid chromatography (HPLC), mass spectroscopy or gel electrophoresis [198]. Any amount of even trace contamination with other proteins may generate unwanted side reactions with ligands or macromolecules and lead to unwanted heat or light polarization effects.

It has been noticed that during the two previously described c-Src purification protocols three proteins were eluted together with the recombinant kinase from the Ni-affinity column (Figures 2.2a and 2.5a). All of them were eliminated after anion exchange chromatography and analytical gel filtration in previous procedures. In the aim to obtain a maximal purity in less purification steps, we have analyzed the protein contaminants and developed faster, two-step purification protocol, generating pure c-Src with no unspecific protein contamination during the purification process.

To determine whether protein contaminants corresponded to proteins that co-purify with 6xHis-c-Src as a complex or alternatively co-elute with 6xHis-c-Src, E.coli BL21 (DE3) transformed with pYopH, but without c-Src, were IPTG-induced and treated using the expression conditions reported above. The lysate was applied to Ni-affinity column and analyzed by gel electrophoresis of the eluted fractions. All three bands were re-appearing on the Coomassie-stained SDS-PAGE, indicating that contaminant proteins corresponded most likely to the over-expressed YopH phosphatase (theoretical mass 50.8kDa) and to two bacterial proteins presumably bound to the metal column that co-eluted with 6xHis c-Src.

Contaminant proteins were identified by Peptide Mass Fingerprint Profiling (PMF). MS analysis has corroborated the presence of YopH phosphatase [169] and has indicated that the two other proteins were from E.coli origin, notably CRP ECO57 (UniProt KB N°P0ACK0) and SlyD (UniProt KB N°P0A9K9), appearing at 23.6 kDa and 20.8 kDa respectively on Coomassie stained SDS-PAGE gels (Figures 2.2a and 2.5a).

SlyD is a nucleotide binding protein in which the incorporation of purine or pyrimidine nucleotides is promoted by bivalent transition metal ions (Zn^{2+}>>Ni^{2+}>Co^{2+}>Cu^{2+}). It has already been described to bind tightly to Ni^{2+}-NTA-agarose due to the presence of several histidines grouped in clusters. This high histidine (and cysteine) density in SlyD supports high affinity binding of bivalent cations, in particular Zn^{2+} and Ni^{2+} [199-201].

CRP ECO57 is a nucleotide binding protein too. Less is known about this protein, but inspection of the primary sequence revealed the presence of a similar histidine reach nucleotide binding motif H^{18}xHxHx^{23} in CRP ECO57 to the one in SlyD (H^{149}xHxHx^{156}). The histidine triad could, in this case, also be involved in binding tightly the Ni-affinity column.

Unspecific binding of YopH phosphatase to the Ni-column was not likely to be a result of its primary sequence since no His- or Cys-clusters are found in this protein. A motif search analysis on the PrositeScan tool showed that YopH sequence does not contain any of the putative metal binding motifs described by Thilakaraj et al. and Sankararamakrishnan et al [202, 203]. Contamination by pYopH during Ni-based IMAC was therefore most probably due to overloading of the IMAC column.

Our first approach to avoid co-elution of c-Src with contaminant protein was to increase the concentration of imidazole in the loading buffer. Having higher affinity for Ni-binding than proteins, imidazole at low concentrations (0mM-50mM) is usually used in loading buffer to avoid unspecific weak binding of contaminant proteins to the Ni-affinity column [204, 205]. SlyD, CRP ECO57 and YopH binding was indeed excluded in presence of 50mM Imidazole into the Ni-affinity loading buffer, but at the expense of a significant decrease in c-Src yields. The amount of protein eluted from the column added up to 5.2 mg compared to 7.7 mg when the protein was loaded in presence of 25mM imidazole (as in the standard procedure) (Figure 2.7).

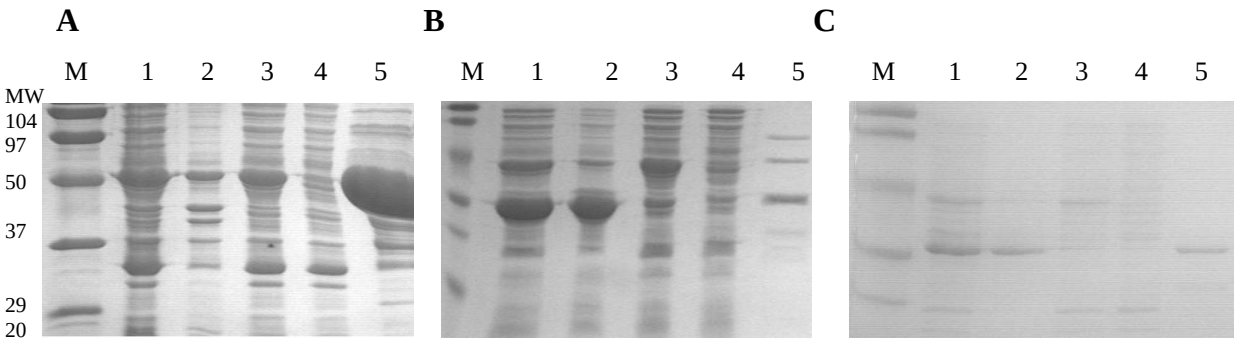

Figure 2.7: Coomassie-blue staining of 12% SDS-PAGE after Ni-IMAC of c-Src co-expressed with YopH phosphatase. Lane M: protei marker; lane 1: total lysate; lane 2: unsoluble fraction; lane 3: soluble franction; lane 4: Ni-IMAC flow-through; lane 5: proteins eluted from the Ni-IMAC resin. **A.** Purification with 0mM imidazole in the loading buffer. **B.** Purification with 25mM imidazole in the loading buffer. **C.** Purification with 50mM imidazole in the loading buffer. YopH phosphatase appears at 50.8kDa; c-Src, at 35.4kDa; CRP ECO57, at 23.6kDa and SlyD, at 20.8kDa.

To preserve elevated amounts of eluted protein after IMAC by obtaining simultaneously highly pure c-Src preparation, we have set up a first step c-Src purification through Co-affinity column. Co-based protein purification resins are known not to bind E. Coli SlyD [205, 206], and indeed, in presence of 25mM imidazole, c-Src was purified at amounts, even higher than after a Ni-affinity purification and without any of the three contaminants mentioned above (Figure 2.8).

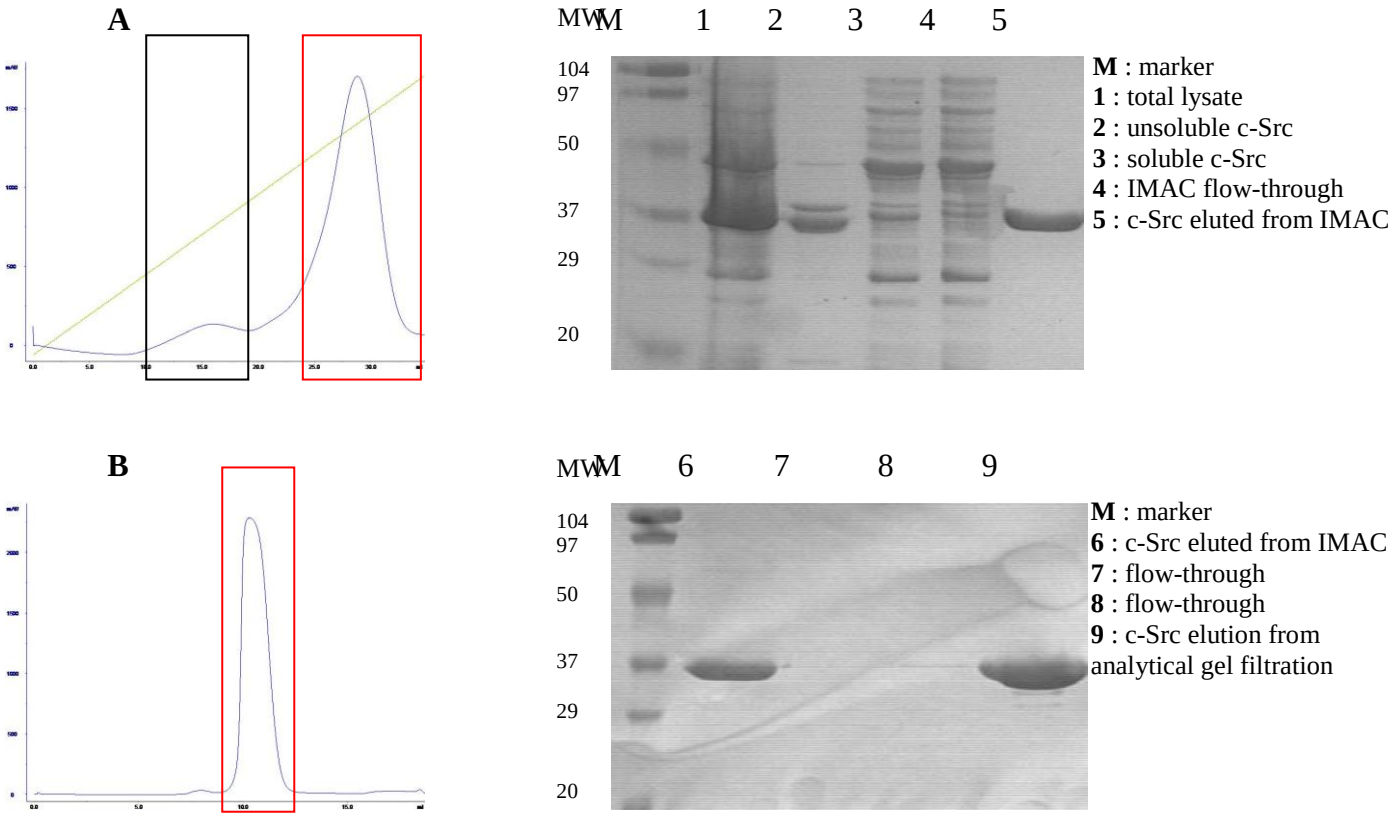

Figure 2.8: Protein purification of c-Src KD for ITC experiments. On the left are shown the chromatograms depicting the absorbance (A=280nm) of purified proteins. Fractions highlighted in red boxes corresponded to c-Src KD. Fractions highlighted in black box corresponded to pYopH phosphatase. Green lines show the buffer gradient. On the right are presented 12% SDS-PAGE gels stained with Coomassie Blue after each purification. **A.** Co-affinity resin; **B.** Size exclusion chromatography. Purified c-Src KD appears at 32.6kDa.

We assume that CRP ECO57 did not bind to the Co-affinity column because of lower affinity towards Co and that higher amount of c-Src bound to the Co-resin impeded YopH contamination.

Given the fact that c-Src eluted from the Co-resin was more than 95% pure (Figure 3.8) and that CD studies were performed without cleavage of the N-terminal 6xHis-tag, the anion exchange purification step was omitted. The kinase domain was submitted directly to a final gel filtration chromatography for exchange against buffers designed for the subsequent CD measurements.

The two-step purification procedure of c-Src for CD studies yielded high amounts of pure, unphosphorylated, active and thermally stable protein (Table 2.3; Figure 2.9 and 2.10), suitable for analysing the impact of c-Src H1-H2 mutations on the structure and stability of the kinase domain (Chapter 4).

Table 2.3: Purification of recombinant c-Src KD. Comparison between original [169] and optimized purification procedure for CD.

c-Src KD mutation	Total protein (mg)		Calculated Mass (Da)	Experimental Mass (Da)	Phosphorylation State After Purification*	Specific Activity* ($M*min^{-1}*mg^{-1}$)**
WT	Lysate	~1000				
	Ni affinity	17.1				
	Ion exchange	7.7				
	Gel filtration	6.8	35344.4	35345.2	Non phopsphoraylated	0.078±0.011
	Lysate	~1000				
WT for CD	Co affinity	11.4				
	Gel filtration	7.2	35344.4	35345.2	Non phosphorylated	0.152±0.013

* Assessed by western Blot and ESI-MS. ** Values are the mean of at least two measures.

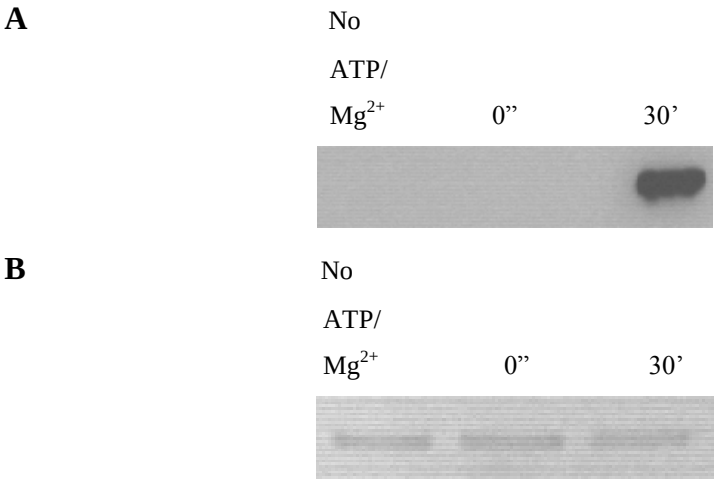

Figure 3.9: Autophosphorylation assay probed with anti-phosphotyrosine antibody 4G10® (Millipore, USA). A. Western blot showing the time course autophosphorylation of c-Src WT purified for CD at time 0” and after 30’ incubation with 20µM ATP and 5mM $MgCl^{2+}$ at 30°C. **B.** Loading control of a) by Coomassie staining.

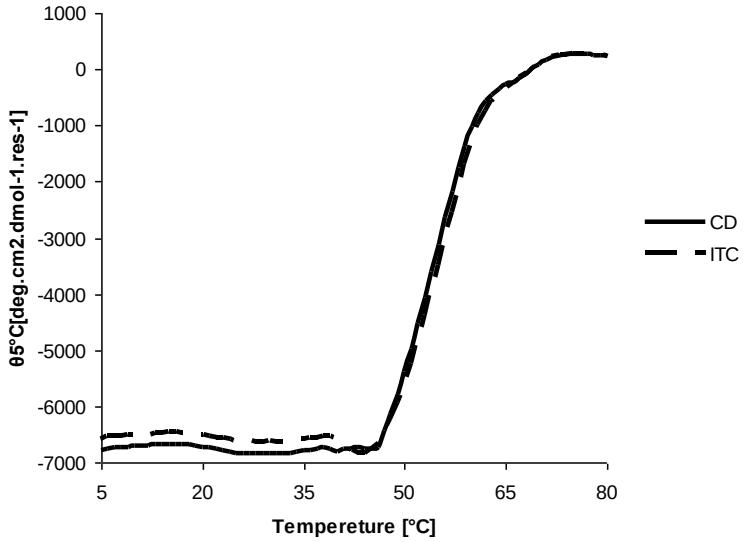

Figure 2.10: Thermal unfolding of uncomplexed c-Src WT KD purified with optimized protocol for CD and of uncomplexed c-Src WT KD purified with optimized protocol for ITC. Unfolding was monitored under the same conditions by CD spectroscopy as described in Materials and methods. Thermal denaturation curves represent the mean of at least 2 measurements and signals are normalized to the buffer. The midpoint of the thermal denaturation curve (T_M) was identical for uncomplexed WT c-Src KD purified for CD and for uncomplexed WT c-Src KD purified for ITC (T_M = 53.4±0.1°C). T_M values were calculated with Spectra Manager (Jasco, Tokyo, Japan).

5. Conclusion

We have presented the vast panorama of c-Src kinase expression and purification techniques. First, a marked emphasis was put in developing techniques for supplying high amounts of pure and active protein for structural and functional studies as well as for inhibitor screening. Over the past decades, understanding kinase physiological role and regulation have confirmed the importance of conformational plasticity on kinase catalysis, specificity and drug resistance. Therefore recent protocols for kinase expression and purification, in particular for c-Src, provide in addition conformationally homogenous protein preparations that consist of an entirely unphosphorylated kinase.

With the aim of studying c-Src KD as case study in understanding mechanisms that control tyrosine kinase domain conformational transition, we have implemented such expression and purification method [169]. We have improved its robustness in obtaining entirely unphosphorylated kinase by adding 1mM EDTA to buffers used in c-Src purification.

We have shown that the optimized purification procedure was providing protein suitable for assays performed at low temperature or over a short time-course like kinetics and crystallization. Kinase yielded by this purification was inappropriate for other biophysical and biochemical assays. Hence, we have established two "tailor made" procedures for c-Src KD purification for ITC and CD. These purification protocols can be a complement to the already adapted c-Src purification method for NMR [169, 207].

Developing specific purification techniques as a function of the subsequent secondary assay read-out might be of big help in implementing different experimental approaches towards protein characterization and in the quest for a better mechanistic understanding of kinase conformational dynamics.

Acknowledgements

We are grateful to Prof. John Kuryian (university of California, Berkeley) for providing the c-Src KD and the YopH phosphatase clones, to Prof. Gérard Hopfgartner for the ESI-TOF MS service, to Andrea Cristiani for useful discussions on the generation of the c-Src mutants and to Sarah-Marie Bendhiaf and Emilio Espinola for contributing to this project in the form of a master's thesis.

CHAPTER 3

Residues within the H1-H2 interface in c-Src putatively controlling the conformational plasticity of the c-Src kinase domain. Site-directed mutagenesis design.

1. Abstract

Conformational plasticity, which allows reversible switching between distinct states of a kinase protein, is a central feature of kinase regulation.

Several in silico and experimental studies [156, 157, 208] have identified hydrophobic interactions as a crucial factor during kinase domain activation.

A recent study on the molecular basis of the whole kinase domain conformational transition has identified virtually a hydrophobic interface formed by a cluster of fourteen amino acids from the N- and the C-lobe of InsR.

To address experimentally the role of the identified H1-H2 interface in kinase domain conformational dynamics and to probe which are the structural and the dynamical effects of replacement of hydrophobic residues of this region, we have identified the H1-H2 interface in c-Src tyrosine kinase.

We have also carried out a rational site directed mutagenesis of c-Src residues from the H1-H2 interface to the corresponding ones in c-Abl in order to investigate on the impact of mutagenesis on conformational stabilisation or dynamics via imatinib binding.

2. Introduction

The idea that a complete description of a globular protein requires not only a static three-dimensional X-ray structure but also an understanding of its flexibility and the role that structural fluctuations may play in protein's function became accepted in the early 80's. At that time Pickover et al. [209] provided some of the first experimental evidences that a globular protein is a fluid, dynamical structure involving conformational fluctuations called "breathing" that allow relatively easy access to buried cavities for small-molecule substrates.

This new vision in protein studies coincided with the discovery of T. Hunter and colleagues who, in 1979, identified the phosphotyrosine as the product of a protein kinase activity in immunoprecipitates of a viral oncoprotein [210].

During the last decades protein tyrosine kinases (PTKs) have been identified as a large family of 93 enzymes that regulate numerous key processes in living cells [103]. All of them transfer the y-phosphate group of ATP to the hydroxyl group of a tyrosine residue from the peptidic substrate and thus control cell division, adhesion and apoptosis.

Multiple sequence alignments identified the catalytic domain as the most conserved part of all tyrosine kinase family members [211, 212]. The catalytic domain also called kinase domain (KD) or SH1 domain was further subdivided into 12 subdomains with conserved secondary structure [212]. This protein domain was also studied extensively under several aspects such as function, regulation, structure and dynamics.

The first X-ray crystal structure of a kinase domain was solved for the Ser/Thr kinase known as protein kinase A (PKA) [106]. To date more than 100 crystallographic apo or ligated structures of the KD are publicly available and demonstrating not only the conserved aspect of the catalytic core but also its exceptional flexibility.

The comparison of the crystallographic structures reveals that the relative position of the two lobes , N- and C-lobe, varies depending on the state of the protein (productive vs. non-productive). Because of this structural phenomenon, PTKs are also known as molecular switches. Principle hallmarks of the kinase domain plasticity seem to be the rotation and bending around the interface of the two lobes. These motions appear to be coupled to the movement of the A-loop, which is supposed to adopt several conformations between the two extreme positions, the "closed" form and the "open" form [104].

Open KD conformations are supposed to be common for all PTKs. They are often similar, stabilized by the phosphorylation of one or several tyrosine residues of the A-loop and are associated with maximal enzymatic activity. The closed kinase domain conformations are more variable among different PTK members since they are not subjected to bind common cofactors (ATP and Mg^{2+}/Mn^{2+}) [118].

Smaller structural changes are revealed at the N-lobe by the relative positions of the C-helix with respect to the β-sheet composed of 5 anti-parallel strands. These motions are supposed to tune the activity via formation of interaction between two conserved residues: the lysine of the third strand and the glutamate from the C-helix. The role of the glutamate is to position correctly the lysine once the latter is bound to ATP.

Important movements are observed for the conserved DFG motif that goes from an Asp-out position in the non-productive state to an Asp-in position in the productive one. This is coupled with the A-loop motion since the DFG forms the N-terminal part of the A-loop. The movement of the DFG serves to align the aspartate of the triad in a position to chelate one of the counter-ions (Mg^{2+}) of the cofactor.

These general mechanisms of the catalytic moiety seem to have evolved with different characteristics for the members of the protein family underscoring the fact that the mechanisms of kinase regulation are as varied as the signaling networks in which these proteins operate. Conformational plasticity which allows reversible switching between distinct states of the kinase is the central feature of these regulatory mechanisms [118, 213].

To understand the molecular mechanism of reversible conformational switching and to gather atomic resolution information about often weak or transient kinase domain interactions with regulating phosphatases and downstream targets, X-ray crystallography data, that provides only static data, has been combined with other techniques that more effectively capture the dynamics of the switching process [118]. In fact, many important structural features of the catalytic pathway may not necessarily be evident from available crystal structures since they may not represent the endpoints of the catalytic pathways but only those stable in crystal packing [207]. Additionally, the activation of protein kinase enzymatic activity may not necessarily involve large changes in conformation that can be characterized by crystal structures alone, but involve changes in dynamics as seen in the case of Eph receptor tyrosine kinase [214].

In this line, several other experimental techniques have been recently used to complete the dynamic concept of the kinase conformational switch.

Time resolved fluorescence anisotropy decay [117] has shed a light on the catalytic dynamics of PKA. Improvements in solution NMR technology and yield optimization in properly folded kinase domain expression have enabled visualization of an important conformational equilibrium within the bacterial histidine kinase NtrC [215] or structural changes upon binding of small molecule inhibitors for members of the Src family kinases (SFK) [207].

Another powerful experimental approach to investigate local and global changes in conformation and conformational mobility in proteins that is successfully applied on protein tyrosine kinases is the Amide Hydrogen-Deuterium Exchange Mass Spectrometry. Using amide H/D exchange MS [208, 216, 217] Ahn and collaborators could identify peptide regions out of the ATP binding pocket that contained an increased flexibility responsive to phosphorylation

In sum, these results provided an experimental evidence for the presence of similar patterns of amino acids involved at different extent in kinase activation.

The concept of conserved structural features implicated in kinase conformational transitions upon kinase domain phosphorylation has been brought up by two important in silico studies as well [156, 157]. The latter describes the surface comparison of active and inactive Ser/Thr and tyrosine kinases concluding that hydrophobic interactions among residues from the N-lobe and the C-lobe of a kinase domain play a significant role in protein kinase plasticity. Hydrophobic interactions seem to be created in a dynamic mode during kinase activation in a way to form “spines” that coordinate the movements of the lobes in the active conformation when the enzyme shuttles through catalysis. Two hydrophobic spines have been described during kinase activation: the C or catalytic spine and the R or regulatory spine (Figure 3.1).

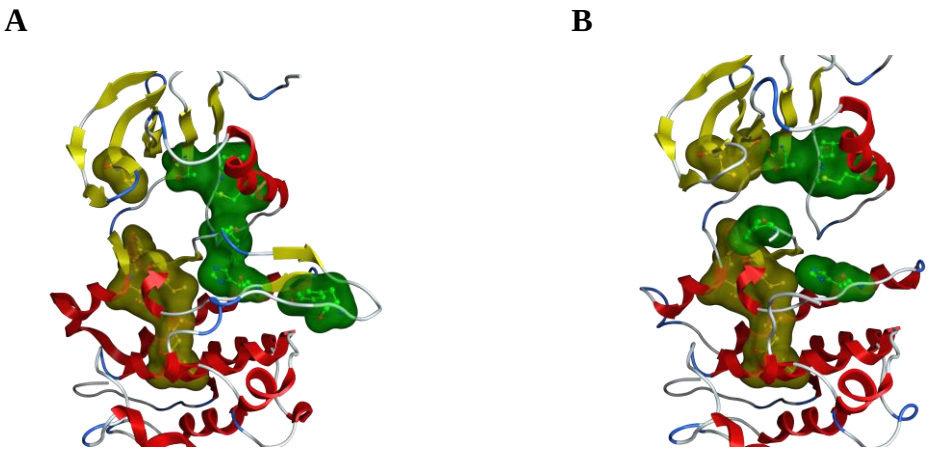

Figure 3.1: R and C spines span the protein kinase core. The hydrophobic part of the R spine is shown as a green molecular surface. The C spine is colored in dark yellow. The adenine ring of ATP (not shown) completes the C spine. **A.** R and C spines in the active conformation of c-Src KD (PDB ID: 1Y57). **B.** R and C spines in the inactive Abl/c-Kit conformation of c-Src KD (PDB ID: 2OIQ). Modified from Kornev et al.

Since the last two studies reported above shed light on the interconnectivity of conserved spatial structures during protein kinase domain activation, a question raised whether there is a correlation between the hydrophobic clusters and the known kinase domain dynamical behavior.

To address this question and to verify whether there are in particular, stretches of amino acids favoring or disfavoring the acquisition of a given conformation throughout the whole catalytic cycle of the enzyme an important work was carried out based on sequence and structure alignment, and on visual inspection of 138 structures of kinase catalytic domains [71].

Observations of the crystallographic structures converged on one hand to the conclusions made by Kornev et al. [218], in particular, to the statement that hydrophobic patterns are similar in the TK family, and on the other hand to the conclusions that structural rearrangements for tyrosine kinases are guided by different dynamical behaviors made by Ahn et al. [208]. Here, observations brought to the definition of two main hydrophobic clusters of amino acids involved together in specific movements and functions:

- The hydrophobic core 1 (H1), defined as the residues taking part of the hydrophobic core of the N-lobe.

- The hydrophobic core 2 (H2), defined as the residues taking part of the hydrophobic core of the C-lobe.

As stated before, the movements of the N-lobe and C-lobe leading to the conformational switch of the kinase domain appeared independent for one hydrophobic core with respect to the other one. This partial freedom in the dynamics of the two lobes prompted the analysis of the interface between H1 and H2 as the putative foundation for KD dynamics.

Thus, based on the crystallographic Insr structures, 6 residues from the H1 and 8 from the H2 were identified and investigated (Figure 3.2). The visual inspection of the two faced regions formed either by residues from H1 or H2, revealed predominant van der Waals contacts and two polar bonds between the oxygen of Ile 1175 and the nitrogen of Val 1187 and between the amino group of Lys1174 and the carboxyl group of Glu1104. Polar bonds have been reported to act as "molecular brakes" around which the remaining hydrophobic parts can change conformation [219].

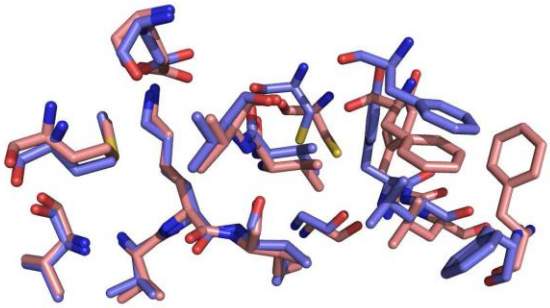

A. Non productive state

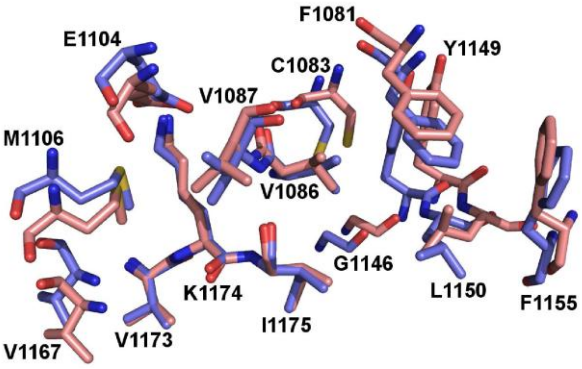

B. Productive state

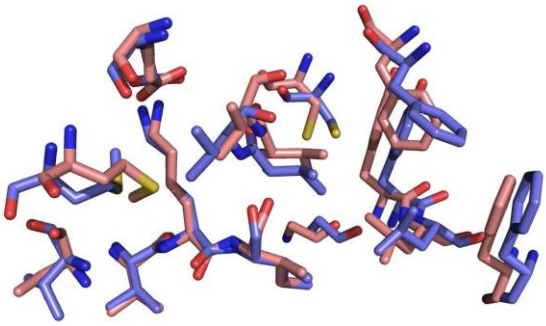

C. Intermediate state

N-lobe residues	C-lobe partners
Phe1081 (1054)	Phe1155 (1128)
	Leu1150 (1123)
	Tyr1149 (1122)
Cys1083 (1056)	Gly1146 (1114)
	Tyr1149 (1122)
Val1086 (1050)	Gly1146 (1114)
	Ile1175 (1148)
Val1087 (1060)	Ile1175 (1148)
	Lys1174 (1147)
Glu1104 (1077)	Lys1174 (1147)
Met1106 (1079)	Val1167 (1140)
	Lys1174 (1147)

Figure 3.2: Structural comparison of H1-H2 interfaces at 0ns and 3ns MD simulation time points for the three KD conformations of the Insr. Residues are depicted in stick representations and color-coded for atoms. Nitrogen is blue, oxygen is red, sulfur is yellow and carbon is light-blue for the conformation at 0ns and light-red for the conformation at 3ns. Labels can be found for the productive state. The structures are superposed for Val 1173, K1174 and Ile 1175. Inset: residues from H1 and their interaction partners in H2. Numbering is set according to the fasta sequence and in between brackets, the corresponding residues from the 1IRK PDB file. Taken from [71].

It appeared that the movements of the N- and the C-lobe have indeed their focus at the H1-H2 interface with changes of the hydrophobic contacts and with conservation of the polar "molecular brake" interactions. Since major rearrangements of this area cannot be expected because of the two electrostatic bonds, this study inferred that small variations within the H1-H2 interface would account for larger ones at the far extremities of the protein structure.

This hypothesis seems to be indirectly proved by the highly conserved nature of the residues of the H1-H2 interface. Interestingly, the variability of such positions is appreciated within the family of TKs (Table 3.1) and with a lower extent among elements of the same subfamily, which was pointed out as a major factor for the diversity at the level of the dynamical behavior for kinase domains.

Table 3.1: Comparative table for corresponding H1 and H2 residues in Insr, Egfr, Src and Vgfr kinase domains. Residues belonging to the H1 and H2 interface in c-Src are in bold.

Insr	Egfr	**c-Src**	Vegfr
F_{1081}	V	**L**	I
C_{1083}	N	**H**	H
V_{1086}	V	**L**	V
V_{1087}	C	**V**	V
E_{1104}	Q	**E**	E
M_{1106}	M	**M**	C
G_{1146}	G	**G**	G
Y_{1149}	Y	**Y**	F
L_{1150}	L	**V**	L
F_{1155}	L	**Y**	C
V_{1167}	V	**V**	L
V_{1173}	V	**C**	V
K_{1174}	K	**K**	K
I_{1175}	I	**V**	I

Thus, both Kornev and Moretti confirmed *in silico* the role of kinase domain residues involved in hydrophobic interactions in influencing the dynamics of the tyrosine kinase catalytic domain.

Our knowledge on the role of kinase domain residues on the plasticity of the enzymatic core was recetly enlarged by the work of Seeliger et al. performed experimentally on c-Src KD [155]. In the latter study, c-Src kinase domain was found to bind to the cancer drug imatinib in the micromolar range, with an inactive Abl/c-Kit conformation [220] and a distributed thermodynamic penalty. Attempts to increase the affinity of c-Src for imatinib by swapping residues of the ATP binding pocket with the corresponding residues in Abl have not been successful. The reported results suggested that the residues that regulate the conformational balance in c-Src are located far from the ATP-binding site.

Therefore the identification of clusters of hydrophobic residues involved in KD plasticity raised the following questions:

- Which are the structural and the dynamical effects upon replacement of hydrophobic residues from the H1-H2 interface?

- Could amino acid variations from the latter regions account for different molecular pathways in the transition from active to inactive kinase conformation?

- Could amino acid disparity from the latter regions influence tyrosine kinase regulation and substrate specificity?

Therefore our strategy to identify experimentally kinase domain residues dictating the kinase conformational plasticity was to perform a mutagenesis study in which the identified residues from the H1-H2 interface of Insr and Abl (all situated far from the ATP-binding site) were compared to the corresponding ones in c-Src kinase domain after a sequence and a structural alignment.

Several reasons guided our choice to c-Src kinase domain for this work. c-Src is actually one of the best studied members of the tyrosine kinome since its encoding gene, c-src, has been described as the first human proto-oncogene. During last decades, data on c-Src have shown that, at the level of the kinase domain, the structural basis of c-Src catalytic activity lies on the capability of the kinase domain to adopt two extreme conformations that can be related to the activation state of the kinase.

So far, over 30 different c-Src protein kinase structures have been solved, providing a general understanding of the reversible switch between distinct states of the kinase. Classified according to the three-dimensional occupation of the structural determinants (DFG, A-loop, Glu310 in the αC-helix) [100]. c-Src structures are hence available in their active [124], intermediate [119] and in inactive state [155].

In addition to the wealth of available structural information, c-Src kinase domain represents a good case study because of the possibility to be expressed quickly, in milligram amounts and in its unphosphorylated state [169], giving the prospect to combine mutagenesis studies on the H1-H2 residues with additional biophysical and biochemical studies on the generated mutants as described in chapters 4 and 5.

3. Materials and methods

All chemicals were purchased from Applichem, Germany, except if otherwise indicated.

3.1 Rational design of c-Src kinase domain site point mutants

The mutations were designed in order to swap residues from c-Src located at the H1-H2 hydrophobic interface between the N-lobe and the C-lobe to the corresponding ones in c-Abl, c-Kit, PDGFR, DDR1, DDR2 and Syk tyrosine kinase domains.

First we structurally aligned on Bodil v 0.8.1 [221] available crystal structures of INSR (1IRK [222] and 1IR3 [223]) to crystal structures of c-Src (1Y57 [124], 2SRC [119], 2OIQ [155]) to identify amino acids involved in the c-Src H1-H2 interface since the hydrophobic interface has been first described for the InsR tyrosine kinase [71]. Structural alignments were also performed for c-Abl [181], c-Kit [220] and Syk [224] tyrosine kinase domains against mentioned crystal structures of InsR. All crystal structures were retrieved from Protein Data Bank (PDB) [225].

Furthermore, we retrieved the amino acid sequences of chicken c-Src, human c-Abl, c-Kit, human PDGFR and human Syk from UniProtKB database, release 14.8 [226], under the following accession numbers: P00523, P00519, P10721, P09619, and P06213. A multiple sequence alignment was carried out using Clustal W [227]. Then the fourteen amino acids located at the hydrophobic interface of InsR were identified in the remaining kinases and the numbering was changed to the one of chicken c-Src.

In total 8 c-Src mutants were designed for c-Src (Figure 3.3).

The Leu at position 317 from the H1 interface was swapped to Ile (1), since the latter is found in c-Abl. The L317I mutation was combined with a replacement of a Val at position 377 from the H2 interface to the corresponding Leu in c-Abl, c-Kit and PDGFR to generate a double mutant (2). Another double mutant was designed to contain the L317I mutation in combination with a Leu322 mutated to Ile as in c-Kit (3). The swap of a Val 377 to Leu from the H2 interface was also used to produce a single c-Src mutant V377L (4). The exchange of a L322 to Ile was also used to produce a single c-Src mutant L322I (5). Another single mutant was constructed by inserting a Gly at position 318, since a glycine residue is present at the H1 interface in c-Kit and PDGFR but not in c-Src (6). Then the G318 insertion was combined with the V377L mutation to generate the double mutant G318-V378 (7). A triple c-Src mutant was designed to contain G318-L323I-V378L mutations (8). Finally, L407G was made since it has been published as the point mutation decreasing the most the thermodynamic penalty in c-Src KD [155] (9).

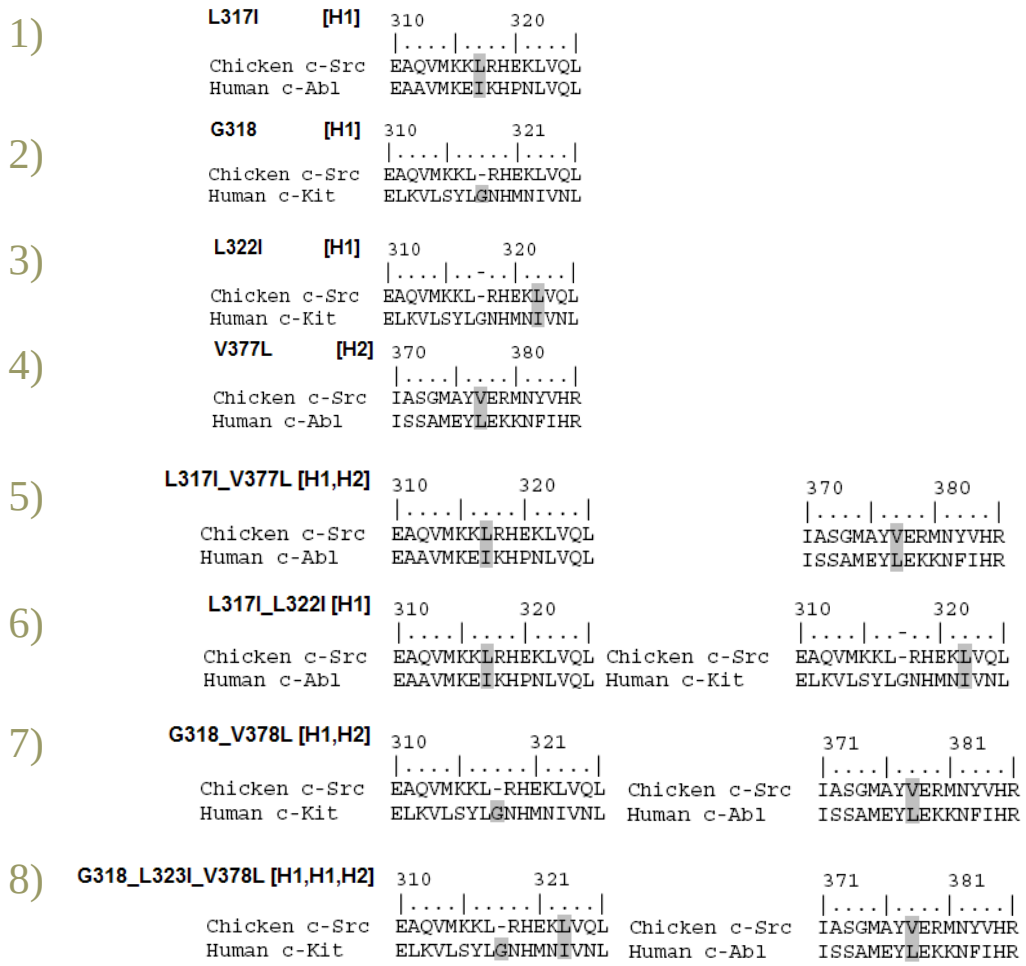

Figure 3.3: Designed mutations and local sequence alignments of chicken c-Src, human c-Abl, human c-Kit and human PDGFR (1-8). Insertion and swapping of amino acids of c-Src to the corresponding ones in c-Abl, c-Kit or PDGFR are depicted in grey bars for each c-Src mutant. The localization of each mutation at the H1 or H2 interface or both is shown between brackets. Sequence alignments were conducted on ClustalW2 [227].

3.2 Site-directed mutagenesis

The kinase domain construct of chicken c-Src, residues 251-533 (GenBank N° V00402), cloned into pET-28a (+) (Novagen) as well as the construct in pCDFCuet-1 (Novagen) for co-expression of full length pYopH phosphatase, were a kind gift from Prof. J. Kuriyan, University of California, Berkley, USA [155].

Mutants of c-Src kinase domain were generated by *in vitro* site-directed mutagenesis. Oligonucleotides were designed using PrimerX [228] and Oligocalc [229] and were synthetized by Microsynth (Balgach, Switzerland) (Table 2.2). All reactions were performed in 50µl reaction mixture and contained 5ng of plasmid pET-28a (+) *c-src* wild type, 2.5U of Pfu DNA Polymerase, Pfu Buffer 10x (Promega, USA), 50pmol of both forward and reverse primers, 0.25 mM of deoxynucleotide triphophosphate (dNTPs) mix (Promega, USA) and 5% Glycerol.

The Polymerase Chain Reaction (PCR) was carried out in a thermocycler Techgene TC-312, Techne, UK. The initial denaturation at 94°C for 2min. was followed by 18 PCR cycles each consisting of denaturation at 94°C for 30sec. , annealing at 52°C for 1 min. and extension at 68°C for 14min. The final extension was at 68°C for 8min. The parental plasmid containing *c-src* wild type was digested at 37°C for 1.5 hours with 1µl of DpnI (NEB, USA) applied directly to the PCR reactions. Mutated plasmids were purified using GenElute PCR Clean-Up Kit (Sigma, USA) and eluted with 10µl of 10% Elution buffer in ddH_2O.

The entire volume of purified plasmid (10µl, ~100ng DNA) was used to transform 60µl competent NovaBlue *E. Coli* cells (Stratagene, USA). Transformed cells were plated on LB agar plates containing 50µg/ml kanamycin and incubated overnight at 37°C.

Table 3.2: Primer sequences for the construction of c-src kinase domain mutants by site directed mutagenesis. Mutated codons are underlined. First six mutants were generated in one PCR reaction. Among the mutants marked by an (*), double mutants were produced in two PCR steps: first a single mutation was introduced and afterwards, this construct was used as template for the second mutation. The triple mutant was created by using construct coding for c-Src V377L as template.

	Mutation	Sence	Primer sequence 5´→ 3´
1)	L317I	Forward	CCCAAGTGATGAAGAAGATCCGGCATGAGAAGCTGG
		Reverse	CCAGCTTCTCATGCCGGATCTTCTTCATCACTTGGG
2)	G318	Forward	CCAAGTGATGAAGAAGCTCGGACGGCATGAGAAGCTGG
		Reverse	CCAGCTTCTCATGCCGTCCGAGCTTCTTCATCACTTGG
3)	L322I	Forward	CCGGCATGAGAAGATTGTTCAGCTGTACGC
		Reverse	GCGTACAGCTGAACAATCTTCTCATGCCGG
4)	V377L	Forward	CGGCATGGCCTATTTGGAGAGGATGAACTACG
		Reverse	CGTAGTTCATCCTCTCCAAATAGGCCATGCCG
5)	L317I_V377L*		
6)	L317I_L322I*		
7)	G318_V378L*		
8)	G318_L323I_V378L*	Forward	GCTCGGACGGCATGAGAAGATTGTTCAGCTGTACGCAGTGG
		Reverse	CCACTGCGTACAGCTGAACAATCTTCTCATGCCGTCCGAGC
9)	L407G	Forward	GGCTGACTTTGGGGGGGCACGCCTCATCG
		Reverse	CGATGAGGCGTGCCCCCCCAAAGTCAGCC

Changes were confirmed by forward anr reverse DNA sequencing performed at Microsynth (Balgach, Switzerland). Obtained electropherograms were verified using Chromas 2.31 (Technelysium Pty Ltd., Queensland, Australia), and edited using Bio Edit v7.0.0 [230]. The comparison between electropherograms was carried out with CodonCode Aligner 2.0.6 [231].

5ng of the purified plasmids containing the designed mutations on the *c-src* construct were then co-transformed into 60ul competent BL21 (DE3) *E. Coli* cells (Stratagene, USA) containing a pCDFDuet-1 plasmid (Novagen, USA), carrying already a construct for pYopH phosphatase.

4. Results and discussion

With the aim to identify key amino acids that dictate the transitions from active to inactive tyrosine kinase domain conformation, we have based our work on recent in silico finding describing two clusters of residues within the kinase domain forming hydrophobic interactions that are alike to play a central role in the molecular control of kinase plasticity.

A deeper observation of the hydrophobic cores of the N-lobe and of the C-lobe in Insr, revealed a special conformation of 14 residues at the interface (Figure 2.2). To verify whether these residues are involved in the dynamical behaviour of tyrosine kinases experimentally and also whether variations of these amino acids at the sequence level may confer differences in kinase activity and enzyme regulation, we constructed nine mutants within the kinase domain of c-Src, which was used as a case study.

Sequence and structure alignments of c-Src KD against the kinase domain of InsR allowed the identification of the amino acids constituting the hydrophobic interface in c-Src (Figure 3.4).

From the 14 residues forming the H1-H2 interface in c-Src, 8 residues were conserved in respect to INSR and 7 were different.

A visual inspection from the inside of c-Src of the two faced regions, formed by either residues from H1 or H2, revealed the formation, as for INSR, of two planes and sort of paws looking the back side (Figure 3.5).

A

Interface	INSR 1IRK	c-Src 2OIQ	c-Abl 1OPJ	c-Kit 1T46	Syk 1XBB
H1	F_{1081}	L_{317}	I_{293}	L_{647}	L_{427}
H1	C_{1083}	H_{319}	H_{295}	H_{650}	N_{429}
H1	V_{1086}	L_{322}	L_{298}	I_{653}	I_{432}
H1	V_{1087}	V_{323}	V_{299}	V_{654}	V_{433}
H1	E_{1104}	E_{339}	E_{316}	E_{671}	E_{449}
H1	M_{1106}	M_{341}	M_{318}	C_{673}	M_{450}
H2	G_{1146}	G_{373}	A_{350}	G_{779}	G_{481}
H2	Y_{1149}	Y_{376}	Y_{353}	F_{782}	Y_{484}
H2	L_{1150}	V_{377}	L_{354}	L_{783}	L_{485}
H2	F_{1155}	Y_{382}	F_{359}	C_{788}	F_{490}
H2	V_{1167}	V_{394}	V_{371}	L_{800}	L_{502}
H2	V_{1173}	C_{400}	V_{377}	T_{806}	A_{508}
H2	K_{1174}	K_{401}	K_{378}	K_{807}	K_{509}
H2	I_{1175}	V_{402}	V_{379}	I_{808}	I_{510}

B

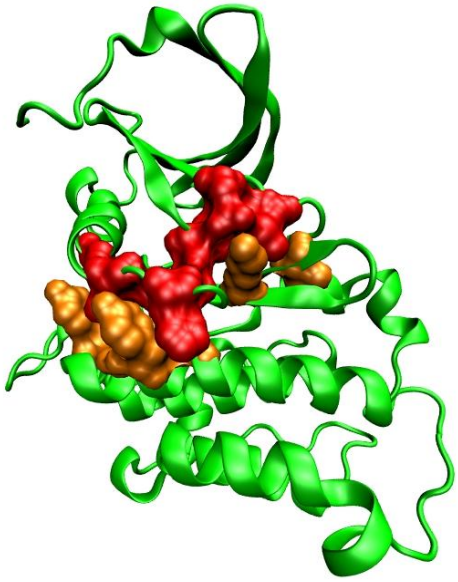

Figure 3.4: The H1-H2 interface in c-Src. A. Residues constituting the hydrophobic interface in InsR, c-Src, c-Abl, c-Kit and Syk KDs identified by comparative sequence (Clustal W) and structural alignment (Bodil, v 0.8.1). Residues from the H1 hydrophobic core are indicated in red and residues from the H2 core are in orange. **B.** The location of the H1(in red) and H2 (in orange) within the 3D structure of c-Src KD (in green).

In details, K401 and Y376 from H2, both well conserved, embed H1 by holding H319, V313 and V323. In the case of c-Src, H319 replaces the Cys 1056 from InsR. This substitution is frequent in the PTK family and remains possible since the counterpart of the hydrophobic interaction that takes place in this position is the highly conserved Gly 373. Glycine at this position is needed to allow the movements of the H1 without sterical hindrance. The "molecular brake" between a glutamate and a lysine is also conserved in c-Src, in respect to INSR (E339 (H1) and K401 (H2)) [219].

A

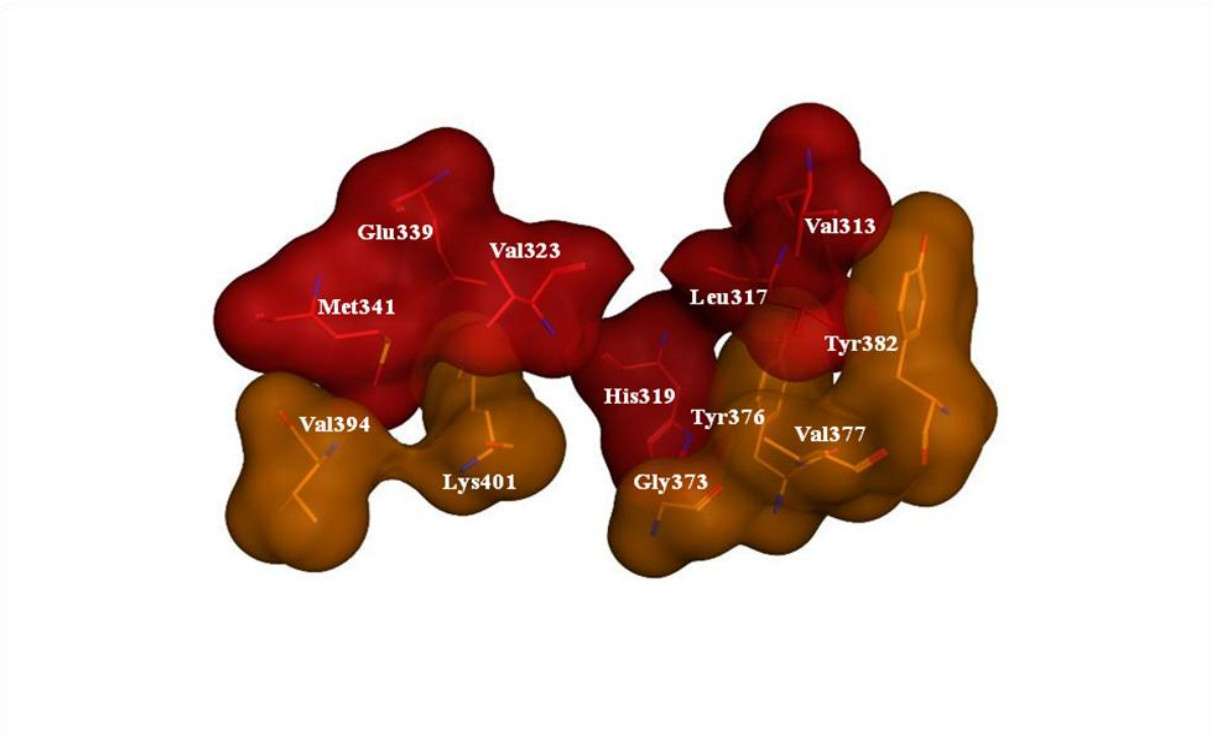

B

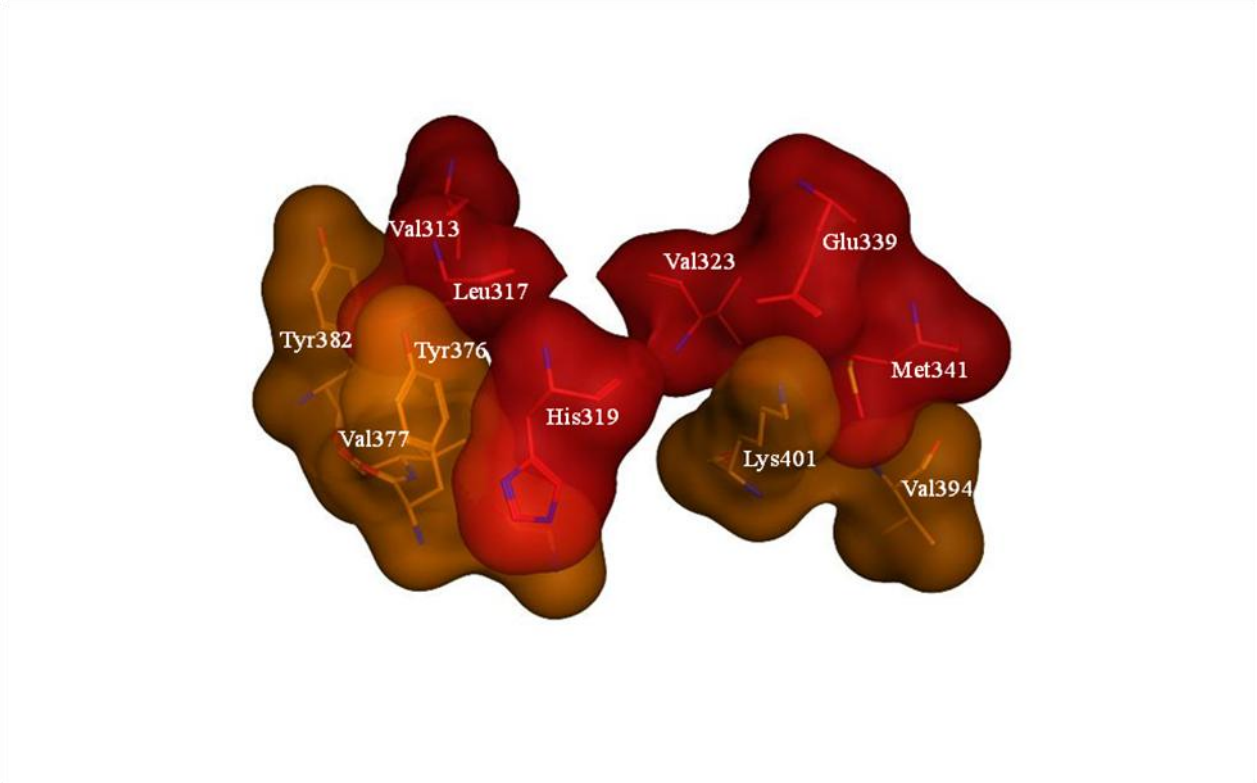

Figure 3.5: H1-H2 interface in the active c-Src KD (PD ID: 1Y57). A. The residues found at the interface are represented as balls, labelled and color-coded for atoms: orange for carbon, red for oxygen, blue for nitrogen and yellow for sulphur. The surfaces for the atoms are also color-coded for clusters, dark yellow for H1 and red for H2. **B.** A view of the H1-H2 interface after rotation of 180°C compared to **A.**

When comparing the variations of the interaction pattern for the defined interface between the non-productive and productive InsR (1IRK and 1IR3, respectively), the major rearrangements were observed for Phe1054, Leu1123 and Phe1128. Interestingly all these three amino acids are different in c-Src (L317, V377 and Y382, respectively).

Further sequence and structure comparison was then conducted for c-Src against all tyrosine kinase domains that are inhibited in the nanomolar range by imatinib (c-Abl and c-Kit) (Figure 3.4). PDGFR, DDR1 and DDR2 tyrosine kinases, which are also inhibited in the nanomolar range by imatinib were not included in the analysis since any crystal structure or molecular model was publically available at the time point of this part of the study. Syk tyrosine kinase was used as a "negative control" within the alignments since Syk is known to be resistant to imatinib inhibition.

Sequence and structure evaluation of the H1-H2 interfaces of c-Abl, c-Kit, PDGFR pointed to a similar pattern. The Glu-Lys "molecular break" was conserved, as well as residues corresponding to H319, V323 in the above mentioned kinases. Y376 was conserved in c-Abl. Here again, the residues L317, V377 and Y382, were not conserved between c-Src and c-Abl. Interestingly, from these three residues only the Leu at position 317 was conserved within c-Src and Syk KD (both resistant to imatinib inhibition) but different (Leu→Ile) between c-Src and c-Abl. Residues at positions 377 and 382 (according to c-Src numbering) were the same for c-Abl and for the "negative control" Syk KD.Thus, the rational design of site point mutants in c-Src consisted in single mutants or a combination of mutations of L317 and V377.

All point mutations were successfully performed as shown on the electropherograms after DNA sequencing of c-src mutants in Figure 3.6 and no frameshift or additional mutations were observed for any of the constructs.

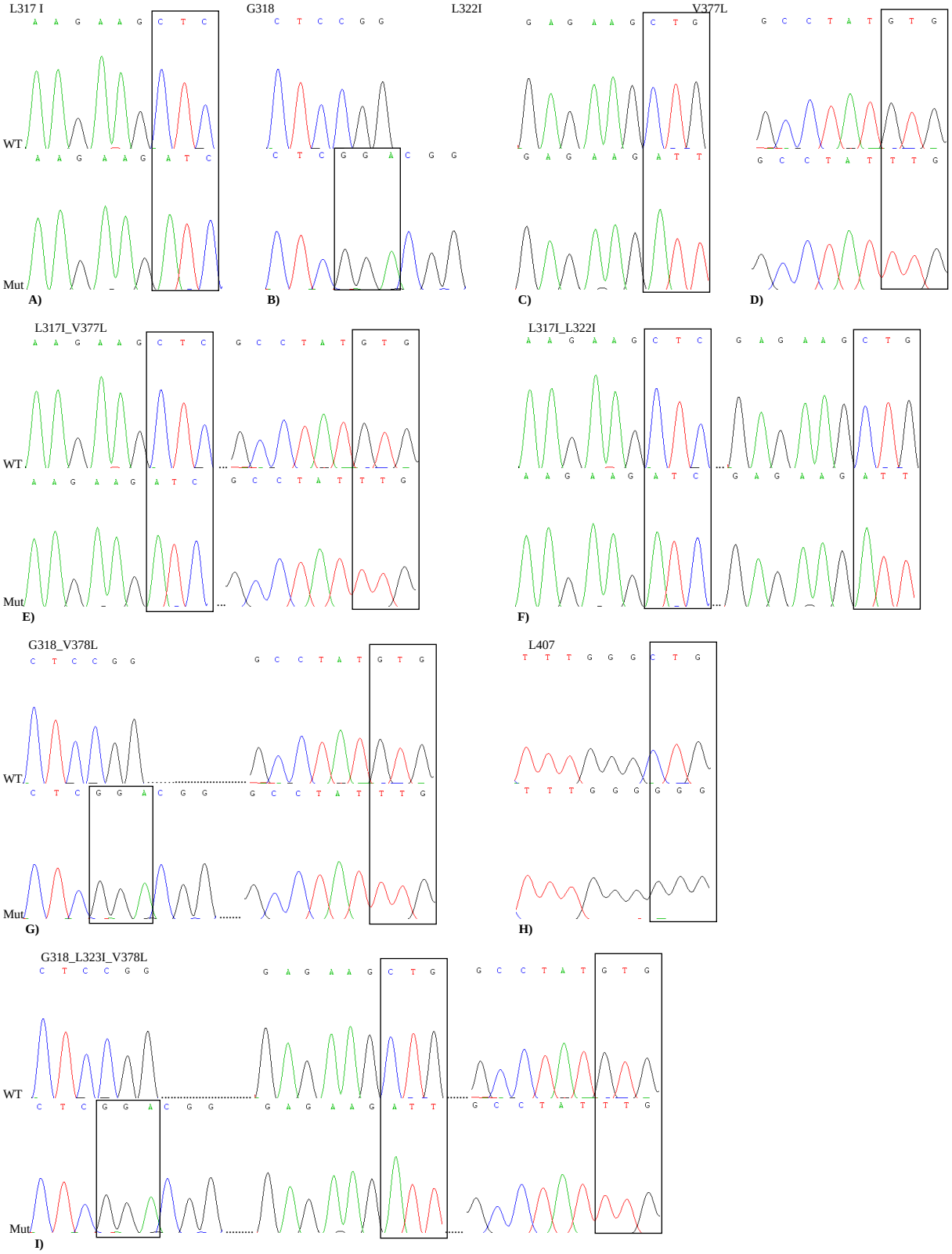

Figure 3.6: Extract of electropherograms after DNA sequencing of c-Src mutants. Each mutant is compared with *c-src* wild type. Mutated codons are shown in frame. **A.** L317I **B.** G318 **C.** L322I **D.** V377L **E.** L317I_V377L **F.** L317I_L322I **G.** G318_V378L **H.** L407G **I.** G318_L323I_V378L.

5. *Conclusion*

It is often postulated that protein motions contribute conformationally and entropically to enzyme catalysis, however relatively little is known about how this really occurs.

By looking at the several structures of kinases in different conformations that are available to date, we have the same impression of their dynamics as if we were looking at a flipbook: sequential stages of the kinase domain movement would create the optical illusion of movement when flipped rapidly, but the mechanism leading the dynamics of the switching process remains elusive. Unfortunately, an experimental technique that can provide a fully detailed molecular analysis of the time evolution in c-Src plasticity is not yet available. This brought our attempts to identifiy the amino acid residues influencing the transition from active to inactive kinase conformation.

Therefore, based on recent *in silico* [156, 157] and *in vitro* [155] studies, we presented here the hypothesis that residues having a key role within the kinase domain dynamics might be located far from the ATP-binding site and might regulate the kinase dynamics via a network of hydrophobic interactions at the interface between the N-lobe and the C-lobe of the kinase domain.

The importance of the amino acids at this interface was addressed by mutagenesis studies and c-Src KD was used as a case study. Thus, the hydrophobic interface was described in c-Src. Eight mutated c-Src KD expression constructs carrying single or coupled mutations within the identified H1-H2 interface were successfully produced by site-directed mutagenesis.

CHAPTER 4

Biochemical and biophysical studies on c-Src tyrosine kinase domain mutants

1. Abstract

In this chapter we report the first experimental approach in understanding the role of H1-H2 residues in the conformational plasticity of c-Src kinase domain *in vitro*. We aimed on answering to the following questions: do residue(s) from the H1-H2 interface influence the thermodynamic penalty conformation of Src for imatinib and how?

To address these questions we have subjected c-Src KD mutants to two main types of biophysical and biochemical protein assays. The first category of protein assays (*i.e* kinase assays, inhibition assays) investigated on the dynamical influence of H1 and H2 residues and was conducted in presence of elements essential for c-Src catalysis: Mg2+, ATP. The second category of protein assays were meant to follow the role of c-Src H1 and H2 mutants on c-Src KD conformational prevalence and were referred to as "static" assays (*i.e* ITC, crystallization and CD).

We could show that residues mainly from the H1 and to a lesser extent from the H2 interface are involved in the regulation of the kinase domain conformational plasticity. These amino acids influence the kinase conformational transition mainly at the level of the the DFG-motif mobility via hydrophobic interactions with the H1 residue at position 317 (c-Src numbering). When L317 in c-Src was replaced by the corresponding Ile in c-Abl, the rate of the DFG flip increased. In consequence, c-Src L317I showed a c-Abl-like sensitivity for imatinib (nanomolar range).

We discuss on the naturally present in primitive multicellular organisms c-Src L317I ortholog and support the hypothesis that it may be considered as an index for the evolutionary history of Src. We believe that its identification can be considered as an important step towards understanding the dynamical aspect of protein tyrosine kinase plasticity.

2. Introduction

About 2% of all human genes encode protein kinases [95], enzymes that play key roles in transducing cellular signals regulating cell growth, differentiation, proliferation migration and survival [94, 232-234]. Given the essential aspect of kinases in cell regulation, it is not surprising that the protein kinase catalytic domain is the protein domain the most commonly encoded by known cancer genes [235], and that protein kinases constitute one of the leading families of drug targets [236].

The kinase catalytic domain is highly conserved among protein kinases with an average sequence identity of about 30% between any two sequences [237]. Its two- subdomains architecture consists of an N-terminal lobe, with five-antiparallel-stranded β-sheets and one prominent α-helix (αC helix), and a C-terminal lobe, with mainly α-helixes. The flexibility of this catalytic domain allows a complex auto-regulatory mechanism.

Crystallographic x-ray structures of human tyrosine kinase domains in different conformations allow clear structural distinctions to be drawn between the inactive and the active states (Figure 4.1). The major movements are observed for three protein elements also referred to as "structural determinants": C-helix, A-loop and P-loop, and seem to be coupled. A switch in one necessitates a switch in the other [118].

The A-loop undergoes a structural change from a closed conformation where it collapses within the active site and blocks the binding of both ATP and substrate, to an opened state where it moves away from the catalytic center aside to the C-lobe [118]. At the N-terminal of the A-loop, the DFG triad switches from Asp-in to Asp-out (described in Chapter 5).

The P-loop, which is made very flexible by the presence of three highly conserved Gly residues, also undergoes a transition from a closed to an open conformation to facilitate sterically the binding of ATP [238].

The C-helix moves in order to bring its conserved Asp towards the active site for coordinating the interaction between a Magnesium cation and the α- and β-phosphate groups of ATP. The conformational change of this element is characterized by two extreme positions: the "swung-in" position towards the mouth of the protein during catalysis and the "swung-out" position, reached with a combination of movements and rotations around its own axis, out of the protein core [115, 239].

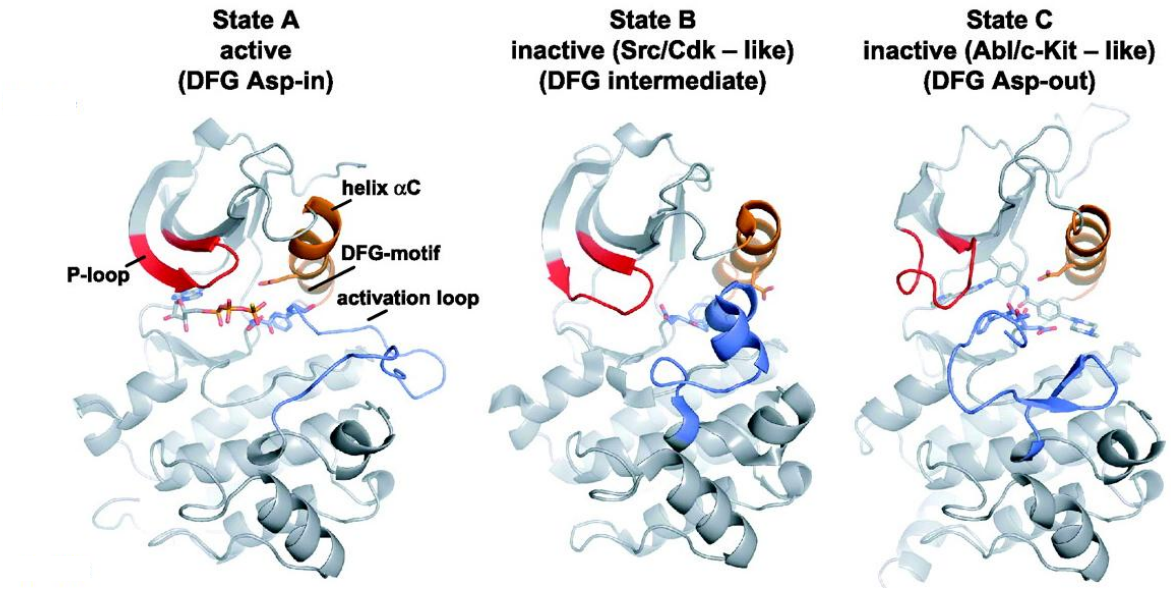

Figure 4.1: Structurally defined conformational states of the c-Src and c-Abl kinase domains. Red, P-loop, orange, αC-helix, blue, A-loop. **State A**, active c-Src kinase (PDB entry 3DQW; [154]); **state B**, inactive c-Src/Cdk-like conformation (PDB entry 1QCF, [120]); **state C**, Abl/c-Kit-like conformation (PDB entry 1OPJ, [181]) with the DFG motif flipped conformation relative to states A and B. Modified from [240].

Given the high sequence similarity at the level of the kinase domain and especially at the level of the ATP-binding site [241], three dimensional structures of different kinase domains in similar conformational states are exploited in rational drug design when structural differences are used to achieve inhibitor specificity. Typically, structural diversity between kinases tends to be larger when the inactive state is targeted [242, 243]. The latter observation has been successfully used for the development of ATP-competitive inhibitors of tyrosine kinases [244, 245]. A major problem encountered with such specific inhibitors is the acquisition of resistance through mutations in the kinase gene that abrogate drug binding. Picturing how the kinase domain dynamically switches from one state to another would allow answering whether there are structural elements other than the A-loop, the P-loop and the C-helix involved in this process. Thus, identifying new key residues or interactions that regulate kinase activity is of great interest for overcoming bottlenecks in kinase inhibitor research, such as limited selectivity and drug resistance [244, 245].

X-ray structures, though rich in information about the two end-points of the structural transition, do not show how the conformational shift occurs and how it might be regulated [168]. One challenge for experiments to obtain the dynamic information is that the conformational switching process is inherently transient [246]. To relate these static structures to the function, the dynamics of protein motion is required to fully monitor the conformational change process [55, 247-249].

The molecular description of the activation of kinase domain has been attempted by computational [246, 250] and furtively by experimental means. A number of these studies report the existence of hydrophobic interactions in the kinase domain that organize the catalytically important residues for the phosphotransfer reaction [156, 157, 251, 252].

By comparison of the distribution patterns of residues of the kinase domain in the active and inactive conformations of many tyrosine kinases, Kornev et al., discovered that four conserved hydrophobic residues in the kinase domain are assembled as a "spine" when a kinase adopts an active conformation. When inactive conformation is adopted, the hydrophobic spine is disassembled [156, 157]. In line with this observation, Bukhtiyarova et al. reported that mutation of one of these four residues in p38 MAP kinase (Phe 185 to Ala, Arg or Gly) completely abolishes the catalytic activity of the kinase [253]. Furthermore, mutation of a Thr338 to a hydrophobic residue in c-Src, PDGF receptor α and β and EGF receptor experimentally increases kinase activity, since it is likely that Thr338 interacts with the hydrophobic spine and influences its assembly [154].

The trend that hydrophobic interactions are fundamental features for the dynamical behaviour of tyrosine kinases was also described in a parallel study by Moretti et al. (cf. Chapter 2). The latter study reported the presence of an H1-H2 interface formed mainly by the hydrophobic interactions of residues from the N- and the C-lobe as the initial point for kinase conformational transition [239].

To validate experimentally the findings described by Moretti et al, we have used c-Src tyrosine kinase as case study and imatinib as conformational reporter.

The kinase domain of c-Src shares 47% sequence identity with c-Abl KD. Nevertheless imatinib binding to c-Src is 2400 times weaker than imatinib-Abl binding [155]. The poor Src-imatinib binding structurally lies on the orientation of the DFG motif. In the unphosphorylated c-Src crystal structure (PDB ID: 2SRC), the DFG backbone shares the same DFG-in orientation as the active c-Abl.

Thus, the Phe side chain overlaps the imatinib-binding site and confers a "thermodynamic penalty" for imatinib to bind c-Src KD (Figure 4.2). Src-imatinib binding could not be increased by mutating residues in direct contact with imatinib [155].

Therefore, our hypothesis was that if we mutate a residue(s) from the H1-H2 interface of c-Src to the corresponding one(s) of c-Abl, this would increase Src-imatinib binding by rendering the conformational equilibrium of c-Src similar to the one of c-Abl.

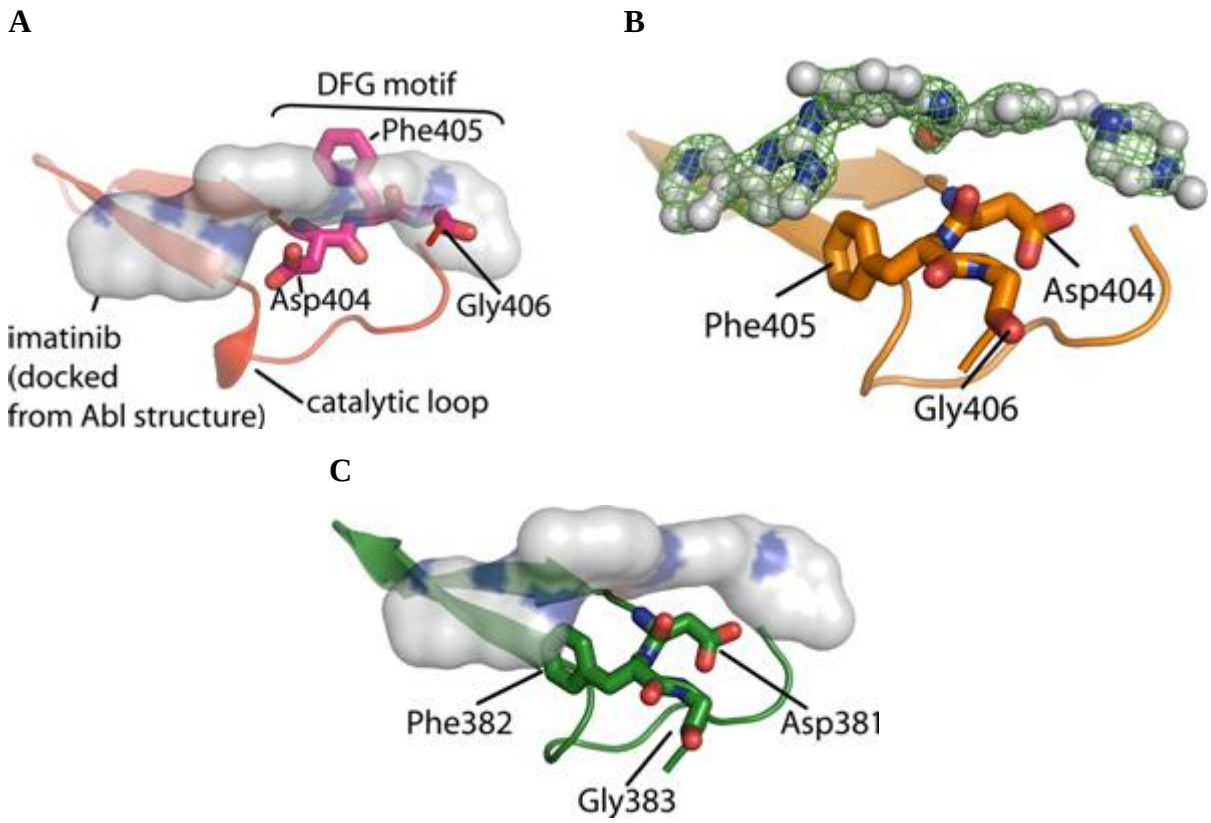

Figure 4.2: The DFG Motif Flip. A. The surface of imatinib bound to Abl (PDB ID: 1OPJ) is shown and is superposed upon inactive c-Src in the Src/CDK or DFG-out conformation (PDB ID: 2SRC). **B.** The c-Src- imatinib complex (PDB ID: 2OIQ). **C.** The Abl-imatinib complex (PDB ID: 1OPJ). For the c-Src-imatinib complex, electron density for imatinib is shown calculated before imatinib was included in the refinement and contoured at 3σ. Protein structures were aligned on the Cα atoms of the displayed Abl fragment (Abl residues 380-403, PDB code 1OPJ) Modified from [155].

Recently, indeed, NMR experiments on a related kinase, p38, showed that the DFG-in and the DFG-out conformations were in dynamic equilibrium over fairly short time-scales (milliseconds) [254]. An x-ray structure revealed that the two inactive conformations could coexist in the same crystal [254]. Both c-Src and c-Abl can interconvert between two inactive conformations, and Abl-like DFG-out conformation and a DFG-in c-Src-like conformation [255].

Therefore, by mutating a residue(s) from the H1-H2 interface of c-Src to the corresponding one(s) of c-Abl, we aimed at answering to the following questions:

- do residue(s) from the H1-H2 interface influence the thermodynamic penalty conformation of c-Src for imatinib?

- if it is the case how; by stabilizing given Src conformation or by influencing the dynamical structural transition of the DFG-motif?

To address these questions we have subjected c-Src KD mutants (described in Chapter 2) to two main types of biophysical and biochemical protein assays.

The first category of protein chararcterization assays investigated on the dynamical influence of H1/ H2 residues and was conducted in presence of elements essential for c-Src catalysis: Mg^{2+}, ATP.

The second category of protein characterization assays were meant to follow the role of c-Src H1/ H2 mutants on c-Src KD conformational prevalence and were referred to as “static” assays.

For both investigations, we have used three different small molecule ATP-inhibitors of c-Src as conformational markers.

Imatinib, 4-(4-methyl-piperazin-1-ylmethyl)-N-(4-methyl-3-(4-pyridin-3-yl-pyrimidin-2-ylamino)-phenyl)-benzamide was used as binder of the c-Src DFG-out conformation (Figure 4.3).

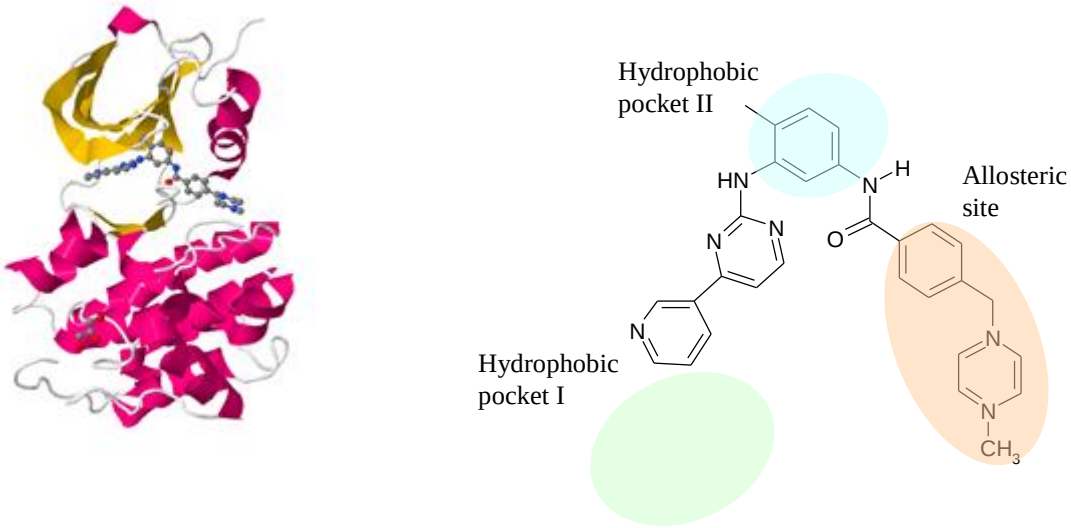

Figure 4.3: Imatinib binding to c-Src kinase domain. Imatinib bound to c-Src kinase domain (PDB ID: 2OIQ) (left). The chemical structure of imatinib (right) depicts hydrophobic regions I (light green) and II (light turquoise) in c-Src. The allosteric pocket exposed in the DFG-out conformation is indicated by the tan shaded area. Modified from [245].

Dasatinib, N-(2-chloro-6-methylphenyl)-2-(6-(4-(2-hydroxyethyl) piperazin-1-yl)-2-methylpyrimidin-4-yl)amino-1,3-thiazole-5-carboxamide was used as binder of the DFG-in/out conformations (Figure 4.4).

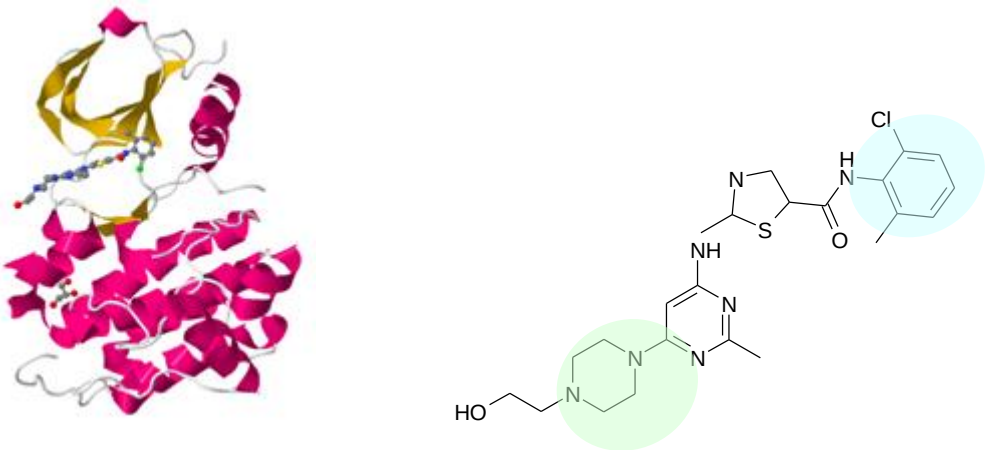

Figure 4.4: Dasatinib binding to c-Src kinase domain. Dasatinib bound to c-Src kinase domain (PDB ID: 3G5D) (left). The chemical structure of dasatinib (right) depicts hydrophobic regions I (light green) and II (light turquoise) in c-Src. Modified from [245].

Finally, the pyrazolopyrimidine 5 compound 1-(4-(4-amino-1-isopropyl-1H-pyrazolo(3,4-d)pyrimidin-3-yl)phenyl)-3-(3-(trifluoromethyl)phenyl) urea, was used as a potent nanomolar binder of the DFG-out c-Src conformation (Figure 4.5) [256].

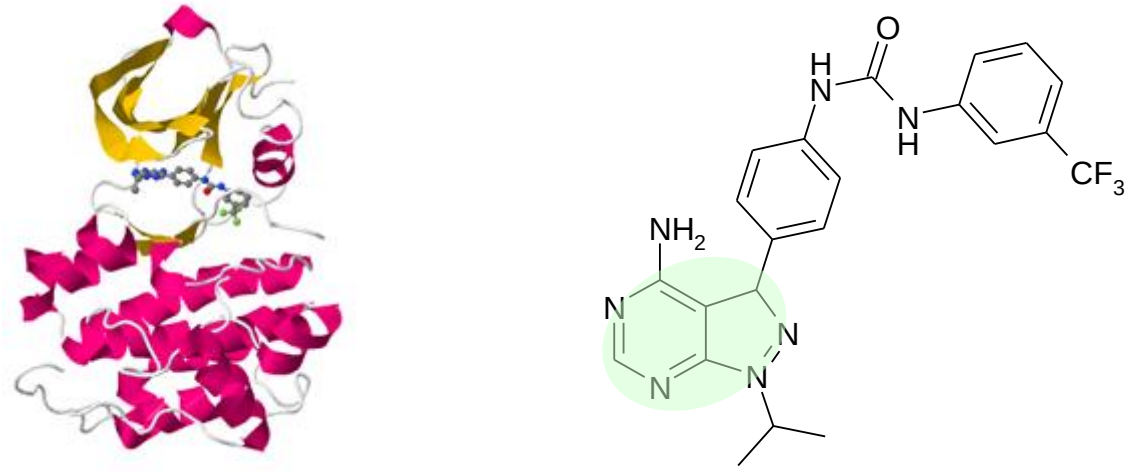

Figure Figure 4.5: Pyrazolopyrimidine 5 compound binding to c-Src kinase domain. Pyrazolopyrimidine 5 compound bound to c-Src kinase domain (PDB ID: 3EL8) (left). The chemical structure of pyrazolopyrimidine 5 compound (right) depicts hydrophobic regions I in c-Src (light green). Modified from [245].

3. Materials and Methods

All chemicals were purchased from Applichem, Germany except if otherwise indicated.

3.1 In vitro tyrosine kinase activity assays

3.1.1 UV-based tyrosine kinase assay

The kinase activity of c-Src was monitored using a continuous spectrophotometric assay. Reactions contained 100mM Tris (pH8.0),1mM DTT, 10mM $MgCl_2$, 275µM ATP, 1mM Phosphoenolpyruvate, 180 µM NADH, 75U/ml pyruvate kinase (PK), 105U/ml lactate dehydrogenase (LDH), 30nM c-Src, 533 µM c-Src peptide substrate (EIYGEFKKK from Peptide2.0 Inc., USA) [155]. Reactions (75µl) were first preincubated for 5min at 30°C and then started through the addition of the peptide substrate. The decrease in absorbance was monitored over 30min at 30°C in a Cary 50 UV-Vis spectrophotometer (Varian, USA) in triplicate for each mutant. The background protein activity was calculated in a sample without peptidic substrate and subtracted from the kinase assays with the peptidic substrate.

The specific activity of the recombinant c-Src KD can be calculated as the amount of product (NAD) produced per unit of time per milligram of enzyme and which is equimolarly related to the produced products of the kinase reaction, ADP and EIY*GEFKKK.

In the UV-based tyrosine kinase assay one molecule of substrate (NADH) used gives one molecule of product (NAD). Therefore the specific activity of c-Src KD can be deduced as the amount of NADH used per unit of time, T (min) and per milligram of enzyme.

$$specific\ activity = \frac{\Delta NADH}{\Delta T * cSrc} \qquad \text{(Equation 1)}$$

The concentration of NADH is given by the Lambert-Beer's law as follows:

$$A = \varepsilon * l * c \qquad \text{(Equation 2)}$$

where c is the concentration of NADH, l is the length of the cuvette (cm) and ε for NADH is $6.22*10^3$ mol^{-1} * l * cm^{-1}. Thus, the normalized specific activity of c-Src is calculated as:

$$specific\ activity = \frac{\Delta A}{\varepsilon * l * \Delta T * cSrc} \quad \{M*min^{-1}*mg^{-1}\} \qquad \text{(Equation 3)}$$

where the variation of the absorbance of NADH over time (ΔA/ΔT) is given by the slope resulting from the activity assay.

To measure the Michaelis constant K_M and v_{max} of c-Src WT for the substrate peptide, variable concentrations of peptide (from 1μM to 2mM) were added to the reaction mix described above (the concentration of ATP was fixed at 275μM). The components were diluted up to 75μl with ddH_2O and pre-incubated for 2min at 30°C before measurement.

To measure the Michaelis constant K_M and v_{max} of c-Src WT for ATP, variable concentrations of ATP (from 10μM to 400μM) were added to the reaction mix described above (the concentration of peptide was fixed at 533μM). The components were diluted up to 75μl with ddH_2O and pre-incubated for 2min at 30°C before measurement.

K_M and v_{max} of c-Src WT for ATP and for the substrate peptide were calculated on GraphPad Prism 4.0 using a Michaelis-Menten equation (equation 4) to determi ne the optimal concentration for the kinase assay.

$$v = \frac{v_{\max} \times peptide}{k_M \times peptide} \qquad \text{(Equation 4)}$$

v is the velocity of the enzymatic reaction (μM*min^{-1}).

κ_{cat} [257] was obtained from the equation 5.

$$k_{cat} = \frac{v_{\max}}{enzyme} \qquad \text{(Equation 5)}$$

3.1.2 Autophosphorylation reaction by Western Blotting

Autophosphorylation of c-Src WT and mutants was followed by Western Blotting. For this assay 1μg of purified protein was mixed with 5mM $MgCl_2$ and Buffer 75 to a final volume of 20μl. The mix was incubated at 30°C for 5min and the reaction was initiated by adding 200μM ATP for different times of incubation (0sec, 15sec, 1min, 10min and 30min.). Reactions were stopped by denaturing the protein with 3xSample Buffer (0.24 M Tris-HCl pH 6.8, 6% SDS, 30% Glycerol, 16% B-mercaptoethanol, and 8.9mM Bromophenol blue).

A negative control was included (no $MgCl_2$, no ATP), as well as a positive phosphorylation control (EGF-Stimulated A431 cell lysate, Millipore, USA). All the samples were boiled for 5min at 95°C and separated on 12% SDS-PAGE. The nitrocellulose membrane and two Watman® papers (with the obtained gel) were equilibrated in water and transfer buffer (Tris 25mM pH 8.5, 0.2M Glycine, 20% Methanol, and 0.05% SDS), respectively, for 30 minutes. The protein transfer was carried out at 19 V, 400mA, for 1.5 hours, in a Trans-Blot Semi-Dry Transfer Cell (Bio-Rad, UK).

Immunodetection was performed on SNAP i.d. Protein Detection System (Millipore, USA) following the standard protocol with the following solutions: 1) Blocking solution (tris buffered saline pH7.6, 0.1% Tween 20, 0.5% non fat dry milk), 2) Washing solution (tris buffered saline pH7.6, 0.1% Tween 20), 3) Primary antibody solution (0.0035mg/ml Monoclonal Anti-Phosphotyrosine-Y_{416} Antibody, clone 4G10 (Millipore, USA) diluted in tris buffered saline pH7.6, 0.1% Tween 20), 4) Secondary antibody solution (0.0015mg/ml Goat Anti-Mouse IgG(H+L)-HRP Conjugate (BioRad, UK).

A FUGI Medical X-Ray film (FUJIFILM Corporation, Tokyo) was used to image the nitrocellulose membrane after 15 seconds of exposure. A picture of each western blot film was taken using the software Quantity One 4.5.1 (BioRad, UK). The densitometric analysis was performed in duplicates on Scion Image (Scion Corporation, Tokyo). Obtained values were corrected for background by subtracting the intensity of the negative control.

3.2 In vitro c-Src inhibition assays

Imatinib and dasatinib were purchased from ChemieTek, USA and the pyrazolopyrimidine 5 compound was synthetized in house as described in [256].

3.2.1 UV-based c-Src inhibition assay

Kinase activity was tested in triplicate (as described in section 3.1.1) over a broad range of inhibitor concentrations to generate a dose-response curve. Inhibitors were all dissolved in dimethylsulfoxyde (DMSO). Stock solutions of each inhibitor were prepared in a way to have 5% DMSO in the final reaction mixture.

The background activity of the proteins at different drug concentrations was determined in experiments without the substrate peptide and subtracted from the kinase assays with the substrate peptide.

The enzymatic inhibition was assessed in two different ways:

1) Inhibition assay with preincubation of unphosphorylated c-Src

The reaction mixtures containing 100mM Tris pH8.0,1mM DTT, 1mM PEP, 180µM NADH, 75 U/ml PK, 105U/ml LDH, 30nM c-Src, were preincubated with the inhibitor for 5min at 30°C. Then, 10mM $MgCl_2$, 275µM ATP and ddH_20 were added to a final volume of 75µl. The assay was initiated with the addition of 533µM of peptide (preincubated at 30°C).

2) Inhibition assay after prephosphorylation of c-Src

The reaction mixture containing 100mM Tris pH8.0, 1mM DTT, 1mM PEP, 180µM NADH, 75 U/ml PK, 105 U/ml LDH, 30nM c-Src, were preincubated for 5min at 30°C together with 10mM $MgCl_2$, 275µM ATP and ddH_20. Then the inhibitor was added and the assay was initiated with the addition of 533µM of the peptide substrate (preincubated at 30°C).
The half maximal inhibitory constant (IC_{50}) was calculated on GraphPad Prism 4.0 (GraphPad Software Inc., USA) using equation 6.

Y = Bottom + (Top – Bottom) / (1+10^ ((LogIC50 – X) * Hill Slope)) (Equation 6)

Where X is the logarithm of concentration and Y is the response.

3.2.2 Inhibition of autophosphorylation monitored by Western Blot

The inhibition of the autophosphorylation rate of c-Src WT and c-Src L317I at different concentrations of imatinib was followed by Western Blot. Here, 120nM of protein were pre-incubated for 5min at 30°C with imatinib (1mM, 200µM and 4nM) and reactions were started through the addition of 10mM MgCl2, 275µM ATP and buffer S75 for 0sec, 15sec, 1min, 10min and 30min. Autophosphorylation was stopped by denaturing the protein with 7µl 3xSample Buffer. A negative control was included (no $MgCl_2$, no ATP), as well as a sample where the autophosphorylation reaction was ran for 30min without inhibitor. All the samples were boiled for 5min at 95°C and separated on 12% SDS-PAGE. Blotting, detection and densitometric analysis were performed as described above.

3.2.3 Inhibitory constant (Ki) determination

Experimental K_i determination was carried out for c-Src WT and c-Src L317I by using the graphical method described by Dixon [258].

Reaction mixtures contained 100mM Tris pH8.0, 1mM DTT, 1mM PEP, 180µM NADH, 75 U/ml PK, 105 U/ml LDN, 30nM c-Src, were preincubated with the inhibitor for 5min at 30°C. Then, 10mM $MgCl_2$, ATP and ddH_2O were added to a final volume of 75µl. The assay was initiated with the addition of the peptide (preincubated at 30°C).

The reciprocal of the initial velocity *(i.e.* 1/V) was plotted against series of 4 different concentrations of inhibitor (0nM, 4nM, 200µM and 600µM) at constant (100µM and 300µM) ATP concentrations resulting in two families of lines. The value of inhibitor concentration at which both lines intersect gave the absolute value of K_i. All measurements were done in duplicate.

For coparison purposes, the ihibitory constants (K_i) were calculated from the inhibitor concentration that causes 50% inhibition (IC_{50}) according to equation 6 as described by Cheng and Prusoff [257].

$$K_i = \frac{IC_{50}}{1 + \frac{ATP}{Km}} \qquad \text{(Equation 7)}$$

(ATP) is the concentration of ATP in the assay (275µM). Km is the Michaelis-Menten constant for ATP, which was defined for c-Src to be 144µM.

3.3 Circular Dichroism (CD)

3.3.1 CD spectra of c-Src WT and mutants

All CD spectra were recorded at 5°C on Jasco model J-815 circular dichroism spectrometer (Tokyo, Japan), equipped with a water cooled Peltier unit in 0.05cm Hellma quartz cuvette model 110-QS (Muellheim, Germany). CD spectra measurements were taken for 10μM protein solutions at a scan rate of 100 nm /min with a data pitch of 0.5nm and a band width of 1nm. Each spectrum represents the average of 2 scans from 800nm to 200nm. Duplicata consisted of a sample from freshly purified protein and from a -80°C overnight frozen sample. Buffer CD (20mM Tris pH 8.0, 100mM NaCl, 1mM TCEP) was used as blank and its spectrum was subtracted from all recorded spectra. For spectra with c-Src inhibitors, the blank consisted in the CD buffer containing 15μM imatinib or dasatinib respectively.

The secondary structure content was estimated by deconvolution procedures using Spectra Manager (Jasco, Tokyo, Japan).

3.3.2 Thermal denaturation of uncomplexed c-Src WT and mutants

To define the midpoint of the thermal denaturation curve (T_M) for c-Src WT and mutants, spectra were collected at 220nm within the temperature range of 5°C- 80°C on Jasco model J-815 circular dichroism spectrometer (Tokyo, Japan), equipped with a water cooled Peltier unit in 0.05cm Hellma quartz cuvette model 110-QS (Muellheim, Germany). For each c-Src mutant and for c-Src WT, CD data were collected from 10μM sample in Buffer CD from both freshly purified protein and from a -80°C overnight frozen sample. The rate of heating was fixed at 1°C /min with data pitch of 1°C and a delay time of 1 sec. T_M calculated with Spectra Manager (Jasco, Tokyo, Japan).

3.3.3 Thermal stability of c-Src WT and c-Src L317I in presence of imatinib

Protein-inhibitor ratio of 1:1.5 was kept identical to the crystallization conditions.

Dissolution of imatinib in DMSO was avoided by using imatinib mesylate (Novartis, Switzerland). Imatinib mesylate was dissolved in water and kept at -20°C until use as a 2mM stock solution. 2.0ul of the stock solution was then added to 248.0ul of CD buffer containing 10μM protein for analysis.

The CD unit used is the mean molar ellipticity per residue (θ) expressed in {deg. cm^2. $dmol^{-1}$. res^{-1}}, where c-Src WT; L317I; L407G; L317_L322I; L317I_L322I; L322I; V377L contained 309 residues and G318, G318_V378L; G318_L323I_V378L contained 310 residues.

3.4 *Crystallization*

3.4.1 c-Src L317I – apo

Crystallization screens were performed in 24-well hanging drop plates (Hampton, USA): 2μl of protein at 7mg/ml in S75c buffer was mixed with 0.5μl of mother liquor solution and equilibrated with 1ml of mother liquor solution (0.1M MES pH6.5, 0.2M NaAc, 4% Glycerol, 12% PEG 4K). Crystals grew overnight at 18°C. For data collection, crystals were transferred to the mother liquor solution supplemented with 30% of glycerol before direct cooling with the cryo-stream (Oxford Cryosystems Ltd, Oxford, UK) at 100K.

3.4.2 c-Src L317I –co-crystals

Crystallization screens were performed in 24-well hanging drop plates (Hampton, USA): 95µl of protein at 7mg/ml in S75c buffer was mixed with 5µl of inhibitor solution in DMSO (10mM imatinib solution, 5mM dasatinib solution and 10mM pyrazolopyrimidine 5 compound solution respectively). 2µl of the protein-inhibitor preparation was mixed with 0.5µl of mother liquor solution (at 18°C for imatinib and at 14°C for dasatinib and for the pyrazolopyrimidine 5 compound) and equilibrated with 1ml of mother liquor solution (0.1M MES pH 6.5, 0.2M NaAc, 4% Glycerol, 12% PEG 4K). Crystals grew overnight at 18°C with imatinib and overnight at 14°C for dasatinib and the pyrazolopyrimidine 5 compound. For data collection, crystals were transferred to the mother liquor solution supplemented with 30% of glycerol and 500µM of imatinib, 250µM dasatinib and 250µM pyrazolopyrimidine 5 compound, respectively before direct cooling with the cryo-stream (Oxford Cryosystems Ltd, Oxford, UK) at 100K.

3.4.3 Data collection, structure solution and refinement

X-ray data sets of c-Src L317I-apo, c-Src L317-imatinib, c-Src L317I-dasatinib and c-Src-pyrazolopyrimidine 5 compound were collected at the beam-line x06da, equipped with a mar225 mosaic CCD detector and tuned at the wavelength of 1 Å, at the synchrotron Swiss Light Source at the Paul Scherrer Institute (Villigen, Switzerland). Angular increment between diffraction images of 1° and a distance crystal-to-detector of 300 mm were chosen for c-Src L317I-apo, c-Src L317I-imatinib and c-Src L317I-dasatinib. For c-Src L317I-pyrazolopyrimidine 5 compoundthe distance crystal-to-detector was fixed at 250nm. Each dataset was obtained from a single crystal. Raw diffraction images were indexed and integrated with MOSFLM version 7.0.1 [259]. Data scaling, merging and reduction was carried out with programs of the CCP4 suite [260].

The structure of L317I c-Src complexed with imatinib was determined by molecular replacement with the program PHASER [261, 262] using the model of the wild-type c-Src complexed with Imatinib as a search model (PBD ID: 2OIQ) [155].

Before starting the molecular replacement procedure the imatinib molecule and solvent molecules were removed from the initial model. The rotation and the translation functions gave two clear single solutions, which corresponded to two molecules in the asymmetric unit. These two molecules located in the asymmetric unit yielded a Matthews coefficient (V_M) of 2.41 $Å^3$/Da and a corresponding solvent content of 49.1% [263]. The 2 solutions found at the end of the molecular replacement were employed in the refinement procedure performed with CNS 1.1 [264, 265] and PHENIX [266] at the end of the refinement procedure. Subsequently, several cycles of refinement were performed and were interchanged with manual rebuilding sessions using the molecular graphics program O [267, 268] and then COOT [267].

The model of L317I c-Src complexed with imatinib was used as a search model to solve by molecular replacement with the program PHASER, the structure of L317I c-Src in the apo form at 2.7 Å and the strucure of L317I cSrc with dasatinib at 2.75Å as well as the structure of c-Src L317I complexed with the pyrazolopyrimidine 5 compound.

Iterative model refinement carried out with PHENIX and manual building done with the program COOT completed the two structures. At the end of the refinement, a translation-libration-screw (TLS) refinement was carried out. For the structure of L317I c-Src in the apo form, each molecule in the asymmetric unit was divided in five TLS groups : group 1- the N-lobe residues 257- 272 and residues 284-298, group 2 (P-loop) residues 273-283, group3 β3-αC loop and αC-helix residues 299-318, group4 activation loop residues 403-427 and group5, C-lobe residues 319-402 and residues

428-533. For the structure of L317I c-Src complexed with dasatinib, each molecule in the asymmetric unit was divided in twenty TLS groups. The choice of the TLS groups was done with the help of the TLSMD server [269].

The stereochemical quality of the three final models were assessed with PROCHECK [270] and MolProbity [271]. Structure solution and refinement were performed by Dr. Lucile Pernot at the University of Geneva, Switzerland.

3.5 Isothermal Titration Calorimetry (ITC)

Thermodynamic binding parameters for the binding of imatinib to c-Src WT and c-Src L317I was obtained through isothermal titration calorimetry using a VP-ITC instrument (Microcal) at 30°C. The sample solution consisted of 2ml 0.1mM protein in MES buffer supplemented with 2% DMSO. The ligand solution was prepared by diluting a 8mM stock solution of imatinib in DMSO with buffer MES to give a final concentration of 0.16mM and 2% DMSO. All solutions were filtered then degassed for 5min with gentle stirring under vacuum. A titration experiment consisted of a first control injection of 1µl followed by 37 injections, each of 8µl and 16sec. duration spaced 300sec. apart. Raw data were collected, corrected for ligand heats of dilution, integrated and fitted to one binding site model using the Origin software package supplied with the instrument.

4. Results and discussion

4.1 Autophosphorylation

We have successfully expressed and purified the eight mutated c-Src kinase domain forms (cf. Chapter 2 and 3) in addition to the wild type. Kinase domain constructs (Q251-L533 from chicken c-Src) contained three extra-N-terminal residues (G-H-M) originating from the tobacco etch virus (TEV) protease cleavage site. ESI-MS and immunodetection with Anti-phospho-Y416 Antibody showed no evidence for post-translational phosphorylation.

As already described for c-Abl [272], a phosphorylation at the level of the activation-loop tyrosine residue (Y416 in c-Src, Y393 in c-Abl) is likely to destabilize the DFG-out position making the conformation of the kinase domain thermodynamically unfavourable for the imatinib binding. In c-Src and many other kinases, it is known that the DFG-out conformation is less stable than the DFG-in conformation, and this can explain at least part of the Src/Abl specificity of type II inhibitors as imatinib[255].

To study the impact of the mutations in the H1-H2 hydrophobic interface of c-Src on the conformational transition of the kinase domain and indirectly on the switch of the DFG-out to the DFG-in conformation, we first measured the time course of kinase autophosphorylation for each mutant and compared it to the wild type protein (Figure 4.6).

All c-Src kinase domain variants autophosphorylated when 1.0µM of protein was incubated over 30 min with 5mM $MgCl_2$ and 200µM ATP at 30°C (Figure 4.6). To ensure that differences in the autophosphorylation level over time were related to the mutations *per se* and not to unequal volumes of loaded proteins, duplicate samples were prepared in parallel and loaded onto duplicate SDS-PAGE gels. Coomassie staining showed that an equal amount of protein sample was loaded in each sample (Figure 4.6 a).

These results clearly indicate that the mutations introduced within the kinase domain do not abolish the catalytic activity of the c-Src KD mutants, thus allowing further analysis.

A semi-quantitative analysis by densitometry on the western blots showed that the c-Src kinase domains containing mutated residues from the H1-H2 interface achieved 100% phosphorylation later than the wild type enzyme, which reached almost complete autophosphorylation after 15sec incubation with with 5mM $MgCl_2$ and 200µM ATP at 30°C (Figure 4.6 b). These results suggest that the mutated c-Src kinase domains have a lower rate of autophosphorylation on Y_{416} over time compared to the wild type c-Src. Therefore, the observed slowdown in phosphorylation could indirectly imply that H1-H2 c-Src mutations are decreasing the rate of c-Src activation. An open question, at this point in the study, was how c-Src kinase domain mutants were influencing the DFG-out/-in equilibrium, by stabilizing the DFG-out c-Abl-like conformation or by increasing the rate of the DFG conformational switch, making the c-Src kinase domain slower in its activation?

A

c-Src	Autophosphorylation (Western Blot, Anti-PY_{416} Antibody)	Loading control (Coomassie staining)
WT	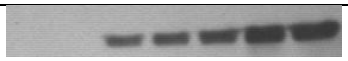	
L317I	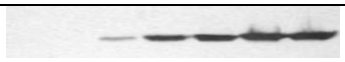	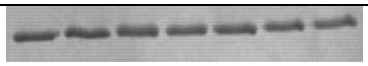
G318	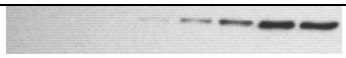	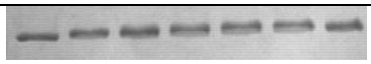
G318_V378L	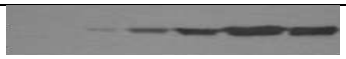	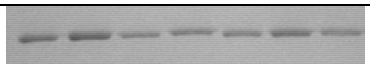
L317I_L322I	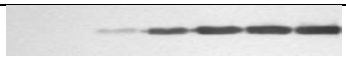	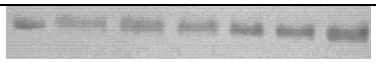
L317I_V377L		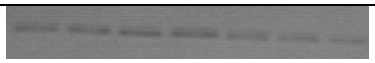
L322I	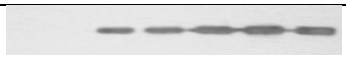	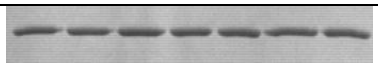
G318_L323I_V378L	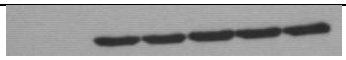	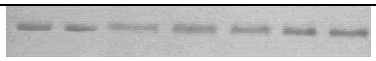
V377L	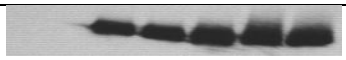	

B

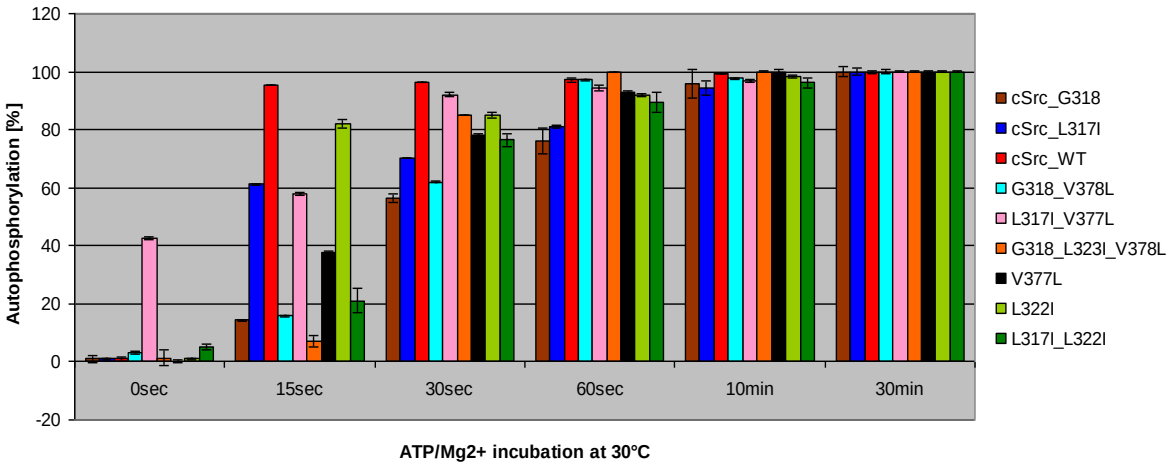

Figure 4.6: Autophosphorylation rate of c-Src wild type and mutant kinase domains over time. A. Western blots and loading controls for wild type and mutant c-Src KD. **B.** Semi-quantitative densitometric analysis was performed with Scion Image® on Western Blots after incubation of 1µg protein kinase domain with 5mM $MgCl_2$ and 200µM ATP.

4.2 ATP and substrate kinetics of c-Src WT and c-Src L317I

ATP and substrate peptide kinetics were measured for the kinase domains of c-Src WT and for one of the c-Src mutants (L317I). Data revealed similar Km values for the mutant and the wild type enzyme, while the Vmax of the mutant appeared to be slightly increased (~1.2 fold) (Figure 4.7). Thus, kinetics data confirm the results of the autophosphorylation assay indicating that the protein activity was not constrained by the L317I mutation. Moreover, the observed increase of V_{max} for the mutant led to the hypothesis that the product inhibition caused by ADP may be altered through modified catalytic dynamics caused by the mutation. In such a case, the product is released by the mutant, conferring a higher turnover rate for c-Src L317I and suggesting a clear impact of the L317I mutation on the dynamical behaviour of c-Src.

Therefore, to get a deeper insight on the impact of residues from the H1-H2 interface on the dynamics of the conformational changes within the c-Src kinase domain, we have analysed the sensitivity of the H1-H2 mutants to three different c-Src inhibitors by using UV-coupled *in vitro* kinase assay. First, we used imatinib as a conformational marker of the DFG-out conformation in analogy to the work published by Seeliger et al. [155]. Secondly, we used dasatinib and the pyrazolopyrimidine 5 compound to explore the conformational impact of the mutants beyond the DFG flip since dasatinib binds the DFG-in conformation [273] and the pyrazolopyrimidine 5 compound binds the DFG-out conformation in wild type c-Src KD without thermodynamic penalty [256].

A

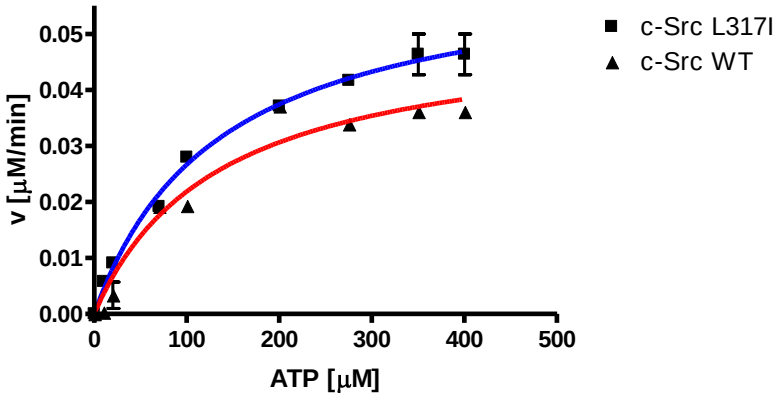

	ATP			
	Km (µM)	Vmax (µM min^{-1})	Kcat (min^{-1})	Kcat/Km ($\mu M^{-1}min^{-1}$)
c-Src WT	134.4±32.2	0.051±0.004	1.7±0.13	0.0125±0.004
c-Src L317I	135.2±17.9	0.062±0.003	2.1±0.1	0.0152±0.005

B

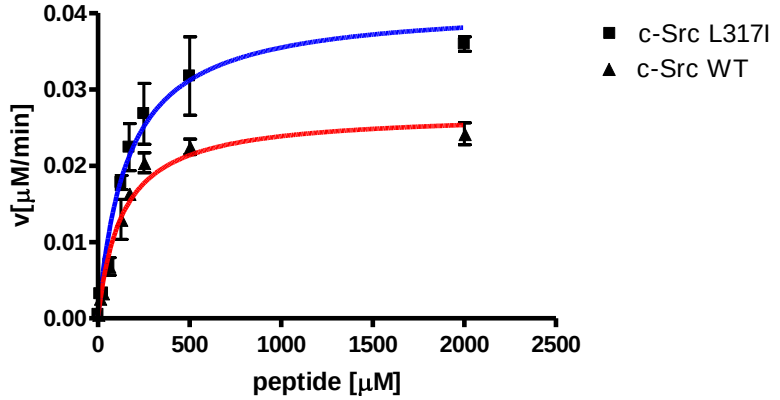

	EIYGEFKKK			
	Km (µM)	Vmax (µM min^{-1})	Kcat (min^{-1})	Kcat/Km ($\mu M^{-1}min^{-1}$)
c-Src WT	131.9±24	0.027±0.002	0.9±0.06	0.006±0.002
c-Src L317I	159.8±39.2	0.041±0.004	1.36±0.13	0.008±0.003

Figure 4.7: ATP and peptide substrate (EIYGEFKKK) kinetics of c-Src WT and c-Src L317I. A. ATP kinetics of c-Src WT and c-Src L317I. **B**. Peptide substrate kinetics of c-Src WT and c-Src L317I. All values represent the mean of at least two measurements. Standard deviations are depicted as error bars.

Km and Vmax values were thus used to establish the concentrations of ATP and substrate peptide that were applied in the UV-coupled *in vitro* kinase assay for all c-Src kinase domain variants. Peptide and ATP concentrations were fixed at no less than two fold the respective Km value to ensure a maximal initial velocity of the kinase and steady state conditions during the inhibition assays. The substrate peptide was used at 533μM (Km_{WT}=132μM) and ATP at 275μM (Km_{WT}=134μM). These conditions were not identical to the c–Src kinase assay described previously [155] where the same substrate peptide was used at 133μM (Km), but they largely guarantee the fulfilment of the Michaelis-Menten condition for substrate(s) excess during the enzymatic reaction (Figure 4.9) [274]. (Figure 4.9; Figure 4.10) [274].

To validate the accuracy and reproducibility of the method, IC_{50} and K_i values for imatinib were measured on c-Src WT and c-Src L407G (Table 4.1). Values were in accordance with data published by Seeliger et al. in [155].

In the case of c-Src L317I, imatinib binding was the most significantly favoured (Figure 4.8). In contrast with c-Src WT (IC_{50}=220μM), it exhibited an inhibition by imatinib in the nanomolar range (IC_{50}=4nM) comparable to the one of c-Abl (IC_{50}=25-200nM) [274]. To date, L317I appears to be the unique mutation that could reverse the "thermodynamic penalty" in c-Src transforming c-Src KD to c-Abl KD in respect to imatinib binding. As a first conclusion, this mutation proves that Leu 317 in the kinase domain of c-Abl may take part in a long range regulation the kinase domain conformational switch.

Not surprisingly, when c-Src L317I inhibition by imatinib was tested on a pre-phosphorylated fraction of the protein (the protein was pre-incubated with ATP before the addition of the inhibitor), the mutant did not show any drastic increase in sensitivity to imatinib (IC_{50}=67.66±0.13μM, Ki=23.25±0.04μM) (Figure 4.8). This was in agreement with the observation made with c-Abl where pre-phosphorylated c-Abl showed a μM range IC_{50} value for imatinib [193]. When compared to the wild type, the remaining seven c-Src kinase domain mutants also showed an increased sensitivity to imatinib. The IC_{50} values spread from low μM to high nM when the mutated enzymes were pre-incubated with the ATP-competitive inhibitor before any addition of ATP and Mg^{2+} (Table 4.1). Eventough any of them could completely reverse the "thermodynamic penalty", their impact on the sensitivity of the c-Src kinase domain to imatinib was globally higher than with mutations that aimed the conversion of sequence motifs in c-Src to the corresponding sequences in c-Abl at the level of the imatinib binding pocket [155].

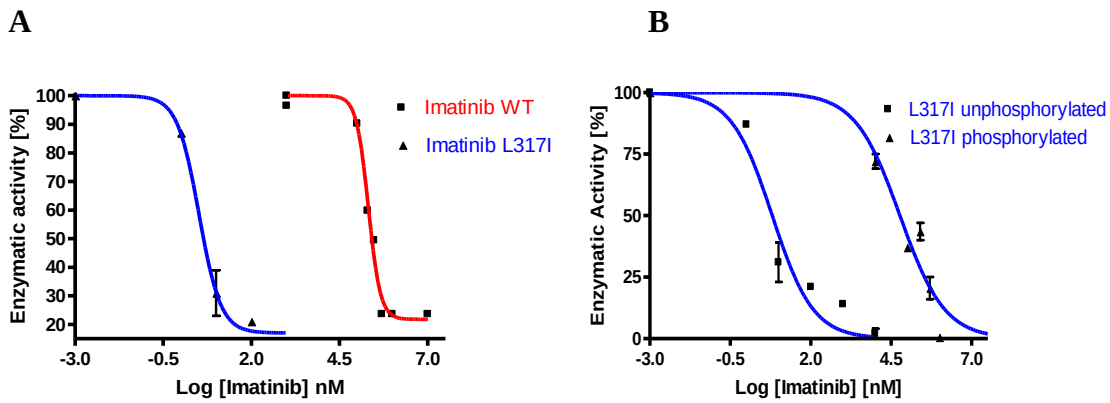

Figure 4.8: IC_{50} values of imatinib for c-Src WT and c-Src L317I from UV-based inhibition assay. A. UV-coupled inhibition assay. IC_{50} values are 4.14±0.2 nM for unphosphorylated c-Src L317I and 221.6 ±10.1 μM for unphosphorylated c-Src WT. **B**. UV-coupled assay comparing the inhibition by imatinib of unphosphorylated vs. pre-phosphorylated c-Src L317I.

An interesting indication within the data in Table 4.1 was the higher impact of mutations from the H1 interface on the "thermodynamic penalty" of c-Src over mutations from the H2 interface. This trend is most likely related to the higher conformational mobility of the residues forming the N-lobe compared to the residues forming the C-lobe.

Table 4.1: Overview of IC_{50} values and calculated K_i values according to the Cheng-Prousoff relationship for c-Src wild type and H1-H2 c-Src mutants with imatinib. Values represent the average of at least two measurements.

	c-Src	Imatinib inhibition		
Mutation	Hydrophobic interface	IC_{50} ± SD (nM) Unphosphorylated*	IC_{50} ± SD (nM) Pre-phosphorylated**	K_i ± SD (nM) Unphosphorylated*
L317I	H1	4.14 ± 0.2	67656± 130	1.42±0.1
L322I	H1	485 ± 17	250000± 340	166.67±5.8
L317I/L322I	H1/H1	3085 ± 15	249000± 305	1060.14±5.1
G318/L323I/V378L	H1/H1/H2	5202 ± 13	4000 ± 13	1787.62±4.5
G318	H1	16624 ± 130	131000± 230	5712.71±44.7
V377L	H2	29441 ± 120	16240± 89	10117.18±41.2
G318/V378L	H1/H2	31846 ± 110	149000± 172	10943.64±37.8
L317/V377L	H1/H2	36400 ± 130	72000± 154	12508.6±44.7
L407G	-	16270± 121	-	5591.1±41.6
WT	-	221600 ± 1011	>200000 ***	76151.2±347.4

* The enzyme was pre-incubated with imatinib before adding ATP/Mg^{2+}. ** The enzyme was pre-incubated with ATP/Mg^{2+} before adding imatinib. *** Not measured experimentally because the value of IC_{50} for unphosphorylated c-Src is already at the upper limit of the enzymatic assay.

The experimental determination of K_i values for c-Src L317I (K_i=3.8±0.02nM) and c-Src WT (K_i=44.9±7.6µM) (Figure 4.9) corroborated the K_i values calculated on the basis of IC_{50} (Table 4.1).

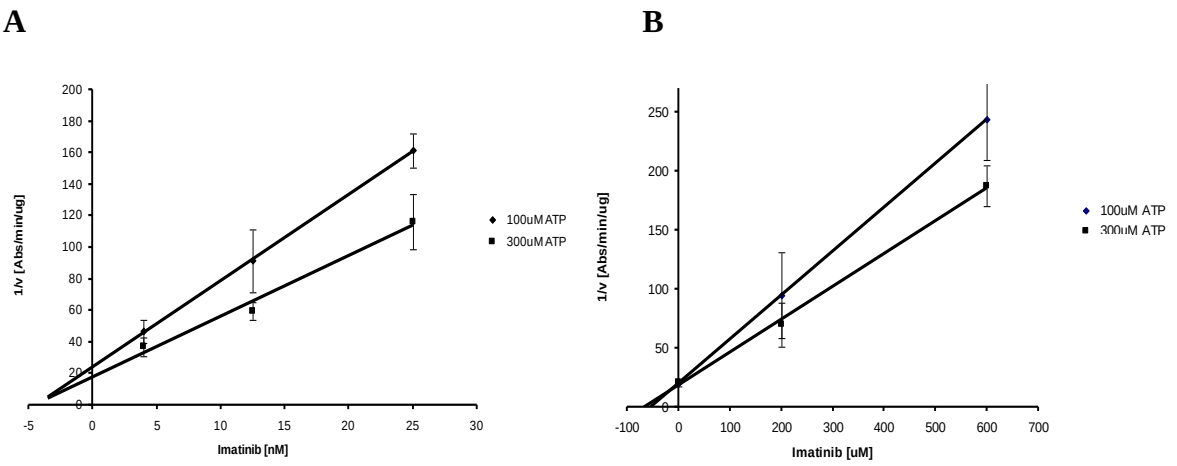

Figure 4.9: Dixon plot for the determination of K_i values of imatinib for c-Src L317I and c-Src WT. A. Dixon plot of c-Src L317I inhibition by imatinib using 100µM and 300 µM of ATP. Resulting Ki value is 3.8±0.02nM. **B.** Dixon plot of c-Src WT inhibition by imatinib using 100µM and 300 µM of ATP. Resulting Ki value is 44.9±7.6µM. All values represent the mean of at least two measurements. Standard deviations are depicted as error bars.

The agreement between experimental and calculated values confirmed that the ATP-competitive nature of imatinib binding to the mutated c-Src kinase was preserved and that the affinity of c-Src L317I for imatinib is indeed 4log higher than the one for the wild type kinase domain.

Results from the UV-coupled inhibition assay for c-Src L317I and c-Src WT were further confirmed by the orthogonal Western Blot assay. Here, IC_{50} values were measured as the effectiveness of imatinib in inhibiting the autophosphorylation of c-Src kinase domains. Obtained data (IC_{50} being 4nM for c-Src L317I and 200µM for c-Src WT) are presented in Figure 4.10.

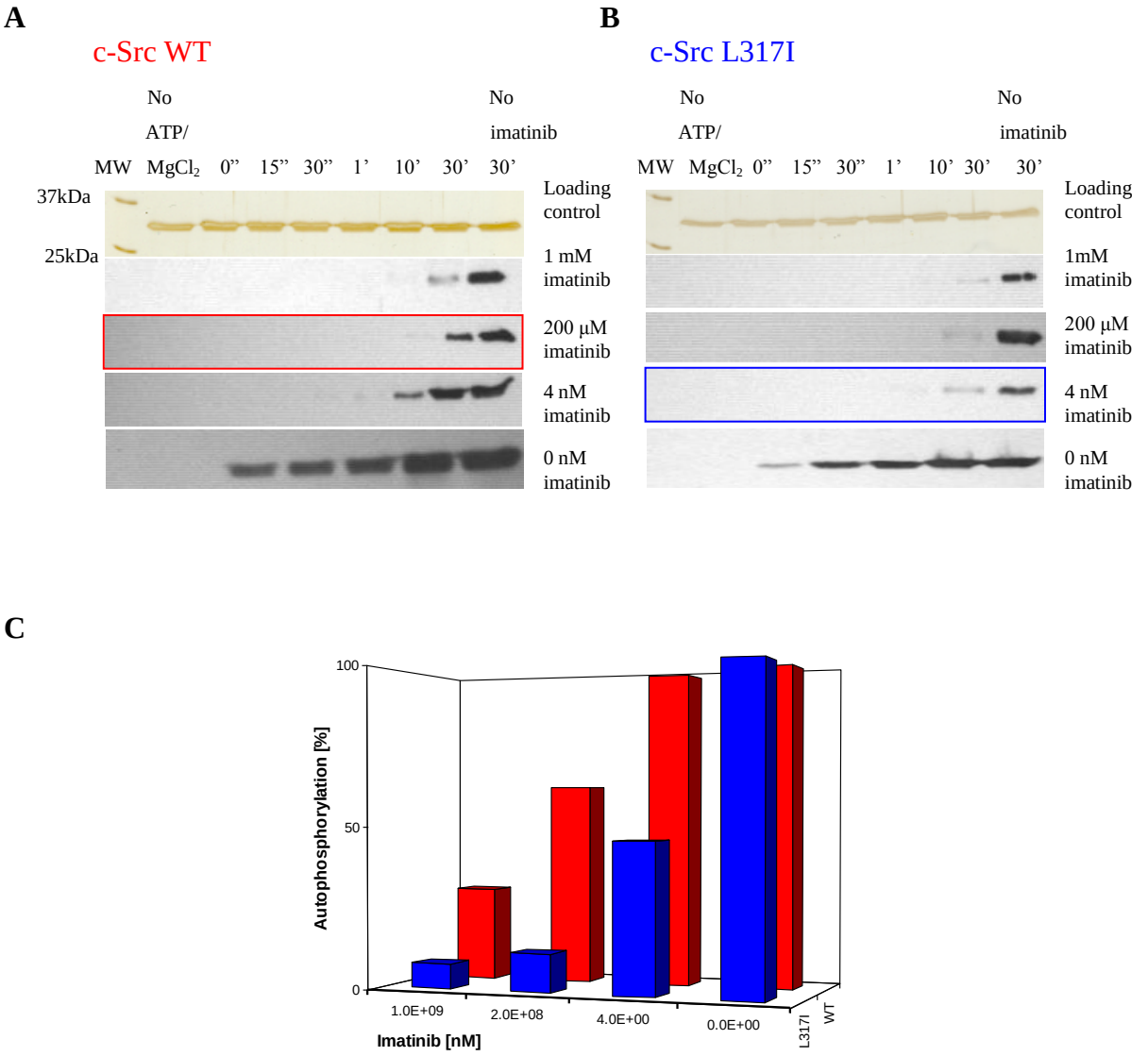

Figure 4.10: IC_{50} values of imatinib for c-Src WT and c-Src L317I from Western Blot-based inhibition assay. Loading control and Western blots showing the autophosphorylation of 120nM c-Src WT (**A**) and c-Src L317I (**B**) in presence of 10mM $MgCl_2$, 275µM ATP and different concentrations of imatinib for 30min at 30°C. Protein phosporylation was detected with an anti-PY_{416} Antibody. Semi-quantitative densitometric analysis (**C**) was performed with Scion Image ®. IC_{50} values are obtained as the percentage of the phosphorylation signal after 30min incubation with imatinib vs. the phosphorylation signal after 30min incubation without imatinib. Estimated IC_{50} values are 4 nM for c-Src L317I and 200 µM for c-Src WT, respectively.

At this point of the kinetic studies on the generated H1-H2 mutants of c-Src we could show that swapping residues from the hydrophobic interface of c-Src to the corresponding ones of c-Abl, c-Kit and PDGFR does not abolish the activity of the c-Src kinase domain. Moreover, the identified residues from the H1-H2 interface in c-Src appear to have a net impact on the conformation of the kinase and in particular at the level of the DFG-flip. This impact is stronger for the amino acids forming the H1-interface, in particular at position 317.

4.3 Dasatinib and pyrazolopyrimidine compound 5 sensitivity of c-Src KD

To investigate whether the residues from the H1-H2 interface affect c-Src KD conformation at regions different than the DFG motif, we tested the sensitivity of the L317I mutant to dasatinib and to the pyrazolopyrimidine 5 compound and compared it against data with c-Src WT (Figure 4.11). Moreover, we tested both compounds on the unphosphorylated as well as on the phosphorylated form of the protein.

Our results (Figure 4.11A) show no significant difference between IC_{50} of Dasatinib for the wild type and the mutant both on their unphosphorylated and their phosphorylated states. Indeed, all measured values were in the low nanomolar range as published for the wild type c-Src and for c-Abl [275]. This lack of difference in IC_{50} can be explained with the fact that dasatinib has less stringent conformational requirements for binding than imatinib [276]. Therefore, similar IC_{50} could indicate that L317I mutation did not affect the conformation or the dynamics of the residues forming the purine binding site, neither the adjacent hydrophobic regions I and II, which are occupied by type I kinase inhibitors such as dasatinib.

A

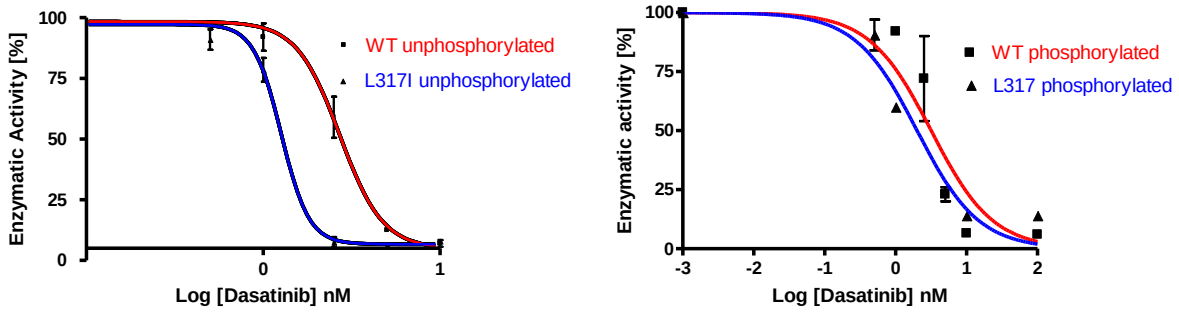

Dasatinib inhibition				
c-Src	IC_{50} ± SD (nM) Unphosphorylated	Ki ± SD (nM) Unphosphorylated	IC_{50} ± SD (nM) Phosphorylated	Ki ± SD (nM) Phosphorylated
WT	2.69±0.19	0.92±0.06	3.13±0.79	1.07±0.07
L317I	1.34±0.09	0.46±0.03	1.08±0.27	0.37±0.02

B

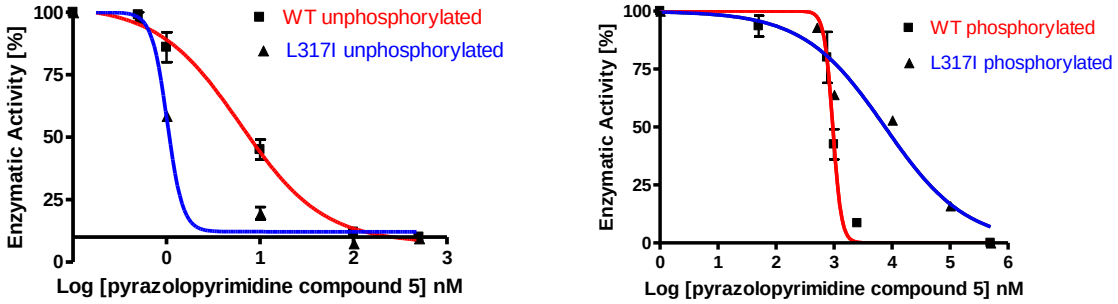

Pyrazolopyrimidine compound N°5 inhibition				
c-Src	IC_{50} ± SD (nM) Unphosphorylated	Ki ± SD (nM) Unphosphorylated	IC_{50} ± SD (nM) Phosphorylated	Ki ± SD (nM) Phosphorylated
WT	6.56±2.31	2.25±0.8	0.9±0.06	0.32±0.02
L317I	1.02±0.02	0.35±0.01	11.15±2.74	3.83±0.94

Figure 4.11: Enzyme activity inhibition of c-Src WT and L317I mutant by dasatinib and pyrazolopyrimidine compound 5. A. Inhibition assay with dasatinib on the unphosphorylated kinase domains of c-Src WT and L317I are depicted on the left. Inhibition assay with dasatinib on the phosphorylated kinase domains is depicted on the right. **B.** Inhibition assay with compound 5 on the unphosphorylated kinase domains of c-Src WT and L317I are depicted on the left. Inhibition assay with compound 5 on the phosphorylated kinase domains is depicted on the right. Determined IC_{50} and calculated K_i values are summarized in tables beneath. All values represent the mean of at least three measurements.

When the inhibition of c-Src L317I by the pyrazolopyrimidine compound 5 was tested, IC_{50} values were in the low nanomolar range for the unphosphorylated and for the pre-phosphorylated c-Src L317I and WT. Data revealed higher sensitivity of the unphosphorylated mutant for the pyrazolopyrimidine 5 compound *vs.* the unphosphorylated wild type c-Src (IC_{50}=1.02±0.02nM for c-Src L317I and IC_{50}=6.56±2.31nM for c-Src WT). In reverse, the phosphorylated wild type c-Src showed higher sensitivity for the pyrazolopyrimidine compound 5 *vs.* c-Src L317I (Figure 4.11B).

To explain these data, we superposed imatinib as it is bound to c-Src WT (PDB ID: 2OIQ) with the crystal structure of the pyrazolopyrimidine compound 5 bound to c-Src WT (PDB ID: 3EL8) (Figure 4.12).

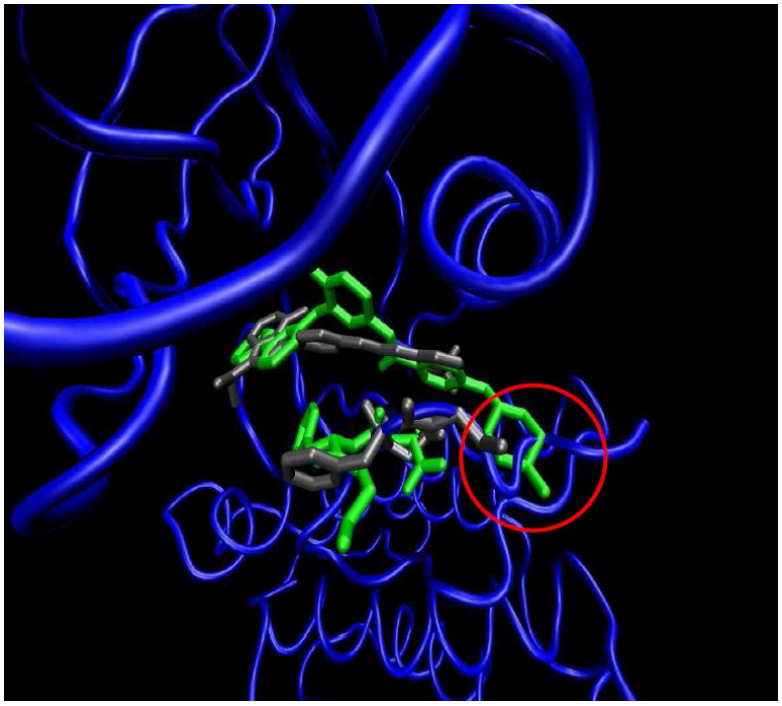

Figure 4.12: Binding mode of imatinib and of pyrazolopyrimidine compound 5 to c-Src WT (PDB ID: 3EL8). Imatinib and the DFG motif of 2OIQ crystal structure are depicted in green; pyrazolopyrimidine compound 5 and the DFG motif of 3EL8 crystal structure are shown in grey. The overall c-Src crystal structure of the c-Src-compound 5 complex (3EL8) is presentd in blue. The red ring shows the clash of the N-methylpiperazine of imatinib with the A-loop in the conformation of c-Src when binding to the pyrazolopyrimidine compound 5.

It appears that the N-methylpiperazine of imatinib clashes with the A-loop in the conformation of c-Src KD bound to the pyrazolopyrimidine compound 5, indicating that c-Src L317I adopts a more extended conformation to bind imatinib than to fit the pyrazolopyrimidine compound 5.

This adaptation may result in an increased thermodynamic barrier leading to the postulated higher thermodynamic penalty [155]. If we assemble these structural observations with the kinetic data from imatinib and compound 5 inhibition on c-Src WT and on L317I, we may presume that the mutation in c-Src favors the transition from the active to the inactive protein conformation not only at the level of the DFG flip but also, eventhough to a lesser extent, of the A-loop, influencing the whole rotation of the N- and C-terminal domains.

4.4 Using CD to elucidate the influence of L317I mutation on the structural stability of c-Src KD

The protein folding and the effect of the H1-H2 mutations on the stability of c-Src KD were evaluated by CD spectroscopy. In this study we subjected not only c-Src L317I but all c-Src kinase domains mutated at the H1-H2 interface. c-Src WT and c-Src L407G mutant [155] were used for comparison.

The CD spectra of all c-Src variants were characteristic of α-helical proteins with minima at 208nm and 220nm (Figure 4.13) and confirmed the correct folding of all generated c-Src mutants. These results were in line with the fact that all mutants were catalytically active (Table 4.1).

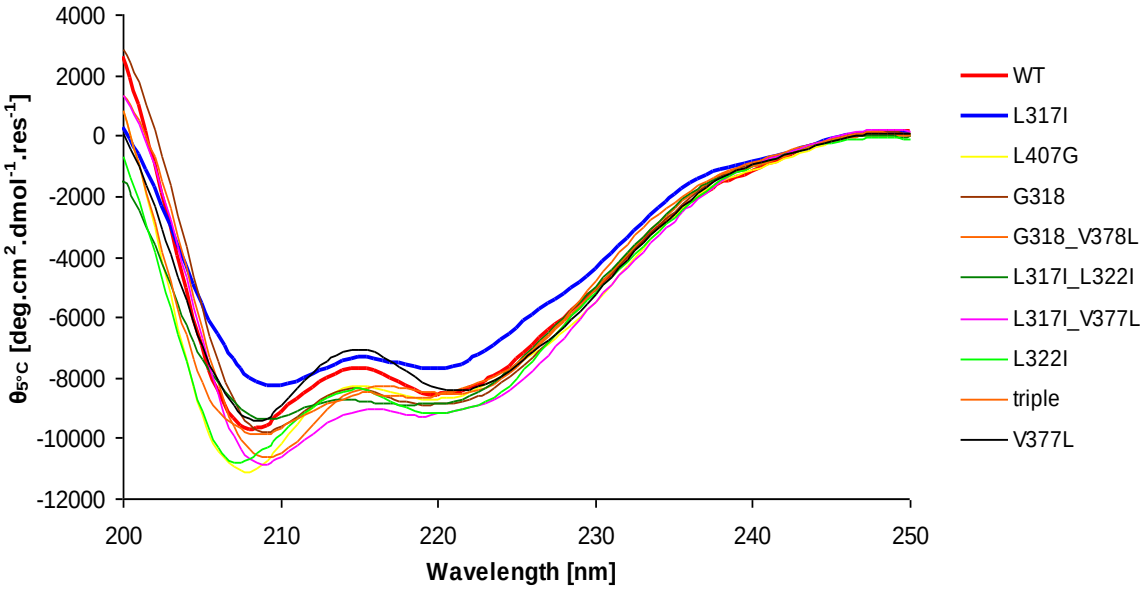

Figure 4.13: CD spectral patterns of wild type and mutant c-Src kinase domains. CD spectra were recorded at 5°C with 10µM protein in 20mM Tris pH 8.0, 100mM NaCl, 1mM TCEP and corrected with buffer spectra. The curves represent the average of at least two independent experiments.

The spectrum of c-Src L317I revealed a decrease in absolute values in mean molar ellipticity per residue suggesting that the mutation at position 317 is accompanied by the main decrease in α-helical content. Since no disruption of α-helix is observed in the crystal structure of the mutant (c.f. part 3.5), one might assume that the mutation L317I influences the conformational dynamics of residues that form mainly α-helices within the kinase domain.

In line with the latter observations, it could be noticed that c-Src L317I showed the lowest CD signal throughout the entire thermal stability measurement at 220nm (Figure 4.14). Here, all transitions were highly cooperative but not reversible. Protein unfolding led to agglomeration in all samples.

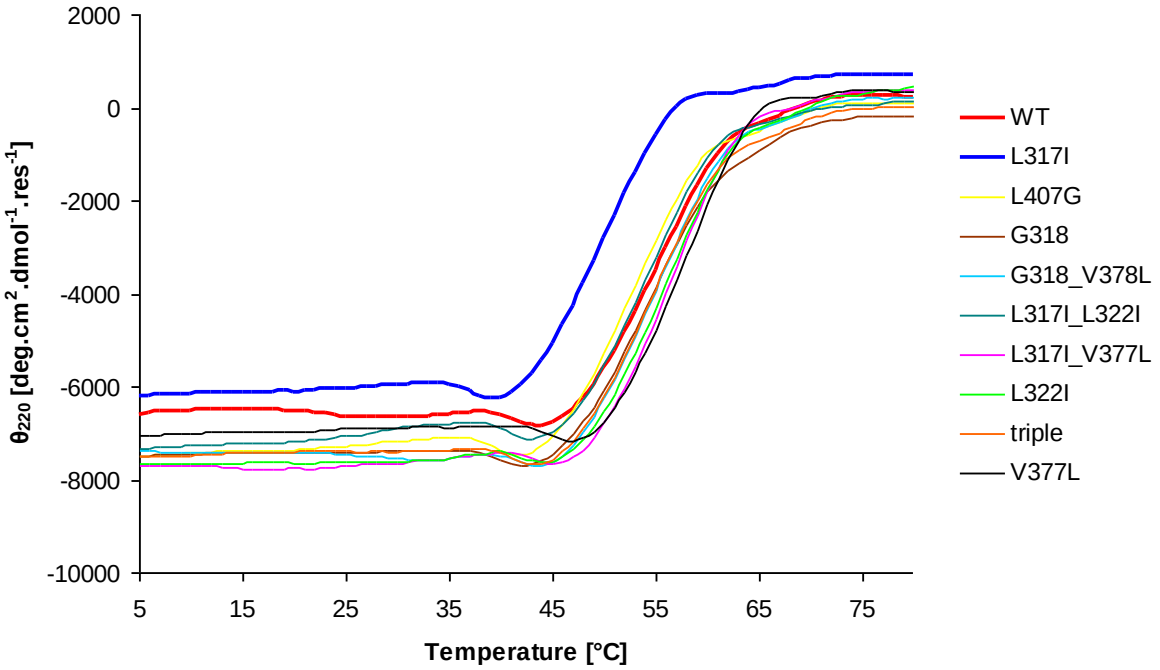

Figure 4.14: Thermal denaturation curves of c-Src WT and mutants. Thermal stability was monitored for 10µM protein in 20mM Tris pH 8.0, 100mM NaCl, 1mM TCEP, at 220nm, within the temperature range of 5-80°C, with a heating rate of 1°C/min. The curves represent the average of at least two independent experiments.

c-Src L317I appeared significantly less stable than the wild type protein and all other c-Src mutants (Figure 4.15). The thermal stability of all c-Src mutants carrying mutations at the level of the H1-H2 interface was significantly modified but could not be correlated to their sensitivity to the DFG-conformational marker imatinib.

While there is no correlation between the T_M and the conformational propensity expressed as sensitivity to imatinib, there is an interesting correlation between the localization of the mutated residue and the resulting thermal stability. Indeed, all c-Src kinase domains containing mutated residues from the H1 interface had lower thermodynamic stability than the WT and that all c-Src kinase domains containing mutated residues from the H2 interface had higher thermodynamic stability than the WT.

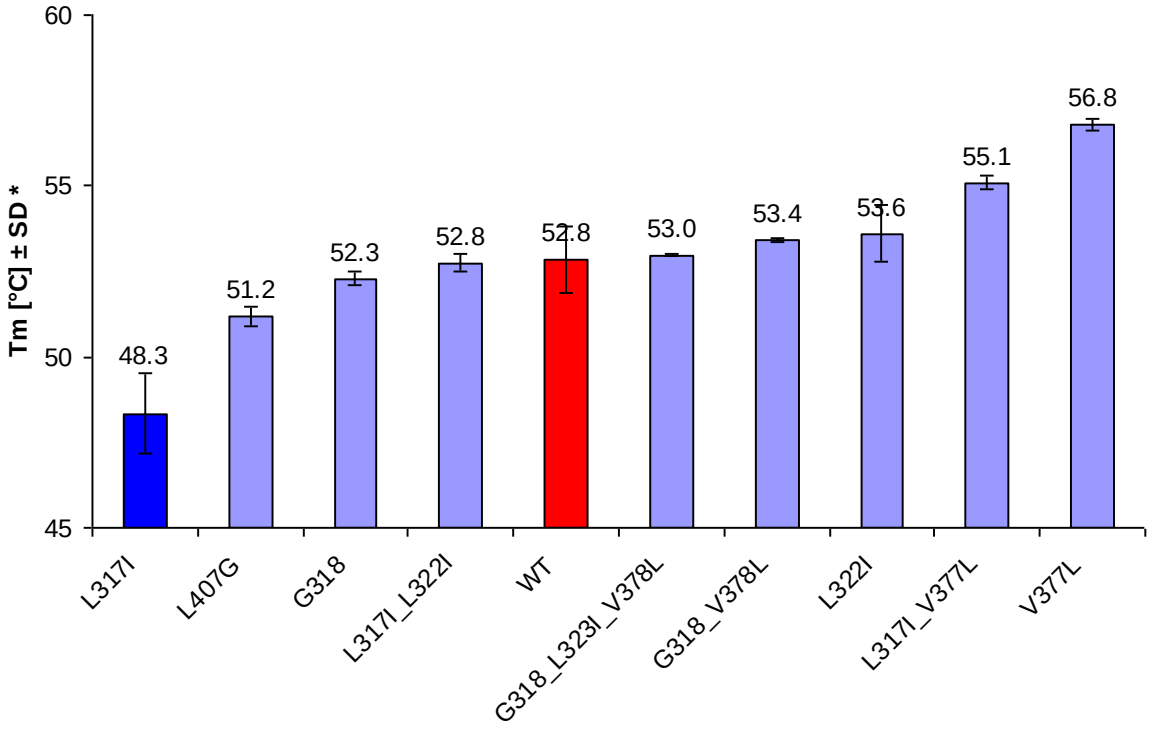

Figure 4.15: Midpoint of the thermal denaturation curve (T_M) for c-Src WT and mutanted kinase domains. Midpoint of thermal denaturation was calculated with Spectra Manager (Jasco, Tokyo, Japan). Standard deviations are represented by vertical bars and represent the average of at least two independent experiments. The trend line (in red) depicts the midpoint of the thermal denaturation of the wild type kinase domain.

Such a tendency was also noticed for the affinity of the c-Src KD variants for imatinib (Figure 4.8) and could be eventually explained by the fact that the conformational motions of H1 residues are more important than fluctuations of H2-residues [71]. To address this issue, molecular dynamic simulations can be used on c-Src kinase domains carrying mutations on the H1 or on the H2 interface.

The CD spectra for c-Src WT and for c-Src L317I in presence of imatinib were characteristic for α-helical proteins with minima at 208nm and 220nm (Figure 4.16) in agreement with the X-ray structures presented in part 3.5

Interestingly, in presence of imatinib, the CD spectrum of c-Src L317I did not reveal a decrease in absolute values in mean molar ellipticity per residue compared to the WT enzyme, indicating a similar secondary structure to the wild type kinase domain. This result seems in line with the analogous crystal structures of c-Src WT and c-Src L317I in complex with Imatinib. Therefore one might dress the hypothesis that the binding of imatinib decreases the dynamical behaviour of c-Src L317I to the level of the wild type kinase domain.

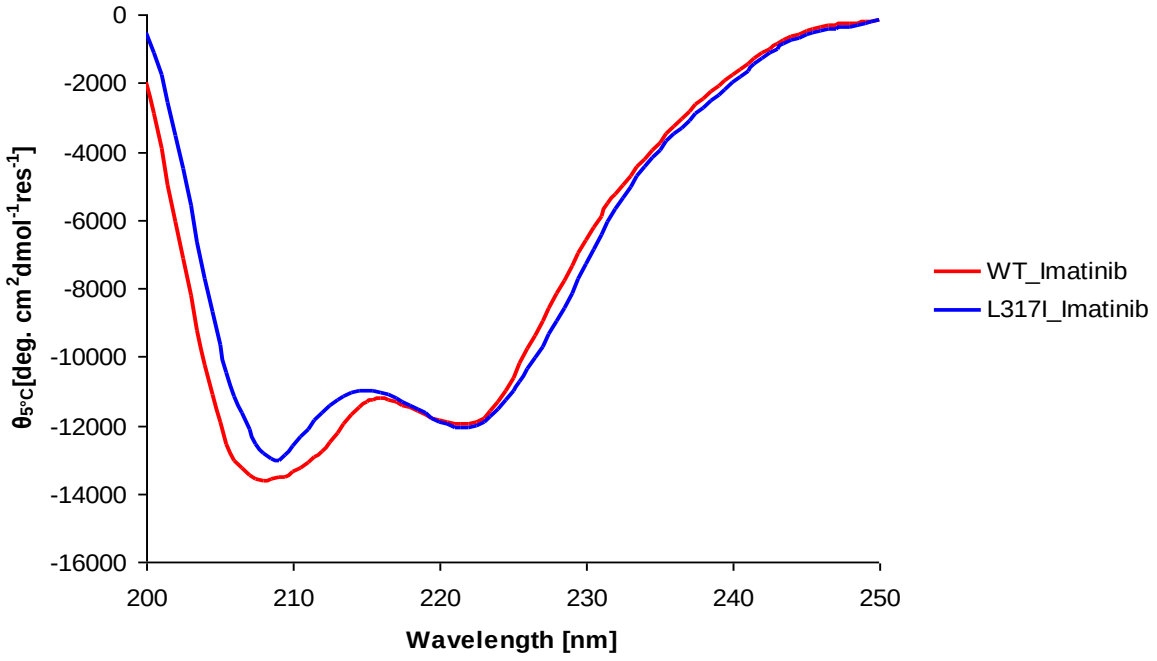

Figure 4.16: Superimposed CD spectra for c-Src WT and c-Src L317I in presence of 15µM Imatinib. CD spectra were recorded at 5°C with 10µM protein in 20mM Tris pH 8.0, 100mM NaCl, 1mM TCEP, 15µM imatinib and corrected with buffer spectra. The curves represent the average of at least two independent experiments.

To determine how the presence of imatinib affected the stability of the mutant *versus* c-Src WT, CD spectra were collected as a function of temperature for both proteins (Figure 4.17).

Here again, both transitions were highly cooperative but not reversible and the protein unfolding led to agglomeration in the samples.

The T_M of c-Src WT did not change significantly in presence of imatinib (52.9 ± 0.1°C) compared to the T_M value calculated for the c-Src kinase domain alone (52.8 ± 0.1°C). For this assay imatinib had to be used at 15μM, which is lower than the Ki (74.5μM) of this inhibitor for the wild type kinase domain. Higher concentrations of imatinib were interfering with the setting of the assay since imatinib is absorbing light at 220nM. Therefore it may be considered that the measured T_M remained unchanged because the concentration of imatinib was not sufficient enough to bind and stabilize the protein.

In contrast, the T_M of the mutant in presence of 15μM imatinib increased the most to a mean of 51.7 ± 0.04 °C (ΔT_M=3.4°C). Such a stabilization of the mutant might be perceived as a confirmation of the hypothesis that imatinib tightly binds and stabilizes the mutated kinase domain at lower concentrations than it does for the wild type c-Src. In line with this statement, the T_M of L322I (Ki of imatinib 98.4 nM) and of L407G (Ki of imatinib 0.8μM) increased to 55 ± 0.05°C (ΔT_M=1.4°C) and 54 ± 0.01°C (ΔT_M=2.8°C) respectively.

A

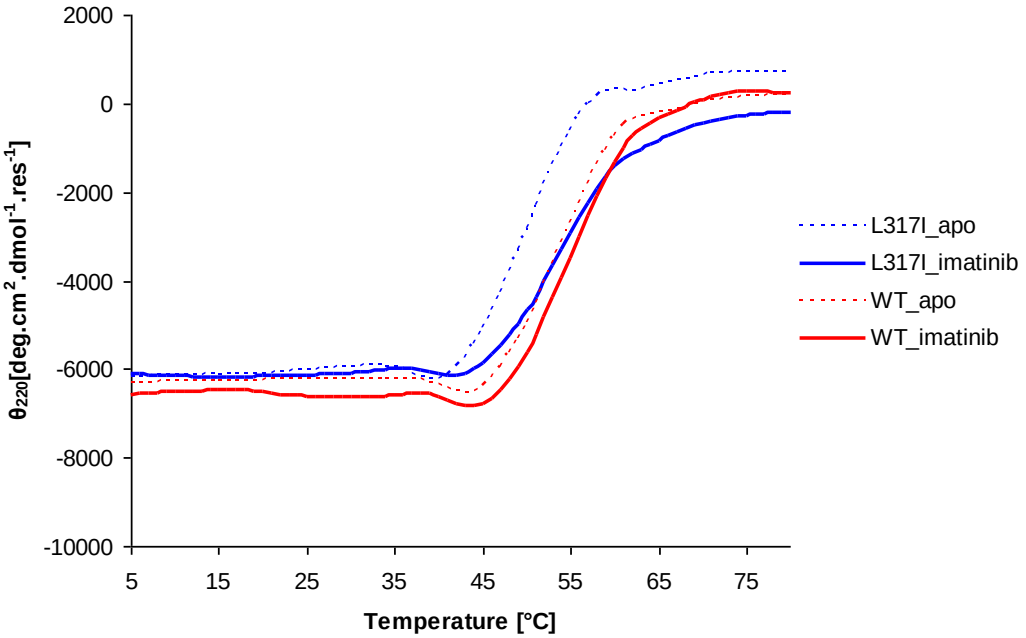

B

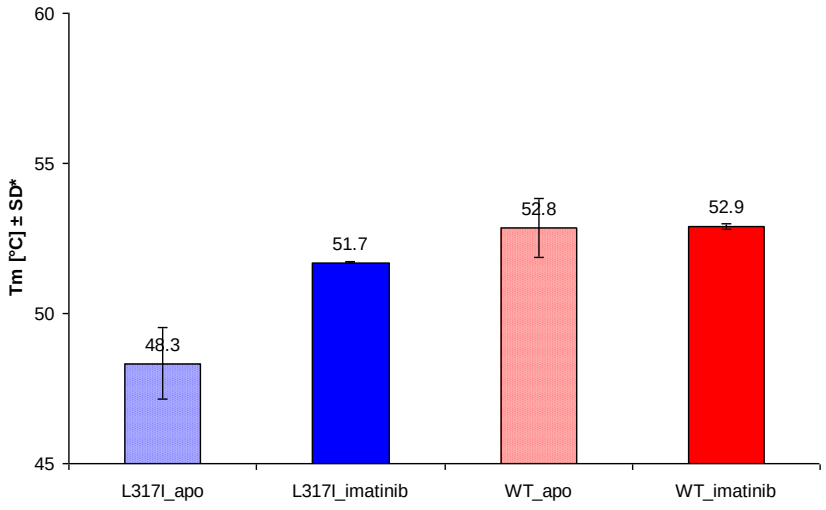

Figure 4.17: Thermal stability of c-Src WT- apo/imatinib and c-Src L317I-apo/imatinib. **A.** Curves were monitored for 10µM protein in 20mM Tris pH 8.0, 100mM NaCl, 1mM TCEP, 15µM imatinib, at 220nm, within the temperature range of 5°C-80°C, with a heating rate of 1°C/min. **B. Midpoint of the thermal denaturation curve (T_M).** T_M was calculated with Spectra Manager (Jasco, Tokyo, Japan). Standard deviations are represented by vertical bars and represent the average of at least two independent experiments.

4.5 Crystal structures of c-Src L317I

Kinetic characterisation of the c-Src kinase domain mutants revealed that residues from the H1-H2 interface have an indirect, but clear influence on c-Src conformational dynamics when they are swapped to the corresponding amino acids of c-Abl, c-Kit or PDGFR. The impact of the latter mutations seems to be focussed mainly at the conformation and/or dynamics of the DFG motif. In addition, kinetic assays with DFG-out binders as the pyrazolopyrimidine compound 5 indicated that L317I mutation influences, to some extent, the conformational equilibrium of c-Src also at the level of the A-loop. Kinetic and CD analysis, though, could not answer to the question whether the swap of L317 to Ile regulated c-Src conformation via stabilization of the inactive c-Abl form of c-Src or by increasing the rate of the conformational dynamics. This major open question prompted us to study the impact of the L317I mutation on a molecular level by means of crystallography on the apo-form of c-Src l317I as well as on it complexes with the conformational markers imatinib, dasatinib and the pyrazolopyrimidine 5 compound.

Apo- and co-crystals grew overnight under the described conditions (cf. Materials and Methods, Chapter 4) as thin needle-like or plate morphology (Figure 4.18). The quasi two dimensional form of c-Src was very similar to the shape of kinase protein crystals in general [277, 278]. Optimization of the crystal growth was approached modifying the composition or concentration of the precipitating agents, the pH of the mother liquor, by different seeding techniques and by reduction of the vapour diffusion in the crystal drop vial using Al's oil (Hampton, USA) over the reservoir solutions but with no success. Fine tuning was finally reached by decreasing the temperature of growth to 14°C. The maximal crystal size (200 x 20 x <5 μm^3) was reached in 24 hours and was similar for all c-Src L317I crystals. All crystals showed satisfying crystallographic properties in terms of crystal mosaicity and diffraction limit.

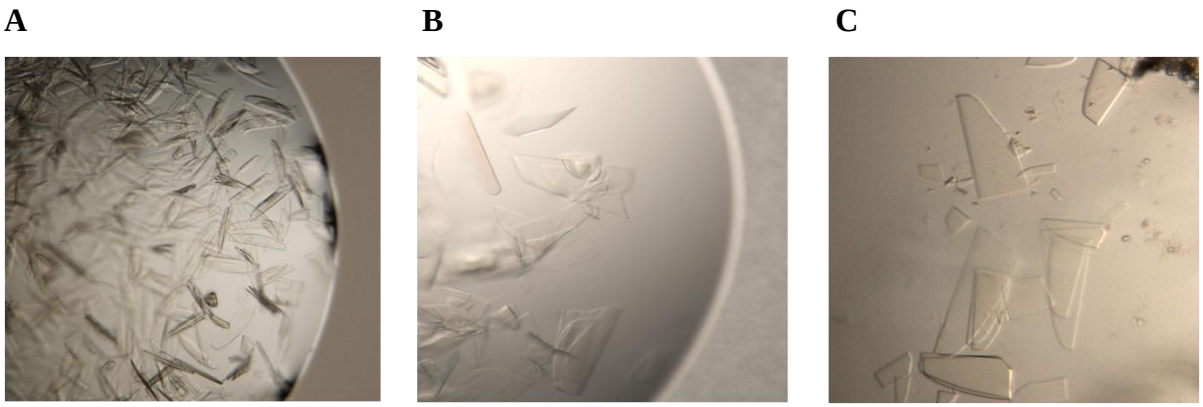

Figure 4.18: A panel of c-Src L317I-dasatinib crystals. Crystals grown under the same conditions. **A, B, C** present different magnifications.

4.6 Crystal structure of c-Src L317I apo form

We report the X-ray crystal structure of c-Src L317I (residues 251-533) at 2.7Å resolution. (Figure 4.19).

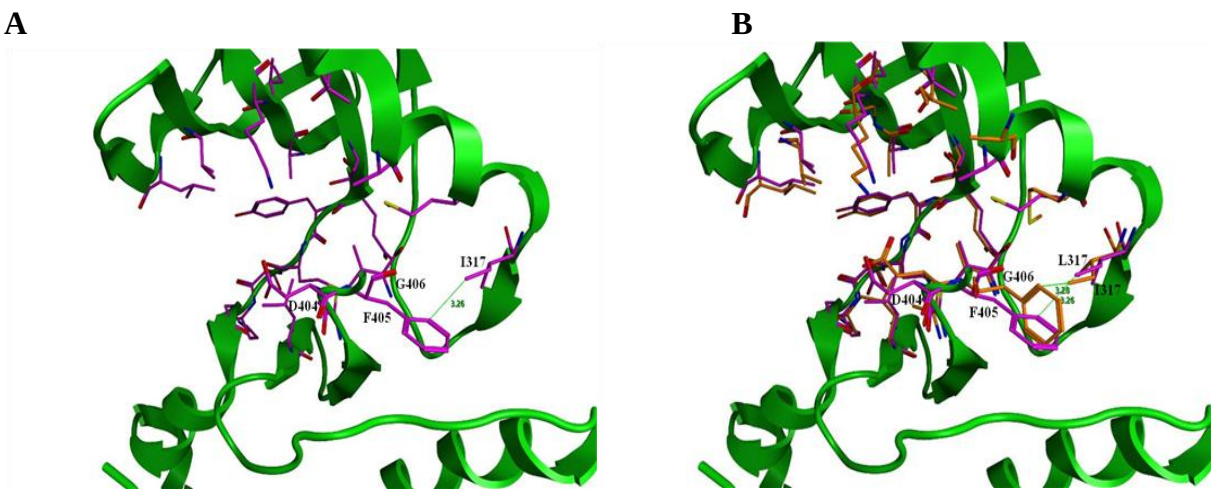

Figure 4.19: The kinase domain of c-Src L317I-apo . A. Ribbon diagram of c-Src L317I-apo structure (PDB ID: 3OF0, in revision). Residues from the ATP-binding site and the DFG-motif of c-Src L317I are shown as sticks (magenta) **B.** Superposition of c-SrcL317I-apo (3OF0) and c-Src WT-imatinib (PDB ID: 2OIQ) kinase domains. Residues from c-Src WT interacting with the ligand and the DFG-motif are shown as sticks (orange). The distances between the aromatic ring of F405 and the side chains of the L317 (in 2OIQ) and I317 (in 3OF0) are shown for each structure.

The crystal had a space group P1. The 3D structure was solved by molecular replacement (PDB ID: 3OFO, in revision. The unit cell was nearly monoclinic. The crystals had two molecules of c-Src L317I in the asymmetric unit, referred to as A and B. A comparison of the two c-Src molecules in the asymmetric unit revealed that their overall conformation was identical and consistent with the general tyrosine kinase fold.

The crystal structure of c-Src L317I is separated in two subdomains or lobes. The smaller N-terminal lobe is composed of a five stranded β-sheet and of one prominent helix, the αC-helix. The C-terminal lobe is larger than the N-terminal and is predominantly helical. The two lobes are connected through a single polypeptide strand (the hinge region) that acts as a linker about which the two domains can rotate with respect to one another and on binding of ATP and/or substrate. The ATP-binding site is in a deep cleft between the two lobes and sits beneath a highly flexible P-loop connecting strands β_1 and β_2. The P-loop contains the conserved (GXGXφG), where φ, a Phe in c-Src, caps the site of phosphate transfer. The structure reveals that the A-loop is partially disordered as indicated by high β-factors and broken electron density. Therefore, it was not possible to define with accuracy the presence of an "open", extended from the ATP-binding site A-loop, or the presence of a "closed", folded back toward the ATP-binding site A-loop.

Phe405 of the L317I mutant is buried in a hydrophobic pocket not accessed by ATP, as it is typically found with activated kinase domains. Therefore we can conclude that the L317I mutation does not stabilize the DFG motif into a flipped, DFG-out conformation, despite this was one of our hypothesis considering the radically higher affinity of the mutant for imatinib (IC_{50}=4nM).

However, the location of Phe405 found in c-Src L317I mutant presents a particular conformation which places the aromatic ring of the amino acid

closer to the side chain of the Ile at position 317 (3.2Å) than it is the case within the wild type c-Src structure where the side chain of Phe405 is 3.8Å apart from the side chain of the Leu317.

In c-Src L317I, the Phe405 forms three other hydrophobic interactions. They are depicted between Phe405 and Val377 from the H2 interface; between Phe405 and the aromatic ring of Tyr382 from the catalytic loop and between Phe405 and the highly conserved His384 from the catalytic loop.

The particular position of Phe405 in respect to the Ile317 in combination with the three hydrophobic interactions that it forms with Val377, Tyr382 and His384, have not been observed neither in the DFG-in structure of c-Src WT (PDB ID: 1FMK), nor in the structure of c-Src WT with dasatinib (PDB ID: 3G5D).

Thus, the location of Phe405 in c-Src L317I can be considered as unique in the "conformational panorama" of c-Src tyrosine domain plasticity and it proves that I317 does influence the position of the Phe405.

In conclusion, the crystal structure of c-Src L317I-apo rather supports the hypothesis ventured upon the *in vitro* inhibition assays, suggesting that the L317I swap may modify the dynamics of the transition from a DFG-in to a DFG-out conformation.

4.7 Crystal structure of c-Src L317I in complex with imatinib

Purified c-Src L317I mutant without the 6xHis-tag was cocrystallized with imatinib. The crystals had space group P1 and difracted at 2.4Å resolution. The 3D structure was solved by molecular replacement (PDB ID: 3OEZ, in revision), (Table 4.2). The unit cell was nearly monoclinic. The crystals had two molecules of c-Src L317I in the asymmetric unit, referred to as A and B. There was a well-defined electron density for imatinib in both molecules (Figure 4.20A), which appeared to be bound with full occupancy. A comparison of the two c-Src L317I molecules in the asymmetric unit revealed that their overall conformation was nearly identical.

L317I in complex with imatinib has been compared to 2OIQ [155] crystal structure which depicts c-Src WT kinase domain in complex with imatinib. Both L317I-imatinib and 2OIQ crystal structures were very well super imposable with an overall CA RMSD of 0.654Å (Figure 4.20B). Imatinib is bound to c-Src L317I in the extended "trans" conformation (Figure 4.20C and D) as in the c-Abl-imatinib (PDB ID: 1OPJ); c-Kit-imatinib (PDB ID: 1T46) and c-Src WT-imatinib complexes (PDB ID: 2OIQ) [155, 220, 272, 279]. The structure of the imatinib-binding pocket was very similar in c-Src L317I, c-Src WT, c-Abl and c-Kit complexes with imatinib. Like in 2OIQ, only two regions in c-Src L317I-imatinib complex deviated significantly from the structure of Abl-imatinib: the P-loop (c-Src residues 273-282) and the A-loop (c-Src residues 404-425), the central portion of which is disordered (c-Src residues 407-423). When compared visually to the Src/CDK inactive conformation (PDB ID: 2SRC), the α-C helix in the c-Src L317I-imatinib complex is rotated inward, the DFG is flipped and the global conformation of the kinase domains is opened to accommodate the small molecule as in the c-Src WT-imatinib complex.

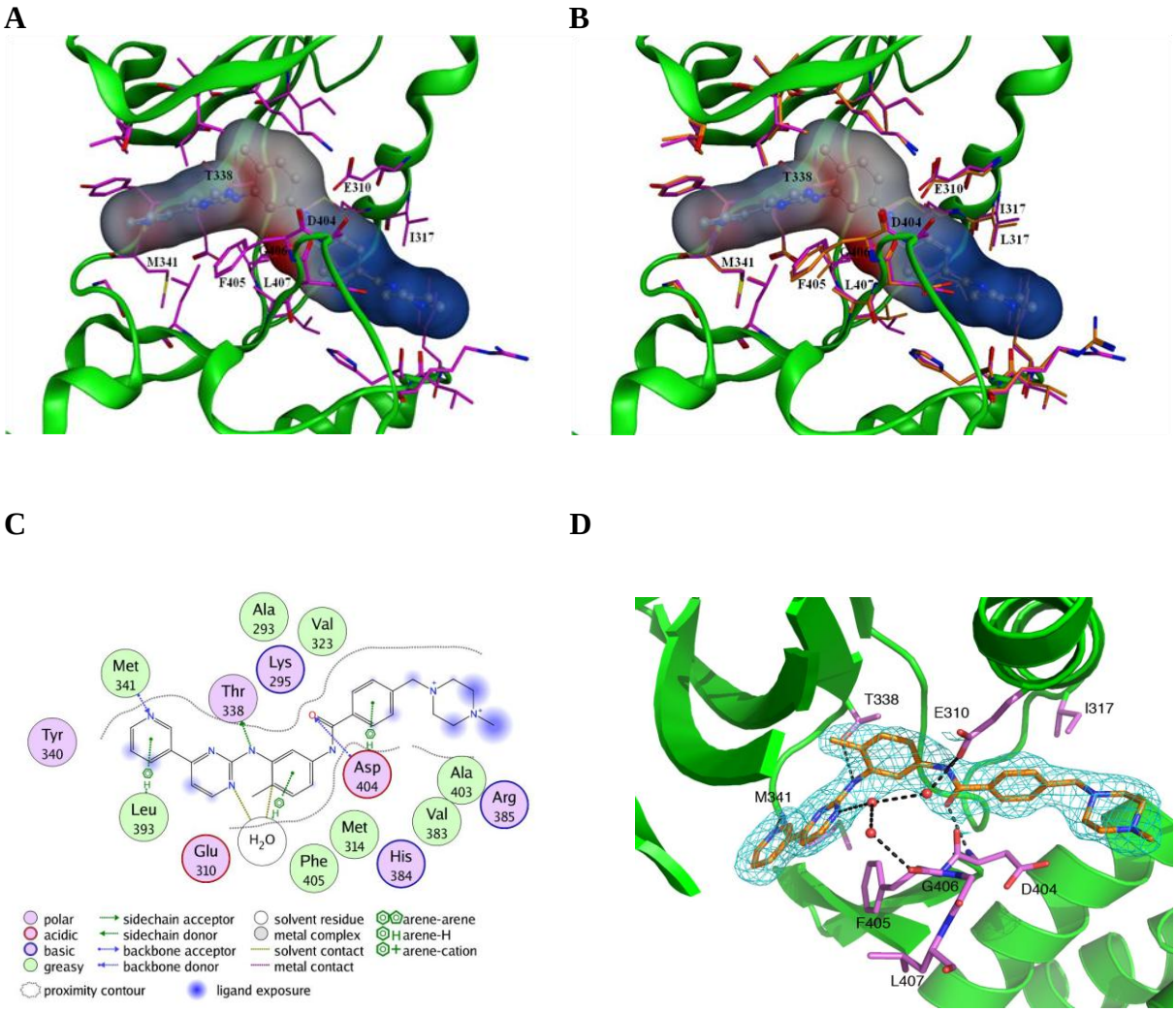

Figure 4.20: Kinase domain of c-Src L317I complexed with imatinib. A. Ribbon diagram of c-Src L317I complexed with imatinb (PDB ID: 3OEZ, in revision). The Connolly surface of imatinib (probe radius of 1.4Å) depicts regions with positive electrostatic potential (blue), negative electrostatic potential (red) and uncharged, hydrophobic regions (gray). Residues from c-Src L317I interacting with the ligand as well as the DFG-motif are shown stick representation (magenta) **B.** Superposition of c-Src L317I (3OEZ, green) and c-Src WT (PDB ID: 2OIQ) both complexed with imatinb. Residues from c-Src WT interacting with the ligand as well as the DFG-motif are shown stick representation (orange). **C.** Interaction map of c-Src L317I with imatinib generated on Moe2010.10 with 3.5Å as maximum interaction distance. Hydrogen bonds are indicated with dotted lines. **D.** Electron density map of imatinib in 3OEZ at 2.4Å after refinement ($2F_0 - F_c$) contoured at $\sigma = 1$.

In the c-Src L317I-imatinib complex, the direction of Arg388 was the same as in the c-Src WT-imatinib crystal. The position of Arg388 in 2OIQ is thought to clash with the A-loop Tyr416 if the central portion of the A-loop were to adopt the conformation observed in Abl-imatinib [155]. c-Src L317I mutant was resolved with disordered residues 407-423. Nevertheless, the conformation of Arg388 could indicate a similar conformation for the A-loop in both c-Src L317I and c-Src WT kinase domain structures with imatinib.

The P-loop conformation in c-Src L317I-imatinib complex was in an extended conformation as in c-Src WT-imatinib and c-Kit-imatinib co-crystals. This made the formation of hydrogen bonds between Tyr253 and Gln252 in the P-loop with the backbone and side chain of Asn322 impossible, but did not hinder imatinib binding.

F405 from the DFG triad had the "out" conformation as visualized in c-Src WT (PDB ID: 2OIQ). The Root Mean Square deviation (RMSD) between L317I and I317 is 0.53Å and the minimal distance between L317 from 2OIQ and imatinib was 3.9Å. This distance was conserved in the c-Src L317I-imatinib structure.

4.8 Crystal structure of c-Src L317I in complex with dasatinib

Purified c-Src L317I mutant was cocrystallized with dasatinib. The crystals had space group P1 and diffracted at 2.75Å resolution. The 3D structure was solved by molecular replacement (Table 4.2) using the published c-Src structure (PDB ID: 3G5D) [280] and the Lyn complex with dasatinib (PDB ID: 2ZVA) [281]. The unit cell was nearly monoclinic. The crystals had two molecules of c-Src L317I in the asymmetric unit, referred to as A and B.

There was a well-defined electron density for dasatinib in both molecules A and B, which appeared to be bound with full occupancy (Figure 4.21A). A comparison of the two c-Src L317I molecules in the asymmetric unit reveals that their overall conformation is nearly identical.

When compared to the c-Abl-dasatinib co-crystal (PDB ID: 2GQG) , c-Src L317I-dastinib complex encompassed the main structural features of an activated kinase domain. The ligand was bound to the DFG-in c-Src conformation. Dasatinib was sitting in the ATP site enveloped by the N-lobe and the C-lobe, with the aminothiazole moiety of the molecule occupying the site normally bound by the adenine group of ATP (Figure 4.21). The 2-chloro-6-methyl phenyl ring of dasatinib was orthogonal to the thiazole carboxamide group and probed into a mostly hydrophobic pocket near Thr338 (in c-Src) that is not occupied by ATP (hydrophobic pocket I). The piperazine group pointed toward the surface-exposed portion of the hinge region. The three hydrogen bonds identified between dasatinib-c-Abl and dasatinib-c-Src WT were present in the complex with c-Src L317I [280, 282].

c-Src L317I in co-crystal with dasatinib was compared to c-Src protein tyrosine kinase bound to dasatinib and deposited in the Protein Data Bank as 3G5D. Both crystal structures are not WT. They contain mutations at different regions.

3G5D contained the mutation S345 to Cys [280]. S345 is a residue positioned at the end of the hinge region. L317I mutation is located in the H1-H2 interface as described in Chapter 2.

We compared both structures by superposing their N-lobes, C-lobes and by performing an overall superposition of the whole kinase domain (Figure 4.21 B).

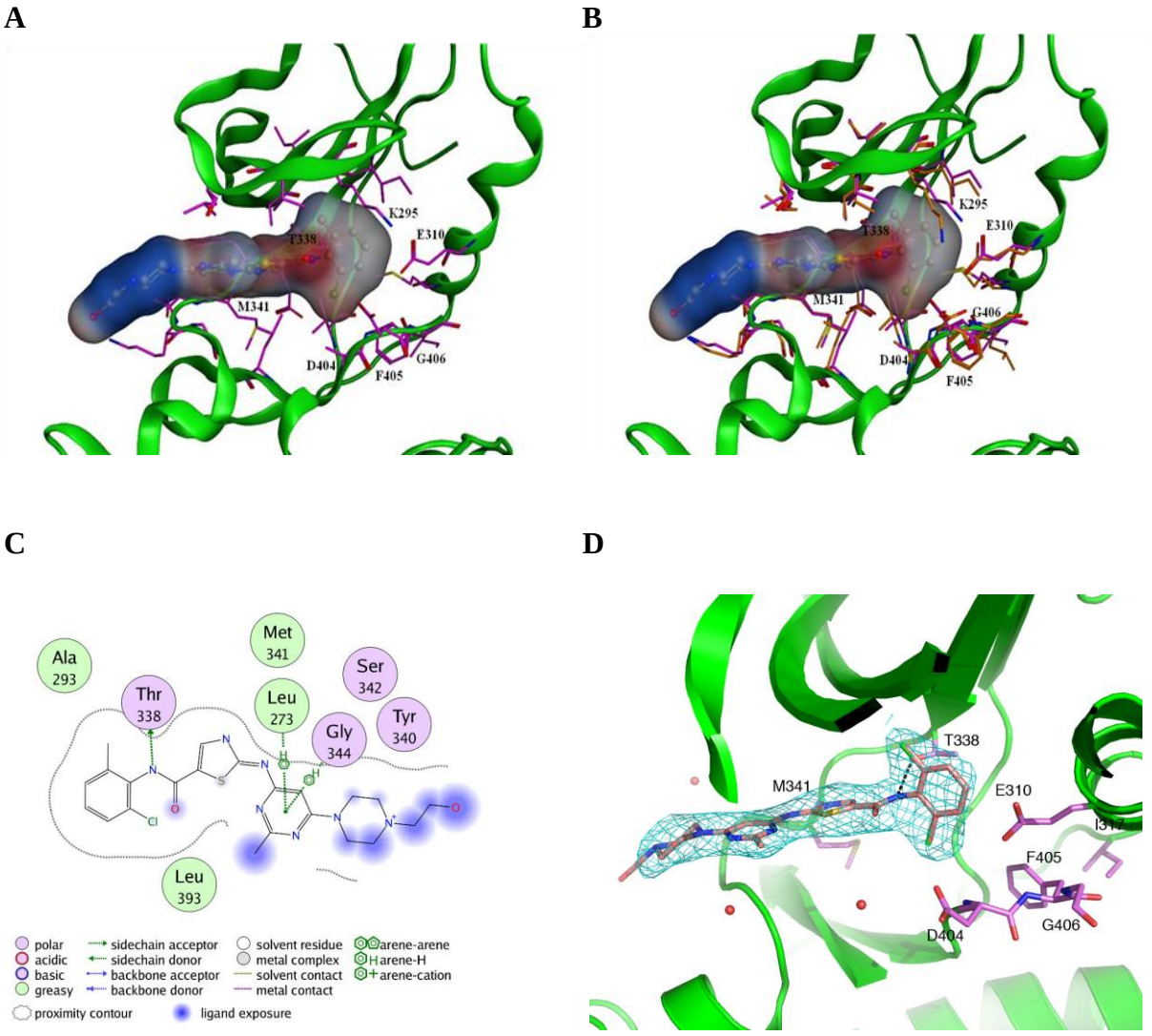

Figure 4.21: Kinase domain of c-Src L317I complexed with dasatinib. A. Ribbon diagram of c-Src L317I complexed with dasatinib (in deposition). The Connolly surface of imatinib (probe radius of 1.4Å) depicts regions with positive electrostatic potential (blue), negative electrostatic potential (red) and uncharged, hydrophobic regions (gray). Residues from c-Src L317I interacting with the ligand as well as the DFG-motif are shown in stick representation (magenta) **B.** Superposition of c-SrcL317I and c-Src WT (PDB ID: 3G5D) both complexed with dasatinib. Residues from c-Src WT interacting with the ligand as well as the DFG-motif are shown stick representation (orange). **C.** Interaction map of c-Src L317I with dasatinib generated on Moe2010.10 with 3.5Å as maximum interaction distance. Hydrogen bonds are indicated with dotted lines. **D.** Electron density map of dasatinib in complex with c-Src L317I at 2.75Å after refinement ($2F_0 - F_c$) contoured at $\sigma = 1$.

S345 of c-Src L317I was very well superimposed to C345 of 3G5D (RMSD 0.3Å). Dasatinib binds the L317I mutant with the same binding mode visualized in 3G5D crystal structure. There were no major differences at the ATP binding site. The ligand binds the DFG-in conformation. The A-loop (residues 407-423 in c-Src) has not been solved as in 3G5D.

The RMSD between K295 of the two proteins was approximately 1.7Å and the salt-bridge interaction with E310 was present (2.9Å). K315 of 2G5D makes a salt bridge with D258 stabilizing the position of the N-terminal tail. K315 has not been solved in c-Src L317I; resulting in a 1.8Å RMSD of D258 with a different orientation compared to 3G5D. The minimum distance between L317 and F405 was 4.2Å in 3G5D and it was comparable to F405-I317 in the mutant (4.1Å).

The crystallographic analysis of this interaction and of the overall structure of the complex showed that the swap L317I in c-Src had no impact in binding dasatinib. I317 did not stabilize the F405 in the "thermodynamical penalty" flipped conformation even in a complex with an inhibitor showing less conformational rigidity for binding.

4.9 Crystal structure of c-Src L317I in complex with pyrazolopyrimidine compound 5

Purified c-Src L317I mutant without the 6xHis-tag as described earlier (Chapter 3) was cocrystallized with pyrazolopyrimidine compound 5 [256]. The crystals had space group P1 and diffracted at 2.75Å resolution. The 3D structure was solved by molecular replacement (Table 4.2) using the published c-Src structure (PDB ID: 3EL8) [256]. The unit cell was nearly monoclinic. The crystals had two molecules of c-Src L317I in the asymmetric unit, referred to as A and B.

In both, the A-loop has not been solved as in the complex between c-Src WT-pyrazoplopyrimidine 5 compound (3EL8). Glu310 within the α-C helix could not be solved neither.

There was a well-defined electron density for pyrazolopyrimidine compound 5 in both molecules A and B, which appeared to be bound with full occupancy (Figure 4.22). Each subunit was co-crystalized with the ligand compared to the structure of c-Src WT (PDB ID: 3EL8) where the pyrazolopyrimidine 5 compound was solved only in subunit A. The binding site of the ligand is the same as in c-Src WT but the hydrogen bond interactions differ from those depicted in 3EL8. In both subunits, the conformation of the DFG-motif is "in" eventhough not identical between subunit A and B (Figure 4.22 depicts the subunit A). This is a major difference to 3EL8, where the DFG-out conformation is present. Therefore the pyrazolopyrimidine 5 compound does not form hydrogen bond interactions with the F405 from the DFG, but with the D404. This observation could lead to the conclusion that the pyrazolopyrimidine 5 compound can bind with the same binding mode with the DFG-in and –out conformations, as we could already expect since both the unphosphorylated and pre-phosphorylated form of c-Src L317I could bind the compound with IC values in the low nanomolar range. The compound is slightly shifted away from the side-chain hydroxyl of the Thr338 gatekeeper and as a result does not form the hydrogen bond seen in 3EL8 with this residue. The pyrazolopyrimidine ring of the compound forms hydrogen bonds with the main chain carbonyl of E339 and with M341. Since the E310 was not solved in this structure of L317I, we cannot state whether the interaction with the side chain of E310 is preserved. In c-Src L317I the urea extension of the compound was found in the pocket lined by the same residues as in 3EL8.

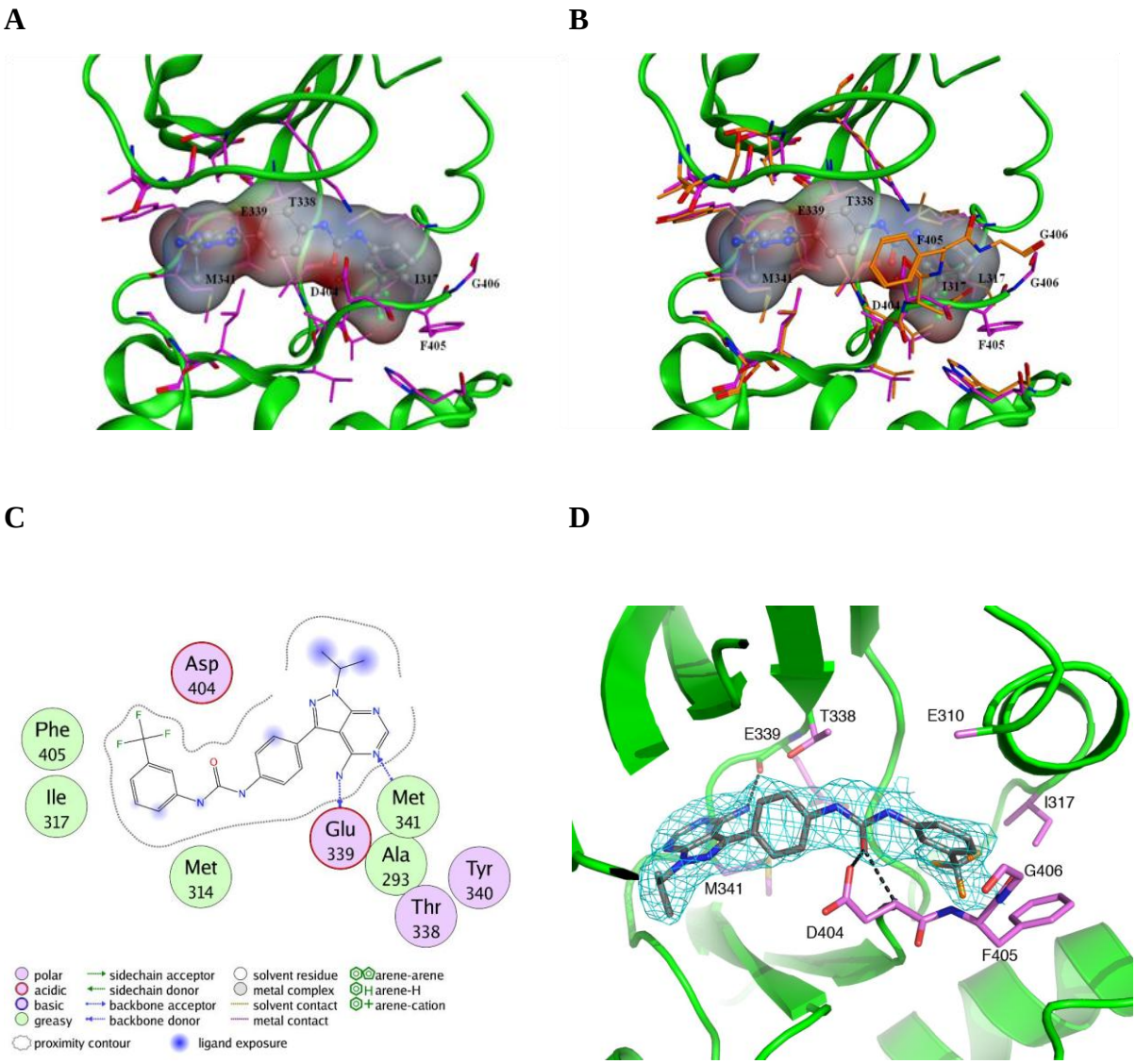

Figure 4.22: Kinase domain of c-Src L317I complexed with pyrazolopyrimidine 5 compound. A. Ribbon diagram of c-Src L317I complexed with pyrazolopyrimidine 5 compound (in deposition). The Connolly surface of imatinib (probe radius of 1.4Å) depicts regions with positive electrostatic potential (blue), negative electrostatic potential (red) and uncharged, hydrophobic regions (gray). Residues from c-Src L317I interacting with the ligand as well as the DFG-motif are shown stick representation (magenta) **B.** Superposition of c-SrcL317I and c-Src WT (PDB ID: 3EL8) both complexed with dasatinib. Residues from c-Src WT interacting with the ligand as well as the DFG-motif are shown stick representation (orange). **C.** Interaction map of c-Src L317I with the pyrazolopyrimidine 5 compound generated on Moe2010.10 with 3.5Å as maximum interaction distance. Hydrogen bonds are indicated with dotted lines. **D.** Electron density map of the pyrazolopyrimidine 5 compound in complex with c-Src L317I at 2.75Å after refinement ($2F_0 - F_c$) contoured at $\sigma = 1$.

Table 4.2: Data collection and refinement statistics

Data Collection	**SLS - x06DA**	**SLS - x06DA**	**SLS - x06DA**	**SLS - x06DA**
Crystal	L317I c-Src Apo	L317I c-Src + imatinib	L317I c-Src + dasatinib	L317I c-Src + pyrazolopyrimidine 5
Space group	*P*1	*P*1	*P*1	*P*1
Unit cell parameters	*a* = 42.07 Å *b* = 63.49 Å *c* = 74.12 Å α = 78.66° β = 89.41° γ = 90.00°	*a* = 41.89 Å *b* = 63.43 Å *c* = 74.14 Å α = 79.16° β = 90.02° γ = 90.19°	*a* = 42.26 Å *b* = 63.49 Å *c* = 74.44 Å α = 100.74° β = 90.18° γ = 90.0°	*a* = 42.27 Å *b* = 63.50 Å *c* = 73.45 Å α = 79.48° β = 90.09° γ = 89.41°
Resolution limits (Å)	32.8 - 2.7	32.7 - 2.4	34.5 - 2.75	33 - 2.75
No. of measured reflections	78503	111593	73645	72272
No. of unique reflections	20128	28323	18788	18749
Redundancy*	3.9 (3.9)	3.9 (3.9)	3.9 (3.8)	3.9 (3.9)
Completeness (%)*	97.3 (97.3)	96.5 (96.5)	95.1 (87.3)	96 (95.2)
I/σ(I)*	9.4 (2.97)	19.3 (3.1)	12.05 (3.1)	10.3 (2.22)
R_{sym} (%)*	11.6 (38.8)	5.6 (32.2)	9.4 (34.1)	11.7 (53.8)
Refinement				
No. of reflections	20120	28322	18782	17811
No. of omitted reflections	977	1379	912	938
No. of proteins residues	511	520	519	507
No. of water molecules	241	287	180	99
No. of Imatinib/Dasatinib	-	2	2	2
R (%) / R_{free} (%)	23.3 / 26.2	19.4 / 24.0	20.0 / 26.85	18.4 / 24.2
Mean on *B*-factors (Å^2)				
Protein / solvent	36.8 / 27.4	40.9 / 37.3	40.1/ 26.1	36.5/ 26.1
Compound	-	43.6	41.3	47.5
r.m.s.d. from ideal geometry				
Bond length (Å)	0.003	0.007	0.006	0.009
Bond angles (°)	0.683	1.035	0.944	1.17

* Numbers in brackets are for the highest shell of resolution: 2.7 - 2.85Å for L317I c-Src apo, 2.4 - 2.53Å for L317I c-Src + imatinib, 2.75 Å - 2.9 Å for L317I c-Src + dasatinib, 2.75 Å - 2.9 Å for L317I c-Src + pyrazolopyrimidine 5.

4.10 Imatinib binding to c-Src L317I: a calorimetric study

We determined the dissociation constants, K_D, of imatinib binding to unphosphorylated c-Src L317I and c-Src WT kinase domains by ITC (Figure 4.23). ITC data indicated that the binding of imatinib to the L317I c-Src mutant (K_D = 7.2 ± 3.14μM) was nearly the same as to the wild type c-Src (K_D = 7.2 ± 2.2 μM) and was not comparable to the binding to c-Abl (K_D = 0.08μM) [155]. These values were not in line with Ki values obtained for unphosphorylated c-Src L317I (K_i = 3.8±0.02nM.) and c-Src WT (K_i = 44.9±7.6μM). Thus, measurements of imatinib binding affinity to c-Src L317I by calorimetry could support the conclusions drawn after the analysis of the c-Src L317I-apo structure excluding the hypothesis that L317I mutation governs the prevalence of the DFG-out conformation in c-Src KD.

An explanation for the disagreement between inhibition and binding affinity most probably lies on the kinetics of binding. There is indeed a substantial difference between the experimental conditions for K_i measurement as compared with conditions for crystallization and ITC. In the first case, c-Src WT and L317I were assayed under "catalytic" conditions (in presence of ATP and Mg^{2+}) allowing the kinase domain to freely undergo the conformational transitions related to its catalytic cycle. ITC experiments were performed in the absence of ATP and Mg^{2+}, and like the crystallization "static" conditions, could give only "snap-shot" information on the role of L317I on the conformation of the DFG-motif.

An orthogonal way for direct measurement of K_D, K_{on} and K_{off} for ligand binding under catalytic conditions for c-Src L317I, could be to adapt a recently described DFG-out fluorescence-based binding assay by J. Simard et al. [244]. In the latter assay, the N-terminal region of the A-loop is specifically labelled with an environmentally sensitive fluorofore using a Cys residue introduced via site-directed mutagenesis into a position that

does not alter the kinetic parameters of the kinase. Fluorescence signals at 475nm and 505nm could then be used as reporters for the position of the DFG in the wild type or mutated c-Src kinase domain.

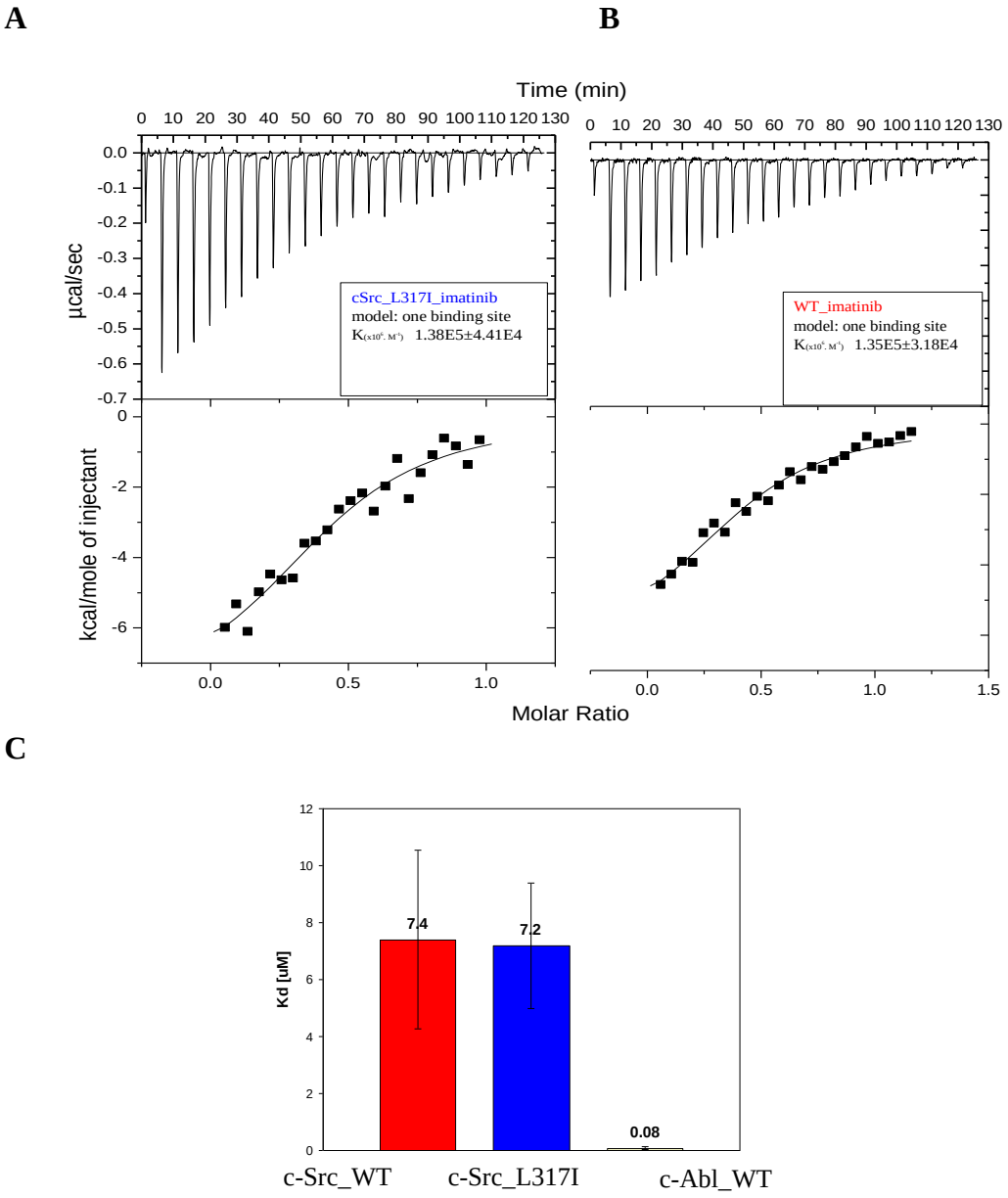

Figure 4.23: ITC assay of imatinib binding to c-Src WT, c-Src L317I. Binding of imatinib to c-Src L317I (**A**) and to c-SrcWT (**B**). The top panel shows heat signals upon 37 injections (8µl) of imatinib (1.5µM) into the sample cell containing 0.1mM protein. The obtained binding isotherm is shown on the lower panel. The solid line represents the non-linear least square fit based on a one-site binding model. **C.** Comparison of KD values obtained by ITC for c-Src WT, c-Src L317I and c-Abl WT.

4.11 H1-H2 naturally occurring mutations in c-Src?

Biophysical and biochemical assays on the H1-H2 c-Src kinase domain mutants have confirmed the hypothesis that residues from the H1-H2 hydrophobic interface in c-Src and in particular at position 317, affect the conformational dynamics of the enzyme mainly at the level of the DFG motif. Since all c-Src kinase domain mutants were generated by swapping H1-H2 residues to the corresponding ones in other cytosolic (c-Abl, c-Kit) or receptor (PDGFR) kinases, we went on investigating whether these mutations existed as natural variants of c-Src in human or other living organisms (Choanoflagellida; Spongillidae; Arthropoda; Viruses and Vertebrates) using multiple sequence alignment performed with ClustaW2 [283].

Since no tyrosine kinases could yet be isolated from plants and characterized, we did not search for H1-H2 c-Src variants in plants [103].

We have found that except of M341I in *Xenopus leavis* (UniProtKB ID: P13115), there is no difference within the primary structure of the H1-H2 domain of c-Src neither in vertebrates, nor in viruses which was found to be identical in both phylogenies. Thus, none of the mutations described in this work exists in vertebrates, or in viruses.

Interestingly, some of the hydrophobic residues (at positions 313, 317, 323, from the H1 and 377, 382 and 394 from the H2 of c-Src) were identical to the corresponding ones in c-Kit, PDGFR and/or c-Abl in phylogenies that are representative of the early evolution in Src, such as Choanoflagellida, Spongilliae and Arthropoda) (Figure 4.24) [284-287].

A

Interface	c-Abl	c-Kit	PDGFRα	c-Src	Residue variations in c-Src species
H1	**I**	L	L	L_{317}	**I** (Spongillidae)
	H	H	H	H_{319}	No variations
	L	I	V	L_{322}	No variations
	V	V	V	V_{323}	No variations
	E	E	E	E_{339}	No variations
	M	C	M	M_{341}	No variations
H2	A	G	G	G_{373}	No variations
	Y	F	F	Y_{376}	No variations
	L	**L**	**L**	V_{377}	**L** (Arthropoda; Spongillidae; Choanoflagellida)
	F	C	C	Y_{382}	**F** (Choanoflagellida)
	V	L	L	V_{394}	No variations
	V	T	**V**	C_{400}	**V** (Arthropoda; Spongillidae; Choanoflagellida)
	K	K	K	K_{401}	No variations
	V	**I**	**I**	V_{402}	**I** (Arthropoda; Spongillidae)
PDB/ sequence ID	**1IEP**	**1T46**	**P16234**	**2OIQ**	

B

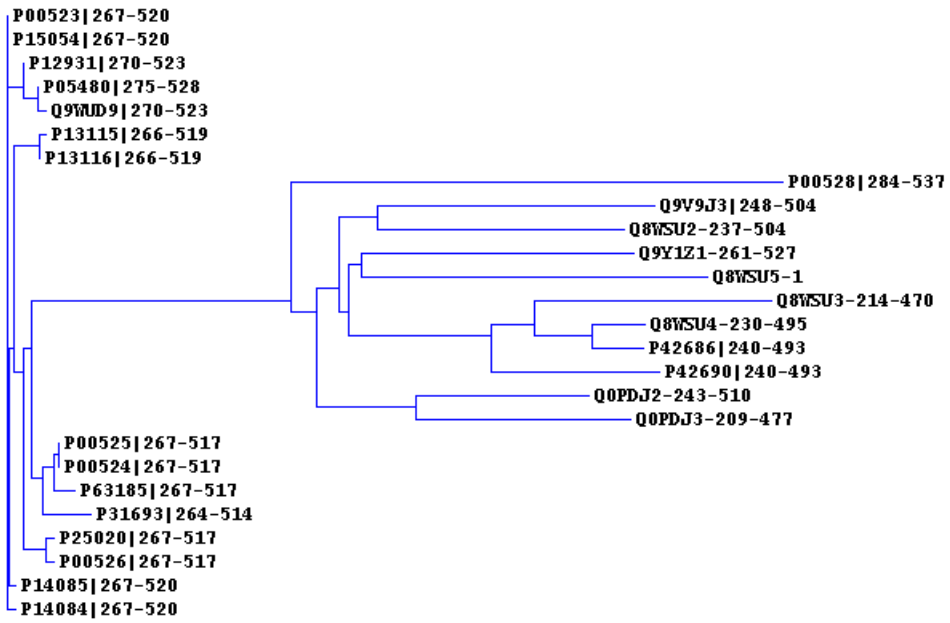

Figure 4.24: Variation and genetic evolution of the H1-H2 forming residues in Src. A. Src orthologues at residues forming the H1-H2 hydrophobic interface. Variant residues within c-Src species are depiced in bold **B.** Phylogram of c-Src from different species after Blast search and ClustaW2 alignment of sequences forming the respective Src kinase domains.

Alignments of these Src orthologs revealed that the kinase domains are nevertheless relatively highly conserved, with amino-acid identities to chicken c-Src ranging from 58% (*E. fluviatilis,* PDB ID: Q8WSU5) to 65% (*Monosiga ovata,* PDB IDs: Q0PDG2-5). All Src orthologs presented in Table 4.23A contain the regulatory SH2 and SH3 domains, as well as conserved critical residues required for intramolecular domain interactions (Y90, Y135 and P250 in chicken c-Src), suggesting that these primitive c-Src relatives may be regulated in a similar manner as Src in vertebrates.

A work published by Segawa et al. [287] stated that these evolutionary intermediate forms of c-Src exhibit a substantial activity even when Y527 is phosphorylated and that the origin of this "unstable" negative regulation, located in the N-lobe, enhances the flexibility of the catalytic pocket. This hypothesis goes in line with the kinetics performed on c-Src L317I KD, which presents a higher V_{max} value than the wild type c-Src kinase domain (Figure 4.7) hence bringing to the supposition that the explanation at the molecular level of the "unstable" negative regulation of c-Src from *E. fluviatilis* may partially lie on the presence of an Ile at position 317.

Thus L317I may be considered as an index for the evolutionary history of Src negative regulation from a unicellular ancestor to multicellular organisms.

The presence of L317I mutation in primitive multicellular organisms and the fact that this mutation apparently increases drastically the affinity of imatinib for Src, opens a discussion on the ecological aspect of released chemotherapies on living organisms that present enhanced sensibility to given therapeutic molecules. On the other hand it comes to support the relatively new field in medicinal chemistry where orthologs of tyrosine kinases in microorganisms might be seen as novel targets for anti-infectious agents [288].

5. Conclusion

Rationally designed and expressed c-Src kinase domain mutants (*cf*. chapters 2 and 3) were subjected to a panel of experimental assays with the intention of answering whether and how residues of the H1-H2 hydrophobic interface control c-Src kinase domain conformational transition.

Activity and autophosphorylation tests could show that H1-H2 c-Src KD mutants present similar enzymatic activity but slower autophosphorylation and provided a first hint on the involvement of the latter residues in c-Src KD dynamics.

Inhibition tests with three different ATP-competitive inhibitors (imatinib, dasatinib and a pyrazolopyrimidine compound) indicated that residues from the H1-H2 interface have a focused impact on the dynamical behaviour of the DFG motif and in some measure, to the remaining part of the A-loop. Remarkably, one of the identified H1 residues, L317, when swapped to an Ile as in the kinase domain of c-Abl, could completely turn imatinib activity toward c-Src from µM to nM. This observation led us to investigate on how L317I mutation affects the conformational selection of c-Src tyrosine kinase domain at the level of the DFG triad.

Despite inhibition data, the crystal structure of c-Src L317I-apo did not depict an abolished thermodynamic penalty conformation for the mutant. On the contrary, the DFG motif presented a new, but still considered as "in" conformation. Furthermore, the c-Src L317I in complex with imatinib showed that the mutation did not influence the binding mode of the inhibitor.

Performed in parallel, ITC measurements for imatinib binding to L317 and WT c-Src kinase domains depicted as well a discrepancy in comparison with inhibition data; K_D values for the mutant and the wild type protein were similar and both in the μM range.

Thus, the crystal structure of c-Src L317I apo-form and thermodynamic characterization of imatinib binding to the mutant suggested that an Ile at position 317 in c-Src does not act on the conformational prevalence of the kinase domain.

The fact that inhibition data, in one hand, were collected in presence of a catalytically active protein and that crystallisation and ITC data, in other hand, were obtained for kinase domains that were not involved in catalysis, let us presume that L317I mutation did have a role in DFG conformation, but rather at the level of its dynamical transition from an "out" to an "in" position.

Acknowledgements

We are grateful to Dr. Remo Perozzo for the useful help in crystal growth and maniplulation, to Dr. Lucile Pernot for performing the crystal solution and refinement, to the Swiss Light Source at the Paul Sherrer Institute and to Didia Graça and Cecilia Borini who contributed to this project in the form of a mastr's thesis.

CHAPTER 5

Inactive-like kinase domain conformation within the catalytic cycle of c-Src

1. Abstract

In Chapter 4, we raised the hypothesis that the impact of L317I mutation in the kinase domain of c-Src was rather based on the dynamics of DFG-in/-out transition (DFG-flip) than on a stabilization of the DFG-out conformation.

Since the DFG-flip has been suggested to promote the ADP release in the kinase reaction [108], we hypothesized that if the rate of DFG-flip was faster in the mutated kinase domain, ADP would be expulsed faster and would inhibit L317I to a lesser extent than the wild type c-Src KD.

A radioactive ADP-inhibition test allowed confirming our hypothesis experimentally. Furthermore, kinetic data corroborated the involvement of the entire DFG-flip in the catalytic cycle of c-Src.

Thus, we suggest that all DFG conformations that are stable enough in time should be considered for targeted drug design, as they are all present within the catalytic cycle of the tyrosine kinase.

2. Introduction

The human kinome and the kinomes of other organisms have provided a rich source of information on the distribution of protein kinases in different physiological environments and the development of signaling pathways that use tyrosine kinases. Over the years, structural studies have demonstrated the stereochemical consequences of phosphorylation of protein targets, revealing a wide variety of mechanisms, but with the common feature that was a tight phosphate-binding site. The ATP-binding site, despite sharing common features among the different kinases, has proved one of the most-druggable site, and, by 2010, there were 12 clinically approved small molecules as human protein kinase inhibitors that target this site. An emerging feature of the kinase studies for ligand interactions has been the importance of not only local interactions, but also the conformational adaptability of the kinase to select a particular conformational state that also provides recognition properties, as seen in imatinib binding to c-Abl [128].

In the process of developing new tyrosine kinase inhibitors, several studies have been directed in order to elucidate the mechanisms that regulate the protein tyrosine kinase reactions. First, studies were driven to understand the kinetic mechanism of TK reactions.

Various models of kinetic mechanisms have been described for enzymes that catalyze two substrates [289-291]. Possible mechanisms in protein tyrosine kinases are shown in Figure 5.1.

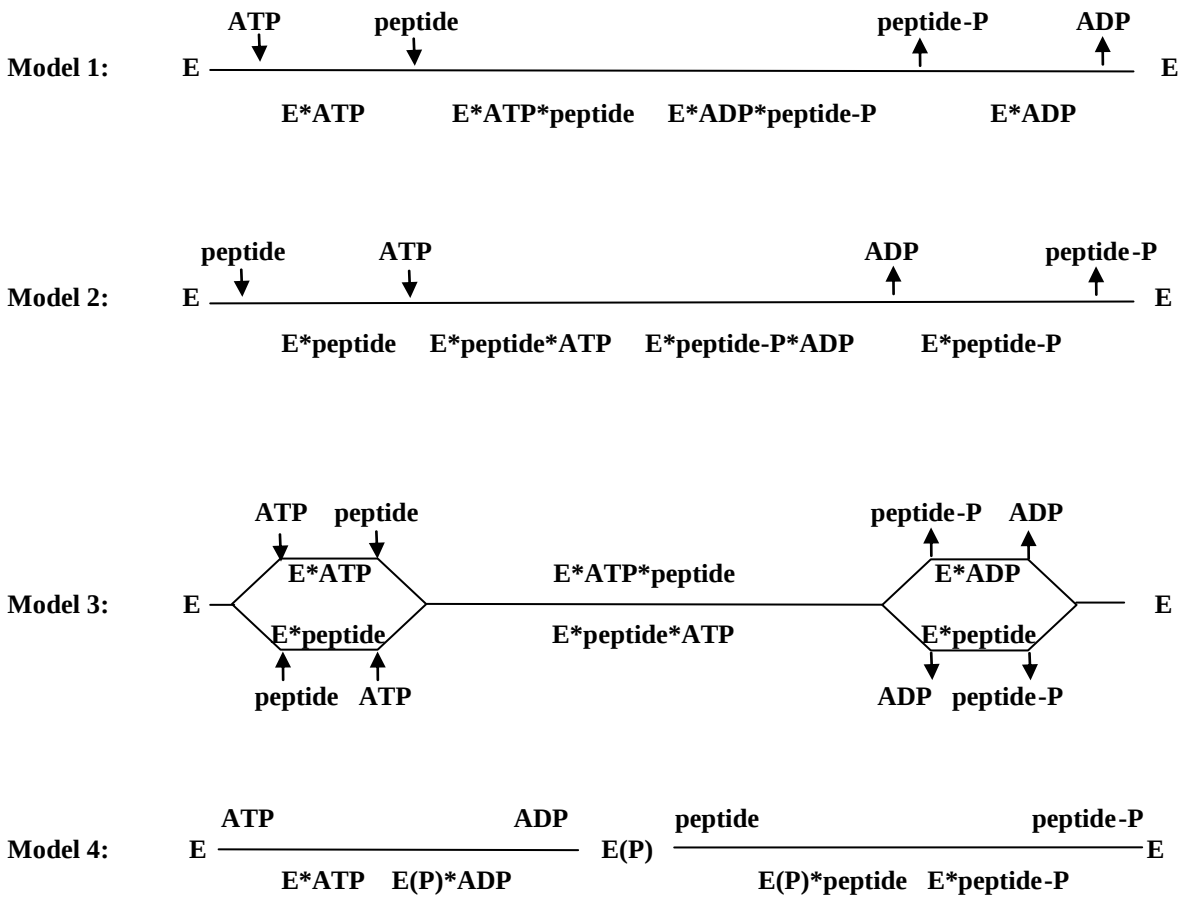

Figure 5.1: Various models of kinetic mechanisms described for enzymes that catalyze two substrates. Model 1, ordered sequential with ATP binding first; **Model 2**, ordered sequential with peptide binding first; **Model 3**, random sequential; **Model 4**, ping-pong. Adapted from [292].

Already in 1982 Cook et al. [293] reported the first kinetic mechanism of a protein kinase in the case of PKA. Following studies described the kinetic mechanisms for the human CSK [294]; EGFR [295, 296]; human placental IR TK [297], IκB-related kinases (IKK) [292]. Wong and Goldberg were the pioneers in describing the mechanism of a Src reaction [298]. They concluded that the v-Src TK reaction proceeds by an ordered mechanism, with a productive reaction only if ATP binds first because binding of the substrate (Val^5)-angiotensin II first excluded ATP binding.

In the matter of c-Src, Boerner et al. [299] demonstrated that the mechanism consisted in a random rapid equilibrium in the forward and reverse reactions with dead end complexes forming when either ATP-Mg^{2+} and a peptide substrate or ADP-Mg^{2+} and a peptide substrate bind to the enzyme. These data showed that both of the substrate binding sites are accessible in the free c-Src enzyme and that there is a negligible binding synergy between substrates in c-Src TK reaction. Moreover, as expected for a random order equilibrium reaction, the product ADP affects only the binding of its parent substrate without affecting the binding of the peptide [300]. Thereafter, authors concluded that either binding assays or catalytic assays could be used to detect inhibitors that bind to the either binding site. At that level, the conformational plasticity of c-Src was not considered within the kinetic mechanism of the kinase.

The striking discrepancy between values from a binding assay of imatinib to c-Src L317I (K_D = 7.2µM) and values from catalytic assays with the same ligand to c-Src L317I (IC_{50} = 4nM) (cf. Chapter 4) let us hypothesize that performing either binding or catalytic assay in kinase studies for ligand interactions did not give a complete picture on the conformational properties of the protein during binding of the inhibitor.

Moreover, it was rather the detected difference, which raised the idea that the impact of L317I mutation lied on increased conformational dynamics at the level of the DFG motif.

The conformational change connecting the DFG-in and DFG-out conformations (“DFG-flip”) has been suggested to promote the ADP release [108, 301], the rate limiting step of the kinase reaction [302-304] by allowing the kinase to adopt the DFG-out conformation [304-306] and thus to potentially facilitate the binding of the ATP-Mg^{2+} complex.

In this part of the work we used c-Src L317I (which presents a rapid DFG-flip) and c-Src WT (which presents a slower DFG-flip) to verify this hypothesis experimentally.

Then we went further and investigated whether the DFG-out (inactive) conformation of c-Src was taking place within the catalytic cycle of the kinase. In other words, whether the kinase mechanism could be related to conformational changes.

We hypothesized that if the DFG-out conformation was part of the catalytic cycle of c-Src and that if the DFG switch was faster in the mutant form of the kinase, ADP as a product and limiting step of the catalysis would inhibit L317I to a lesser extent than c-Src WT.

3. Materials and Methods

All chemicals were purchased from Applichem, Germany except if otherwise indicated.

3.1. Protein expression and purification

c-Src WT and c-Src L317I kinase domains were expressed as described in Chapter 2 (Materials and Methods).

For the ADP-inhibition assay, wild type and mutant c-Src kinase domains have been purified based on the protocol reported in Chapter 2 with the following three differencies:

- The filtrated supernatant from cell lysis was applied on a 5ml Chelating Column (GE Healthcare, UK) charged with $CoCl_2$ (Acros Organics, Belgium) according to the producer's protocol.

- After Co-affinity purification, fractions containing the kinase domain of c-Src were directly diluted to 50ml Buffer QA without cleavage of the 6xHis-tag, then filtered and loaded on the Hi-Trap HP column.

- Gel filtration on a S75 Column (GE Healthcare, UK) was carried out in buffer containing HEPES pH 7.2, 10mM MgCl2, 0.2mM DTT, 1mg/ml BSA.

3.2. ADP-inhibition assay

A radiometric filter-binding assay was used to assess ADP inhibition on c-Src.

The assay was performed in a total volume of 50µl by diluting c-Src WT or c-Src L317I in kinase reaction buffer (HEPES pH 7.2, 10mM MgCl2, 0.2mM DTT, 1mg/ml BSA) to a concentration of 10nM and pre-incubated with 133µM of the phospho-acceptor peptide (EIYGEFKKK from Peptide2.0 Inc., USA) and varying concentrations of ADP (0-10mM) for 2min at RT. At a given concentration of ADP, a series of kinase reactions were initiated by addition of (10µM, 35µM, 70µM, 105µm, 140µM, 200µM and 400µM) cold ATP supplemented with 5µCi γ^{32}P ATP (Perkin Elmer, Switzerland) and allowed to proceed for 10min at RT. At 10min after the addition of ATP, 1µl of the reactions were spotted onto 2cm squares of P81 phosphocellulose paper (Millipore, Switzerland). P81 squares were immediately immersed in 75mM phosphoric acid. Papers were washed 5 times in phosphoric acid, air dried and transferred radioactivity was measured by Cerenkov counting (i.e., without liquid scintillation fluid) in a scintillation counter (Beckman LS 6500 Scintillation System) using a ^{32}P program. For each series of kinase reactions, two controls were included: a control containing peptide and ATP, but no protein to assess contamination for any free ATP not incorporated into substrate, alongside a control lacking a peptide, but containing ATP and protein to correct for any autophosphorylation. Experiments were completed 3 times to derive mean values.

The activity of the undiluted protein kinase solutions in U/ml was calculated as:

$$\frac{(-b) \div sa \times 50 \times 1000 \times c}{10 \times 0.0003534} \qquad \text{(Equation 1)}$$

where *r* is the c.p.m. incorporated into the substrate in the protein kinase reaction, *b* is the average c.p.m. associated with the phosphocellulose paper in the reaction controls, *sa* is the specific radioactivity of ATP (c.p.m. $nmol^{-1}$), *50* is the correction for transfer of only 2% of the reaction to the P81 squares, *1000* corrects for the addition of only 1µl of diluted protein kinase to each assay, *c* is the fold dilution of hot ATP in respect to the final ATP concentration within a sample, *10* is the incubation time per minute and 0.0003534 is the amount of c-Src KD in mg within 1ml 10nM c-Src KD solution.

3.3. Kinetic analysis

K_M and V_{max} were calculated on GraphPad Prism 4.0 using a Michaelis-Menten Equation (Equation 2) where v is the velocity of the enzymatic reaction (U/mg).

$$v = \frac{v_{\max} \times peptide}{K_m \times peptide} \qquad \text{(Equation 2)}$$

K_i values were obtained using the graphical method described by Dixon [258]. Here, the reciprocal of the initial velocity *(i.e.* 1/V) was plotted against a series of 3 different concentrations of ADP (0mM, 1mM and 10mM) at constant (100µM and 300µM) ATP concentrations resulting in two families of data. The value of inhibitor concentration at which both lines intersect gave the absolute value of K_i.

4. Results and discussion

To assess experimentally whether the DFG-flip takes place within the catalytic cycle of c-Src tyrosine kinase in order to release ADP, we have adapted a kinase radiometric inhibition assay [154, 307] in which ADP was used as inhibitor against c-Src WT and c-Src L317I kinase domains.

According to a random order of substrate addition in c-Src and to the findings that ADP competes only with its parent substrate (i.e ATP), experiments were carried out by titrating increasing amounts of ADP in the presence of a fixed concentration of peptide substrate and varying concentrations of ATP.

The resulting mechanism of inhibition with respect to ATP for c-Src WT and c-Src L317I is reported in Figure 5.2, along with the corresponding apparent ADP dissociation constant (K_i).

Km values for ATP for both wild type and mutant protein calculated from the radiometric assay (Km_{WT}=82.14±20.4; Km_{L317I}=146.25±53.8μM) were close to Km values for ATP calculated from the UV-coupled enzymatic assay (Km_{WT}=134.4±32.2μM; Km_{L317I}=135.2±17.9μM) confirming the interchangeability of both methods.

The apparent ADP dissociation constant for c-Src L317I (K_i =1.0mM) was found to be 1log higher than for c-Src WT (K_i =0.1mM), indicating that ADP binds less tightly to c-Src L317I than to c-Src WT. This implies that the formed product ADP is released faster by the mutated kinase domain.

A

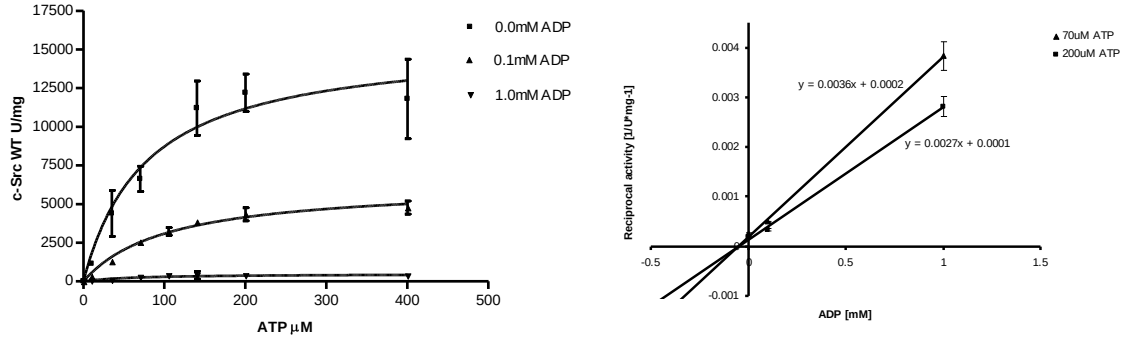

ADP				
	Ki (mM)	Type of inhibition	Effects on binding constants	Molecular target
c-Src WT	0.1 ± 0.01	Mixed	Vmax decreased, Km constant	Free enzyme

B

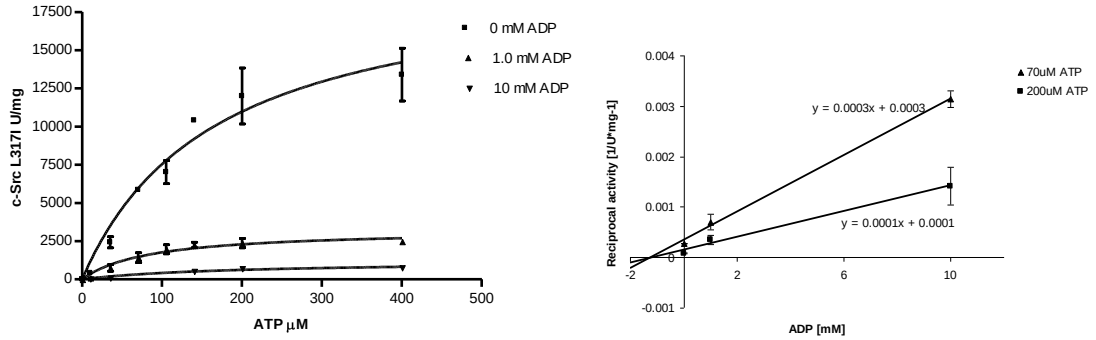

ADP				
	Ki (mM)	Type of inhibition	Effects on binding constants	Molecular target
c-Src L317I	1.0 ± 0.05	Mixed	Vmax decreased, Km constant	Free enzyme

Figure 5.2: ATP kinetics of c-Src WT and c-Src L317I kinase domains versus ADP. A. ATP kinetics of c-Src WT kinase domain versus ADP. **B.** ATP kinetics of c-Stc L317I kinase domain versus ADP. Standard deviations are shown as vertical bars and represent the means of three independent experiments. Dixon plot analysis was used to determine inhibition constants.

In Chapter 4, we have demonstrated that L317I mutation increased the rate of the DFG conformational transition in c-Src. In this context, the results from the ADP-inhibition assay could suggest that the faster release of ADP by the mutated kinase is due to the higher rate of the DFG-flip in c-Src L317I. Thus, the resistance to ADP inhibition in c-Src L317I confirmed experimentally that the flip of the DFG motif is the most probable molecular mechanism for the release of ADP at the end of the kinase catalytic cycle.

To support kinetic data, we have superimposed the non-hydrolysable ATP-analog adenosine 5'-(β, γ-imido) triphosphate tetralithium salt hydrate (AMP-PNP) as bound to the kinase domain of c-Src/DFG-in (PDB ID: 2SRC) with the kinase domain of c-Src/DFG-out conformation (PDB ID: 2OIQ). Figure 5.3 shows the Connolly surfaces of the AMP-PNP and of the flipped DFG motif. Connolly surfaces represent the volume occupied by the atoms. The image depicts a co-penetration of both surfaces involving the Phe405 and the β- and γ- phosphate of the ATP analogue meaning an incompatibility of the DFG-out conformation with the binding of an analogue of ADP/ATP. Therefore, it is likely that the DFG-out conformation helps releasing the ADP temporarly by modifying its ADP binding site.

Furthermore, kinetic data corroborate the involvement of the total DFG-flip and not only of the DFG-in form within the catalytic cycle of c-Src [305]. The latter statement implies that both, -in and –out, positions of the DFG motif are present as intermediates during the flip in a catalytically productive c-Src.

Since the DFG-in conformation is believed to be important to ATP-binding (Asp404 coordinates the ATP-bound magnesium cation [308, 309]), our model confirms experimentally the central role of the DFG motif in both nucleotide binding and release and provides an additional reason for the high degree of conservation of the DFG motif in protein tyrosine kinases.

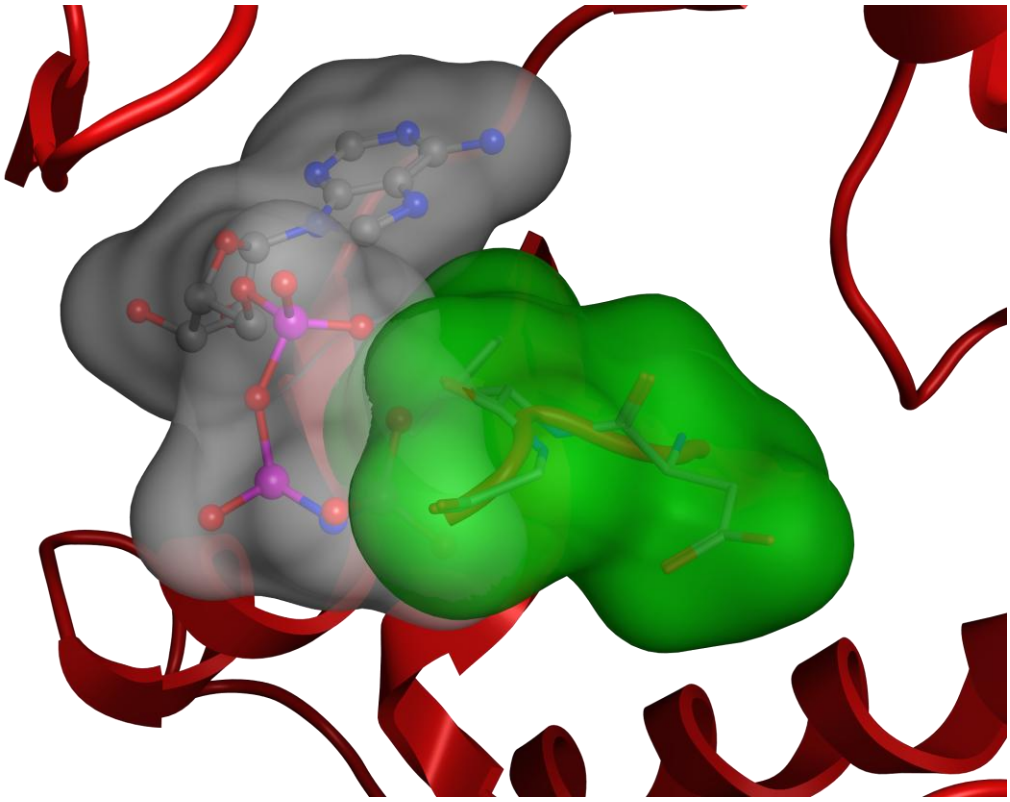

Figure 5.3: Clash of β- and γ-PO_4 from an ATP analogue with flipped Phe405 in c-Src KD. Superposition of AMP-PNP (Connolly surface in grey) as bound c-Src DFG-in (PDB ID: 2SRC) and c-Src DFG-out (PDB ID: 2OIQ) in red. The Connolly surface of the flipped DFG is depicted in green and penetrates the Connolly surface of the phosphate groups of AMP-PNP. Protein structures were aligned on the Cα atoms of the c-Src 2OIQ fragment.

The assumption that a multitude of different DFG conformations composes the DFG-flip may also explain why our data did not show ADP as a pure competitive inhibitor with respect to ATP but rather as a mixed type inhibitor.

5. Conclusion

Toward a deeper understanding of kinase enzymatic activity through conformational transitions, we have set up an experimental approach which revealed the DFG-flip as a central feature in the catalytic cycle of c-Src tyrosine kinase domain.

We have demonstrated experimentally that nucleotide release in c-Src KD is promoted by the DFG-flip and that the entire turnover of the DFG motif is involved in the catalytic cycle of the kinase.

This new structural vision on the catalytic cycle of c-Src, may give an important input in kinase drug design and in particular for choosing targetable c-Src conformations. To date, the DFG-in conformation was targeted for two main reasons. First, it was considered less flexible in terms of interlobe motions as part of the kinase domain hydrophobic spine [156, 157]. The DFG-in conformation was also believed responsible for oncogenicity since ATP/Mg^{2+} and protein substrate are bound when the Asp404 points into the ATP-binding site [310]. On the other hand, the more flexible DFG-out form was targeted for achieving drug selectivity [245, 311, 312].

Our catalytic model shows that during the catalytic cycle of c-Src the whole DFG-in/DFG-out transition is present and that any of the extreme or intermediate conformations that are stable enough in time should be considered as "targetable" for drug design. Therefore, as already stated for c-Abl [305], intermediate DFG conformations in c-Src obtained by in silico simulations, crystallography or NMR studies may present new opportunities for inhibitor design.

Moreover, a combination of binding and catalytic kinase assays should be used in *in vitro* inhibitor studies to elucidate kinetic mechanism through conformational plasticity.

Acknowledgements

We are grateful to Mr. Pascal Damay from the group of Prof. David Shore (University of Geneva, Switzerland) for the useful instructions in performing the radiometric assay and data-collection.

CHAPTER 6

Final conclusions and outlook

Final conclusions and outlook

The aim of this thesis consisted in the identification of key amino acid residues governing the transition from active to inactive protein kinase domain conformation to better understand the molecular basis of the conformational plasticity of tyrosine kinases.

We used c-Src tyrosine kinase domain as a case study because of the wealth of structural and computational information on this protein.

To define the residues involved in the regulation of c-Src kinase domain plasticity, we have leaned upon a recent comparative structural study on tyrosine kinase domains. The latter study depicted a pool of 14 residues forming a hydrophobic interface in between the bi-lobed structure of the InsR kinase domain that appeared to be important for the protein conformation and motion. Thus, we first carried out a structural alignment against the kinase domain of InsR and defined the corresponding residues in the kinase domain of c-Src.

To verify experimentally whether the identified residues were indeed controlling the kinase domain plasticity, we have mutated them to the corresponding ones in tyrosine kinases (*i.e* c-Abl, c-Kit, Syk and PDGFR) that are inhibited in a nanomolar range by the DFG-Asp-out conformation specific inhibitor, imatinib. The wild type kinase domain of c-Src is faintly inhibited by imatinib (IC_{50}=220μM) due to the thermodynamic penalty conformation of the DFG-motif which sterically hinders the binding of the inhibitor while adopting a DFG-in conformation.

Therefore, by mutating one or several residues from the hydrophobic interface of c-Src to the corresponding ones of c-Abl, c-Kit, Syk and PDGFR, we constructed eight c-Src kinase domain mutants (as detailed in Chapter 3) with the aim at answering to the following questions: Do

residues from the hydrophobic interface in c-Src influence the conformational prevalence of c-Src? If yes, how do they do it? Is it by stabilizing a DFG-favourable conformation for imatinib binding or by influencing dynamically the transition from DFG-out to DFG-in conformation?

All c-Src kinase domain mutants together with the wild type c-Src kinase domain were expressed and purified in milligram amounts. Different purification strategies were then adopted in accordance to two main types of biophysical and biochemical protein characterization assays necessary to reply to the above addressed issues. In Chapter 2 we report the protocols for c-Src purification tailor-made for each type of protein characterization assay.

The first category of assays investigated on the influence of the mutated residues on the dynamics of the DFG-flip and was conducted in presence of elements essential for c-Src catalysis, notably Mg^{2+}, peptide substrate and ATP. The second category of assays was meant to follow the role of the mutations on the conformational prevalence of the c-Src kinase domain. The latter were referred to as "static" assays and were conducted without Mg^{2+}, and ATP. Results from protein characterization assays are detailed in Chapter 4.

Kinetics and circular dichroism data showed that all c-Src mutants were active and properly folded, with a decreased thermodynamic stability of c-Src kinase domains carrying mutations of hydrophobic residues from the N-lobe of the kinase domain.

Data from UV-coupled imatinib inhibition assay demonstrated that all c-Src mutants were more sensitive to imatinib inhibition than the wild type kinase domain when their unphosphorylated form was pre-incubated with the inhibitor before addition of Mg^{2+}, and ATP.

c-Src variants carrying mutations of hydrophobic residues from the N-lobe of the kinase domain, showed higher inhibition than c-Src variants carrying mutations of hydrophobic residues from the C-lobe of the kinase domain. Among them c-Src L317I exhibited an inhibition by imatinib in the nanomolar range (IC_{50}=4nM, K_i=3.8nM) which was comparable to the one of c-Abl (IC_{50}=25-200nM, K_i=45µM) in both the UV-coupled inhibition assay as well as in an orthogonal autophosphorylation inhibition assay.

Thus, we could show that the identified residues from the hydrophobic interface in c-Src appear to have a net impact on the conformation of the kinase in particular at the level of the DFG-motif.

c-Src L317I revealed also a higher sensitivity to the inhibition with pyrazolopyrimidine 5 compound. Since the pyrazolopyrimidine 5 compound has been reported as an inhibitor that binds to the DFG-out conformation without thermodynamic penalty, we could presume that L317I mutation influences the plasticity of the kinase domain of c-Src not only at the level of the DFG-motif but also, to a lesser extent, of the A-loop, influencing the whole rotation of the N-and C-terminal domains.

Despite inhibition data, the crystal structure of c-Src L317I-apo did not depict an abolished thermodynamic penalty conformation for the mutant. On the contrary, the DFG motif presented a new, but still considered as DFG-Asp-in conformation. Furthermore, the 3D structure of c-Src L317I in complex with imatinib showed that the mutation did not influence the binding mode of the inhibitor.

Performed in parallel, ITC measurements for imatinib binding to L317 and WT c-Src kinase domains depicted as well a discrepancy in comparison with inhibition data; K_D values for the mutant and the wild type protein were similar and both in the µM range.

Hence, the crystal structure of c-Src L317I apo-form and thermodynamic characterization of imatinib binding to the mutant suggested that an Ile at position 317 in c-Src does not act on the conformational prevalence of the kinase domain by stabilizing the DFG-Asp-out conformation but at the level of the DFG dynamical transition from an "out" to an "in" position.

To assess experimentally this hypothesis and whether the DFG-flip takes place within the catalytic cycle of c-Src tyrosine kinase in order to release ADP, we have adapted a kinase radiometric inhibition assay in which ADP was used as inhibitor against c-Src WT and c-Src L317I kinase domains.

The apparent ADP dissociation constant for c-Src L317I (K_i =1.0mM) was found to be 1 log higher than for c-Src WT (K_i =0.1mM), indicating that ADP binds less tightly to c-Src L317I than to c-Src WT. Moreover, c-Src L317I KD demonstrated higher turnover numbers (for ATP and peptide substrate) over c-Src WT (Figure 4.7). This data led us to the conclusion that the formed product (ADP) is released faster by the mutated kinase domain and could suggest that the faster release of ADP by the mutated kinase is due to the higher rate of the DFG-flip in c-Src L317I. Resistance to ADP inhibition in c-Src L317I confirmed experimentally that the flip of the DFG motif is the most probable molecular mechanism for the release of ADP at the end of the kinase catalytic cycle.

Substantial support for that hypothesis was given by a study conducted by F. Gervasio (CNIO, Madrid) and A. Cristiani (UNIGE, Geneva), in which large scale classical MD simulations at high-temperature, metadynamics and biased-exchange MD simulations of both WT and L317I c-Src were recently performed. MD studies revealed that the mutation to Ile did favour the in/out flip-rate of the DFG and that the particular orientation of Phe405 in the apo structure of c-Src L317I is indeed in energetical minima within the trajectory of the DFG-flip (personal communication).

Interestingly, L317I mutation was found to be naturally present in phylogenies that are representative of the early evolution in Src (*E. fluviatilis,* Spongilliae). The presence of L317I mutation in primitive multicellular organisms and the fact that this mutation apparently increases drastically the affinity of imatinib for Src, opens a discussion on the ecological aspect of released chemotherapies on living organisms that present enhanced sensibility to given therapeutic molecules. On the other hand it comes to support the relatively new field in medicinal chemistry where orthologs of tyrosine kinases in microorganisms might be seen as novel targets for anti-infectious agents.

Additional experimental data should, of course, still be collected in order to prove undeniably the central role of Ile 317 in the dynamic regulation of the kinase domain.

Currently on-going NMR binding studies in "catalytic" conditions (CNIO, Madrid) are expected to enable to "see" the difference between the DFG-flip rates in c-Src WT and L317I.

The impact of L317I mutation in c-Src still remains to be assessed on the whole protein *in vivo*. To consider c-Src L317I inhibition by imatinib, dasatinib or by a DFG-out binder as the pyrazolopyrimidine compound 5 in cellular systems, PC3 and DU145 prostate carcinoma cell lines should be treated with different concentrations of the respective inhibitor and one should monitor the phosphorylation state of c-Src Tyr416 and FAK Tyr576/Tyr577 since FAK is known as a direct c-Src substrate [280].

Another point in this direction would be to conduct the assays described above on the c-Abl I293L mutant, which would be expected to present c-Src WT "behaviour". Unfortunately the attempt in generating c-Abl I293L mutant within the frame of this work failed.

In conlusion, we believe that the experimental identification of amino acid 317 in c-Src, as a residue involved in the kinase conformational transition, as well as the molecular mechanism by which this control is done, is an important step towards understanding the dynamical aspect of tyrosine kinase plasticity and towards establishing a rational experimental design in the study of dynamical phenomena in proteins.

Bibliography

1. *Kunz, H. and Emil Fischer- Unequalled Classicist, Master of Organic Chemistry Research, and Inspires Trailblazer of Biological Chemistry. Vol. 41. 2002: Angewandte Chemie International Edition.*
2. *Griffiths, An introduction to genetic analysis. 2000, New York: W. H. Freeman.*
3. *Fersht, A.R., From the first protein structures to our current knowledge of protein folding: delights and scepticisms. Nat Rev Mol Cell Biol, 2008. **9**(8): p. 650-4.*
4. *Fishbein, W.N., K. Nagarajan, and W. Scurzi, Urease catalysis and structure. IX. The half-unit and hemipolymers of jack bean urease. J Biol Chem, 1973. **248**(22): p. 7870-7.*
5. *Northrop, J.H., Crystalline Pepsin. Science, 1929. **69**(1796): p. 580.*
6. *Perutz, M.F., et al., Structure of haemoglobin: a three-dimensional Fourier synthesis at 5.5-A. resolution, obtained by X-ray analysis. Nature, 1960. **185**(4711): p. 416-22.*
7. *Kendrew, J.C., et al., Structure of myoglobin: A three-dimensional Fourier synthesis at 2 A. resolution. Nature, 1960. **185**(4711): p. 422-7.*
8. *Koshland, D.E., The Key–Lock Theory and the Induced Fit Theory. Angewandte Chemie International Edition in English, 1995. **33**(23-24): p. 2375-2378.*
9. *Hartsuck, J.A., et al., Carboxypeptidase a, Ii. The Three-Dimensional Electron Density Map at 6 a Resolution. Proc Natl Acad Sci U S A, 1965. **53**(2): p. 396-403.*
10. *Steitz, T.A., M. Shoham, and W.S. Bennett, Jr., Structural dynamics of yeast hexokinase during catalysis. Philos Trans R Soc Lond B Biol Sci, 1981. **293**(1063): p. 43-52.*
11. *Gerstein, M., A.M. Lesk, and C. Chothia, Structural mechanisms for domain movements in proteins. Biochemistry, 1994. **33**(22): p. 6739-49.*
12. *Frauenfelder, H., S.G. Sligar, and P.G. Wolynes, The energy landscapes and motions of proteins. Science, 1991. **254**(5038): p. 1598-603.*
13. *Bourgeois, D., et al., Extended subnanosecond structural dynamics of myoglobin revealed by Laue crystallography. Proc Natl Acad Sci U S A, 2006. **103**(13): p. 4924-9.*
14. *Austin, R.H., et al., Dynamics of ligand binding to myoglobin. Biochemistry, 1975. **14**(24): p. 5355-73.*
15. *Frauenfelder, H., G.A. Petsko, and D. Tsernoglou, Temperature-dependent X-ray diffraction as a probe of protein structural dynamics. Nature, 1979. **280**(5723): p. 558-63.*
16. *Frauenfelder, H., F. Parak, and R.D. Young, Conformational substates in proteins. Annu Rev Biophys Biophys Chem, 1988. **17**: p. 451-79.*
17. *Frauenfelder, H., P.W. Fenimore, and R.D. Young, Protein dynamics and function: insights from the energy landscape and solvent slaving. IUBMB Life, 2007. **59**(8-9): p. 506-12.*
18. *Henzler-Wildman, K. and D. Kern, Dynamic personalities of proteins. Nature, 2007. **450**(7172): p. 964-72.*
19. *Wales, D.J., The energy landscape as a unifying theme in molecular science. Philos Transact A Math Phys Eng Sci, 2005. **363**(1827): p. 357-75; discussion 375-7.*
20. *Zhuravlev, P.I. and G.A. Papoian, Functional versus folding landscapes: the same yet different. Curr Opin Struct Biol. **20**(1): p. 16-22.*
21. *Wales, D.J., Energy landscapes: some new horizons. Curr Opin Struct Biol. **20**(1): p. 3-10.*

22. *Straub, J.E. and D. Thirumalai, Exploring the energy landscape in proteins. Proc Natl Acad Sci U S A, 1993.* ***90****(3): p. 809-13.*
23. *Gavish, B. and M.M. Werber, Viscosity-dependent structural fluctuations in enzyme catalysis. Biochemistry, 1979.* ***18****(7): p. 1269-75.*
24. *Careri, G., P. Fasella, and E. Gratton, Enzyme dynamics: the statistical physics approach. Annu Rev Biophys Bioeng, 1979.* ***8****: p. 69-97.*
25. *McCammon, J.A., P.G. Wolynes, and M. Karplus, Picosecond dynamics of tyrosine side chains in proteins. Biochemistry, 1979.* ***18****(6): p. 927-42.*
26. *Karplus, M., et al., Local and collective motions in protein dynamics. Ciba Found Symp, 1983.* ***93****: p. 271-90.*
27. *Karplus, M. and J.A. McCammon, Dynamics of proteins: elements and function. Annu Rev Biochem, 1983.* ***52****: p. 263-300.*
28. *Kamerlin, S.C. and A. Warshel, At the dawn of the 21st century: Is dynamics the missing link for understanding enzyme catalysis? Proteins.* ***78****(6): p. 1339-75.*
29. *Warshel, A. and W.W. Parson, Dynamics of biochemical and biophysical reactions: insight from computer simulations. Q Rev Biophys, 2001.* ***34****(4): p. 563-679.*
30. *Billeter, S.R., et al., Hydride transfer in liver alcohol dehydrogenase: quantum dynamics, kinetic isotope effects, and role of enzyme motion. J Am Chem Soc, 2001.* ***123****(45): p. 11262-72.*
31. *Dodson, G.G., D.P. Lane, and C.S. Verma, Molecular simulations of protein dynamics: new windows on mechanisms in biology. EMBO Rep, 2008.* ***9****(2): p. 144-50.*
32. *Daniel, R.M., et al., The molecular basis of the effect of temperature on enzyme activity. Biochem J.* ***425****(2): p. 353-60.*
33. *Saen-Oon, S., et al., Remote mutations and active site dynamics correlate with catalytic properties of purine nucleoside phosphorylase. Biophys J, 2008.* ***94****(10): p. 4078-88.*
34. *Henzler-Wildman, K.A., et al., A hierarchy of timescales in protein dynamics is linked to enzyme catalysis. Nature, 2007.* ***450****(7171): p. 913-6.*
35. *Henzler-Wildman, K.A., et al., Intrinsic motions along an enzymatic reaction trajectory. Nature, 2007.* ***450****(7171): p. 838-44.*
36. *Kale, S., et al., Efficient coupling of catalysis and dynamics in the E1 component of Escherichia coli pyruvate dehydrogenase multienzyme complex. Proc Natl Acad Sci U S A, 2008.* ***105****(4): p. 1158-63.*
37. *Daniel, R.M., et al., The role of dynamics in enzyme activity. Annu Rev Biophys Biomol Struct, 2003.* ***32****: p. 69-92.*
38. *Gabdoulline, R.R. and R.C. Wade, Biomolecular diffusional association. Curr Opin Struct Biol, 2002.* ***12****(2): p. 204-13.*
39. *Mittag, T., et al., Structure/function implications in a dynamic complex of the intrinsically disordered Sic1 with the Cdc4 subunit of an SCF ubiquitin ligase. Structure.* ***18****(4): p. 494-506.*
40. *Winn, P.J., et al., Comparison of the dynamics of substrate access channels in three cytochrome P450s reveals different opening mechanisms and a novel functional role for a buried arginine. Proc Natl Acad Sci U S A, 2002.* ***99****(8): p. 5361-6.*
41. *Wriggers, W. and K. Schulten, Investigating a back door mechanism of actin phosphate release by steered molecular dynamics. Proteins, 1999.* ***35****(2): p. 262-73.*
42. *Smock, R.G. and L.M. Gierasch, Sending signals dynamically. Science, 2009.* ***324****(5924): p. 198-203.*
43. *Tokuriki, N. and D.S. Tawfik, Protein dynamism and evolvability. Science, 2009.* ***324****(5924): p. 203-7.*

44. *Schultes, E.A. and D.P. Bartel, One sequence, two ribozymes: implications for the emergence of new ribozyme folds. Science, 2000.* ***289****(5478): p. 448-52.*
45. *Wagner, A., Neutralism and selectionism: a network-based reconciliation. Nat Rev Genet, 2008.* ***9****(12): p. 965-74.*
46. *Bornberg-Bauer, E. and H.S. Chan, Modeling evolutionary landscapes: mutational stability, topology, and superfunnels in sequence space. Proc Natl Acad Sci U S A, 1999.* ***96****(19): p. 10689-94.*
47. *Wei, Y. and M.H. Hecht, Enzyme-like proteins from an unselected library of designed amino acid sequences. Protein Eng Des Sel, 2004.* ***17****(1): p. 67-75.*
48. *Yadid, I. and D.S. Tawfik, Reconstruction of functional beta-propeller lectins via homo-oligomeric assembly of shorter fragments. J Mol Biol, 2007.* ***365****(1): p. 10-7.*
49. *de Visser, J.A., et al., Perspective: Evolution and detection of genetic robustness. Evolution, 2003.* ***57****(9): p. 1959-72.*
50. *Anantharaman, V., L. Aravind, and E.V. Koonin, Emergence of diverse biochemical activities in evolutionarily conserved structural scaffolds of proteins. Curr Opin Chem Biol, 2003.* ***7****(1): p. 12-20.*
51. *Vilardaga, J.P., et al., Conformational cross-talk between alpha2A-adrenergic and mu-opioid receptors controls cell signaling. Nat Chem Biol, 2008.* ***4****(2): p. 126-31.*
52. *Kurakin, A., Scale-free flow of life: on the biology, economics, and physics of the cell. Theor Biol Med Model, 2009.* ***6****: p. 6.*
53. *Tousignant, A. and J.N. Pelletier, Protein motions promote catalysis. Chem Biol, 2004.* ***11****(8): p. 1037-42.*
54. *Rousseau, F. and J. Schymkowitz, A systems biology perspective on protein structural dynamics and signal transduction. Curr Opin Struct Biol, 2005.* ***15****(1): p. 23-30.*
55. *Kern, D. and E.R. Zuiderweg, The role of dynamics in allosteric regulation. Curr Opin Struct Biol, 2003.* ***13****(6): p. 748-57.*
56. *Kern, D., E.Z. Eisenmesser, and M. Wolf-Watz, Enzyme dynamics during catalysis measured by NMR spectroscopy. Methods Enzymol, 2005.* ***394****: p. 507-24.*
57. *Bourgeois, D. and A. Royant, Advances in kinetic protein crystallography. Curr Opin Struct Biol, 2005.* ***15****(5): p. 538-47.*
58. *Englander, S.W., Hydrogen exchange and mass spectrometry: A historical perspective. J Am Soc Mass Spectrom, 2006.* ***17****(11): p. 1481-9.*
59. *Bai, Y., Protein folding pathways studied by pulsed- and native-state hydrogen exchange. Chem Rev, 2006.* ***106****(5): p. 1757-68.*
60. *Pervushin, K., et al., Attenuated T2 relaxation by mutual cancellation of dipole-dipole coupling and chemical shift anisotropy indicates an avenue to NMR structures of very large biological macromolecules in solution. Proc Natl Acad Sci U S A, 1997.* ***94****(23): p. 12366-71.*
61. *Palmer, A.G., 3rd, M.J. Grey, and C. Wang, Solution NMR spin relaxation methods for characterizing chemical exchange in high-molecular-weight systems. Methods Enzymol, 2005.* ***394****: p. 430-65.*
62. *Mittermaier, A. and L.E. Kay, New tools provide new insights in NMR studies of protein dynamics. Science, 2006.* ***312****(5771): p. 224-8.*
63. *Kay, L.E., NMR studies of protein structure and dynamics. J Magn Reson, 2005.* ***173****(2): p. 193-207.*
64. *Palmer, A.G., 3rd, NMR characterization of the dynamics of biomacromolecules. Chem Rev, 2004.* ***104****(8): p. 3623-40.*
65. *Giepmans, B.N., et al., The fluorescent toolbox for assessing protein location and function. Science, 2006.* ***312****(5771): p. 217-24.*

66. *Greenfield, N.J., Analysis of the kinetics of folding of proteins and peptides using circular dichroism. Nat. Protocols, 2007.* ***1****(6): p. 2891-2899.*
67. *Hunt, N.T., 2D-IR spectroscopy: ultrafast insights into biomolecule structure and function. Chemical Society Reviews, 2009.* ***38****(7): p. 1837-1848.*
68. *Balakrishnan, G., et al., Protein dynamics from time resolved UV Raman spectroscopy. Current Opinion in Structural Biology, 2008.* ***18****(5): p. 623-629.*
69. *Borbat, P.P., et al., Electron Spin Resonance in Studies of Membranes and Proteins. Science, 2001.* ***291****(5502): p. 266-269.*
70. *Adcock, S.A. and J.A. McCammon, Molecular dynamics: survey of methods for simulating the activity of proteins. Chem Rev, 2006.* ***106****(5): p. 1589-615.*
71. *Moretti, L., Exploring structure and plasticity of tyrosine kinase for drug discovery, in faculté des sciences. 2007, Université de Genève, Università degli studi di Padova: Geneva. p. 168.*
72. *Day, R., D. Paschek, and A.E. Garcia, Microsecond simulations of the folding/unfolding thermodynamics of the Trp-cage miniprotein. Proteins.* ***78****(8): p. 1889-99.*
73. *Shaw, D.E., et al., Atomic-Level Characterization of the Structural Dynamics of Proteins. Science, 2010.* ***330****(6002): p. 341-346.*
74. *Ma, J. and M. Karplus, Ligand-induced conformational changes in ras p21: a normal mode and energy minimization analysis. J Mol Biol, 1997.* ***274****(1): p. 114-31.*
75. *Jacobs, D.J., et al., Protein flexibility predictions using graph theory. Proteins, 2001.* ***44****(2): p. 150-65.*
76. *Wells, S., et al., Constrained geometric simulation of diffusive motion in proteins. Phys Biol, 2005.* ***2****(4): p. S127-36.*
77. *Scheraga, H.A., M. Khalili, and A. Liwo, Protein-folding dynamics: overview of molecular simulation techniques. Annu Rev Phys Chem, 2007.* ***58****: p. 57-83.*
78. *Hamelberg, D., J. Mongan, and J.A. McCammon, Accelerated molecular dynamics: a promising and efficient simulation method for biomolecules. J Chem Phys, 2004.* ***120****(24): p. 11919-29.*
79. *Marti, M.A., et al., Nitric oxide reactivity with globins as investigated through computer simulation. Methods Enzymol, 2008.* ***437****: p. 477-98.*
80. *Noé, F. and S. Fischer, Transition networks for modeling the kinetics of conformational change in macromolecules. Current Opinion in Structural Biology, 2008.* ***18****(2): p. 154-162.*
81. *Yuan, Z., T.L. Bailey, and R.D. Teasdale, Prediction of protein B-factor profiles. Proteins, 2005.* ***58****(4): p. 905-12.*
82. *Westenhoff, S., et al., Time-resolved structural studies of protein reaction dynamics: a smorgasbord of X-ray approaches. Acta Crystallogr A.* ***66****(Pt 2): p. 207-19.*
83. *Schotte, F., et al., Picosecond time-resolved X-ray crystallography: probing protein function in real time. J Struct Biol, 2004.* ***147****(3): p. 235-46.*
84. *Yang, D. and L.E. Kay, Contributions to conformational entropy arising from bond vector fluctuations measured from NMR-derived order parameters: application to protein folding. J Mol Biol, 1996.* ***263****(2): p. 369-82.*
85. *Jarymowycz, V.A. and M.J. Stone, Fast time scale dynamics of protein backbones: NMR relaxation methods, applications, and functional consequences. Chem Rev, 2006.* ***106****(5): p. 1624-71.*
86. *Kay, L.E., D.A. Torchia, and A. Bax, Backbone dynamics of proteins as studied by 15N inverse detected heteronuclear NMR spectroscopy: application to staphylococcal nuclease. Biochemistry, 1989.* ***28****(23): p. 8972-9.*

87. *Pelupessy, P., S. Ravindranathan, and G. Bodenhausen, Correlated motions of successive amide N-H bonds in proteins. J Biomol NMR, 2003.* ***25****(4): p. 265-80.*
88. *Lundstrom, P., F.A. Mulder, and M. Akke, Correlated dynamics of consecutive residues reveal transient and cooperative unfolding of secondary structure in proteins. Proc Natl Acad Sci U S A, 2005.* ***102****(47): p. 16984-9.*
89. *Wang, T., et al., Changes in calmodulin main-chain dynamics upon ligand binding revealed by cross-correlated NMR relaxation measurements. J Am Chem Soc, 2005.* ***127****(3): p. 828-9.*
90. *LeMaster, D.M., Structural determinants of the catalytic reactivity of the buried cysteine of Escherichia coli thioredoxin. Biochemistry, 1996.* ***35****(47): p. 14876-81.*
91. *Doster, W., S. Cusack, and W. Petry, Dynamical transition of myoglobin revealed by inelastic neutron scattering. Nature, 1989.* ***337****(6209): p. 754-6.*
92. *Zhong, D., Ultrafast catalytic processes in enzymes. Curr Opin Chem Biol, 2007.* ***11****(2): p. 174-81.*
93. *Zewail, A.H., 4D ultrafast electron diffraction, crystallography, and microscopy. Annu Rev Phys Chem, 2006.* ***57****: p. 65-103.*
94. *Hubbard, S.R. and J.H. Till, Protein tyrosine kinase structure and function. Annu Rev Biochem, 2000.* ***69****: p. 373-98.*
95. *Manning, G., et al., The protein kinase complement of the human genome. Science, 2002.* ***298****(5600): p. 1912-34.*
96. *Fabbro, D.M., F., ed. Protein tyrosine kinases. From inhibitors to useful drugs. 2005, H. Press: New Jersey.*
97. *Nagar, B., c-Abl tyrosine kinase and inhibition by the cancer drug imatinib (Gleevec/STI-571). J Nutr, 2007.* ***137****(6 Suppl 1): p. 1518S-1523S; discussion 1548S.*
98. *Ubersax, J.A. and J.E. Ferrell, Jr., Mechanisms of specificity in protein phosphorylation. Nat Rev Mol Cell Biol, 2007.* ***8****(7): p. 530-41.*
99. *Cowan-Jacob, S.W., et al., Structural biology contributions to the discovery of drugs to treat chronic myelogenous leukaemia. Acta Crystallogr D Biol Crystallogr, 2007.* ***63****(Pt 1): p. 80-93.*
100. *Cowan-Jacob, S.W., Structural biology of protein tyrosine kinases. Cell Mol Life Sci, 2006.* ***63****(22): p. 2608-25.*
101. *Blume-Jensen, P. and T. Hunter, Oncogenic kinase signalling. Nature, 2001.* ***411****(6835): p. 355-65.*
102. *Hanks, S.K., Genomic analysis of the eukaryotic protein kinase superfamily: a perspective. Genome Biol, 2003.* ***4****(5): p. 111.*
103. *Miranda-Saavedra, D. and G.J. Barton, Classification and functional annotation of eukaryotic protein kinases. Proteins, 2007.* ***68****(4): p. 893-914.*
104. *Hubbard, S.R., M. Mohammadi, and J. Schlessinger, Autoregulatory mechanisms in protein-tyrosine kinases. J Biol Chem, 1998.* ***273****(20): p. 11987-90.*
105. *Knighton, D.R., et al., Structure of a peptide inhibitor bound to the catalytic subunit of cyclic adenosine monophosphate-dependent protein kinase. Science, 1991.* ***253****(5018): p. 414-20.*
106. *Knighton, D.R., et al., Crystal structure of the catalytic subunit of cyclic adenosine monophosphate-dependent protein kinase. Science, 1991.* ***253****(5018): p. 407-14.*
107. *Cowan-Jacob, S.W., H. Mobitz, and D. Fabbro, Structural biology contributions to tyrosine kinase drug discovery. Curr Opin Cell Biol, 2009.* ***21****(2): p. 280-7.*
108. *Kannan, N. and A.F. Neuwald, Did protein kinase regulatory mechanisms evolve through elaboration of a simple structural component? J Mol Biol, 2005.* ***351****(5): p. 956-72.*

109. *Nolen, B., S. Taylor, and G. Ghosh, Regulation of protein kinases; controlling activity through activation segment conformation. Mol Cell, 2004.* ***15****(5): p. 661-75.*
110. *Hu, J., et al., Structural basis for recruitment of the adaptor protein APS to the activated insulin receptor. Mol Cell, 2003.* ***12****(6): p. 1379-89.*
111. *Favelyukis, S., et al., Structure and autoregulation of the insulin-like growth factor 1 receptor kinase. Nat Struct Biol, 2001.* ***8****(12): p. 1058-63.*
112. *Furdui, C.M., et al., Autophosphorylation of FGFR1 kinase is mediated by a sequential and precisely ordered reaction. Mol Cell, 2006.* ***21****(5): p. 711-7.*
113. *Gotoh, N., et al., A highly conserved tyrosine residue at codon 845 within the kinase domain is not required for the transforming activity of human epidermal growth factor receptor. Biochem Biophys Res Commun, 1992.* ***186****(2): p. 768-74.*
114. *Ogawa, A., et al., Structure of the carboxyl-terminal Src kinase, Csk. J Biol Chem, 2002.* ***277****(17): p. 14351-4.*
115. *Levinson, N.M., et al., A Src-like inactive conformation in the abl tyrosine kinase domain. PLoS Biol, 2006.* ***4****(5): p. e144.*
116. *Adams, J.A., Kinetic and catalytic mechanisms of protein kinases. Chem Rev, 2001.* ***101****(8): p. 2271-90.*
117. *Li, F., et al., Evidence for an internal entropy contribution to phosphoryl transfer: a study of domain closure, backbone flexibility, and the catalytic cycle of cAMP-dependent protein kinase. J Mol Biol, 2002.* ***315****(3): p. 459-69.*
118. *Huse, M. and J. Kuriyan, The conformational plasticity of protein kinases. Cell, 2002.* ***109****(3): p. 275-82.*
119. *Xu, W., et al., Crystal structures of c-Src reveal features of its autoinhibitory mechanism. Mol Cell, 1999.* ***3****(5): p. 629-38.*
120. *Schindler, T., et al., Crystal structure of Hck in complex with a Src family-selective tyrosine kinase inhibitor. Mol Cell, 1999.* ***3****(5): p. 639-48.*
121. *Young, M.A., et al., Dynamic coupling between the SH2 and SH3 domains of c-Src and Hck underlies their inactivation by C-terminal tyrosine phosphorylation. Cell, 2001.* ***105****(1): p. 115-26.*
122. *Harrison, S.C., Variation on an Src-like theme. Cell, 2003.* ***112****(6): p. 737-40.*
123. *Lerner, E.C. and T.E. Smithgall, SH3-dependent stimulation of Src-family kinase autophosphorylation without tail release from the SH2 domain in vivo. Nat Struct Biol, 2002.* ***9****(5): p. 365-9.*
124. *Cowan-Jacob, S.W., et al., The crystal structure of a c-Src complex in an active conformation suggests possible steps in c-Src activation. Structure, 2005.* ***13****(6): p. 861-71.*
125. *Hantschel, O., et al., A myristoyl/phosphotyrosine switch regulates c-Abl. Cell, 2003.* ***112****(6): p. 845-57.*
126. *Lamers, M.B., et al., Structure of the protein tyrosine kinase domain of C-terminal Src kinase (CSK) in complex with staurosporine. J Mol Biol, 1999.* ***285****(2): p. 713-25.*
127. *Pawson, T. and M. Kofler, Kinome signaling through regulated protein-protein interactions in normal and cancer cells. Curr Opin Cell Biol, 2009.* ***21****(2): p. 147-53.*
128. *Johnson, L.N., The regulation of protein phosphorylation. Biochem Soc Trans, 2009.* ***37****(Pt 4): p. 627-41.*
129. *Rous, P., The challenge to man of the neoplastic cell. Science, 1967.* ***157****(784): p. 24-8.*
130. *Czernilofsky, A.P., et al., Nucleotide sequence of an avian sarcoma virus oncogene (src) and proposed amino acid sequence for gene product. Nature, 1980.* ***287****(5779): p. 198-203.*

131. *Czernilofsky, A.P., et al., The nucleotide sequence of an untranslated but conserved domain at the 3' end of the avian sarcoma virus genome. Nucleic Acids Res, 1980.* ***8****(13): p. 2967-84.*
132. *Duesberg, P.H. and P.K. Vogt, Differences between the ribonucleic acids of transforming and nontransforming avian tumor viruses. Proc Natl Acad Sci U S A, 1970.* ***67****(4): p. 1673-80.*
133. *Martin, G.S., The hunting of the Src. Nat Rev Mol Cell Biol, 2001.* ***2****(6): p. 467-75.*
134. *Collett, M.S. and R.L. Erikson, Protein kinase activity associated with the avian sarcoma virus src gene product. Proc Natl Acad Sci U S A, 1978.* ***75****(4): p. 2021-4.*
135. *Levinson, A.D., et al., Evidence that the transforming gene of avian sarcoma virus encodes a protein kinase associated with a phosphoprotein. Cell, 1978.* ***15****(2): p. 561-72.*
136. *Hunter, T. and B.M. Sefton, Transforming gene product of Rous sarcoma virus phosphorylates tyrosine. Proc Natl Acad Sci U S A, 1980.* ***77****(3): p. 1311-5.*
137. *Carragher, N.O., et al., A novel role for FAK as a protease-targeting adaptor protein: regulation by p42 ERK and Src. Curr Biol, 2003.* ***13****(16): p. 1442-50.*
138. *Carragher, N.O. and M.C. Frame, Calpain: a role in cell transformation and migration. Int J Biochem Cell Biol, 2002.* ***34****(12): p. 1539-43.*
139. *Yeatman, T.J., A renaissance for SRC. Nat Rev Cancer, 2004.* ***4****(6): p. 470-80.*
140. *Zamir, E. and B. Geiger, Molecular complexity and dynamics of cell-matrix adhesions. J Cell Sci, 2001.* ***114****(Pt 20): p. 3583-90.*
141. *Johnson, F.M. and G.E. Gallick, SRC family nonreceptor tyrosine kinases as molecular targets for cancer therapy. Anticancer Agents Med Chem, 2007.* ***7****(6): p. 651-9.*
142. *Perl, A.K., et al., A causal role for E-cadherin in the transition from adenoma to carcinoma. Nature, 1998.* ***392****(6672): p. 190-3.*
143. *Schenone, S., F. Manetti, and M. Botta, SRC inhibitors and angiogenesis. Curr Pharm Des, 2007.* ***13****(21): p. 2118-28.*
144. *Summy, J.M. and G.E. Gallick, Src family kinases in tumor progression and metastasis. Cancer Metastasis Rev, 2003.* ***22****(4): p. 337-58.*
145. *Irby, R.B., et al., Activating SRC mutation in a subset of advanced human colon cancers. Nat Genet, 1999.* ***21****(2): p. 187-90.*
146. *Oneyama, C., et al., Functional dissection of transformation by c-Src and v-Src. Genes Cells, 2008.* ***13****(1): p. 1-12.*
147. *Kaplan, J.M., et al., The first seven amino acids encoded by the v-src oncogene act as a myristylation signal: lysine 7 is a critical determinant. Mol Cell Biol, 1988.* ***8****(6): p. 2435-41.*
148. *Gingrich, J.R., et al., Unique domain anchoring of Src to synaptic NMDA receptors via the mitochondrial protein NADH dehydrogenase subunit 2. Proc Natl Acad Sci U S A, 2004.* ***101****(16): p. 6237-42.*
149. *Yu, H., et al., Solution structure of the SH3 domain of Src and identification of its ligand-binding site. Science, 1992.* ***258****(5088): p. 1665-8.*
150. *Fushman, D., R. Xu, and D. Cowburn, Direct determination of changes of interdomain orientation on ligation: use of the orientational dependence of 15N NMR relaxation in Abl SH(32). Biochemistry, 1999.* ***38****(32): p. 10225-30.*
151. *Cartwright, C.A., et al., Cell transformation by pp60c-src mutated in the carboxy-terminal regulatory domain. Cell, 1987.* ***49****(1): p. 83-91.*
152. *Moarefi, I., et al., Activation of the Src-family tyrosine kinase Hck by SH3 domain displacement. Nature, 1997.* ***385****(6617): p. 650-3.*

153. *Gonfloni, S., et al., Crosstalk between the catalytic and regulatory domains allows bidirectional regulation of Src. Nat Struct Biol, 2000.* ***7****(4): p. 281-6.*
154. *Azam, M., et al., Activation of tyrosine kinases by mutation of the gatekeeper threonine. Nat Struct Mol Biol, 2008.* ***15****(10): p. 1109-18.*
155. *Seeliger, M.A., et al., c-Src binds to the cancer drug imatinib with an inactive Abl/c-Kit conformation and a distributed thermodynamic penalty. Structure, 2007.* ***15****(3): p. 299-311.*
156. *Kornev, A.P., et al., Surface comparison of active and inactive protein kinases identifies a conserved activation mechanism. Proc Natl Acad Sci U S A, 2006.* ***103****(47): p. 17783-8.*
157. *Kornev, A.P., S.S. Taylor, and L.F. Ten Eyck, A helix scaffold for the assembly of active protein kinases. Proc Natl Acad Sci U S A, 2008.* ***105****(38): p. 14377-82.*
158. *Moretti, L., Exploring Structure and Plasticity of Tyrosine Kinase Domains for Drug Discovery, in Faculté des Sciences. 2007, Université de Genève, Università degli Studi di Padova: Geneva. p. 168.*
159. *Cooper, J.A., Oncogenes and anti-oncogenes. Curr Opin Cell Biol, 1990.* ***2****(2): p. 285-95.*
160. *Spector, D.H., H.E. Varmus, and J.M. Bishop, Nucleotide sequences related to the transforming gene of avian sarcoma virus are present in DNA of uninfected vertebrates. Proc Natl Acad Sci U S A, 1978.* ***75****(9): p. 4102-6.*
161. *Simon, M.A., T.B. Kornberg, and J.M. Bishop, Three loci related to the src oncogene and tyrosine-specific protein kinase activity in Drosophila. Nature, 1983.* ***302****(5911): p. 837-9.*
162. *Irby, R.B. and T.J. Yeatman, Role of Src expression and activation in human cancer. Oncogene, 2000.* ***19****(49): p. 5636-42.*
163. *Corey, S.J. and S.M. Anderson, Src-related protein tyrosine kinases in hematopoiesis. Blood, 1999.* ***93****(1): p. 1-14.*
164. *Finn, R.S., Targeting Src in breast cancer. Ann Oncol, 2008.* ***19****(8): p. 1379-86.*
165. *Giaccone, G. and P.A. Zucali, Src as a potential therapeutic target in non-small-cell lung cancer. Ann Oncol, 2008.* ***19****(7): p. 1219-23.*
166. *Kim, L.C., L. Song, and E.B. Haura, Src kinases as therapeutic targets for cancer. Nat Rev Clin Oncol, 2009.* ***6****(10): p. 587-95.*
167. *Capdeville, R., et al., Glivec (STI571, imatinib), a rationally developed, targeted anticancer drug. Nat Rev Drug Discov, 2002.* ***1****(7): p. 493-502.*
168. *Gan, W., S. Yang, and B. Roux, Atomistic view of the conformational activation of Src kinase using the string method with swarms-of-trajectories. Biophys J, 2009.* ***97****(4): p. L8-L10.*
169. *Seeliger, M.A., et al., High yield bacterial expression of active c-Abl and c-Src tyrosine kinases. Protein Sci, 2005.* ***14****(12): p. 3135-9.*
170. *Varshney, G.C., et al., Tyrosine kinases in normal human blood cells. Platelet but not erythrocyte band 3 tyrosine kinase is p60c-src. FEBS Lett, 1986.* ***205****(1): p. 97-103.*
171. *Presek, P., et al., High-yield purification of a pp60c-src related protein-tyrosine kinase from human platelets. Biochim Biophys Acta, 1988.* ***969****(3): p. 271-80.*
172. *Feder, D. and J.M. Bishop, Purification and enzymatic characterization of pp60c-src from human platelets. J Biol Chem, 1990.* ***265****(14): p. 8205-11.*
173. *Gilmer, T.M. and R.L. Erikson, Rous sarcoma virus transforming protein, p60src, expressed in E. coli, functions as a protein kinase. Nature, 1981.* ***294****(5843): p. 771-3.*
174. *McGrath, J.P. and A.D. Levinson, Bacterial expression of an enzymatically active protein encoded by RSV src gene. Nature, 1982.* ***295****(5848): p. 423-5.*

175. *Chambers, S.P., et al., High-throughput screening for soluble recombinant expressed kinases in Escherichia coli and insect cells. Protein Expr Purif, 2004.* ***36****(1): p. 40-7.*
176. *Williams, D.M., D. Wang, and P.A. Cole, Chemical rescue of a mutant protein-tyrosine kinase. J Biol Chem, 2000.* ***275****(49): p. 38127-30.*
177. *Waksman, G., et al., Crystal structure of the phosphotyrosine recognition domain SH2 of v-src complexed with tyrosine-phosphorylated peptides. Nature, 1992.* ***358****(6388): p. 646-53.*
178. *Saya, H., et al., Bacterial expression of an active tyrosine kinase from a protein A/truncated c-src fusion protein. FEBS Lett, 1993.* ***327****(2): p. 224-30.*
179. *Garcia, P., et al., Phosphorylation of synthetic peptides containing Tyr-Met-X-Met motifs by nonreceptor tyrosine kinases in vitro. J Biol Chem, 1993.* ***268****(33): p. 25146-51.*
180. *Weijland, A., et al., The purification and characterization of the catalytic domain of Src expressed in Schizosaccharomyces pombe. Comparison of unphosphorylated and tyrosine phosphorylated species. Eur J Biochem, 1996.* ***240****(3): p. 756-64.*
181. *Nagar, B., et al., Structural basis for the autoinhibition of c-Abl tyrosine kinase. Cell, 2003.* ***112****(6): p. 859-71.*
182. *Gasteiger, E. Protein Identification and Analysis Tools on the ExPASy Server. 2005; Humana Press:[*
183. *Barker, S.C., et al., Characterization of pp60c-src tyrosine kinase activities using a continuous assay: autoactivation of the enzyme is an intermolecular autophosphorylation process. Biochemistry, 1995.* ***34****(45): p. 14843-51.*
184. *Songyang, Z. and L.C. Cantley, Recognition and specificity in protein tyrosine kinase-mediated signalling. Trends Biochem Sci, 1995.* ***20****(11): p. 470-5.*
185. *Wang, Y.H., et al., A new strategy to produce active human Src from bacteria for biochemical study of its regulation. Biochem Biophys Res Commun, 2006.* ***346****(2): p. 606-11.*
186. *Guan, K.L. and J.E. Dixon, Protein tyrosine phosphatase activity of an essential virulence determinant in Yersinia. Science, 1990.* ***249****(4968): p. 553-6.*
187. *Bliska, J.B., et al., Tyrosine phosphate hydrolysis of host proteins by an essential Yersinia virulence determinant. Proc Natl Acad Sci U S A, 1991.* ***88****(4): p. 1187-91.*
188. *Ahmadibeni, Y., et al., Metal-binding properties of a dicysteine-containing motif in protein tyrosine kinases. Chembiochem, 2007.* ***8****(13): p. 1592-605.*
189. *Lee, N.Y., T.L. Hazlett, and J.G. Koland, Structure and dynamics of the epidermal growth factor receptor C-terminal phosphorylation domain. Protein Sci, 2006.* ***15****(5): p. 1142-52.*
190. *Singh, D., et al., Human spleen tyrosine kinase (Syk) recombinant expression systems for high-throughput assays. Biotechnol J.* ***5****(2): p. 201-12.*
191. *Narhi, L.O., et al., Changes in conformation and stability upon SCF/sKit complex formation. J Protein Chem, 1998.* ***17****(5): p. 387-96.*
192. *Falsone, S.F., et al., Oncogenic mutations reduce the stability of SRC kinase. J Mol Biol, 2004.* ***344****(1): p. 281-91.*
193. *Wang, W., et al., Structural characterization of autoinhibited c-Met kinase produced by coexpression in bacteria with phosphatase. Proc Natl Acad Sci U S A, 2006.* ***103****(10): p. 3563-8.*
194. *Caspers, P., M. Stieger, and P. Burn, Overproduction of bacterial chaperones improves the solubility of recombinant protein tyrosine kinases in Escherichia coli. Cell Mol Biol (Noisy-le-grand), 1994.* ***40****(5): p. 635-44.*
195. *Amrein, K.E., et al., Purification and characterization of recombinant human p50csk protein-tyrosine kinase from an Escherichia coli expression system overproducing the*

bacterial chaperones GroES and GroEL. Proc Natl Acad Sci U S A, 1995. ***92****(4): p. 1048-52.*

196. *de Marco, A., et al., Chaperone-based procedure to increase yields of soluble recombinant proteins produced in E. coli. BMC Biotechnol, 2007.* ***7****: p. 32.*
197. *Haacke, A., et al., Chaperone over-expression in Escherichia coli: Apparent increased yields of soluble recombinant protein kinases are due mainly to soluble aggregates. Protein Expression and Purification, 2009.* ***64****(2): p. 185-193.*
198. *Greenfield, N.J., Using circular dichroism spectra to estimate protein secondary structure. Nat Protoc, 2006.* ***1****(6): p. 2876-90.*
199. *Finzi, A., J. Cloutier, and E.A. Cohen, Two-step purification of His-tagged Nef protein in native condition using heparin and immobilized metal ion affinity chromatographies. J Virol Methods, 2003.* ***111****(1): p. 69-73.*
200. *Martino, L., et al., The interaction of the Escherichia coli protein SlyD with nickel ions illuminates the mechanism of regulation of its peptidyl-prolyl isomerase activity. FEBS J, 2009.* ***276****(16): p. 4529-44.*
201. *Mitterauer, T., et al., Metal-dependent nucleotide binding to the Escherichia coli rotamase SlyD. Biochem J, 1999.* ***342 (Pt 1)****: p. 33-9.*
202. *Thilakaraj, R., et al., In silico identification of putative metal binding motifs. Bioinformatics, 2007.* ***23****(3): p. 267-71.*
203. *Sankararamakrishnan, R., S. Verma, and S. Kumar, ATCUN-like metal-binding motifs in proteins: identification and characterization by crystal structure and sequence analysis. Proteins, 2005.* ***58****(1): p. 211-21.*
204. *Healthcare, G., Affinity Chromatography Principles and Methods. 2007.*
205. *Graslund, S., et al., Protein production and purification. Nat Methods, 2008.* ***5****(2): p. 135-46.*
206. *Hengen, P., Purification of His-Tag fusion proteins from Escherichia coli. Trends Biochem Sci, 1995.* ***20****(7): p. 285-6.*
207. *Piserchio, A., R. Ghose, and D. Cowburn, Optimized bacterial expression and purification of the c-Src catalytic domain for solution NMR studies. J Biomol NMR, 2009.* ***44****(2): p. 87-93.*
208. *Wang, W., et al., Structural and mechanistic insights into Mps1 kinase activation. J Cell Mol Med, 2009.* ***13****(8B): p. 1679-94.*
209. *Pickover, C.A., Spectrographic representation of globular protein breathing motions. Science, 1984.* ***223****(4632): p. 181-2.*
210. *Eckhart, W., M.A. Hutchinson, and T. Hunter, An activity phosphorylating tyrosine in polyoma T antigen immunoprecipitates. Cell, 1979.* ***18****(4): p. 925-33.*
211. *Gosselin, E.J., H.P. Tony, and D.C. Parker, Characterization of antigen processing and presentation by resting B lymphocytes. J Immunol, 1988.* ***140****(5): p. 1408-13.*
212. *Hanks, S.K. and T. Hunter, Protein kinases 6. The eukaryotic protein kinase superfamily: kinase (catalytic) domain structure and classification. FASEB J, 1995.* ***9****(8): p. 576-96.*
213. *Taylor, S.S., et al., PKA: a portrait of protein kinase dynamics. Biochimica et Biophysica Acta (BBA) - Proteins & Proteomics, 2004.* ***1697****(1-2): p. 259-269.*
214. *Wiesner, S., et al., A change in conformational dynamics underlies the activation of Eph receptor tyrosine kinases. EMBO J, 2006.* ***25****(19): p. 4686-96.*
215. *Volkman, B.F., et al., Two-state allosteric behavior in a single-domain signaling protein. Science, 2001.* ***291****(5512): p. 2429-33.*
216. *Busenlehner, L.S., et al., Stress sensor triggers conformational response of the integral membrane protein microsomal glutathione transferase 1. Biochemistry, 2004.* ***43****(35): p. 11145-52.*

217. *Sours, K.M., et al., Hydrogen-exchange mass spectrometry reveals activation-induced changes in the conformational mobility of p38alpha MAP kinase. J Mol Biol, 2008.* ***379****(5): p. 1075-93.*
218. *Kornev, A.P., S.S. Taylor, and L.F. Ten Eyck, A helix scaffold for the assembly of active protein kinases. Proceedings of the National Academy of Sciences, 2008.* ***105****(38): p. 14377-14382.*
219. *Chen, H., et al., A molecular brake in the kinase hinge region regulates the activity of receptor tyrosine kinases. Mol Cell, 2007.* ***27****(5): p. 717-30.*
220. *Mol, C.D., et al., Structural basis for the autoinhibition and STI-571 inhibition of c-Kit tyrosine kinase. J Biol Chem, 2004.* ***279****(30): p. 31655-63.*
221. *Lehtonen, J.V., BODIL: a molecular modeling environment for structure-function analysis and drug design. 2004, Journal of Computer Aided MolecularDesign.*
222. *Hubbard, S.R., L. Wei, and W.A. Hendrickson, Crystal structure of the tyrosine kinase domain of the human insulin receptor. Nature, 1994.* ***372****(6508): p. 746-754.*
223. *Hubbard, S.R., Crystal structure of the activated insulin receptor tyrosine kinase in complex with peptide substrate and ATP analog. EMBO J, 1997.* ***16****(18): p. 5572-5581.*
224. *Atwell, S., et al., A novel mode of Gleevec binding is revealed by the structure of spleen tyrosine kinase. J Biol Chem, 2004.* ***279****(53): p. 55827-32.*
225. *Berman, H., Announcing the worldwide Protein Data Bank, in Nature Structural Biology. 2003, Nature. p. 980.*
226. .
227. *Larkin, M.A., Clustal W and Clustal X version 2.0, in Bioinformatics. 2007, Oxford University Press. p. 21.*
228. *C. Lapid, Y.G. 2003; Available from: http://www.bioinformatics.org/primerx.*
229. *Kibbe, W.A. OligoCalc: an online oligonucleotide properties calculator. 2007; Available from: http://basic.northwestern.edu/biotools/OligoCalc.html.*
230. *Tom Hall, I.t., BioEdit v7.0.5.*
231. *Corporation, C., CodonCode Aligner 3.5.6. 2009.*
232. *Kuriyan, J. and D. Eisenberg, The origin of protein interactions and allostery in colocalization. Nature, 2007.* ***450****(7172): p. 983-90.*
233. *Robinson, D.R., Y.M. Wu, and S.F. Lin, The protein tyrosine kinase family of the human genome. Oncogene, 2000.* ***19****(49): p. 5548-57.*
234. *Pawson, T. and P. Nash, Assembly of cell regulatory systems through protein interaction domains. Science, 2003.* ***300****(5618): p. 445-52.*
235. *Futreal, P.A., et al., A census of human cancer genes. Nat Rev Cancer, 2004.* ***4****(3): p. 177-83.*
236. *Cohen, P., Protein kinases--the major drug targets of the twenty-first century? Nat Rev Drug Discov, 2002.* ***1****(4): p. 309-15.*
237. *Kinnings, S.L. and R.M. Jackson, Binding site similarity analysis for the functional classification of the protein kinase family. J Chem Inf Model, 2009.* ***49****(2): p. 318-29.*
238. *Taylor, S.S., et al., PKA: a portrait of protein kinase dynamics. Biochim Biophys Acta, 2004.* ***1697****(1-2): p. 259-69.*
239. *Moretti, L., Exploring structure and plasticity of tyrsine kinase domains for drug discovery, in Faculté des Sciences. 2007, Université de Genève, Univesità degli studi di Padova: Geneva.*
240. *Seeliger, M.A., et al., Equally potent inhibition of c-Src and Abl by compounds that recognize inactive kinase conformations. Cancer Res, 2009.* ***69****(6): p. 2384-92.*
241. *Vulpetti, A. and R. Bosotti, Sequence and structural analysis of kinase ATP pocket residues. Farmaco, 2004.* ***59****(10): p. 759-65.*

242. *Liu, Y. and N.S. Gray, Rational design of inhibitors that bind to inactive kinase conformations. Nat Chem Biol, 2006. **2**(7): p. 358-64.*
243. *Johnson, L.N., Protein kinase inhibitors: contributions from structure to clinical compounds. Q Rev Biophys, 2009. **42**(1): p. 1-40.*
244. *Simard, J.R., et al., A new screening assay for allosteric inhibitors of cSrc. Nat Chem Biol, 2009. **5**(6): p. 394-6.*
245. *Zhang, J., P.L. Yang, and N.S. Gray, Targeting cancer with small molecule kinase inhibitors. Nat Rev Cancer, 2009. **9**(1): p. 28-39.*
246. *Yang, S. and B. Roux, Src kinase conformational activation: thermodynamics, pathways, and mechanisms. PLoS Comput Biol, 2008. **4**(3): p. e1000047.*
247. *Formaneck, M.S., L. Ma, and Q. Cui, Reconciling the "old" and "new" views of protein allostery: a molecular simulation study of chemotaxis Y protein (CheY). Proteins, 2006. **63**(4): p. 846-67.*
248. *Flynn, T.C., et al., Allosteric transition pathways in the lactose repressor protein core domains: asymmetric motions in a homodimer. Protein Sci, 2003. **12**(11): p. 2523-41.*
249. *Chennubhotla, C. and I. Bahar, Markov propagation of allosteric effects in biomolecular systems: application to GroEL-GroES. Mol Syst Biol, 2006. **2**: p. 36.*
250. *Yang, S., N.K. Banavali, and B. Roux, Mapping the conformational transition in Src activation by cumulating the information from multiple molecular dynamics trajectories. Proc Natl Acad Sci U S A, 2009. **106**(10): p. 3776-81.*
251. *Ten Eyck, L.F., S.S. Taylor, and A.P. Kornev, Conserved spatial patterns across the protein kinase family. Biochim Biophys Acta, 2008. **1784**(1): p. 238-43.*
252. *Cheng, H.C., et al., Allosteric networks governing regulation and catalysis of Src-family protein tyrosine kinases: implications for disease-associated kinases. Clin Exp Pharmacol Physiol. **37**(1): p. 93-101.*
253. *Bukhtiyarova, M., et al., Mutagenesis of p38alpha MAP kinase establishes key roles of Phe169 in function and structural dynamics and reveals a novel DFG-OUT state. Biochemistry, 2007. **46**(19): p. 5687-96.*
254. *Vogtherr, M., et al., NMR characterization of kinase p38 dynamics in free and ligand-bound forms. Angew Chem Int Ed Engl, 2006. **45**(6): p. 993-7.*
255. *Aleksandrov, A. and T. Simonson, Molecular dynamics simulations show that conformational selection governs the binding preferences of imatinib for several tyrosine kinases. J Biol Chem. **285**(18): p. 13807-15.*
256. *Dar, A.C., M.S. Lopez, and K.M. Shokat, Small molecule recognition of c-Src via the Imatinib-binding conformation. Chem Biol, 2008. **15**(10): p. 1015-22.*
257. *Cheng, Y. and W.H. Prusoff, Relationship between the inhibition constant (K1) and the concentration of inhibitor which causes 50 per cent inhibition (I50) of an enzymatic reaction. Biochem Pharmacol, 1973. **22**(23): p. 3099-108.*
258. *Dixon, M., The determination of enzyme inhibitor constants. Biochem J, 1953. **55**(1): p. 170-1.*
259. *Leslie, A.G.W., Recent changes to the MOSFLM package for processing film and image plate data. Newsletter on Protein Crystallography, 1992(26).*
260. *Evans, P., Scaling and assessment of data quality. Acta Crystallogr D Biol Crystallogr, 2006. **62**(Pt 1): p. 72-82.*
261. *McCoy, A.J., Solving structures of protein complexes by molecular replacement with Phaser. Acta Crystallogr D Biol Crystallogr, 2007. **63**(Pt 1): p. 32-41.*
262. *McCoy, A.J., et al., Phaser crystallographic software. J Appl Crystallogr, 2007. **40**(Pt 4): p. 658-674.*
263. *Matthews, B.W., Solvent content of protein crystals. J Mol Biol, 1968. **33**(2): p. 491-7.*

*264. Brunger, A.T., et al., Crystallography & NMR system: A new software suite for macromolecular structure determination. Acta Crystallogr D Biol Crystallogr, 1998. **54**(Pt 5): p. 905-21.*

*265. Brunger, A.T., P.D. Adams, and L.M. Rice, Recent developments for the efficient crystallographic refinement of macromolecular structures. Curr Opin Struct Biol, 1998. **8**(5): p. 606-11.*

*266. Adams, P.D., et al., PHENIX: building new software for automated crystallographic structure determination. Acta Crystallogr D Biol Crystallogr, 2002. **58**(Pt 11): p. 1948-54.*

*267. Emsley, P. and K. Cowtan, Coot: model-building tools for molecular graphics. Acta Crystallogr D Biol Crystallogr, 2004. **60**(Pt 12 Pt 1): p. 2126-32.*

*268. Jones, T.A., et al., Improved methods for building protein models in electron density maps and the location of errors in these models. Acta Crystallogr A, 1991. **47 (Pt 2)**: p. 110-9.*

*269. Painter, J. and E.A. Merritt, Optimal description of a protein structure in terms of multiple groups undergoing TLS motion. Acta Crystallogr D Biol Crystallogr, 2006. **62**(Pt 4): p. 439-50.*

*270. Laskowski, R.A., D.S. Moss, and J.M. Thornton, Main-chain bond lengths and bond angles in protein structures. J Mol Biol, 1993. **231**(4): p. 1049-67.*

*271. Davis, I.W., et al., MolProbity: all-atom contacts and structure validation for proteins and nucleic acids. Nucleic Acids Res, 2007. **35**(Web Server issue): p. W375-83.*

*272. Schindler, T., et al., Structural mechanism for STI-571 inhibition of abelson tyrosine kinase. Science, 2000. **289**(5486): p. 1938-42.*

*273. Zhou, T., et al., Structural Analysis of DFG-in and DFG-out Dual Src-Abl Inhibitors Sharing a Common Vinyl Purine Template. Chemical Biology & Drug Design. **75**(1): p. 18-28.*

*274. von Bubnoff, N., et al., Inhibition of wild-type and mutant Bcr-Abl by pyrido-pyrimidine-type small molecule kinase inhibitors. Cancer Res, 2003. **63**(19): p. 6395-404.*

*275. Lombardo, L.J., et al., Discovery of N-(2-chloro-6-methyl- phenyl)-2-(6-(4-(2-hydroxyethyl)- piperazin-1-yl)-2-methylpyrimidin-4- ylamino)thiazole-5-carboxamide (BMS-354825), a dual Src/Abl kinase inhibitor with potent antitumor activity in preclinical assays. J Med Chem, 2004. **47**(27): p. 6658-61.*

*276. Kantarjian, H., et al., Dasatinib. Nat Rev Drug Discov, 2006. **5**(9): p. 717-8.*

*277. Diskin, R., D. Engelberg, and O. Livnah, High-resolution diffracting crystals of intrinsically active p38alpha MAP kinase: a case study for low-throughput approaches. Acta Crystallogr D Biol Crystallogr, 2007. **63**(Pt 2): p. 260-5.*

*278. Kim, K.M., et al., Post-translational modification of the N-terminal His tag interferes with the crystallization of the wild-type and mutant SH3 domains from chicken src tyrosine kinase. Acta Crystallogr D Biol Crystallogr, 2001. **57**(Pt 5): p. 759-62.*

*279. Nagar, B., et al., Crystal structures of the kinase domain of c-Abl in complex with the small molecule inhibitors PD173955 and imatinib (STI-571). Cancer Res, 2002. **62**(15): p. 4236-43.*

*280. Getlik, M., et al., Hybrid compound design to overcome the gatekeeper T338M mutation in cSrc. J Med Chem, 2009. **52**(13): p. 3915-26.*

*281. Williams, N.K., et al., Crystal structures of the Lyn protein tyrosine kinase domain in its Apo- and inhibitor-bound state. J Biol Chem, 2009. **284**(1): p. 284-91.*

*282. Tokarski, J.S., et al., The structure of Dasatinib (BMS-354825) bound to activated ABL kinase domain elucidates its inhibitory activity against imatinib-resistant ABL mutants. Cancer Res, 2006. **66**(11): p. 5790-7.*

283. *Thompson, J.D., T.J. Gibson, and D.G. Higgins, Multiple sequence alignment using ClustalW and ClustalX. Curr Protoc Bioinformatics, 2002.* ***Chapter 2****: p. Unit 2 3.*
284. *Yadav, S.S. and W.T. Miller, The evolutionarily conserved arrangement of domains in SRC family kinases is important for substrate recognition. Biochemistry, 2008.* ***47****(41): p. 10871-80.*
285. *Suga, H., K. Katoh, and T. Miyata, Sponge homologs of vertebrate protein tyrosine kinases and frequent domain shufflings in the early evolution of animals before the parazoan-eumetazoan split. Gene, 2001.* ***280****(1-2): p. 195-201.*
286. *Li, W., et al., Signaling properties of a non-metazoan Src kinase and the evolutionary history of Src negative regulation. J Biol Chem, 2008.* ***283****(22): p. 15491-501.*
287. *Segawa, Y., et al., Functional development of Src tyrosine kinases during evolution from a unicellular ancestor to multicellular animals. Proc Natl Acad Sci U S A, 2006.* ***103****(32): p. 12021-6.*
288. *Cozzone, A.J., Bacterial tyrosine kinases: novel targets for antibacterial therapy? Trends Microbiol, 2009.* ***17****(12): p. 536-43.*
289. *Segel, I.H., Enzyme Kinetics. 1975, New York: John Wiley & Sons.*
290. *Copeland, R.A., Enzymes. 1996, New York: VCH Publishers, Inc.*
291. *Cleland, W.W., Statistical analysis of enzyme kinetic data. Methods Enzymol, 1979.* ***63****: p. 103-38.*
292. *Huynh, Q.K., et al., Kinetic mechanisms of IkappaB-related kinases (IKK) inducible IKK and TBK-1 differ from IKK-1/IKK-2 heterodimer. J Biol Chem, 2002.* ***277****(15): p. 12550-8.*
293. *Cook, P.F., et al., Adenosine cyclic 3',5'-monophosphate dependent protein kinase: kinetic mechanism for the bovine skeletal muscle catalytic subunit. Biochemistry, 1982.* ***21****(23): p. 5794-9.*
294. *Cole, P.A., et al., Evaluation of the catalytic mechanism of recombinant human Csk (C-terminal Src kinase) using nucleotide analogs and viscosity effects. J Biol Chem, 1994.* ***269****(49): p. 30880-7.*
295. *Posner, I., M. Engel, and A. Levitzki, Kinetic model of the epidermal growth factor (EGF) receptor tyrosine kinase and a possible mechanism of its activation by EGF. J Biol Chem, 1992.* ***267****(29): p. 20638-47.*
296. *Erneux, C., S. Cohen, and D.L. Garbers, The kinetics of tyrosine phosphorylation by the purified epidermal growth factor receptor kinase of A-431 cells. J Biol Chem, 1983.* ***258****(7): p. 4137-42.*
297. *Walker, D.H., et al., Substrate specificity and kinetic mechanism of human placental insulin receptor/kinase. Biochemistry, 1987.* ***26****(5): p. 1428-33.*
298. *Wong, T.W. and A.R. Goldberg, Kinetics and mechanism of angiotensin phosphorylation by the transforming gene product of Rous sarcoma virus. J Biol Chem, 1984.* ***259****(5): p. 3127-31.*
299. *Boerner, R.J., S.C. Barker, and W.B. Knight, Kinetic mechanisms of the forward and reverse pp60c-src tyrosine kinase reactions. Biochemistry, 1995.* ***34****(50): p. 16419-23.*
300. *Crespan, E., et al., Dual Src and Abl inhibitors target wild type Abl and the AblT315I Imatinib-resistant mutant with different mechanisms. Bioorg Med Chem.* ***18****(11): p. 3999-4008.*
301. *Cheng, H.C., et al., Allosteric networks governing regulation and catalysis of Src-family protein tyrosine kinases: implications for disease-associated kinases. Clin Exp Pharmacol Physiol, 2010.* ***37****(1): p. 93-101.*
302. *Lew, J., S.S. Taylor, and J.A. Adams, Identification of a partially rate-determining step in the catalytic mechanism of cAMP-dependent protein kinase: a transient kinetic*

study using stopped-flow fluorescence spectroscopy. Biochemistry, 1997. ***36****(22): p. 6717-24.*

303. Shaffer, J., G. Sun, and J.A. Adams, Nucleotide release and associated conformational changes regulate function in the COOH-terminal Src kinase, Csk. Biochemistry, 2001. ***40****(37): p. 11149-55.*

304. Shaffer, J. and J.A. Adams, Detection of conformational changes along the kinetic pathway of protein kinase A using a catalytic trapping technique. Biochemistry, 1999. ***38****(37): p. 12072-9.*

305. Shan, Y., et al., A conserved protonation-dependent switch controls drug binding in the Abl kinase. Proc Natl Acad Sci U S A, 2009. ***106****(1): p. 139-44.*

306. Masterson, L.R., et al., Allosteric cooperativity in protein kinase A. Proc Natl Acad Sci U S A, 2008. ***105****(2): p. 506-11.*

307. Hastie, C.J., H.J. McLauchlan, and P. Cohen, Assay of protein kinases using radiolabeled ATP: a protocol. Nat Protoc, 2006. ***1****(2): p. 968-71.*

308. Zheng, J., et al., Crystal structure of the catalytic subunit of cAMP-dependent protein kinase complexed with MgATP and peptide inhibitor. Biochemistry, 1993. ***32****(9): p. 2154-61.*

309. Bossemeyer, D., et al., Phosphotransferase and substrate binding mechanism of the cAMP-dependent protein kinase catalytic subunit from porcine heart as deduced from the 2.0 A structure of the complex with Mn2+ adenylyl imidodiphosphate and inhibitor peptide PKI(5-24). EMBO J, 1993. ***12****(3): p. 849-59.*

310. Greenman, C., et al., Patterns of somatic mutation in human cancer genomes. Nature, 2007. ***446****(7132): p. 153-8.*

311. Davies, S.P., et al., Specificity and mechanism of action of some commonly used protein kinase inhibitors. Biochem J, 2000. ***351****(Pt 1): p. 95-105.*

312. Bain, J., et al., The selectivity of protein kinase inhibitors: a further update. Biochem J, 2007. ***408****(3): p. 297-315.*

Appendix A

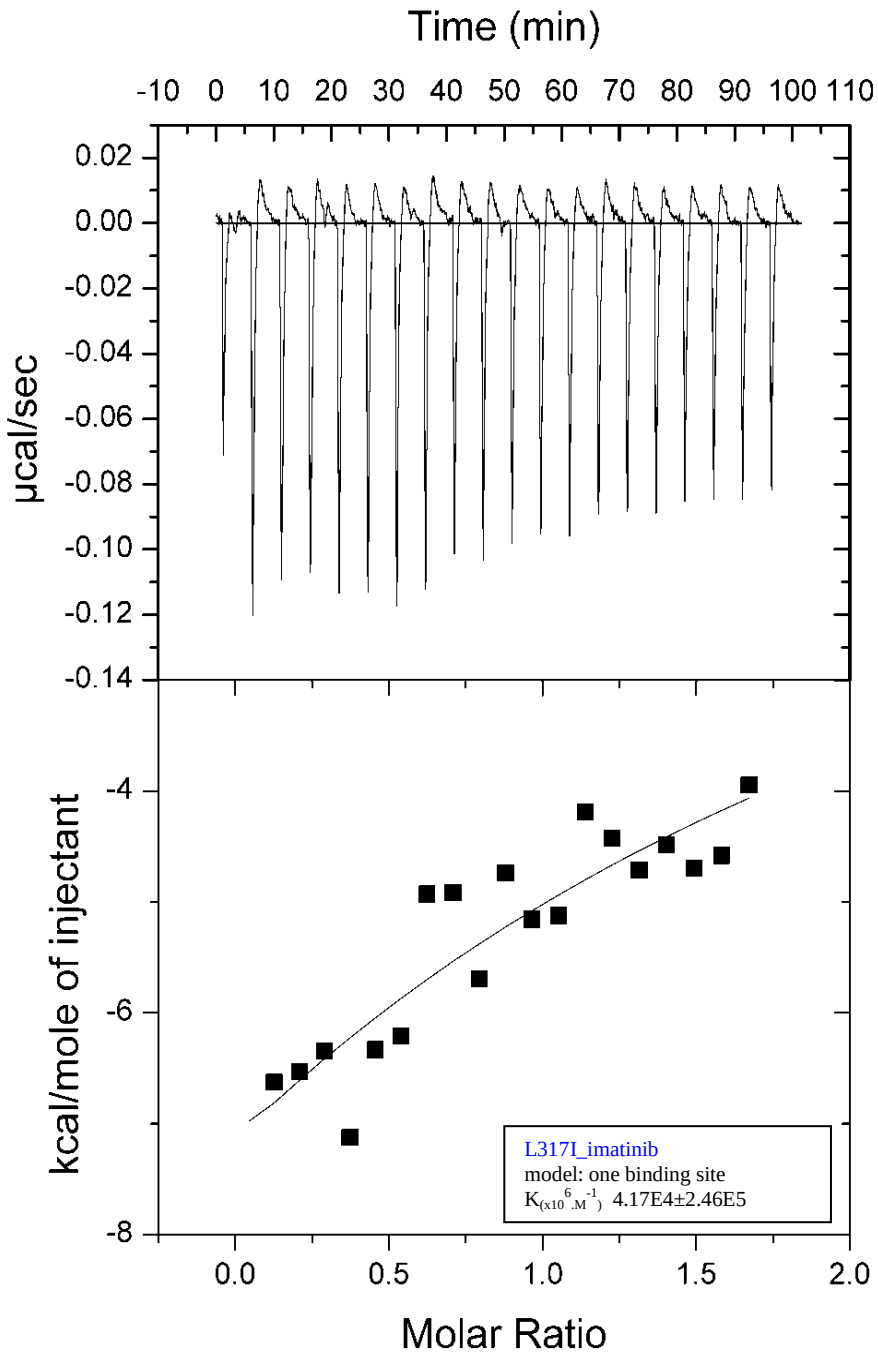

ITC assay of imatinib binding to c-Src L317I upon purification protocol for kinase assay and crystallization. The top panel shows heat signals upon 20 injections (8.8µl) of imatinib (40µM) into the sample cell containing 3µM protein. The obtained binding isotherm is shown on the lower panel. The solid line represents the non-linear least square fit based on a one-site binding model.

Acknowledgements

This work is not only mine. It is the end-point of a long way I was fortunate to travel along with many wonderful people. That is why I owe it to you and I would like to deeply thank you.

A first thank goes to Prof. Leonardo Scapozza. I first met you at 2005 as a student and I was immediately impressed by your strong and supportive relationship with peers and students. You have not only offered me the opportunity of carrying out my PhD at the University of Geneva but also guided me throughout this project and in life, with a lot of wisdom and trust. You have also supported me in my decision of pursuing my science career in protein formulation.

I want to thank the members of my PhD jury, Prof. Alexander Levitzki, Dr. Neil McDonald, Dr. Doriano Fabbro and Dr. Francesco Luigi Gervasio for evaluating my research work.

Dr. Remo Perozzo is also in this list. You are doing research with a lot of knowledge and enthusiasm. All the wet-lab people would like to resemble you.

Of course, I thank all the past, present and invited members of Prof. Scapozza's lab who will remain lifelong friends: Andrea (so bright in science, in informatics and in music, I was glad to share this project with you), Leo (you find a solution to every problem, except of growing basil), Anja (whom I miss so much in Geneva), Dr. Lucile Pernot (for your precious help in crystallography and interesting discussions), Loris and Sabine (the pioneers), Pernilla, Simon and Emma-Sophie (a future pharmacist?), Patricia (so nice and smart, you break the clichés), Yvonne, Alessandra, Surekha, Shaheen, Agatha, Majdeline, Claudia.

I am also thankful to my four diploma students who knew joys and frustrations in research with me. Thank you, Sarah-Marie, Emilio, Didia and Cecilia!

Big thank goes to Dr. Pierre-Alain Menoud who encouraged me to start a PhD.

БЛАГОДАРЯ to my family Dora, Emil and Emo. I have recently heard a citation saying "Wisdom is to have dreams big enough not to lose sight when we pursue them". You have inspired and supported my dreams.

A thankful hug goes to my aunt, Violette. She was there when, at the age of thirteen, I fell in love at first sight with Switzerland!

A special thank goes to my beloved friends Christophe and Inna. You were there all the way through and your friendship is very precious to me.

Last but not least is Florian. On s'est connu au début de cette thèse et tu as vécu toutes les émotions de ce travail avec moi. Merci pour ton amour, ton support, ton aide et tes encouragements. Merci aussi à Cornelia, Philippe, Coralie, Lionel et Liza, car vous êtes ma famille suisse.

If I could arrive at this point it is thank to all people I acknowledged above and to many others who I have not mentioned but they know what they meant to me…

Thank you.